Longitudinal Dispersion due to Surcharged Manholes

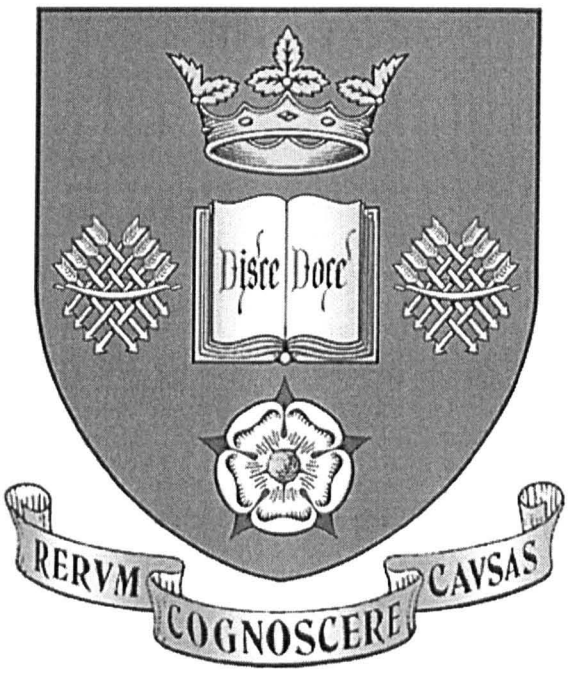

by

Peter Dennis

Thesis submitted in partial fulfilment of the requirements for the Degree of Doctor of Philosophy

University of Sheffield
Department of Civil and Structural Engineering

March 2000

Summary

Greater environmental considerations and the desire to reduce pollution overflows to watercourses are requiring engineers to develop a better understanding of the processes involved in pollution transport through sewer networks. Furthermore, developments in modelling techniques and computer power are allowing urban drainage modellers to increase the complexity of their software and so demand additional data that can be incorporated. Presently, an important aspect is quantifying the retention time and dispersion of pollutants entering an urban drainage system.

Manholes provide a means of sewer access for maintenance and inspection. Under storm flow conditions they are liable to surcharge above the level of the pipe soffit. This creates a storage volume that has an impact on the longitudinal dispersion and travel time of soluble pollutants in sewer systems. A laboratory investigation has been completed to quantify these effects for various manhole configurations. These include step heights between the inlet and outlet pipes, benching and extreme high surcharge conditions. In addition, re-analysis of previously acquired data has allowed variations in manhole diameter to be considered.

Numerical modelling using computational fluid dynamics, combined with laser light sheet visualisation of the flow structures within manholes, has provided greater insight into the processes causing longitudinal dispersion.

The coefficients required for two existing longitudinal dispersion models, the advection dispersion equation and the aggregated dead zone model, have been determined by means of an optimisation process. This has been undertaken with computer software specifically written for the purpose. The technique adopted for optimisation is fully detailed. Final conclusions regarding the longitudinal dispersion due to surcharged manholes are presented.

"It is not the critic who counts, not the man who points out how the strong man stumbles or where the doer of deeds could have done them better. The credit belongs to the man who is actually in the arena, whose face is marred by dust and sweat and blood, who strives valiantly, who errs and comes up short again and again because there is no effort without error and shortcomings, who knows the great devotion, who spends himself in a worthy cause, who at best knows in the end the high achievement of triumph and who at worst, if he fails while daring greatly, knows his place shall never be with those timid and cold souls who know neither victory nor defeat."

Theodore Roosevelt

Contents

Summary
Contents iii
List of Figures vi
List of Tables x
Notation xi

1 Introduction 1

2 Literature Review 3
2.1 Sewer systems 3
2.1.1 Manholes in sewer systems 5
2.2 Head loss 7
2.2.1 Manhole shape and size 9
2.2.2 Flow conditions 10
2.2.3 Surcharge level 11
2.2.4 Step height 11
2.2.5 Benching 13
2.3 Sewer systems modelling 13
2.4 Real time control 15
2.5 Longitudinal dispersion 16
2.5.1 Introduction 16
2.5.2 Mixing theory 17
2.5.3 Advection Dispersion Equation (ADE) 19
2.5.4 Aggregated Dead Zone (ADZ) equation 22
2.6 Longitudinal dispersion in manholes 29
2.7 Computational fluid dynamics 34
2.7.1 Introduction 34
2.7.2 Governing equations of fluid dynamics 35
2.7.3 The k-ε model 36
2.7.4 The Reynolds Stress Model (RSM) 36
2.7.5 Previous related use of CFD 37
2.8 Summary 38

3 Experimental Procedures 39
3.1 Introduction 39
3.2 Laboratory system 39
3.2.1 General arrangement 39
3.2.2 Manhole details 40
3.3 Instrumentation 42
3.3.1 Instrumentation for head loss 42
3.3.2 Instrumentation for longitudinal dispersion 44

3.3.3 Data logging instrumentation 46
3.4 Calibration 46
3.4.1 Calibration of pressure transducers 46
3.4.2 Calibration of fluorometers 47
3.5 Test preparation 49
3.6 Test procedure 49
3.7 Test Schedule 50
3.8 Laser light sheet visualisation 52

4. Experimental Results 53
4.1 Introduction 53
4.2 Processing of laboratory data 53
4.3 Optimisation of travel time and longitudinal dispersion coefficients 53
4.3.1 Data preparation 54
4.3.2 Data optimisation 64
4.4 Laboratory results 70
4.4.1 Flow regimes 70
4.4.2 Head loss results 73
4.4.3 ADE results 77
4.4.4 ADZ results 87
4.4.5 Laser imaging 96

5 Discussion 100
5.1 Introduction 100
5.2 Head loss 100
5.2.1 Comparison of head loss results with other researchers 100
5.3 Re-analysis of manhole diameter data 101
5.4 ADE longitudinal dispersion 104
5.5 ADZ longitudinal dispersion 112
5.5.1 Equivalent pipe length analysis 118
5.6 Flow patterns 119
5.7 Dispersive fraction 120
5.8 Relationship between head loss and ADZ parameters 125
5.9 Simulation of longitudinal dispersion in a sewer 128

6 Numerical Modelling 131
6.1 The application of a CFD model 131
6.1.1 Geometry input 131
6.1.2 Grid generation 132
6.1.3 Boundary conditions 133
6.1.4 Simulation 133
6.2 Application of Fluent for manhole investigation 134
6.3 Results 136
6.3.1 Flow Profiles 136
6.3.2 Head loss 140
6.3.3 Particle Image Velocimetry (PIV) 142

7 Further Work 144
7.1 Introduction 144
7.2 Continuation of laboratory studies 144
7.3 Data analysis 145
7.4 Numerical modelling 148
7.5 Field testing 149

8 Conclusions 151

References 152
Acknowledgements 156

List of Figures

Figure 2.1 Combined sewer system. 3
Figure 2.2 Separate sewer systems. 4
Figure 2.3 Features of a manhole. 6
Figure 2.4 Plan of offset benching design. 6
Figure 2.5 Drop manhole configuration. 7
Figure 2.6 Calculation of head loss from pressure transducer measurements. 8
Figure 2.7 Proposed shape factor values (Bo Pedersen and Mark, 1990). 10
Figure 2.8 Head loss coefficient variation with step height (Kusuda and Arao, 1996). 12
Figure 2.9 Time averaging of turbulent velocity. 18
Figure 2.10 ADE routing of multiple discrete inputs representing an upstream temporal concentration distribution. 21
Figure 2.11 ADZ routing of a single, instantaneous tracer injection. 25
Figure 2.12 ADZ routing of multiple discrete inputs representing an upstream temporal concentration distribution. 25
Figure 2.13 Arrangement for laser induced fluorescence experiments. 31
Figure 2.14 Variation in solute concentration within manhole with time. (Q = 0.9l/s, Surcharge = 200mm). Guymer *et al* (1998). 32
Figure 2.15 Comparison of longitudinal dispersion prediction from MOUSETRAP and laboratory data (diameter = 400mm, Q = 1.98l/s) (Guymer *et al*, 1998). 33

Figure 3.1 Schematic arrangement of laboratory apparatus. 40
Figure 3.2 Laboratory manhole with 1.5D step height. 41
Figure 3.3 Benching arrangement for 1.5D step manhole. 42
Figure 3.4 Potential source of error in head loss measurement. 43
Figure 3.5 Diagram of fluorometer adapter (O'Brien, 2000). 45
Figure 3.6 Fluorometer and adapter fitted in position on manhole pipeline. 45
Figure 3.7 Example calibration lines for pressure transducers. 47
Figure 3.8 Diagram of fluorometer calibration flow circuit. 47
Figure 3.9 Example of calibration for fluorometers (temperature adjusted to 15° Celsius). 48

Figure 4.1 Example of manhole dye tracer data collected by upstream and downstream fluorometers (388mm manhole, no step, Q = 6.0l/s, surcharge = 402mm). 55
Figure 4.2 Sensitivity analysis for rate of sampling data. 56
Figure 4.3 Location of temporal concentration profile start and end points. 58
Figure 4.4 Sensitivity for profile cut off determination. 59
Figure 4.5 Examples of tracer temporal concentration profiles for variations in surcharge at low discharge (388mm unbenched manhole with no step). 61
Figure 4.6 Examples of tracer temporal concentration profiles for variations in surcharge at high discharge (388mm unbenched manhole with no step). 62
Figure 4.7 Examples of tracer temporal concentration profiles for variations in surcharge at high discharge (388mm unbenched manhole with 1.5D step). 63

Figure 4.8 Representation of the matrix optimisation procedure. 66
Figure 4.9 3-D surface representation of matrix optimisation results. 67
Figure 4.10 Measured downstream temporal concentration profile with ADE predictions. (388mm manhole with no step, Q = 6.0l/s, surcharge = 402mm). 68
Figure 4.11 Measured downstream temporal concentration profile with ADZ predictions (388mm manhole with no step, Q = 6.0l/s, surcharge = 402mm). 69
Figure 4.12 Longitudinal dispersion coefficients from 5 repeat tests with standard and optimised analysis (388mm manhole with no step). 69
Figure 4.13 Flow condition 1. 71
Figure 4.14 Flow condition 2. 71
Figure 4.15 Flow condition 3. 71
Figure 4.16 Flow condition 4. 72
Figure 4.17 Flow condition 5. 72
Figure 4.18 Flow condition variation with surcharge and discharge (step = 0.0D). 73
Figure 4.19 Flow condition variation with surcharge and discharge (step = 2.0D). 73
Figure 4.20 Variation of head loss with surcharge (388mm unbenched manhole). 75
Figure 4.21 Variation of surcharge averaged head loss with velocity head (388mm unbenched manhole). 76
Figure 4.22 Sample results from piezometer readings (388mm unbenched manhole, Q = 6.0l/s, surcharge = 402mm). 77
Figure 4.23 Variation of ADE travel time with surcharge (388mm unbenched manhole). 80
Figure 4.24 Variation of surcharge averaged ADE travel time with discharge. 81
Figure 4.25 Variation of dispersion coefficient with surcharge (388mm unbenched manhole). 83
Figure 4.26 Variation of surcharge averaged dispersion coefficient with discharge. 84
Figure 4.27 Comparison of travel time for benched and unbenched manholes. 85
Figure 4.28 Comparison of dispersion coefficient for benched and unbenched manholes. 85
Figure 4.29 Comparison of variation of surcharge averaged ADE travel time with discharge for benched and unbenched manholes and straight pipe (pipe data from Guymer and O'Brien, 2000). 86
Figure 4.30 Comparison of variation of surcharge averaged dispersion coefficient with discharge for benched and unbenched manholes and straight pipe (pipe data from Guymer and O'Brien, 2000). 86
Figure 4.31 Variation of ADZ travel time with surcharge. 89
Figure 4.32 Variation of reach time delay with surcharge. 91
Figure 4.33 Variation of surcharge averaged ADZ travel time with discharge. 92
Figure 4.34 Variation of surcharge averaged reach time delay with discharge. 93
Figure 4.35 Comparison of variation of ADZ travel time with surcharge for benched and unbenched manholes. 94
Figure 4.36 Comparison of variation of reach time delay with surcharge for benched and unbenched manholes. 94
Figure 4.37 Comparison of variation of ADZ surcharge averaged travel time with discharge for benched and unbenched manholes and straight pipe (pipe data from Guymer and O'Brien, 2000). 95
Figure 4.38 Comparison of variation of surcharge averaged reach time delay with discharge for benched and unbenched manholes and straight pipe (pipe data from Guymer and O'Brien, 2000). 95
Figure 4.39 Passage of tracer and particles through unbenched manhole with no step (Q = 1.5l/s, surcharge = 150mm). 97

Figure 4.40 Passage of tracer through unbenched manhole with 1.5D step at low surcharge (388mm manhole, Q = 4.0l/s, surcharge = 288mm). 98
Figure 4.41 Passage of tracer through unbenched manhole with 1.5D step at high surcharge (388mm manhole, Q = 4.0l/s, surcharge = 798mm). 99

Figure 5.1 Comparison of head loss coefficient with Kusuda and Arao (1996). 101
Figure 5.2 Variation of discharge averaged dispersion coefficient with surcharge determined with standard ADE procedure (O'Brien, 2000). 103
Figure 5.3 Comparison of ADE travel time data from Author and O'Brien (≈388mm unbenched manhole with no step). 105
Figure 5.4 Comparison of dispersion coefficient data from Author and O'Brien (≈388mm unbenched manhole with no step). 106
Figure 5.5 Variation of ADE travel time with surcharge for manhole diameters. 108
Figure 5.6 Variation of ADE travel time threshold surcharge with manhole diameter. 108
Figure 5.7 Variation of dispersion coefficient with surcharge for manhole diameters. 111
Figure 5.8 Comparison of travel time data from Author and O'Brien (≈388mm unbenched manhole with no step). 112
Figure 5.9 Comparison of time delay data from Author and O'Brien (≈388mm unbenched manhole with no step). 113
Figure 5.10 Variation of travel time with surcharge. 115
Figure 5.11 ADZ travel time threshold. 115
Figure 5.12 Variation of time delay with surcharge. 117
Figure 5.13 Variation of ADZ post threshold travel time with discharge for manhole diameters. 117
Figure 5.14 Variation of surcharge averaged reach time delay with discharge for manhole diameters. 118
Figure 5.15 Variation of dispersive fraction with surcharge. 123
Figure 5.16 Comparison of dispersive fraction data for benched and unbenched-benched manholes. 124
Figure 5.17 Variation of dispersive fraction with discharge. 125
Figure 5.18 Velocity distribution and diffusion region in a circular free jet (Albertson *et al*, 1950) 126
Figure 5.19 The effect of step height on the volume of jet diffusion region. 127
Figure 5.20 Variation of dispersive fraction with head loss coefficient. 128
Figure 5.21 Sewer simulation input concentration profile with ADZ prediction for longitudinal dispersion due to 100 metres of pipe. 129
Figure 5.22 Simulation of longitudinal dispersion through 100 metres of sewer pipe. 129

Figure 6.1 Process of CFD grid generation. 132
Figure 6.2 Comparison of Cartesian and body fitted co-ordinate grid systems. 133
Figure 6.3 CFD model solving process. 134
Figure 6.4 Surface grid for 388mm manhole with a step height of 1.0D. 135
Figure 6.5 Velocity magnitude prediction (388mm unbenched manhole, step = 0.0D, Q = 1.0l/s). 137
Figure 6.6 Velocity magnitude prediction (388mm benched manhole, step = 0.0D, Q = 1.0l/s). 138
Figure 6.7 Velocity magnitude prediction (388mm unbenched manhole, step = 1.0D, Q = 1.0l/s). 139
Figure 6.8 Determination of head loss due to manhole (388mm unbenched manhole, Q = 1.0l/s and step = 0.0D). 140
Figure 6.9 Boundary layer cell sizing. 141
Figure 6.10 Flow patterns in manhole determined from particle image velocimetry (388mm manhole, Q = 1.0l/s, surcharge = 429mm). 142

Figure 7.1 ADZ parallel model. 146
Figure 7.2 Comparison of ADZ parallel and ADZ optimised predictions (388mm unbenched manhole, no step, Q = 6.0l/s, surcharge = 402mm). 147
Figure 7.3 Possible Monte Carlo simulation results. 148

List of Tables

Table 2.1 Recommended maximum spacing for sewer manholes. 5
Table 2.2 Recommended manhole diameters. 5
Table 2.3 Proposed manhole head loss coefficient, K_H, values (Archer *et al*, 1978). 9
Table 2.4 Circulation regimes (Johnston and Volker, 1990). 11

Table 3.1 Summary of laboratory tests. 51

Table 4.1 Boundary settings for first optimisation matrix calculation. 65
Table 4.2 Ultimate resolution values for matrix boundary coefficients. 67
Table 4.3 Mean and standard deviation values for surcharge averaged head loss, H_s. 76
Table 4.4 Mean and standard deviation values for surcharge averaged ADE travel time, $\bar{t}_s$. 81
Table 4.5 Mean and standard deviation values for surcharge averaged dispersion coefficient, K_s. 84
Table 4.6 Comparison of benched and unbenched manhole mean and standard deviation values for surcharge averaged ADE parameters. 87
Table 4.7 Mean and standard deviation values for surcharge averaged ADZ travel time, $\bar{t}_s$. 92
Table 4.8 Mean and standard deviation values for surcharge averaged reach time delay, τ_s. 93
Table 4.9 Comparison of benched and unbenched manhole mean and standard deviation values for surcharge averaged ADZ parameters. 96

Table 5.1 Head loss coefficients. 100
Table 5.2 Summary of manhole diameter tests completed by O'Brien (2000). 102
Table 5.3 Surcharge averaged dispersive fraction values. 125

Table 6.1 Summary of manhole CFD simulations. 136
Table 6.2 Comparison of CFD and laboratory head loss coefficients. 141

Table 7.1 Coefficients for ADZ parallel and ADZ optimised models. 147

Notation

A	Cross sectional area
B	Mass balance factor
C	Cross-sectional average concentration
C_d	Coefficient of discharge
c	Concentration
$\bar{c}$	Temporal mean concentration
c'	Temporally fluctuating concentration component
D	Pipe diameter
D_m	Manhole diameter
E_k	Shear flow diffusion coefficient
E_m	Molecular diffusion coefficient
E_t	Turbulent diffusion coefficient
g	Acceleration due to gravity
h	Manhole step height
H	Head loss
H	Head over weir
J_x	Molecular diffusive flux parameter in x direction
K	Longitudinal dispersion coefficient
K_H	Head loss coefficient
M	Mass of tracer
P	Pressure
Q	Discharge
r	Pipe radius
Re	Reynolds number
R_t^2	Coefficient of determination of best fit
t	Time
$\bar{t}$	Travel time
T	Residence time
$\bar{t}_i$	Time of occurrence of temporal concentration profile centroid at location i
t_i'	Time of occurrence of temporal concentration profile first arrival at location i
U	Cross-sectional average velocity
u	Velocity
$\bar{u}$	Temporal mean velocity
u'	Temporally fluctuating velocity component
u^*	Shear velocity
v	Velocity
V	Volume
V_e	Effective dead zone volume
Z^{-p}	Backward shift operator

δ	Discrete time equivalent of reach time delay
γ	Dispersive fraction
γ	Integration variable
θ	V-notch weir angle
ρ	Density
σ_t^2	Temporal variance
τ	Reach time delay
τ_o	Shear stress at wall boundary
υ	Kinematic viscosity
ζ	Manhole shape factor

Subscripts

d	Downstream
s	Surcharge averaged
t	Time
t	Post surcharge threshold
u	Upstream
x, y, z	Three-dimensional co-ordinate directions

Chapter 1

Introduction

In many parts of the world sewers are designed as combined sewer systems. The principle is that wastewater from populations and industrial sources is conveyed to treatment by a pipe network. In addition, at times of rainfall, water that lands on impervious areas such as rooftops and roads is also passed into the same network of sewer pipes. During dry weather flow conditions and light rainfall the function of these combined sewers is generally satisfactory. However, periods of more intense rainfall can cause the flow in parts of the network to exceed the maximum capacity of the pipes or the treatment works. Under these circumstances of heavy flow, it is common for specially designed chambers known as Combined Sewer Overflows (CSOs) to begin operation. These are constructed within the sewers and are designed to pass the least polluted volumes of sewer flow to nearby receiving waters, thus providing flow relief for the system. However, the spill of flow from CSO chambers is predominantly untreated sewage and often has an undesirable impact on watercourses.

Many regions served by combined sewer systems have undergone extensive urban development since the original pipe network was designed and constructed. This means that areas of natural landscape have become locations for housing and industry. These changes have a considerable impact on the urban drainage systems and cause a greatly increased rainfall runoff. In many cases there has been no overall management of wastewater systems to deal with these changes and hence there has been an inefficient use of resources. This has often resulted in unnecessary pollution including excessive spills from combined sewer overflows and even surface flooding.

The Urban Pollution Management manual (Foundation for Water Research, 1994) provides details for an environmentally responsible approach to the management and operation of sewer systems. An engineering understanding is applied to the principle of total catchment management to ensure that the best solutions for given circumstances are found. The aim is to minimise the social, economic and environmental costs associated with the operation of an entire urban drainage network, from the entrance of the water to its successful discharge into receiving waters.

An important development in the design and operation of urban drainage networks is the use of sewer water quality models. These are generally extensions of the widely employed sewer hydraulic models that have been used with success to predict discharges and flow depths at locations throughout a sewer system. The models are useful for enabling comparisons to be made between possible design options and to investigate problems in current networks. They are also the basis for assessment of the potential of real time control operation of sewers. This is where computer controlled gates and weirs allow for more advanced operation by better controlling the flow and using storage volumes throughout the network to prevent CSO spills.

At present these models have demonstrated a good capability to model the sewer flow quantities and some reasonable quality predictions are claimed. However, many simplifications and omissions are made due to there being a lack of understanding regarding the interaction and transport of pollutants in sewers. One detail that is not well accounted for is the passage of sewer flow through

urban drainage structures, in particular the numerous manhole chambers. Under storm flow conditions where the water level may rise above the pipe soffit and the manhole chamber become surcharged, passing pollutants are liable to be entrained within this additional storage volume. This will result in them becoming more dispersed through the system and will retard their overall travel downstream.

Extensive research has been undertaken in the past to determine the head loss coefficients for manholes that were incorporated in the models for the hydraulics of sewers. Only recently, as the models have developed and computing power has increased, has there been a need to develop an understanding of the physical processes involved as pollutants travel through manholes. The current models available assume either no mixing or complete mixing of soluble pollutants at manhole junctions. These are the two extremes and without a reliable prediction of the actual circumstances, other aspects of the models concerning decay rates or chemical reaction times will be unreliable. Therefore, the primary aim of the current study has been to accurately quantify the longitudinal dispersion due to surcharged manholes.

Laboratory experiments using a variety of manhole geometries and flow conditions have been used to determine longitudinal dispersion parameters under different circumstances and to highlight the conditions that are most critical. In addition, a relationship between the head loss and the dispersion has been sought and flow patterns through a surcharged manhole have been examined. The aim has been to provide the results quantifying longitudinal dispersion in a form that could be incorporated into sewer water quality models, thus improving their capabilities as a tool for optimum sewer design.

Chapter 2

Literature Review

2.1 Sewer systems

The trend of urbanisation through history in the UK, and the associated changes of land use from agriculture to habitation, has led to greatly increased rainfall run off volumes. In many cases from early civilisations through to the middle ages, open street sewers have been the major provision for draining storm and foul sewage. Comprehensive provision of reliable drainage schemes for large urban communities became regarded as essential in the nineteenth century (Colyer and Pethick, 1976). The prime requirements for the design of sewer systems initially concentrated on fulfilling hydraulic needs. The aim was to convey the rapidly increasing runoff volumes to the sea or nearest river. These schemes were commonly evolved from earlier systems incorporating networks of streams that had been converted to culverts and built over. Thus both foul and storm sewage was conveyed in the same pipe network, giving rise to the term combined sewerage system (Figure 2.1).

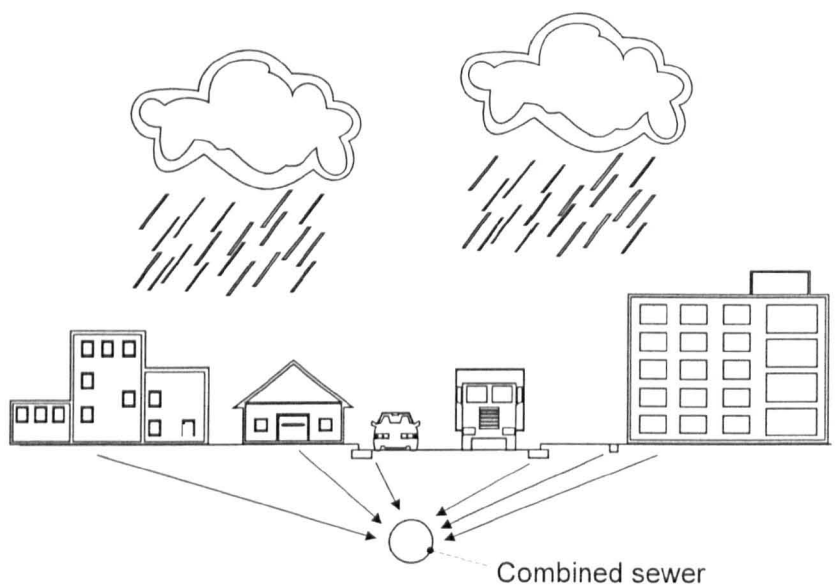

Figure 2.1 Combined sewer system.

The design and further development of combined sewerage systems encountered two problems (Colyer and Pethick, 1976). Firstly, whilst the construction of a drainage system capable of efficiently conveying solely foul sewage was relatively simple, the issue was complicated by the need to incorporate pipe sizes that were able to transport the greatly increased discharges during rainfall events. Catering for extreme rainfall, especially with a network spanning large distances, would require oversized and uneconomic sewers. Therefore a decision had to be made about the proposed capacity of a particular sewer, and what storm event return period it was designed for. The second problem arose from the increasing demand to provide treatment for foul sewage. The construction of expensive treatment works operating considerably below maximum capacity except during

infrequent storm flow conditions was undesirable, especially since the foul flow during storm events is greatly diluted by the rain water volume.

A common solution for dealing with sewer discharges greater than a combined sewer system has been designed for is the provision of Combined Sewer Overflows (CSOs). These structures have taken a wide variety of forms but all with the same principle intention of limiting the discharge that continues to the treatment facility and passing the excess volume to a nearby natural watercourse. A result of employing CSOs is that there will inevitably be spills of a proportion of the sewer flow at times of heavy rain. Increasing urbanisation has led to greater discharges in sewers and more frequent CSO spills. Therefore research has investigated CSO performance and compared the ability of different designs to separate the flow into dirty and predominantly clean portions (Saul *et al*, 1993). This separation is not easily achieved given that pollution in sewer flow can occur in the bed load, suspended and dissolved load, and floating matter.

An alternative sewerage system conveys foul and storm flow by means of totally separate pipes (Figure 2.2). In the past the economics of constructing a twin pipe network with manual bricklaying restricted the use of separate sewers. Furthermore, there was no need for anything other than a combined system since prior to widespread use of wastewater treatment facilities, all sewer flow was conveyed to the same destination. These factors are no longer limitations and new urban development tends towards the totally separate system (Colyer and Pethick, 1976). An intermediate, partially separate, system is also a possibility. This was introduced to convey foul sewage and runoff from the rear of houses in one pipe, and the runoff from the front of houses in a separate pipe. This principle was usually applied to expanses of terraced housing in industrial towns.

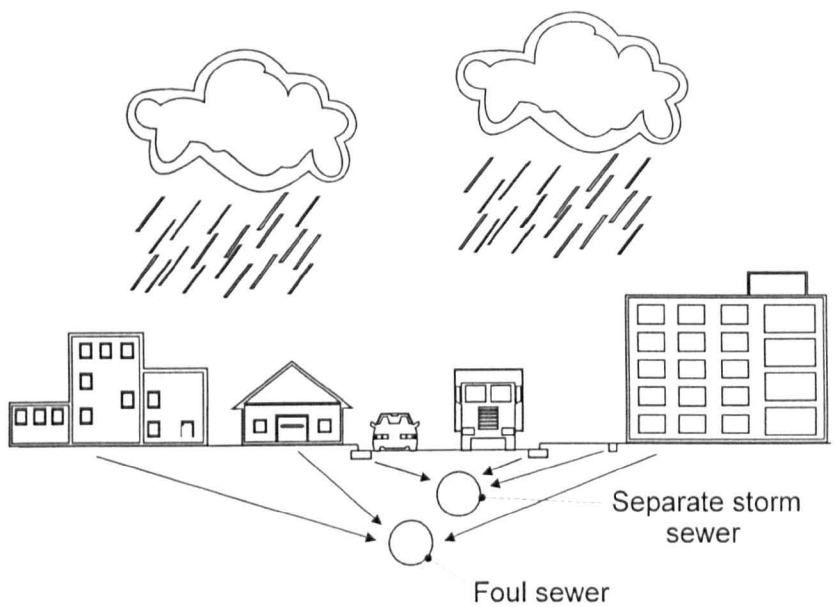

Figure 2.2 Separate sewer systems.

The use of combined or partially separate sewer systems remains extensive. Indeed, such systems have the advantage of applying treatment to at least some of the surface runoff from urban impermeable areas. This is of particular importance with regards to the first foul flush. Thornton and Saul (1986) described this phenomenon as the initial period of storm sewer flow during which the concentration of sediments and pollutants entrained in the flow was observed to be significantly greater than at later stages of the storm event. This effect arises primarily from the erosion and re-

suspension of sediments previously deposited on the sewer bed and from runoff collecting pollutants on the catchment surface (Verbanck *et al*, 1994).

2.1.1 Manholes in sewer systems

In early sewer systems, manholes were employed as a means of removing silt and other obstructions from the flow. Today, the primary function of a manhole chamber is to allow human access to the sewer for the purposes of inspection, cleaning, maintenance and repair. It is these functions, along with the construction materials and local geography, which largely dictate the size and shape of a chamber.

In this country, the common maxim for locating manholes is that they should be at every change of pipe size or type, gradient, direction, and at junctions of pipes. Furthermore, to ensure that cleaning tools such as rods can be used effectively, straight unchanging lengths of sewer should have manholes spaced at no more than a distance given by the pipe diameter (Table 2.1) Hammer (1986).

Pipe diameter (mm)	Maximum manhole spacing (m)
457-762	150
< 381	120 (sometimes 90 for smaller pipes)

Table 2.1 Recommended maximum spacing for sewer manholes.

According to Bartlett (1981), manholes vary in size relative to the pipe diameter. For instance, with pipes up to 300mm in diameter, rectangular brick or in-situ concrete manholes should have a minimum size of 1350mm by 788mm. These measurements are based on the use of standard brick dimensions. With larger sewer pipes, the width of the chamber must be great enough for the pipe channel and the platform known as benching. Hence for pipes varying from 375mm to 750mm in diameter, the associated minimum manhole widths should be from 1125mm to 1575mm. Sewers deeper than 8 metres are usually constructed with an access shaft 788mm by 675mm which descends to a broader chamber. This lower chamber should have a height clearance of at least 2 metres, and minimum plan dimensions of 1350mm by 1125mm.

In the case of manholes constructed with pre-cast concrete rings the diameter to be used should be selected according to the largest pipe size at the junction, as outlined in Table 2.2 (Bartlett, 1981).

Largest pipe diameter (mm)	Diameter of manhole (mm)
150 - 400	1200
450 - 700	1500
750 - 900	1800

Table 2.2 Recommended manhole diameters.

White (1987) highlights the problems of constructing manholes to the specified dimensions when space is limited. It is rarely possible to achieve the required headroom for chambers if sewers are laid at an economic depth. A solution for very shallow sewers is the construction of small inspection chambers, however it is often the case that a sewer is too deep for these and too shallow for full headroom to be provided. In these circumstances the access shaft itself provides the headroom and the necessary space for rodding equipment. For this reason, the shaft is required to be located at an

upstream corner of the manhole, to facilitate rodding in the more usual downstream direction. (Figure 2.3).

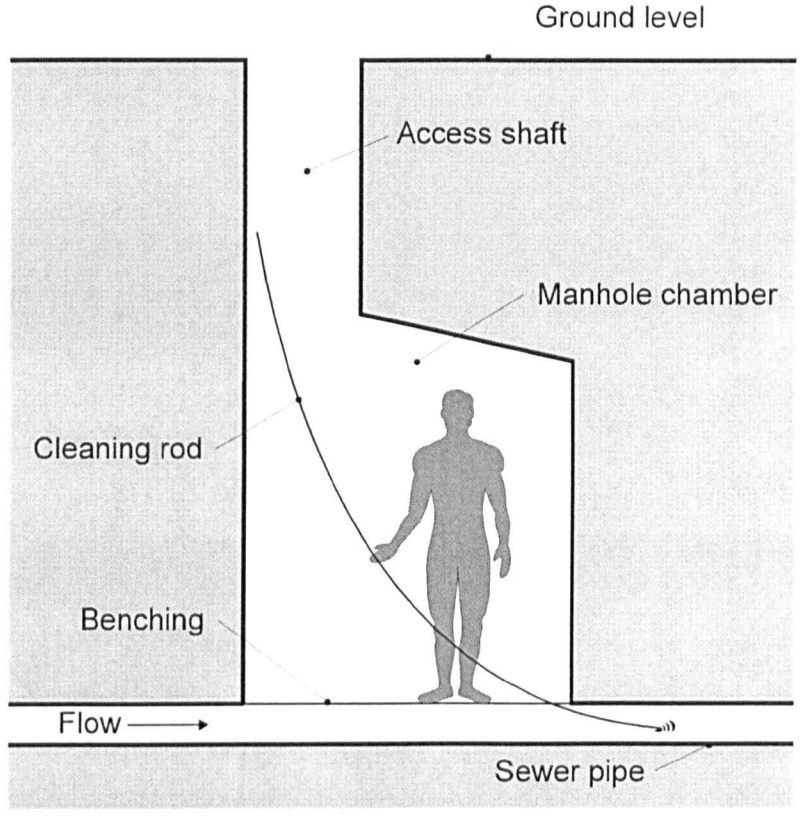

Figure 2.3 Features of a manhole.

It is common for manholes to be constructed with an arrangement at the base known as benching. This usually consists of a platform that provides a secure, flat surface to work from for personnel accessing the chamber. A channel is included to convey some flow from the manhole inlet to the outlet, thus keeping the benching surface free from flooding under dry weather flow conditions. It is possible to offset the channel through a manhole (Figure 2.4) so that adequate space is provided on the benching without having to build extra width into the manhole (White, 1987).

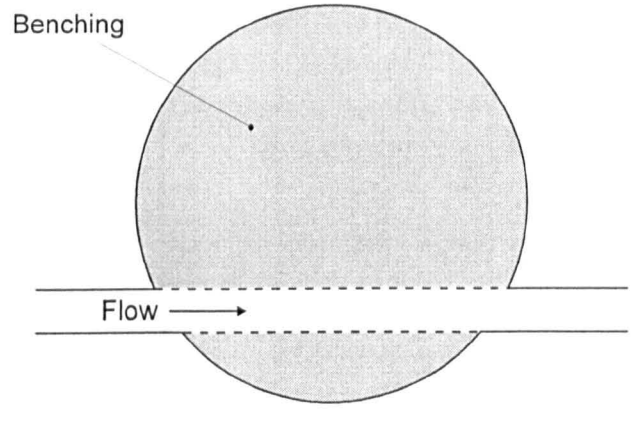

Figure 2.4 Plan of offset benching design.

A sewer with steep gradients, which requires deep excavations, can be constructed more economically if the pipes are laid at gradients sufficient for the hydraulic requirements and connected to lower sewer pipes at manhole junctions. This can result in manholes where there is a

step height between the inlet and the outlet pipe. A ramp formed in the benching is usually provided to accommodate the change in level (Bartlett, 1970). If the step height between the inlet and outlet pipes at a manhole is greater than 600mm then it is usual to construct a drop manhole (Bartlett, 1970; Hammer, 1986). As shown in Figure 2.5, this design allows the sewer flow to drop before entering the manhole thus protecting personnel entering the chamber and avoiding solids splashing onto the walls of the chamber.

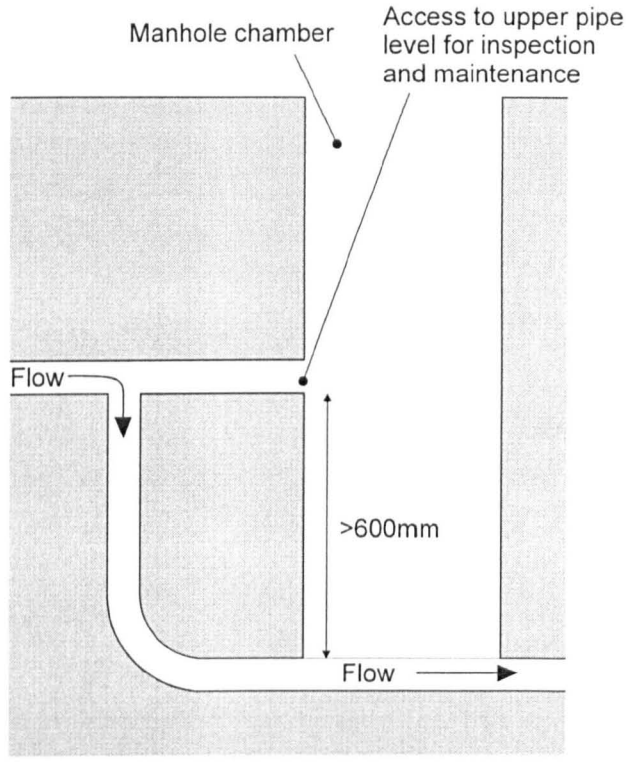

Figure 2.5 Drop manhole configuration.

2.2 Head loss

A great deal of research has been undertaken internationally in an attempt to define the head loss characteristics of manholes and pipe junctions in sewer systems. The majority of this work has used laboratory models of manholes, studied under considerable variations of discharge, surcharge, geometry, pipe size and slope and other factors. A small proportion of the work has been conducted in field tests where measurements have been taken in real sewer networks. Since there is little problem with sewer operation under dry weather flow conditions, most researchers have considered flood conditions where the manhole chamber is surcharged and the water surface is above the level of the pipe soffit. Surcharging is likely to be fairly common in many sewer systems since the return periods of the storms used for design are commonly quite low, such as one year (Archer *et al*, 1978). However, there is usually a large margin of safety between a water level causing surcharging, with the surcharge going unnoticed, and a water level that causes flooding on the paved surface.

There have been two major reasons for the extensive research into head losses at surcharged manholes. Firstly, computer models that simulate the hydraulics of a sewer system are able to employ the fundamentals of pipe flow theory except at manholes where empirically derived head loss coefficients are required (Archer *et al*, 1978). The resulting improved model accuracy provides a

better tool for sewerage designers and managers to examine the behaviour of proposed or existing networks. Friction losses for flows in pipes are well understood and can be estimated with use of the Colebrook-White equation. No such reliable theory exists for other structures in sewers, and quantifying head loss in such structures has primarily been by laboratory determination. This is due to the difficulties associated with making observations in active sewers, and the relative infrequency of surcharge events from an experimental point of view. Secondly, studies have been conducted which look at design alterations such as baffle plates and benching configurations to examine the effect on the head loss caused by a given manhole (Marsalek and Greck, 1988; Johnston and Volker, 1990). Such changes added to a present sewer system lead to an increased efficiency, which allows the sewer to transport greater volumes of flow without flooding or CSO spills to watercourses.

Researchers have generally followed the principle of Sangster *et al* (1958) in determining the head loss. A method of establishing the hydraulic grade line in the pipes upstream and downstream of the manhole is required for this. Piezometric tappings connected to measurement scales have been commonly used (Sangster *et al*, 1958; Marsalek, 1984; Johnston and Volker, 1990), although calibrated electronic devices such as water level transmitters (Howarth and Saul, 1984; Elgattas, 1995) and pressure transducers (Guymer and O'Brien, 2000) have also been successfully employed for the same purpose. The hydraulic grade lines are then extrapolated to the manhole centre line (Figure 2.6), and the head loss recorded between them, H, at this location is used to determine the head loss coefficient, K_H (Equation [2.1]).

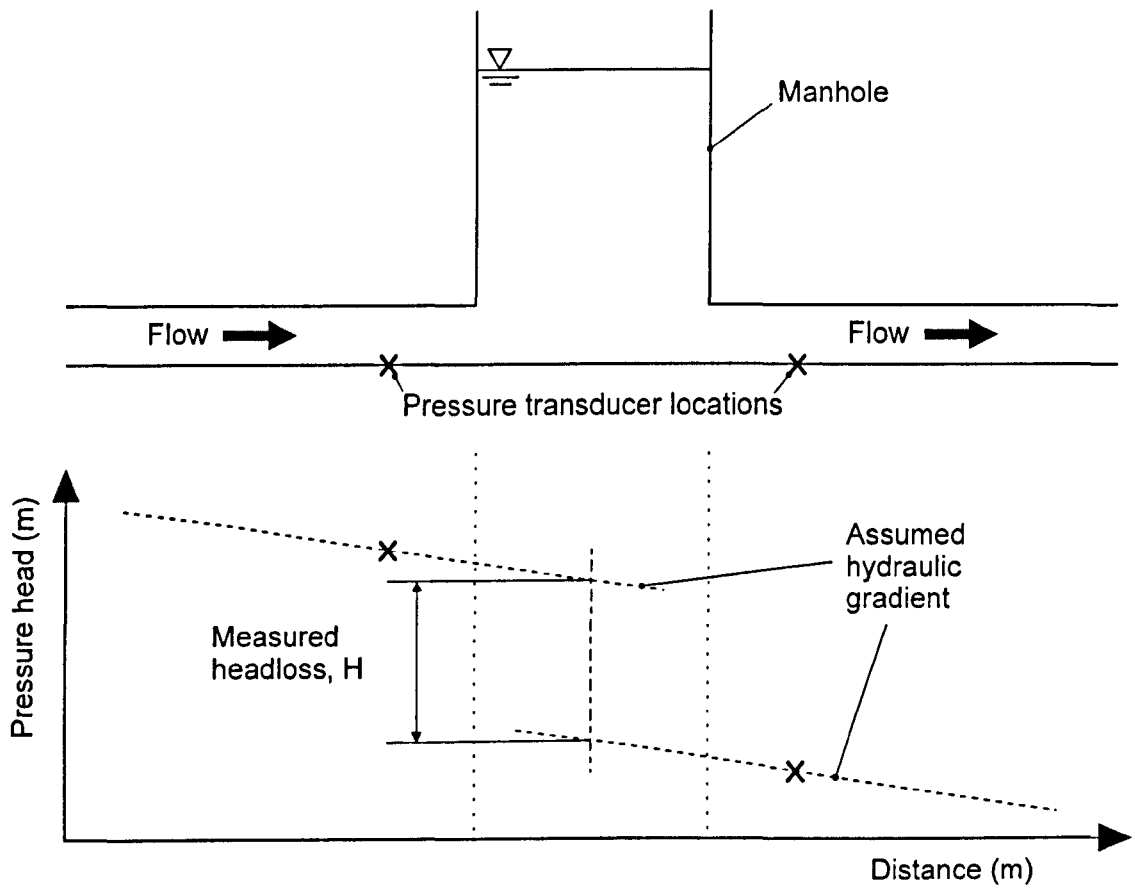

Figure 2.6 Calculation of head loss from pressure transducer measurements.

$$H = K_H \frac{v^2}{2g} \qquad [2.1]$$

where H is the difference in level between the upstream and downstream hydraulic grade lines at the manhole centreline, K_H is the head loss coefficient, v is the mean flow velocity in the pipe and g is the acceleration due to gravity.

There are a wide variety of potential configurations of manhole structure. Unfortunately, it is not always straightforward to extend the results of the laboratory configurations that have been studied to other conditions not covered. However, the previous head loss studies do assist in determining which factors, such as manhole dimensions and shape, pipe size, surcharge level, step height and benching configurations have the greatest impact on the head loss.

2.2.1 Manhole shape and size

Archer *et al* (1978) conducted laboratory head loss experiments on both circular and rectangular plan shape manholes incorporating a benching design. They considered both straight through alignments and variations in the angle of deflection between the inlet and outlet pipes. Their results showed that the head loss coefficient was dependent upon the deflection angle and, to a much lesser extent, the cross sectional shape of the manhole. Marsalek and Greck (1988) also found that the plan shape had little effect on the head loss coefficient in the case of benched and unbenched manholes with a 90 degree turn. Archer *et al* (1978) proposed constant values for K_H as given in Table 2.3.

Shape	Straight pipe	30 degree deflection	60 degree deflection
Rectangular	0.10	0.40	0.85
Circular	0.15	0.50	0.95

Table 2.3 Proposed manhole head loss coefficient, K_H, values (Archer *et al*, 1978).

Whilst Archer *et al* (1978) considered manholes of similar proportion, Sangster *et al* (1958) examined variations in the relative manhole size and concluded that the observed head losses increased with increases in manhole to pipe diameter ratio, D_m/D, although only minor differences occurred with D_m/D greater than 2.0, and there was no increase in head loss for D_m/D greater than 2.5. In contrast, the results of other researchers (Howarth and Saul, 1984; Bo Pedersen and Mark, 1990) from laboratory experiments demonstrated that the loss coefficient for a manhole continued to increase up to D_m/D values of at least 4.0.

Bo Pedersen and Mark (1990) showed with their theory and laboratory experiments that a relationship existed between the head loss coefficient and the manhole diameter ratio, D_m/D. They proposed that for engineering applications the experimental results could be approximated with a function involving the diameter ratio and a shape factor, ζ (Equation [2.2]).

$$K_H = \zeta\left(\frac{D_m}{D}\right) \qquad [2.2]$$

This relationship was shown to be useful for predicting loss coefficients for both square and circular manholes using data from previous researchers. Combining experimental results from themselves

and others, Bo Pedersen and Mark (1990) estimated the shape factor for various straight through manhole designs (Figure 2.7). Since the shape factor could only be estimated from the laboratory experiments undertaken, they point out that the equation was restricted to the few geometries from which it had been determined.

Shape ($D_m/D \leq 4$)	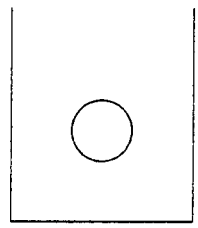 A	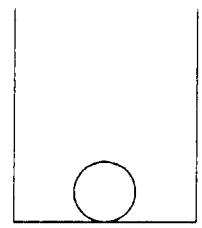 B	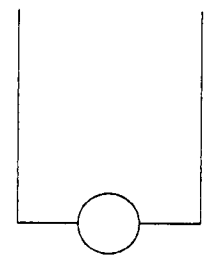 C	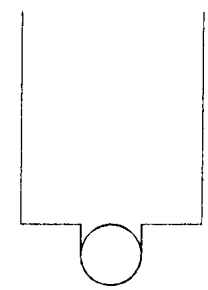 D
ζ	0.24	0.12	0.07	0.025

Figure 2.7 Proposed shape factor values (Bo Pedersen and Mark, 1990).

The pipe slope has been shown to have an insignificant effect on the head loss caused by a manhole (Archer *et al*, 1978; Elgattas, 1995).

2.2.2 Flow conditions

Howarth and Saul (1984) completed laboratory experiments to compare the energy loss coefficients for manholes with steady flow conditions with those that were obtained with time varying discharges. Archer *et al* (1978) concentrated on steady flow conditions and applied the derived coefficients for all flow rates. Howarth and Saul felt that this assumption required validation since hydraulic models were able to predict unsteady flow conditions. A computer controlled valve in the laboratory apparatus allowed various simulated discharge-time hydrographs to be applied to the system. A total of five manhole configurations were examined, three circular manholes with straight through flow and half pipe depth benching, a circular manhole with an offset and deeply benched channel and a square shaped chamber, again with half pipe depth benching.

An important discovery by Howarth and Saul was the fact that certain geometry and flow conditions were likely to lead to considerable swirling of the flow in a manhole. The presence of this swirl flow caused a marked increase in the head loss that occurred, and invalidated the assumptions of previous work that a single loss coefficient was applicable to a particular manhole shape.

Howarth and Saul (1984) established loss coefficients approximately equal to 0.15 for all manhole shapes when swirl was not present. This is similar to the values of 0.10 to 0.15 proposed by Archer *et al* (1978) for square and circular manholes respectively. However, with swirl conditions present these values increased to averages of 1.0 for the circular manhole, 0.4 for the equivalent square manhole and 0.2 for the deeply benched offset manhole. Hence for circular manholes it was possible to obtain head loss coefficients approximately seven times the magnitude of the values that were proposed by Archer *et al* (1978) as being applicable for all surcharged flow conditions. Swirl was less likely to occur in the square manhole, which the authors attribute to quiescent zones in the corners.

Johnston and Volker (1990) observed different circulation regimes within the manhole during their laboratory study. They grouped these into five categories (Table 2.4). It was suggested that these regimes had a strong correlation with the manhole head loss determined during the experiments.

Regime	Surcharge	Water surface fluctuation (mm)	Circulation description
1	0.7D	±8.0	Violent oscillations or seiching across diagonals
2	1.1D	±4.0	Predominant wave on downstream face of box with two equal eddies in wake
3	1.2D	±1.0	No wave, equal eddies, fairly calm
4	3.3D	±0.5	No wave, single eddy, fairly calm
5	3.7D	±0.5	Random circulations, very calm

Table 2.4 Circulation regimes (Johnston and Volker, 1990).

2.2.3 Surcharge level

Archer *et al* (1978) conducted a series of tests where the surcharge level varied up to a maximum where the water level was five pipe diameters above the outlet pipe soffit. This showed that at a constant discharge the head loss that occurred was independent of the surcharge level. Later research found that this was not necessarily the case. Howarth and Saul (1984) found that one of the factors that affected whether swirl would occur, thus giving rise to greater head loss, was the level of surcharge in the manhole chamber. Hence the ratio of surcharge depth to manhole diameter was considered an important factor in the head loss coefficient values. Johnston and Volker (1990) found that at lower pipe velocities there was a tendency for the head loss coefficient to increase in value with surcharge from a small value until the surcharge reached 0.5D, then reduce with further increases in water depth. This pattern compares favourably with that described by Lindvall (1984) and Kusuda and Arao (1996). In these cases, the greatest head loss coefficient values occurred when the water depth in the manhole was less than 2.0D. This was attributed to the strong surface swirling motions that were observed at low surcharges and which decreased as the surcharge increased. From these later studies it would appear that there is a threshold level of surcharge above which the head loss tends to becomes constant for a given discharge.

2.2.4 Step height

Kusuda *et al* (1993) and Kusuda and Arao (1996) present the results from a comprehensive investigation of head loss at circular manholes that included a step height between the inlet and outlet pipes. The manhole diameters to outlet pipe diameter ratios tested were in the range of 1.4 to $3.6D_m/D$, the upstream pipe diameter was 50mm and the downstream pipe was 50 or 60mm. Step heights between the inverts of the upstream and downstream pipes of between 0.0 and 4.0D were used, and flow rates were between 0.48 and 3.82 litres per second. The hydraulic grade line was established from three piezometer measurements either side of the manhole.

For step heights up to almost 1.5D the head loss coefficient increased as the step height increased. However, further increases in step height resulted in no further increase in the head loss coefficient. The effect of a step height in the range of 0.0 to 1.5D on the head loss coefficient was significant. For

a manhole with no step and $D_m/D = 3.6$, the value of K_H was approximately 0.4, whilst for step height of 1.5D this increased to almost 2.0 (Figure 2.8). The head loss coefficients were expressly given for higher surcharge levels where the head loss was found to be almost constant.

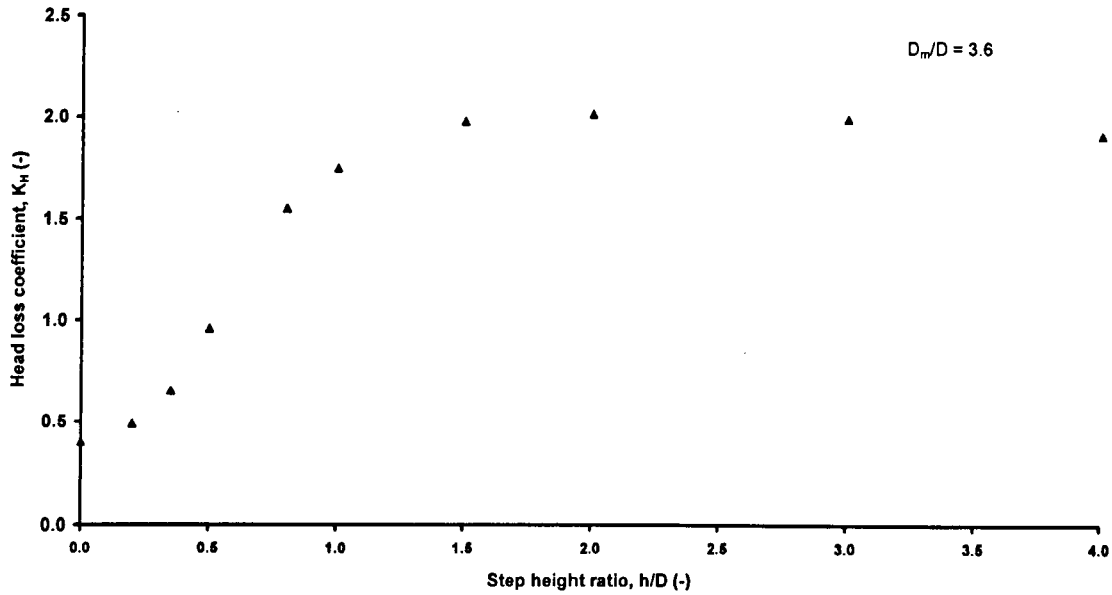

Figure 2.8 Head loss coefficient variation with step height (Kusuda and Arao, 1996).

Head losses for manholes with a step height between the inlet and outlet pipes have also been investigated by Elgattas (1995). A laboratory arrangement of manhole and delivery pipes was employed for the study. The manholes were circular with internal diameters of 340mm, 388mm and 488mm. The upstream pipe was always 88mm in diameter whereas three diameters of 88mm, 110mm and 130mm were used for the downstream pipe. Step heights between the inverts of the inlet and outlet pipes at the manhole junction were set between 0.0D and 2.0D in 0.5D intervals, where D was the outlet pipe diameter. All manholes were tested with no benching and a small number of tests were completed with a simple half pipe benching arrangement in the 340mm manhole.

The results for the variation of the head loss coefficient with step height presented by Elgattas (1995) appear to vary from the trends of those of Kusuda *et al* (1996). Elgattas does not describe a step height above which the value of K_H becomes almost constant, but found a continual increase of K_H with step height. This was attributed to the lesser ability of the manhole geometry to guide the flow towards the outlet, resulting in an increase in head loss.

Elgattas (1995) described an empirically derived expression to predict the head loss within the range of geometries and flow conditions studied in the laboratory. A curve fitting exercise was applied to each configuration of upstream and downstream pipe diameter ratio and manhole to pipe diameter ratio to find the relationship between the head loss and variables such as surcharge, step height and the Reynolds number. Further curve fitting allowed the surcharge to be described in terms of the Reynold's number and thus the empirical model for head loss in terms of step height ratio and Reynolds number in the downstream pipe was produced (Equation [2.3]). The a_i, b_i and c_i coefficients were listed by Elgattas for all the geometries considered. These were upstream to downstream pipe diameter ratios in the range of 0.68 to 1.0 and manhole to downstream pipe diameter ratios between 2.62 and 5.55.

$$H = \left[\left(a_1 + b_1\left(\frac{h}{D}\right) + c_1\left(\frac{h}{D}\right)^2\right) + \left(a_2 + b_2\left(\frac{h}{D}\right) + c_2\left(\frac{h}{D}\right)^2\right)(A_1 + B_1 Re) + \left(a_3 + b_3\left(\frac{h}{D}\right) + c_3\left(\frac{h}{D}\right)^2\right)(A_1 + B_1 Re)^2\right]\frac{V^2}{2g} \quad [2.3]$$

where

$$A_1 = a_4 + a_5\left(\frac{h}{D}\right) \quad [2.4]$$

$$B_1 = b_4 + b_5\left(\frac{h}{D}\right) \quad [2.5]$$

and h is the step height, D the downstream pipe diameter, Re the Reynold's number and v is the velocity in the downstream pipe.

Unfortunately, the presentation of this empirical analysis is rather poor and somewhat confusing, and the equation is limited to the flow conditions and manhole configurations from which it was developed. The extensive curve fitting procedure to determine the numerous coefficients must be a cause for concern as to the validity of applying the equation as a method for predicting head loss.

Research into the head loss coefficients for stepped manholes has continued with Arao and Kusuda (1999) considering the effects of a combination of a step height and an angle between the inlet and outlet pipes. For manholes with no step, the head loss coefficient at most surcharge levels was approximately three times greater for a 90 degree angle than for the straight through configuration. However, the straight through manhole head loss increased considerably as the step height was raised to 1.0D, but the head loss for the angled arrangement increased little further. Thus, the difference in head loss coefficients for straight and angled manholes was negligible at this step height.

2.2.5 Benching

The effect of benching within manholes has been shown to have a large influence on the measured head loss coefficient. Marsalek (1984) examined square and circular manholes with three different benching arrangements. These were shapes B, C and D in Figure 2.7. The lowest head losses occurred with the deep channel benching and were found to be approximately half that of the unbenched manholes. This concurred with the benched manhole test results of Johnston and Volker (1990). Howarth and Saul (1984) noticed that the bed configuration of the manhole had considerable importance on the occurrence of swirling flows and benching was observed to prevent swirl and so reduce the head loss. In chambers with a 90 degree turn between the inlet and outlet pipe Marsalek and Greck (1988) concluded that half pipe diameter benching gave little reduction in the head loss over that for an unbenched manhole. However, the provision of a full pipe diameter depth channel in the benching produced significant head loss reductions.

2.3 Sewer systems modelling

Greater environmental considerations and a desire to design and operate more efficient urban drainage networks has led to the increased use of computer based sewer simulation models. The original models concentrated on computing the hydraulics of a sewer system. It was required that

these models reached a satisfactory performance before consideration was given to including the far more complex water quality aspects. Extensive work was conducted by many researchers into determining the head loss characteristics of manhole structures to allow the inclusion of appropriate coefficients in the models. Research continues now to develop the ability of these models to produce reliable predictions for the water quality aspects of sewer flow.

Herath *et al* (1999) provide a summary of the features and application of three current urban drainage models, all of which to a greater or lesser extent incorporate some provision for modelling wastewater quality. These are HydroWorks, MOUSETRAP and SWMM, produced by Hydraulic Research Wallingford, the Danish Hydraulic Institute and the United States Environmental Protection Agency respectively. Only one of these models, MOUSETRAP (Crabtree *et al*, 1994; Garsdal *et al*, 1995), uses both advection and dispersion processes in the routing of dissolved and sediment pollution through the sewer system. Whilst this complicates the model, it provides for the longitudinal dispersion effects of manholes to be incorporated.

Garsdal *et al* (1995) describe the development of the numerical model MOUSETRAP for describing water quality processes in urban drainage networks. They identify that the design, management and operation of sewer systems would be greatly enhanced with knowledge of pollutant concentrations at combined sewer overflows and treatment works. The modelling tool developed was based on the MOUSE hydrodynamic package produced by the Danish Hydraulic Institute. The model attempts to describe the physical transport of pollutants, both dissolved and attached to sediments, together with chemical and biological water quality processes. In their work, the authors detail the extent to which water quality considerations are taken into account. A module of the software has been developed to include processes such as degradation of organic matter, bacterial fate, exchange of oxygen with the atmosphere and oxygen demand. The equations formulated to describe these complex processes often include time dependent growth rates or decay constants. In these cases any retention that occurs in sewer structures such as manholes that is not taken into consideration will result in misleading predictions for these processes. MOUSETRAP also has an advection dispersion module that is dynamically coupled with the water quality module. This requires longitudinal dispersion coefficients to be applied so as to predict the transport of pollutants through the sewer system.

The authors applied these two modules to a 5km length of gravity sewer in northern Jutland, Denmark. Tests were conducted with Rhodamine dye as a tracer to allow residence times for solutes to be determined and used for calibration of the advection dispersion module. The conclusions were that the advection dispersion equation describes solute transport in sewers effectively. Whilst Taylor's (1954) work demonstrates this to be applicable for the straight pipe sections of sewer, and theoretically a good approximation of unsurcharged flow through benched manholes, the application of the equation to sewers where manholes are surcharged and cause changes in flow cross sections is less certain. It is possible that the validation of the advection dispersion equation for a real length of sewer (Garsdal *et al*, 1995) was completed predominantly for dry weather flow conditions where manhole structures would remain unsurcharged.

A more complete description of the application of the advection dispersion module of the MOUSE software is given by Mark *et al* (1996). The model has been applied to a sewer network in Ljubljana, Slovenia, using inputs of industry loadings to the sewer system and measured dry weather flow concentrations. Only conservative pollutants were considered with this particular work, thus negating concerns over decay coefficients being involved. The final calibrated model gave good

simulations of the selected pollutant (ammonium) concentration, including temporal variations, at several locations within the system.

The difference between the accuracy and efficiency of quantitative storm water simulation models, which are widely and reliably used, and those attempting to include water quality aspects is emphasised by Ahyerre *et al* (1998). There are many problems associated with simulating the complex nature of the physical, chemical and biological processes involved. Whilst the current sewer quality software is regularly used for research models, their application as management tools is restricted by the cost of obtaining reliable calibration parameters. Further research is required to make improvements in the modelling approach and to develop understanding of the water quality processes and pollution transport mechanisms involved in order that managers of urban drainage systems will be convinced that the models are cost effective and accurate.

Computer model development continues with the ultimate aim of producing an accurate and fully integrated software package. This would be able to predict the flow rates and the pollutant concentration levels from the rainfall event to the downstream river flow, divided into sections for rainfall prediction, sewer modelling, wastewater treatment facilities and pollution transport in watercourses. The advantages of such a model would be extensive. With regards to the urban drainage section of the package, the benefits would assist in improved management and operation of the network resulting in a reduction of pollutant loading on nearby watercourses.

2.4 Real time control

A major development in sewer design and operation is Real Time Control (RTC). As explained by Schilling (1996) the primary aim of real time control is to reduce spills from Combined Sewer Overflow (CSO) chambers without constructing any extra capacity within a sewer. Computer simulations are used to compare the advantages and disadvantages of possible control strategies. Furthermore, if an urban drainage network is to be designed with storm control chambers and moveable remote controlled weirs and gates so that the bulk of pollutant concentrations can be stored for later treatment then a computer model could be employed. This would assist in determining the ideal size and location for new chambers, or indeed the best procedure for utilising available sewer storage volumes and would be a critical factor in saving costs and reducing CSO spills.

Furthermore, improved flow simulations would allow wastewater treatment facilities to better predict the arrival time and concentration of pollutants and so adapt their process accordingly. In addition, any CSO spills that were predicted by the model would have a known pollutant concentration, and hence the ability of the receiving watercourse to cope with the spill could be more accurately assessed. Ultimately, the use of such a model would enable water companies to successfully reduce the environmental impact and the cost of operating an urban drainage network. Engineers must consider an integrated control strategy where the consequences of adding small pollutant loads to highly sensitive receiving waters must be weighed against the damage of larger loads into waters more capable of receiving them. Schilling (1996) highlights that current and future research is concentrated upon these quality orientated aspects, and that on-line simulation models will play a crucial role in developments. Therefore, improvements in these models are a prime concern.

Weinreich *et al* (1997) discuss an extension of a real time control strategy and its operation on the Oslo interceptor sewer tunnel. In a reflection of early sewer simulation models, real time control strategies have been heavily based on minimising volumes of discharges via CSOs. The work of Weinreich *et al* looks at the development of these strategies to include pollution concentration elements, termed a Pollution Based Real Time Control (PBRTC) strategy. The tool developed for this work consists of three modules. A flow model combined with a simple pollution transport model, a control module and a provision for numerical optimisation. The optimisation procedure utilised linear functions considering the relative costs of overflow, discharge and storage. By modifying the cost of overflow so that it depends on the pollutant concentration, it becomes possible to direct the main polluted discharge on to the treatment works. The authors claim a reduction in total phosphorus and ammonia nitrogen at the overflows of 48 and 51 percent respectively by using the pollution based real time control model on a simplified model of the Oslo interceptor sewer. This compares favourably with reductions of 42 percent for both examined pollutants with purely a volume based real time control strategy. Their conclusions highlight the advantages of regarding pollutant loads rather than volumes, especially as developments in computing power increase the feasibility of more complex methods. However, the concern is expressed as to whether the accuracy of pollution transport models is sufficient to make best use of these advantages.

Petruck *et al* (1998) express the two main aims of their real time control project as a reduction in the volume and pollution content of CSO spills and an improvement in the efficiency of the wastewater treatment plant. As with Weinreich *et al* (1997) they consider the effectiveness of a pollution based real time control system, in this case applied to the catchment of the stream Rapphofs Muehlenbach in Germany. The principle is again to maximise the pollutant load to the treatment facilities, and to minimise the discharge of pollution into the watercourse. In this case, only knowledge of the sewer system itself is required. As a possible continuation however, Petruck *et al* (1998) discuss the possibilities for applying a Water Quality Based Real Time Control (WQBRTC) strategy. In this extension of previous control proposals, the aim would be to reduce the occurrence of so called critical conditions in the receiving waters. Hence, the requirement is for flow volume and quality measurements to be taken for both the sewer system and the associated stream. In this way the discharge of CSOs could be determined with regard to the quality of the receiving water. The authors predict that this strategy would give further efficiency over pollution based real time control. However, the success of further complexities in control strategies will ultimately depend on the accuracy of the hydraulic and quality modelling predictions.

2.5 Longitudinal dispersion

2.5.1 Introduction

Longitudinal dispersion is the tendency for a cloud of soluble tracer travelling with a fluid flow to spread along the flow direction axis. This effect reduces the cross sectional averaged peak concentration of the tracer measured at locations downstream, and spreads the solute over a greater longitudinal distance. For many years the importance of this phenomenon has been understood by researchers interested in riverine water quality modelling. The theory and experimental work covering longitudinal dispersion in open channels and rivers is extensive, and in many cases it is now possible to produce reliable predictions of field conditions. In the case of urban drainage, there has not yet been the same emphasis on research into the longitudinal dispersion that occurs in sewer flow. Only now, as computer modelling techniques for urban drainage have reached a level

comparable with river modelling, are coefficients required that will allow the models to accurately reflect the effects of longitudinal dispersion. Previous models concentrated on the sewer hydraulics where coefficients for head loss were the prime concern. With increased environmental considerations being applied to sewers, the development of computing power and software capabilities, and the desire to produce urban drainage design solutions that are integrated from the rainfall event to the final impact on receiving waters, a prime requirement for modellers is to include longitudinal dispersion considerations.

The first theoretical and experimental analysis of longitudinal dispersion in fluid flow began with the pipe flow experiments conducted by Taylor (1953, 1954) considering both laminar and turbulent flow conditions. This work proved fundamental in the determination of equations describing the dispersive effects of particular flow regimes. These equations are still widely used today as a means of predicting downstream solute concentrations from an upstream source.

2.5.2 Mixing theory

If a single drop of tracer were to be statically released into a second tranquil fluid, Brownian motion of the molecules would result in the spread of the tracer mass from the region of high concentration into the surrounding volume of fluid. So long as the two fluids were of comparable density and viscosity, this process would continue until the originally steep concentration gradient became zero and the tracer was evenly distributed throughout the entire volume. It was shown by Fick that the tracer would move from a region of high concentration to one of lower concentration at a rate proportional to the concentration gradient. Molecular diffusion for tranquil conditions in a single direction is described by Fick's first law (Equation [2.6]).

$$J_x = -E_m \frac{\partial c}{\partial x} \qquad [2.6]$$

Where J_x is the tracer flux in the x direction, E_m is the molecular diffusion coefficient and $\partial c/\partial x$ is the spatial tracer concentration gradient in the x direction.

Holley (1969) considered the progress of a tracer travelling within a two dimensional channel flow. This situation was described by applying the principle of mass conservation to an elemental control volume. A continuum mechanics approach, with the assumption that the fluid conveyed the tracer at a rate dependent on both the velocity, u, and the concentration, c, gave rise to a two dimensional molecular diffusion equation (Equation [2.7]) that is capable of describing dispersion in laminar flow. This is also commonly known as Fick's second law.

$$\frac{\partial c}{\partial t} + u_x \frac{\partial c}{\partial x} = E_m \left(\frac{\partial^2 c}{\partial x^2} + \frac{\partial^2 c}{\partial y^2} \right) \qquad [2.7]$$

where u_i is the uniform velocity in the i direction.

A fully turbulent flow is characterised by being composed of randomly fluctuating velocity components at any location within the flow. A similar equation to [2.7] can be produced for circumstances where the flow is turbulent.

$$\frac{\partial c}{\partial t} + u_x \frac{\partial c}{\partial x} + u_y \frac{\partial c}{\partial y} = E_m \left(\frac{\partial^2 c}{\partial x^2} + \frac{\partial^2 c}{\partial y^2} \right) \qquad [2.8]$$

where u_x, u_y and c represent instantaneous values.

A distinctive character of turbulent flow is the formation of eddies, which can range in size from the molecular level to easily visible swirls in the flow. This feature necessitates the inclusion of the advective term $u_y(\partial c/\partial y)$ in the equation, since although the primary flow is in the x direction, turbulent motion in the y direction will be present. The difficulty in determining instantaneous measurements of velocity and concentration means that these are expressed as time averaged values comprising a mean value and a turbulent fluctuation (Figure 2.9). Thus, the instantaneous value is represented by a time average value (overbar) and a fluctuating component (prime), such that in the case of velocity

$$u = \bar{u} + u' \qquad [2.9]$$

with a similar definition for concentration.

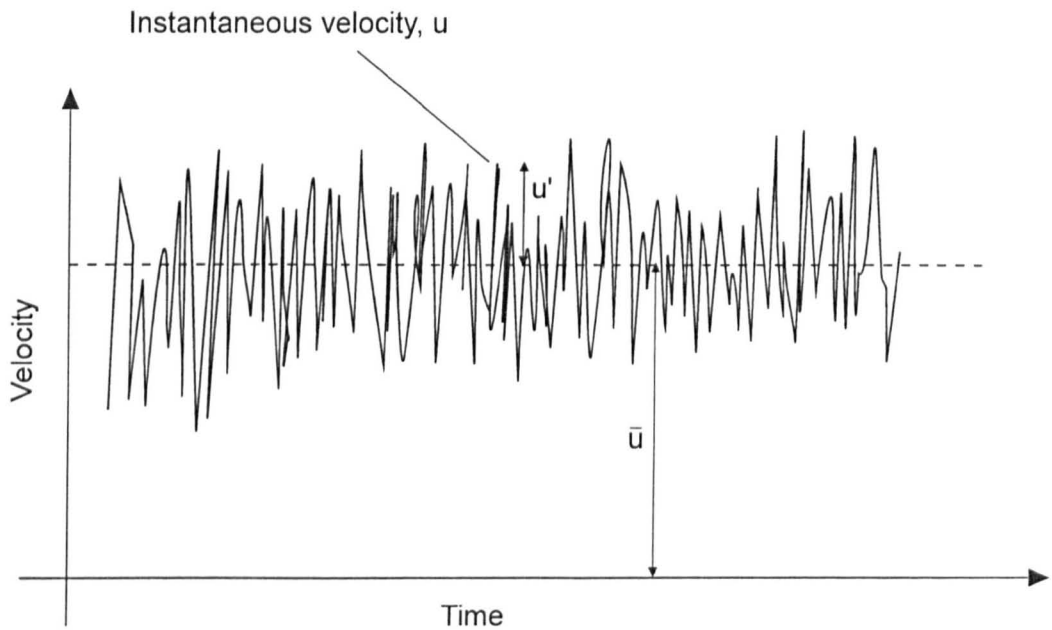

Figure 2.9 Time averaging of turbulent velocity.

Turbulent diffusion causes a random scattering of particles due to the random eddy forms that exist. The process of time averaging leads to an equation where the turbulent diffusion coefficient, E_t, is defined with analogy to molecular diffusion (Equation [2.10]) (Holley, 1969). This equation includes the effects of both molecular and turbulent diffusion on the transport of a tracer.

$$\frac{\partial \bar{c}}{\partial t} + \bar{u}_x \frac{\partial \bar{c}}{\partial x} = (E_m + E_t) \frac{\partial^2 \bar{c}}{\partial x^2} + (E_m + E_t) \frac{\partial^2 \bar{c}}{\partial y^2} \qquad [2.10]$$

where $\bar{c}$ and $\bar{u}_x$ are the time averaged concentration and velocity values respectively.

If a tracer has been present in a two dimensional continuum long enough, turbulent transport will have mixed it throughout the depth of the fluid. This means that most variation in concentration will now occur in the longitudinal direction. Equation [2.10] is still valid under these circumstances, however, it can be simplified since there is no longer any significant variation in concentration in the vertical direction. This is done by depth averaging the turbulent diffusion equation and again developing a diffusion coefficient, this time to represent the effects of shear flow, by analogy with molecular diffusion.

$$\frac{\partial C}{\partial t} + U\frac{\partial C}{\partial x} = \left(E_m + E_t + E_k\right)\frac{\partial^2 C}{\partial x^2} \qquad [2.11]$$

where C and U are the cross-sectional average values for the concentration and the velocity respectively and E_k is a coefficient for the diffusion due to shear flow.

These three diffusion processes can be combined and a single dispersion coefficient, K, used to represent their combined effects (Equation [2.12]).

$$\frac{\partial C}{\partial t} + U\frac{\partial C}{\partial x} = K\frac{\partial^2 C}{\partial x^2} \qquad [2.12]$$

where K is the longitudinal dispersion coefficient.

This is the Fickian model of longitudinal dispersion, otherwise known as the Taylor Advection Dispersion Equation (ADE) since it originates from his work studying mixing in pipes (Taylor, 1953, 1954). The concentration and velocity are cross sectional averages and so the equation is unable to model variations of these across a section. The longitudinal dispersion coefficient includes the effects of the velocity shear, the turbulent mixing and the molecular diffusion. However, it is important to note that the latter two are very small effects in comparison to the velocity shear, and hence $K \approx E_k$.

The spreading of a tracer along the pipe length is increased by velocity shear leading to an increase in transverse concentration gradient whilst the transverse mixing acts to smooth these gradients and create more uniform concentrations thus counteracting the longitudinal dispersion effects of velocity shear. The combination of velocity shear and turbulent diffusion can be termed dispersion, and once a solute is fully mixed over the cross section then it is this dispersion that is the dominant mixing process.

2.5.3 Advection Dispersion Equation (ADE)

Close to the source of injection of a tracer the concentration is not uniform over the cross section. This region is known as the advective zone, acknowledging the significance of the velocity profile for the mixing in this region. The tracer concentration profiles measured within the advective zone are highly skewed. Taylor (1954) showed that further downstream the effects of the longitudinal dispersion being increased by the velocity shear are balanced by the turbulent diffusion, which tends to reduce longitudinal dispersion. This region is termed the equilibrium zone. The distinctive features of this region of mixing are that the variance of cross sectional averaged concentration profiles increase linearly with time and the skewness remaining from the advective zone reduces slowly until a spatially measured profile becomes Gaussian. The final region of mixing where the concentration profiles have this shape is known as the Gaussian zone.

This theory requires several assumptions to be met. Firstly, as explained above, sufficient time must have elapsed from the time of injection. Also, the flow must be steady and the turbulence independent of time. Furthermore, the flow cross section must remain constant and the tracer must be conservative.

Taylor (1954) and others (French, 1986; Rutherford, 1994) supply solutions to the Fickian longitudinal dispersion model (Equation [2.12]). If U and K are assumed to be constant then the solution for a single, instantaneous tracer injection is given by Equation [2.12].

$$C_{x(t)} = \frac{M}{A\sqrt{4\pi Kt}} \exp\left[-\frac{(x-Ut)^2}{4Kt}\right] \qquad [2.13]$$

where M is the mass of tracer injected at location x = 0 at time t = 0, and A = cross sectional area of the channel.

This equation, known as Taylor's solution for longitudinal dispersion, predicts Gaussian spatial concentration profiles. It is very unlikely that measured concentration profiles will have an exact Gaussian shape, for two reasons. Firstly, laboratory and field measurements are usually restricted to temporal concentration profiles where the concentration of the tracer as it passes a fixed site is measured with respect to time. Spatial concentration profiles would require the concentration to be measured with respect to distance at an instantaneous moment in time. Longitudinal dispersion that occurs during the time taken for the tracer cloud to pass the measuring site imparts a skewness onto the profile. Secondly, equation [2.13] assumes that the Fickian dispersion model is valid within the advective zone, which is not the case. Concentration profiles in this zone are heavily skewed and this skewness can remain long into the equilibrium zone (Fischer, 1966). It can take a considerable time and reach length for the skewness to decay sufficiently for Taylor's solution to become valid.

Whilst equation [2.13] is strictly only valid once the asymmetry of a tracer profile has decayed, it is still widely used as a longitudinal dispersion model. The application of Taylor's analysis requires that a downstream temporal concentration profile can be predicted from a profile measured at an upstream site. In many cases, the 'frozen cloud approximation' is used. This assumes that the advection in a system dominates the dispersion such that no longitudinal dispersion occurs as a tracer cloud passes a measuring site (Fischer, 1968; Rutherford, 1994). Fischer *et al* (1979) describe how the principle of superposition can be used as a means of routing an upstream concentration profile. Assuming that each discrete time concentration at the upstream site was an instantaneous release of tracer it is possible to predict the downstream profile produced from each individual upstream injection. The sum of the predicted downstream concentrations for each upstream injection gives the overall downstream temporal concentration distribution (Figure 2.10). The concentration profile at the downstream measuring location at time t after the first arrival of the tracer at the upstream location is given by

$$C_{d(t)} = \int_{\gamma=-\infty}^{\infty} \frac{C_{u(t)}U}{\sqrt{4\pi K(\bar{t}_d - \bar{t}_u)}} \exp\left[-\frac{U^2(\bar{t}_d - \bar{t}_u - t - \gamma)^2}{4K(\bar{t}_d - \bar{t}_u)}\right] d\gamma \qquad [2.14]$$

where $\bar{t}_i$ is the time of passage of the tracer centroid at site i and γ is an integration variable.

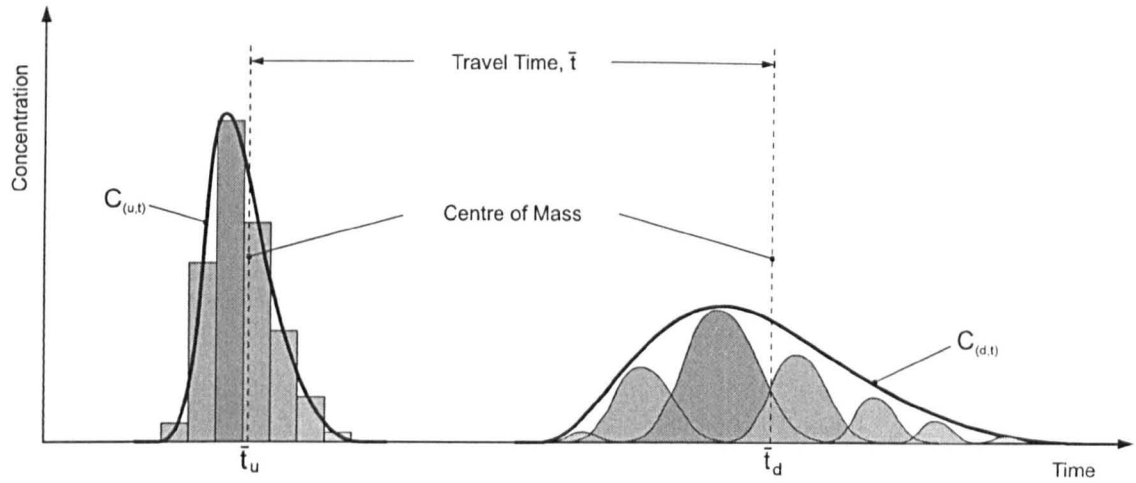

Figure 2.10 ADE routing of multiple discrete inputs representing an upstream temporal concentration distribution.

In order to use equation [2.14] to predict a downstream concentration profile, it is necessary to determine a suitable dispersion coefficient. Taylor (1954) studied turbulent flow in a straight pipe and proposed a theoretical relationship to predict the dispersion coefficient value (Equation [2.15]).

$$K = 10.1ru^{*} \qquad [2.15]$$

where r is the pipe radius and u^{*} is the shear velocity, given by equation [2.16].

$$u^{*} = \sqrt{(\tau_0 / \rho)} \qquad [2.16]$$

where τ_0 is the shear stress at the pipe wall and ρ is the density of the fluid.

Fischer (1966) provided analysis to show that the dispersion coefficient could be estimated if both upstream and downstream concentration distributions were available (Equation [2.17]) since, at a sufficient distance from the tracer injection point, the variance of concentration profiles was shown to increase linearly with time.

$$K = \frac{U^2}{2}\left[\frac{\sigma^2_{t(d)} - \sigma^2_{t(u)}}{\bar{t}_d - \bar{t}_u}\right] \qquad [2.17]$$

where $\bar{t}_i$ is the time of passage of the centroid of the tracer cloud at location i. This is calculated as

$$\bar{t}_i = \frac{\int_{t=-\infty}^{\infty} tC_{i(t)}dt}{\int_{t=-\infty}^{\infty} C_{i(t)}dt} \qquad [2.18]$$

and $\sigma^2_{t(i)}$ is the temporal variance at site i, given by

$$\sigma^2_{t(i)} = \frac{\int_{t=-\infty}^{\infty} \left(t - \bar{t}_i\right)^2 C_{i(t)}dt}{\int_{t=-\infty}^{\infty} C_{i(t)}dt} \qquad [2.19]$$

One of the main features of data collected from field tests on real rivers, which do not comply with the restrictions to Taylor's analysis such as homogeneous turbulence and constant channel shape, is that there is a heavily skewed shape to concentration profiles. An obvious feature of many observed temporal concentration distributions is a long tail of low concentration at the end of the profile. The reason for this is the presence of dead zones, which are areas of the channel cross section where the flow is somewhat isolated from the main flow and is re-circulating or is relatively still. These areas can be caused by the shape of the channel sides and any obstructions such as vegetation or rocks. Also, roughness elements in the channel bed will have spaces around them which retain some of the passing flow (Valentine and Wood, 1977). Fischer (1967) noted that physical observations of these dead zones showed that a proportion of a tracer cloud passing them was retained and mixed within them and was gradually released back to the main flow. The slow release of tracer from the dead zone volumes is the cause of the low concentration tail that is measured after the majority of the tracer mass. Valentine and Wood (1977) observed that the effect of dead zones on longitudinal dispersion was primarily governed by the proportion of the boundary area covered by, and the individual depth of, the dead zones.

2.5.4 Aggregated Dead Zone (ADZ) equation

Taylor's analysis is unable to provide good approximations of the skewness often observed in measured tracer concentration profiles. The skewness is caused by mechanisms in the flow that invalidate the Fickian model for dispersion. Dead zones have been highlighted as a major factor in the non-Fickian dispersion that is often observed in natural channels. This has led researchers to consider other methods for predicting longitudinal dispersion for cases where dead zones are present. It is important to consider how dead zone effects have been accommodated into theoretical principles and models since a surcharged manhole chamber interrupting pipe flow may be assumed to provide a re-circulating storage volume.

One such development is the Cells-In-Series (CIS) simulation presented in detail by Stefan and Demetracopoulos (1981). This is a complete diversion from efforts to modify and adapt the advection dispersion model (Valentine and Wood, 1977), and has a great benefit of simplifying the complex nature of those models into a relatively simple first order differential equation.

The CIS method of analysis is based on the modelling of reactor tanks, which has commonly been employed in the chemical engineering industry. A series of equal volume units, or cells, is used to represent the flow reach in question, and complete mixing is said to occur in each cell. Mass transport of a conservative tracer through an individual cell is described by

$$V\frac{dC}{dt} = M(t) - QC \qquad [2.20]$$

where V is the cell volume, C is the tracer concentration within the cell, M(t) is the external mass input of tracer to the cell in time t, either from the upstream cell or as a direct input, Q is the flow rate out of the cell.

The solution for equation [2.20], giving the tracer concentration in the cell any time after an instantaneous injection of mass M at time t = 0 is

$$C_{(t)} = \frac{M}{V} e^{-\left(\frac{Qt}{V}\right)} \qquad [2.21]$$

where t is the discrete time interval and M is the total mass of tracer injected.

With an impulse input to the first cell of a series of cells, the concentration in the nth cell is given by

$$C_{(n,t)} = \frac{MQ^{n-1}t^{n-1}}{V^n(n-1)!} e^{-\left(\frac{Qt}{V}\right)} \qquad [2.22]$$

Using this theory, Stefan and Demetracopoulos (1981) demonstrate that the centroid, variance and skewness of the temporal concentration profiles produced by this equation are all simple functions of the number of cells used. Clearly the technique has a great simplicity advantage over the more traditional advection dispersion method of analysis for longitudinal dispersion. There is also the benefit that the CIS model is applicable for the advective zone of transport, and it requires no extra terms to incorporate skewness into the predicted concentration profiles.

The terms of the CIS model, such as number of cells and effective cell volume, do not necessarily have any direct relationship with actual physical features of a reach length, but they can be determined by dye tracing experiments.

A major disadvantage with this approach is the fact that both the advection and dispersion terms of the model are dependent upon the number of cells (Rutherford, 1994). This means that it is not possible to vary these aspects independently and hence the potential for applying the model is restricted. Indeed, Stefan and Demetracopoulos (1981) applied the model to a series of river reaches and found that although in general the travel time could be predicted reliably, there was no improvement in the quality of the temporal concentration profiles over those generated from the advection dispersion equation.

The concept of a cells-in-series model was extended into a model with improved potential by Beer and Young (1983). They highlight the interdependent nature of the CIS coefficients, which becomes an extreme problem for situations where the time delay is large compared with the dispersion constants. The development is known as the Aggregated Dead Zone (ADZ) model and Beer and Young proposed that longitudinal dispersion could be modelled with a combination of a plug flow chamber and a completely mixed tank connected in series. The principle behind the ADZ model is simple. Whereas the travel time and dispersion of the CIS model are not able to be independently modified, the ADZ technique circumvents this problem. The effect of all the dead zones in the particular reach are assumed to be modelled by a single dead zone cell i.e. the completely mixed tank, and the required plug flow travel time parameter is introduced prior to the input concentration entering the dead zone cell by adding a pure advection cell before it.

Both simulated tanks have a residence time associated with them, reach time delay, τ, for the plug flow and residence time, T, for the completely mixed tank. The travel time, $\bar{t}$, through the entire system, or ADZ cell, is then the sum of these residence times and is equivalent to the average time a

particle resides in the system.

The ADZ model mass balance equation is

$$\frac{dC_{(d,t)}}{dt} = \frac{1}{T}\left(C_{(u,t-\tau)} - C_{(d,t)}\right) \qquad [2.23]$$

where T, the dead zone residence time, is equal to V_e/Q, with V_e being the effective dead zone volume.

The solution for an instantaneous injection of mass M at time t = 0 is

$$C_{(d,t)} = \frac{M}{V_e}\exp\left[\frac{1}{T}(t-\tau)\right] \qquad [2.24]$$

which is valid for any time where $t > \tau$.

It is important for the applicability of the model that it can be discretised with respect to time, since almost all field and laboratory investigations of longitudinal dispersion are performed on the basis of concentration samples at regular time intervals. The discrete form of the ADZ equation is

$$C_{(d,t)} = -\alpha C_{(d,t-1)} + (1+\alpha)C_{(u,t-\delta)} \qquad [2.25]$$

where $C_{(i,t)}$ = tracer concentration at position i at time t, where i = u or d represents the upstream and downstream measurement locations respectively.

α = $-e^{\left(\frac{-\Delta t}{T}\right)}$

T = residence time, $\bar{t} - \tau$

$\bar{t}$ = travel time, $\bar{t}_d - \bar{t}_u$

τ = time delay, $t'_d - t'_u$

t'_i = time of first arrival of tracer at location i

δ = the discrete time equivalent of the time delay, τ (which is equal to the nearest integer value of $\tau/\Delta t$)

Δt = the time step or sampling interval

The transport of a single, instantaneous input of tracer into the ADZ cell is represented in Figure 2.11. This shows how the model applies the combined effects of advection and exponential decay to the injection of tracer to determine the downstream profile.

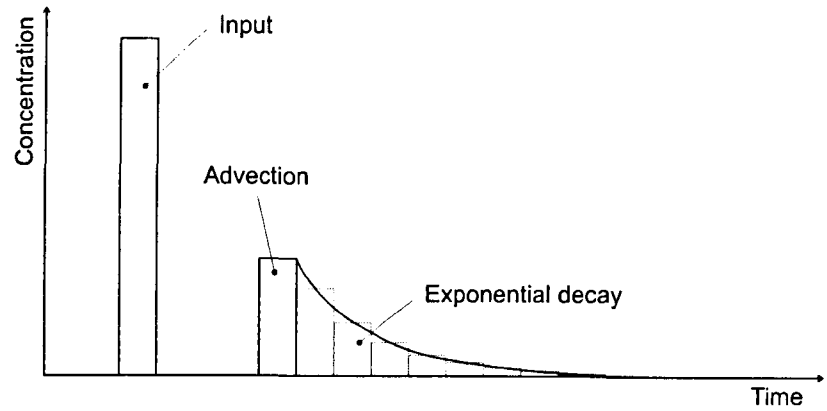

Figure 2.11 ADZ routing of a single, instantaneous tracer injection.

The ADZ equation [2.25] is applied to actual data by using a discrete time representation of the measured concentration profile. In this way, each discrete time concentration value is transported downstream in the manner of Figure 2.11. In this situation, however, each previous discrete time value of concentration at the downstream location will continue to decay exponentially. Therefore, the downstream concentration profile prediction is generated from the sum of the tracer advected from upstream and the decaying concentration at the previous downstream time step (Figure 2.12).

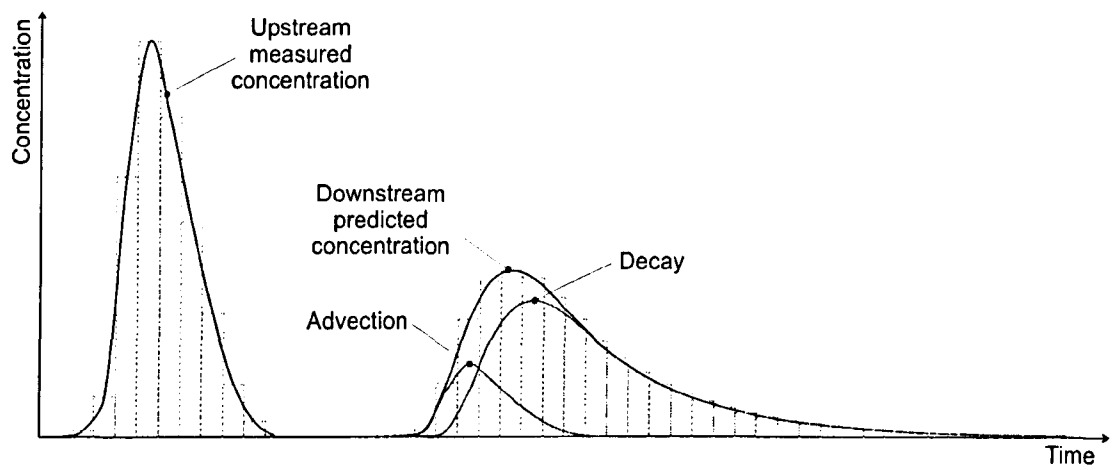

Figure 2.12 ADZ routing of multiple discrete inputs representing an upstream temporal concentration distribution.

The success and potential that the work of Beer and Young displayed with the ADZ model encouraged continuing development of the work. Researchers such as Wallis *et al* (1989a) have attempted to connect the physical characteristics of a river reach and the ADZ model parameters. This has been done by conducting river dye tracing experiments for different short river reaches over a range of discharge conditions. The choice of short (100-150m) reach lengths has allowed study of the simplest first order ADZ model, which can be developed further by considering higher orders of model if it is deemed better for longer reach lengths.

As explained by Wallis *et al* (1989a) dead zones have been considered as volumes usually located at the edges of a flow which the main discharge passes by but where some form of mixing takes place. Solute in the main body of the flow may encounter a dead zone and enter it, mixing with the volume the dead zone contains and only be released back to the main flow gradually after a period of time. The concept of pipe flow encountering a surcharged manhole chamber clearly fits with this image,

but as highlighted by the authors it is not so simple to make the comparison for river reaches. Although in a river there will often be dead zone regions in the bed and sides of the channel there are also considerable other mixing phenomena, such as eddies, wakes behind large roughness elements and reverse flows which could occur at bends or similar channel irregularities. It is therefore important to understand that the term dead zone used in an ADZ model represents the summation of all the various mixing effects even though there are differences in time and length scales. In this way all the dispersive effects are lumped together and represented by a single parameter, which gives the term lumped parameter model. This is the crucial assumption of the ADZ model (Wallis *et al*, 1989a). The aggregated effect of all the dispersive processes in a reach must be capable of being described by a single dead zone equation using an effective dead zone volume. This assumption is only justified so far by the practical results of field tests using dye trace experiments.

With longer reach lengths, where the channel or flow conditions are greatly variable between different portions of the total reach length, it is likely that a series of individual ADZ elements may be required. Indeed, there are possibilities for ADZ elements to be used in combinations of series and parallel.

The first order ADZ model equation (equation [2.25]) can be written in the form

$$C_{d,t} = -aC_{d,t-1} + bC_{u,t-\delta} \qquad [2.26]$$

The development of this equation to allow higher order models to be applied uses a backward shift operator introduced by Beer and Young (1983).

$$Z^{-p}X_k = X_{k-p} \qquad [2.27]$$

Where Z^{-p} is the backward shift operator. Applying this to the first order model described by equation [2.26] gives

$$C_{d,t} = -aZ^{-1}C_{d,t} + bZ^{-\delta}C_{u,t} \qquad [2.28]$$

$$C_{d,t}\left(1 + aZ^{-1}\right) = bZ^{-\delta}C_{u,t} \qquad [2.29]$$

$$C_{d,t} = \frac{bZ^{-\delta}}{\left(1 + aZ^{-1}\right)}C_{u,t} \qquad [2.30]$$

The equation above can be generalised in the form

$$C_{d,t} = \frac{B\left(Z^{-1}\right)\left(Z^{-\delta}\right)}{A\left(Z^{-1}\right)}C_{u,t} \qquad [2.31]$$

where

$$A\left(Z^{-1}\right) = 1 + a_1Z^{-1} + a_2Z^{-2} + \ldots + a_nZ^{-n} \qquad [2.32]$$

$$B\left(Z^{-1}\right) = b_0 + b_1Z^{-1} + b_2Z^{-2} + \ldots + b_nZ^{-n} \qquad [2.33]$$

Applying second order $A(Z^{-1})$ and $B(Z^{-1})$ polynomials to the generalised ADZ equation (Equation [2.31]) gives

$$C_{d,t} = \frac{\left(b_0 + b_1 Z^{-1}\right) Z^{-\delta}}{\left(1 + a_1 Z^{-1} + a_2 Z^{-2}\right)} C_{u,t} \qquad [2.34]$$

$$C_{d,t}\left(1 + a_1 Z^{-1} + a_2 Z^{-2}\right) = \left(b_0 + b_1 Z^{-1}\right) Z^{-\delta} C_{u,t} \qquad [2.35]$$

$$C_{d,t} + a_1 C_{d,t-1} + a_2 C_{d,t-2} = b_0 C_{u,t-\delta} + b_1 C_{u,t-\delta-1} \qquad [2.36]$$

which leads to the second order ADZ equation

$$C_{d,t} = -a_1 C_{d,t-1} - a_2 C_{d,t-2} + b_0 C_{u,t-\delta} + b_1 C_{u,t-\delta-1} \qquad [2.37]$$

Young and Wallis (1986) and Wallis *et al* (1989a) discuss the calibration of the ADZ model with data from four small rivers in north-west England. This has been done by examining upstream and downstream temporal concentration profiles and statistically examining these to determine the most appropriate model order and time delay and then estimating the remaining parameters. Repeating the analysis for different time delays and model orders allows the best fit coefficients to be obtained, using a normalised measure of the model fit, R_t^2, described by Young *et al* (1980).

$$R_t^2 = 1 - \left[\frac{\sum_{t=1}^{n} (c_t - p_t)^2}{\sum_{t=1}^{n} c_t^2} \right] \qquad [2.38]$$

where c_t and p_t are the measured and predicted data values at time t. By this definition, a prediction with an exact fit to the measured downstream data would give a value of unity for R_t^2.

When applying their method to actual river data, Wallis *et al* (1989a) compare the quality of fit between the measured downstream data and ADZ predictions made from different order models. Their results show that although the simplest first order models gave adequate longitudinal dispersion predictions, higher order models produced better descriptions of the data. However, it was noted that the parameters for higher order models were less well defined.

For two of the four test reaches, a second order ADZ model, which factorises into two parallel first order cells gave an extremely good fit to the data including the long tail effect. The assumption made is that one ADZ element represents a slow moving layer near the bed whilst the other element simulates a faster moving layer of the flow in the remaining channel volume. This is supported by the physical bed configuration of these two channels, which consisted of cobbles and hence perhaps explains the presence of an ADZ element with a larger residence time. Third order or greater models were identified as being over parameterised and were rejected for the field data in question on this basis.

Young and Wallis (1986) and Wallis *et al* (1989a) discuss the concept of the dispersive fraction, γ. This is the ratio of residence time to travel time (Equation [2.39]).

$$\gamma = \frac{T}{\bar{t}} \qquad [2.39]$$

This value is a measure of the length of time a solute is being dispersed as a proportion of the total time spent in the reach by the solute, and hence is also a measure of the proportion of the total reach volume that is dispersing the solute. Although the authors point out that the relationship between the dispersive fraction and actual physical reach characteristics remains unclear, it appears from the results that any particular reach can be expected to have an almost constant dispersive fraction regardless of the discharge. This relationship has potential, since it implies that if the dispersive fraction is established for a reach by a single dye trace experiment, and a relationship between discharge and travel time is known or estimated from channel hydraulics, then the ADZ model can be calibrated for all discharge rates. The value for the dispersive fraction was found to be consistently lower for smooth constructed channels when compared to results from natural river reaches. As yet, a technique for predicting the dispersive fraction of a particular river or channel by examining the geometry alone is not available. However, with the more simple dead zone geometry of a surcharged manhole there is perhaps a greater possibility of relating the dispersive fraction to the physical features.

Wallis *et al* (1989b) examined upstream and downstream temporal concentration profiles of a dye tracer collected over a 20 metre reach in a rectangular laboratory flume operated at a series of flow rates. From the profiles, values for the travel time and time delay were determined, and hence the residence time and dispersive fraction could be calculated. Plotting these variables against discharge and fitting both power and inverse law relationships to the results showed that either relationship gave a high quality fit to the data. The plot for dispersive fraction suggested that there was a slight tendency for the dispersive fraction to decrease with discharge. With their earlier work, Wallis *et al* (1989a) concluded that for field tests in small river reaches the dispersive fraction was independent of discharge.

As with the application of other models, the ADZ method requires calibration for the reach concerned. The high quality of fit of the model parameters to a relationship with discharge means that only a few tracer experiments would be required to calibrate the model over a wide discharge range with confidence. This is all that is required for first order model predictions and if these are deemed adequate there is no need to consider more complex model orders. If an improved fit is required then the authors Wallis *et al* (1989b) recommend that the time delay and residence time values should be halved and applied to two identical first order models positioned in series. It is possible to continue extending this to further higher orders of model but as discussed earlier Wallis *et al* (1989a) found no justification for models above third order. The longitudinal dispersion predictions can then be made for the reach using the model order identified as most suitable.

Wallis *et al* (1989b) highlight three possible reasons for limitations with the downstream concentration predictions using this technique. Firstly that this method of applying the model involves no optimisation to achieve best fit criteria. Secondly the discrete time version of the ADZ equation can only ever be an approximation of the original differential equation and finally there will be some experimental error in the derived parameters for the model.

2.6 Longitudinal dispersion in manholes

Detailed examination of the longitudinal dispersion of solutes due to manholes in urban drainage networks began with the work of Guymer and O'Brien (1995). Their study was aimed at quantifying the contribution that surcharged manhole chambers made in the overall dispersion within a sewer and to provide this information in a format that could be employed by sewer modelling software designers. Further investigations by Guymer *et al* (1996, 1998), Guymer and O'Brien (2000) and O'Brien (2000) analysed laboratory data with both the advection dispersion equation and with the aggregated dead zone model.

The original work of Guymer and O'Brien (1995) formulated the basic laboratory apparatus arrangement and the measurement instrumentation. A circular, unbenched 390mm internal diameter manhole was positioned between 2.6 metre lengths of 88mm internal diameter clear perspex pipe. Flow was provided from a constant head tank through a control valve, and was measured with a V-notch weir. The level of surcharge in the manhole could be varied by means of an adjustable weir at the downstream end of the system. Small quantities of Rhodamine WT dye were injected into the flow well upstream of the manhole and its concentration was measured either side of the manhole. To do this fluorometers were modified so that the flow through measuring volume became the entire 88mm diameter delivery pipe as opposed to the usual 12mm diameter arrangement. Importantly this technique was non-intrusive and so there was no disruption to the flow patterns, although it requires the assumption that the tracer is cross-sectionally well mixed at both locations.

Although the configuration of a pipe and surcharged manhole combination does not conform to the requirements for Taylor's (1954) analysis to be applied, the widespread use of the advection dispersion equation with river reaches and in urban drainage software led Guymer and O'Brien to apply it for the manhole arrangement. The tracer measurements gave upstream and downstream temporal concentration profiles from which the travel time and dispersion coefficient were obtained.

Their results show that over the range of tests covered the surcharge appears to have a relatively small effect on the solute mean travel time compared with the discharge. By assuming that variations in surcharge had no effect on the travel time for a particular discharge a relationship between the surcharge mean travel time and the discharge could be formulated. This showed that the delay effect caused by the manhole in comparison to that of a straight pipe was greater at higher discharges.

Guymer and O'Brien (1995) concluded that structures such as manholes have significant effects on the longitudinal dispersion. They highlight the fact that this conventional method of modelling the dispersion may not be fully justified with a surcharged manhole, but tentatively suggest that predictions for the geometry considered could be made. With further work they proposed that it would be possible to incorporate the mixing and retention effects of manholes into numerical modelling schemes.

Guymer *et al* (1996) rejected the advection dispersion equation in favour of the aggregated dead zone model proposed by Beer and Young (1983). The pronounced skewness, which is a feature of the concentration profiles from this work, and the fact that visual observation showed the manhole to act as a storage volume justified trying an ADZ approach. In their work Guymer *et al* (1996) used a similar laboratory system to the earlier work, although this time with a 357mm internal diameter benched manhole and with 100mm internal diameter pipework.

Difficulties were encountered in establishing the precise start and end points of the recorded temporal concentration profiles once the background level had been removed. This was due to noise generated by the fluorometers as the data was recorded. The method adopted for extracting the profile worked away from the peak concentration and cut the profile at the first data point value to be less than the best fit background concentration. As pointed out by the authors this defined a start time which was invariably too late and also truncated the tail at the end of the distribution. Furthermore the exaggerated cut off had a greater effect on the downstream distribution since this regularly contained a long low concentration tail. It was a simple method, however, and allowed a provisional study of the effectiveness of the ADZ technique in these circumstances.

Once determined, the upstream and downstream temporal concentration profiles were examined to find the travel time and time delay coefficients. They presented the manhole travel time by subtracting the theoretical pipe length travel time estimated from continuity. The residence time for the ADZ model incorporates the mixing of the solute, but the contribution on mixing of the short pipe lengths was unknown, so the data was presented as total spread, T_s, of the solute due to both the manhole and the pipe lengths. As with Guymer and O'Brien (1995), this work suggested that the travel time was independent of surcharge for the range considered. Although researchers investigating manhole head loss coefficients (Howarth and Saul, 1984; Johnston and Volker, 1990) observed differing circulation regimes, Guymer *et al* (1996) claimed that these had little effect on the mixing and so proposed that a solute introduced into the flow does not become fully mixed with the manhole. They felt that the circulation cells and flow structure formed within the manhole may prevent the tracer reaching all parts of the surcharged volume. This could not be confirmed by the authors without analysis of the internal flows in the chamber.

As a method of simplifying their results to make them more accessible for practical applications, Guymer *et al* (1996) considered the travel time as a multiple of the travel time for equivalent pipe lengths. Hence the travel time for the manhole was divided by the theoretical travel time for a pipe of the same diameter as the supply pipes and of a length equal to the manhole diameter. The equivalence factor was found to be reasonably constant and in the region of ten pipe lengths, establishing the significance of surcharged manholes on the travel time of soluble pollutants through sewer systems. This is especially so considering that the requirements for the provision of manholes ensure that they are numerous.

The variation of total spread of the solute showed more variation with surcharge than the travel time results, and no clear trends. It was difficult for any conclusions to be drawn, but the final presentation of results given by the authors averaged the total spread across the surcharge range. An ADZ prediction of a downstream concentration profile made using the surcharge mean travel time and total spread values had quite good agreement with measured results. The peak concentration and the profile shape were well predicted but advection was slightly overestimated.

Guymer *et al* (1998) continued the manhole mixing research by attempting to fill in some remaining gaps in the knowledge gained from previous work. There were three new aspects to their work, which considered visualisation of flow structures within the manhole, travel times and dispersion for cases where the manhole was free flowing rather than surcharged and a brief examination of the application of the advection dispersion model for manholes in sewer modelling software.

For the purposes of flow visualisation, a similar laboratory system to previous arrangements used at the University of Sheffield was equipped with a Laser Induced Fluorescence (LIF) facility developed by

Guymer and Harry (1996). A rapid scanning laser light beam was positioned to form a narrow vertical sheet of light along the centre line of the manhole parallel with the primary flow direction (Figure 2.13). Any fluorescent dye present in the two dimensional light plane emits light with an intensity proportional to the concentration.

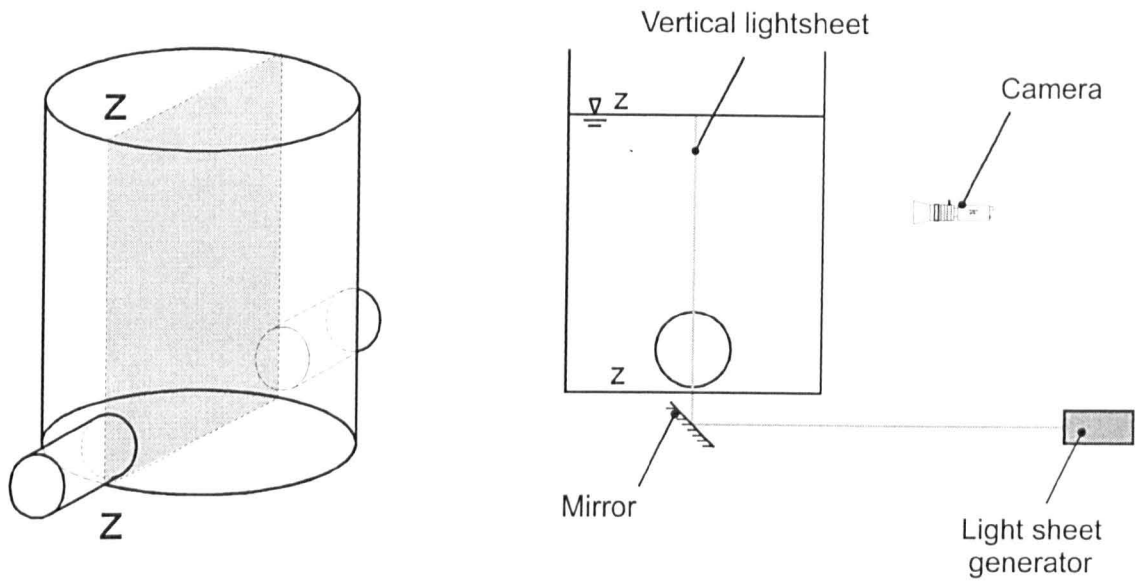

Figure 2.13 Arrangement for laser induced fluorescence experiments.

The technique was originally planned as a non-intrusive method for determining the longitudinal dispersion, with the ability to determine tracer concentrations spatially and temporally throughout the manhole. Calibration tests, however, proved that the laser used was not powerful enough for quantitative measurements of concentration but the LIF work did prove useful for providing a preliminary qualitative analysis of flow structures within the manhole. A series of images presented by Guymer *et al* (1998) show an injection of dye passing through the manhole (Figure 2.14). In this case the flow was 0.9 litres per second and the surcharge was 200mm. The retention of tracer in the surcharged volume for a considerable period of time after the majority of tracer cloud mass has passed, and the gradual release of the tracer from this volume is obvious.

The images show how the dye entering with the flow from the left hand side becomes mixed on the plane of the manhole centre line. Eddies associated with the jet diffusion region (Abertson *et al*, 1950) can be observed entraining tracer into the surcharge volume and later re-entraining quantities into the flow exiting the manhole. The re-circulation pattern can be seen in Figure 2.14b where a central region of low dye concentration is present. Furthermore, Figure 2.14c clearly demonstrates how the incoming jet of water is compressed slightly upon entry into the manhole chamber by the re-circulation of water pressing from above.

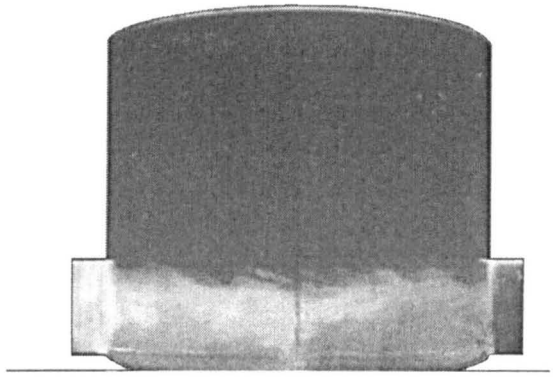

Figure 2.14a After 2 seconds

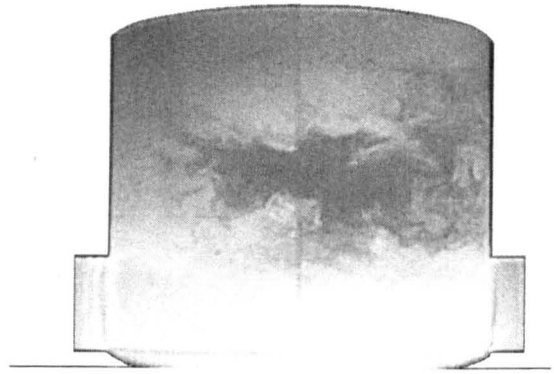

Figure 2.14b After 28 seconds

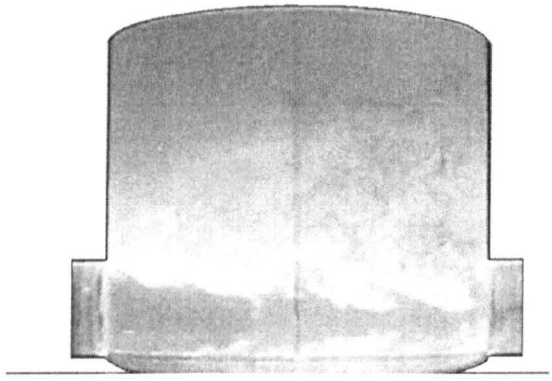

Figure 2.14c After 38 seconds

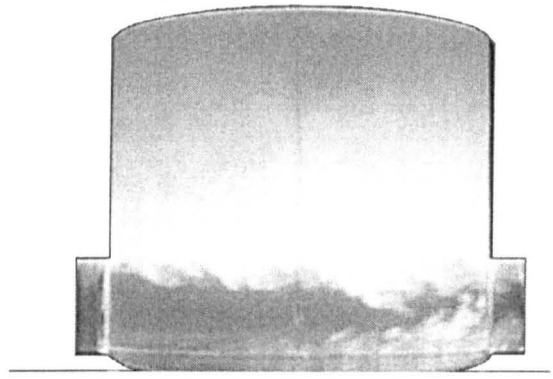

Figure 2.14d After 67 seconds

Figure 2.14 Variation in solute concentration within manhole with time. (Q = 0.9l/s, Surcharge = 200mm). Guymer *et al* (1998).

The experimental study comparing surcharged and unsurcharged flow and the effect of benching was conducted using a very fine sediment as the tracer. Not only does fine sediment behave in a similar manner to solutes in the flow, it is also important to bear in mind that many sewer pollutants are attached to fine sediments. In this case a ground olive stone material was used, and the concentration was detected using nephelometers fitted into the pipe lengths upstream and downstream of the manhole to detect the turbidity of the passing flow. As before, the authors encountered problems in distinguishing the start and end points of the temporal sediment concentration profiles. For this work a slightly more complex statistical method was employed with the aim or retaining better consistency between tests. The authors chose to pursue the advection dispersion method of analysing the data since this is the theory used for pollution transport in the MOUSE sewer modelling software (Garsdal *et al*, 1995). Unsurcharged flow was found to cause less dispersion and a reduction in travel time whilst benching was shown to have a significant effect in reducing these values.

In their discussion of numerical modelling for sewer manholes, Guymer *et al* (1998) highlight how the assumption of instantaneous full mixing at surcharged manholes, as currently made in the quality model MOUSETRAP, overestimates the degree of mixing that occurs. The effect of representing a surcharged manhole as a completely mixed tank is shown by the data in Figure 2.15. A proposed method of dealing with this is to reduce the dispersion coefficient that is applied to neighbouring pipe lengths. This technique was successfully applied to a MOUSETRAP model for the city of Ljubljana in Slovenia (Mark *et al*, 1996). However, they advocate that a better method is perhaps to develop the ADZ theory in combination with jet theory (Bo Pedersen and Mark, 1990) to give a more accurate description of the actual manhole mixing.

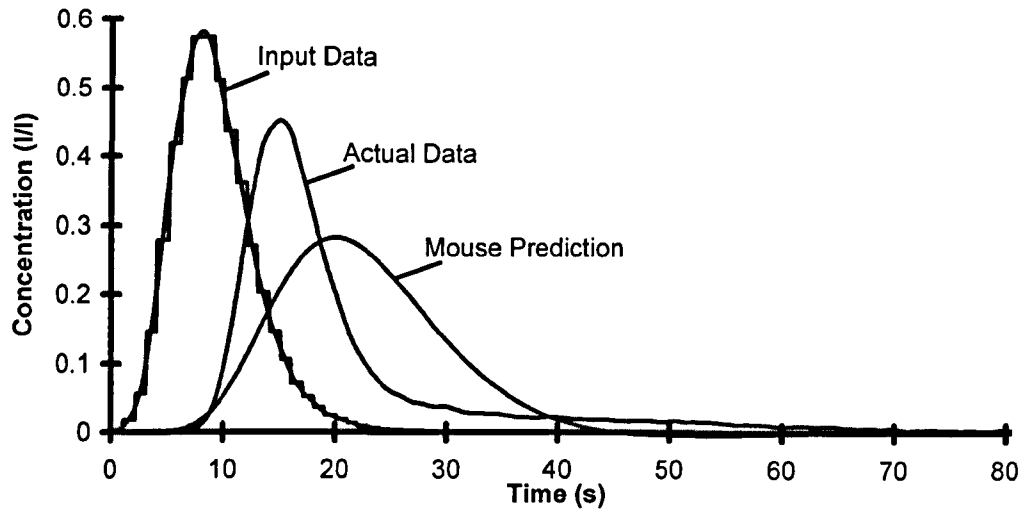

Figure 2.15 Comparison of longitudinal dispersion prediction from MOUSETRAP and laboratory data (diameter = 400mm, Q = 1.98l/s) (Guymer *et al*, 1998).

A development in obtaining longitudinal dispersion coefficients for manholes is the use of optimisation techniques. A simple optimisation approach for the advection dispersion equation was described by French (1986) and similar methods have also been applied to ADZ models (Wallis *et al*, 1989a; Antonopoulos, 1997). French gives several methods for determining a dispersion coefficient for temporal concentration data from a river reach. One of these suggests choosing a trial value for the dispersion coefficient and using this in combination with the advection dispersion equation (Equation [2.14]) to produce a downstream concentration prediction from the upstream data. A measure of the quality of fit to the actual downstream data is obtained by computing the mean squared concentration difference between the predicted and measured profiles. Trying other values for the dispersion coefficient determines whether there is a value that gives the best fit. This value is than taken as the dispersion coefficient for that particular set of data.

Antonopoulos (1997) analysed an extensive set of data obtained from fluorescent dye tracer laboratory experiments with a 500mm internal diameter unbenched manhole. The standard ADZ coefficients of travel time and reach time delay for the flow between the fluorometer locations were obtained in the usual fashion from the temporal concentration distributions. The author pinpointed some of the failings of the output produced using these standard coefficients. There was a tendency for over-prediction of the advection and dispersion, and hence the predicted curve appeared later on the timescale than the measured data, had a smaller peak concentration value, showed less skewness and was without the long tail present in the actual data profiles. One of the reasons put forward for this by Antonopoulos (1997) was that although Guymer *et al* (1996) obtained adequate ADZ predictions for surcharged manholes it may be that the dead zone aggregation involved with complex river reaches gives better results with a straightforward application of the ADZ model than the less complex geometry of a manhole and pipe configuration. Antonopoulos (1997) gives full details of optimisation procedure conducted for the ADZ analysis of the data, similar in principle to the recommendations of French (1986). A measurement of the goodness of fit was defined using a root mean square error parameter, which was a minimum for the closest match between actual and predicted profiles. For a given value of time delay, a Newton Raphson approach revealed the minimum error as a function solely of residence time. It was demonstrated that for any particular time delay value, there was a unique residence time giving the minimum error and hence the best fit to the observed data. Repeating this process for the range of possible time delay values, from zero to

the time between the first upstream arrival and the final downstream arrival, revealed the pair of ADZ parameters which best optimised the model to the recorded data. The remarkable improvement in the ability of the optimised ADZ predictions to describe the longitudinal dispersion was evident, and the author suggested that this optimisation procedure had great further potential. Depending upon the practical application of the optimised ADZ model, it would be possible to create a more complex best fit coefficient that was weighted towards factors such as peak concentration, peak arrival time, first arrival time and accuracy of tail prediction.

Dennis *et al* (1999) incorporated similar optimisation procedures to Antonopoulos (1997) into a FORTRAN computer program. An optimised ADZ model was used to examine the effect of a step height between the inlet and outlet pipe levels on the travel time of solutes passing through a surcharged manhole. The optimisation procedure used a matrix based system to optimise both the travel time and the time delay coefficients simultaneously. It was clearly demonstrated that for a particular data set there was only a single coupling of the coefficients that gave a downstream prediction with the very best fit to the measured data. Dennis *et al* (1999) give an example of how the optimisation method produces a predicted profile that accurately reflects the peak concentration and its arrival time. For the purposes of urban drainage design and operation it is deemed that this is the most crucial aspect of the trace and it is more important to model this accurately than the low concentration tail effects. The step height of one pipe diameter in the manhole geometry was demonstrated to cause an increase of approximately 100 percent in the travel time for the system, whilst actually reducing the reach time delay slightly.

2.7 Computational fluid dynamics

2.7.1 Introduction

Computational Fluid Dynamics (CFD) is becoming a widely used technique for research and industrial applications associated with fluid flow. It offers a different approach to the investigation of fluid flow from that of physical modelling, and as such it has several advantages. Developments in computer power and the software itself bring increasingly complex geometries and flow regimes within the scope of detailed CFD analysis. The main advantage of employing CFD techniques is that, once calibrated, a model can be used to examine the effects of changes in geometry without the need for the reconstruction of a laboratory model, which may prove time consuming and expensive. Thus it can be applied as a decision making tool for considering design options. Furthermore, a flow problem analysed by means of a numerical model calculates a very complete data set over the control volume so values for variables such as velocity and pressure can be obtained for all locations within the computational domain.

In the case of longitudinal dispersion due to surcharged manholes, the advantages of a CFD approach could be exploited. For instance, once a solution was obtained for a particular manhole configuration, velocities and pressure details for other arrangements could be obtained with relative ease. Many CFD packages are also capable of modelling two species of fluid within the same flow, for example water and a soluble tracer. In this way the process could be used as a means of identifying critical factors causing longitudinal dispersion as flow passes through a surcharged manhole. Furthermore, the CFD solutions offer an interpretation of the flow mechanisms within the manhole, which would assist the interpretation of laboratory results.

2.7.2 Governing equations of fluid dynamics

CFD packages use the governing equations of fluid dynamics and incorporate special techniques for the description of turbulent flow conditions. For three dimensional incompressible flow the following equations can be applied.

Conservation of mass is given by the continuity equation

$$\frac{\partial u_x}{\partial x}+\frac{\partial u_y}{\partial y}+\frac{\partial u_z}{\partial_z}=0 \qquad [2.40]$$

and conservation of momentum in the x direction is given by

$$\frac{\partial u_x}{\partial t}+u_x\frac{\partial u_x}{\partial x}+u_y\frac{\partial u_x}{\partial y}+u_z\frac{\partial u_x}{\partial z}=-\frac{1}{\rho}\frac{\partial P}{\partial x}+g_x+\upsilon\left(\frac{\partial^2 u_x}{\partial x^2}+\frac{\partial^2 u_x}{\partial y^2}+\frac{\partial^2 u_x}{\partial z^2}\right) \qquad [2.41]$$

with similar equations for y and z flow directions (often collectively referred to as the Navier-Stokes equations).

Where u_i is the instantaneous velocity component in the i direction, ρ is the density, P is the instantaneous static pressure, υ is the kinematic viscosity and g_i is the acceleration due to gravity in the i direction. These equations are derived from first principles in many fluid dynamics text books, an example derivation being provided by Anderson (1995).

At present there is no numerical procedure to solve these equations directly for turbulent flow conditions. Therefore the statistical technique of Reynolds averaging is applied to modify the equations and allow modelling of turbulent conditions, which are more likely to be encountered in practice. As an example of this, consider the instantaneous fluid velocity in the x direction, which is separated into a temporal mean velocity, represented by an overbar, and a temporally fluctuating component, marked with a prime (Figure 2.9 and Equation [2.42])

$$u_x=\overline{u_x}+u'_x \qquad [2.42]$$

where the mean component is defined by

$$\overline{u_x}=\frac{1}{(t_2-t_1)}\int_{t_1}^{t_2}u_x dt \qquad [2.43]$$

with $t_2 - t_1$ being long in comparison with the time scale for the turbulent fluctuations.

The fluctuating component of equation [2.43] is defined such that

$$\overline{u'_x}=0 \qquad [2.44]$$

The same Reynold's averaging principle applies to other flow directions and to the instantaneous value of pressure in all directions. Substituting these time averaged varaibles into the fluid flow

equations (Equation [2.40] and [2.41]) produces

$$\frac{\partial \overline{u_x}}{\partial x}+\frac{\partial \overline{u_y}}{\partial y}+\frac{\partial \overline{u_z}}{\partial z}=0 \qquad [2.45]$$

and for the x direction Navier-Stokes equation

$$\frac{\partial \overline{u_x}}{\partial t}+\overline{u_x}\frac{\partial \overline{u_x}}{\partial x}+\overline{u_y}\frac{\partial \overline{u_x}}{\partial y}+\overline{u_z}\frac{\partial \overline{u_x}}{\partial z}=-\frac{1}{\rho}\frac{\partial \overline{P}}{\partial x}+g_x+\frac{\partial}{\partial x}\left(\upsilon\frac{\partial \overline{u_x}}{\partial x}-\overline{u'_x u'_y}\right)+ \frac{\partial}{\partial y}\left(\upsilon\frac{\partial \overline{u_x}}{\partial y}-\overline{u'_y u'_z}\right)+\frac{\partial}{\partial z}\left(\upsilon\frac{\partial \overline{u_x}}{\partial z}-\overline{u'_z u'_x}\right) \qquad [2.46]$$

The averaging process introduces into the equation correlations between the velocity fluctuations ($u'_x u'_y$ and similar) that are unknown (Rodi, 1984). They represent the transport of momentum that is attributable to the fluctuating fluid velocity. When multiplied by the density these correlations are defined as stresses acting on the fluid, which gives them the name Reynold's stresses.

There are more unknowns over three flow directions than there are equations, which leads to the necessity to obtain a mathematical description of the Reynolds stress values. Different techniques are available to overcome this difficulty, which is known as the "closure problem". Two of the most common methods are described in the following sections.

2.7.3 The k-ε model

The k-ε turbulence model is described in detail by Rodi (1984). The closure problem is solved by employing the Boussinesq hypothesis for eddy viscosity where the Reynolds stresses are assumed to be proportional to the mean velocity gradients. The constant of proportionality is termed the turbulent, or eddy, viscosity, μ_t. This theory was founded on the concept of considering the volume of fluid in a turbulent eddy to behave in an analogous manner to molecules, which collide and exchange momentum. The molecular viscosity is proportional to the average velocity and mean free path of the molecules. Similarly, the eddy viscosity is said to be proportional to a velocity representing the fluctuating motion and the length of this motion, termed the mixing length. Whilst the molecular viscosity is a fluid property, the turbulent viscosity depends on the local turbulence and thus may vary considerably over different locations within the flow. Therefore, whilst the closure problem has been solved, it is necessary to determine the turbulent viscosity at particular locations. This is done within the model by means of two parameters, k, the turbulent kinetic energy, and ε, the dissipation rate of k. These are used to calculate the velocity and length scales from which, in turn, the turbulent viscosity is computed (Fluent, 1993).

2.7.4 The Reynolds Stress Model (RSM)

The k-ε model employs an isotropic description of the turbulence to determine the Reynolds stresses. This assumes that the turbulence velocity and length scales are equal in all directions. In more complex flows, and especially where there is a tendency for high degrees of swirling, it is likely that there will be significant variations in the velocity and length scales in different directions. This makes the k-ε model inappropriate and an alternative option is the Reynolds Stress Model (RSM), which calculates individual values for the Reynolds stresses. Although this model is capable of providing a

more accurate prediction of complex and swirling flows, the disadvantage is an increase in computation time required to reach a solution.

2.7.5 Previous related use of CFD

Rodi (1984) demonstrated that the k-ε turbulence model was capable of describing the velocity features of jets. Turbulent jets have been examined with computational fluid dynamics by Dimenna and Lee (1996) and also Ali and Othman (1997), who considered jet-forced water circulation in reservoirs. This work has provided an insight into the ability of CFD software to model re-circulating flow regimes and jet flows. In most cases the authors achieved good agreement for the velocity profiles between the models and laboratory data. Dimenna and Lee (1996) found that the results were particularly sensitive to the computational mesh. Ali and Othman (1997) used two dimensional numerical models, which gave depth averaged results. This resulted in good agreement with uniform shape laboratory scale reservoirs. However, when extended to models of more realistically profiled reservoir shapes the CFD model had less agreement with the measured circulations. This was attributed to the fact that a 5:1 vertical exaggeration was used for the laboratory scale model. They concluded that CFD was a useful method of examining the jet-forced circulations in reservoirs, but that for the more complex geometries further verification with undistorted physical models was required.

Harwood and Saul (1996) used the Fluent CFD software package to assist in the design of a new combined sewer overflow. A full-scale laboratory model of an hydrodynamic separator was tested with a simple particle imaging system to calibrate the flow fields at several locations within the chamber. A hydrodynamic separator CSO structure is designed to induce extensive swirling of the flow within. The demonstrated ability of the CFD package Fluent to model these flows with good agreement suggests it also has potential as a tool for examining the flow structures and re-circulations within a surcharged manhole.

Asztély and Lyngfelt (1996) used a numerical model in a preliminary feasibility study to determine whether a three dimensional numerical model could be used to calculate the head loss coefficients for surcharged manholes. A series of assumptions were made in establishing the model. The inlet conditions were determined by using the outlet conditions of a separate model of a straight pipe, 60 pipe diameters in length. A circular half pipe benched manhole was modelled including short sections of pipe on either side of the chamber itself. Although free surface modelling is possible with some numerical models it adds extra complications to the solution process, and in most cases is probably unnecessary for steady flow conditions. Asztély and Lyngfelt (1996) chose to fix the free surface at a specified level, effectively using a wall condition to seal the surface, but unlike the other boundary walls the perpendicular velocity was set to zero and the tangential velocity components had frictionless conditions applied to them. This requires that the free surface has little influence on the energy loss, which may not be the case at low surcharges and high flow rates when the surface is highly turbulent. A further step to reduce the computational domain of the model was to use a plane of symmetry along the manhole centre line parallel with the main flow direction. In a similar fashion to the fixed surface, this boundary is given frictionless conditions. However, this method restricts the applicability of the model to symmetrical flow conditions. With the seiching and swirling flows noted by researchers using laboratory manhole studies, this may be a rather restrictive assumption as was confirmed by the authors when comparing their predicted head loss with the experimental work of Lindvall (1984).

The simulations completed discovered that pipe lengths of approximately 10 pipe diameters upstream and 20 pipe diameters downstream were required to achieve pipe flow at these extremes that was not influenced by flow disturbance from the manhole. Three water levels of 3.6, 4.6 and 5.6 times the pipe diameter and two manhole diameters of 2.6 and 4.1 pipe diameters were examined. A single flow rate giving a Reynolds number of 2.4×10^5 was used. The work highlighted an interesting feature of the pressure measured along the centreline of the pipes, which was an additional drop in the pressure immediately prior to the manhole inlet. This has not been noted by any laboratory researchers and is not included in theoretical approaches. It was explained as a result of the increase in flow velocity in this section of pipe, which in turn is caused by the re-circulation in the manhole compressing the flow area at the inlet.

Head loss coefficients were compared with the laboratory results of Lindvall (1984) and found to give good agreement in the region where the flow depth to pipe diameter ratio was between 2.5 and 6.0. Below this value, where Lindvall had obtained greatly increased coefficients, the CFD compared less favourably. This was attributed to the failure of the CFD model to successfully simulate the non-symmetric and swirling flow patterns that were a feature of the higher head loss flows. Asztély and Lyngfelt (1996) concluded that the use of CFD technology was valid for examining flow structures within manholes. Reliable simulation results could be obtained with their model for symmetrical flow regimes with little influence from the free surface.

2.8 Summary

Manhole chambers are extensively located throughout urban drainage networks to provide a means of sewer access for inspection and maintenance. A wide variety of geometrical variations have been examined in laboratory investigations to determine the head loss caused by a manhole under surcharged conditions. The head loss is regarded as being proportional to the velocity head, $v^2/2g$, with the constant of proportionality being termed the head loss coefficient, K_H. The value of this coefficient has been shown to vary with factors such as manhole to pipe size ratio, surcharge level, benching arrangement and step height.

Urban drainage modelling and real time control operation are becoming more widespread as understanding of sewer quality processes improves. In addition, developments in computing power and modelling techniques are resulting in better predictions of pollution transport through sewers. This brings benefits by allowing better management and operation of sewer networks to reduce pollution spills into watercourses during storm flow.

Longitudinal dispersion is the process by which a tracer spreads whilst being transported by a flow. The advection dispersion model and the aggregated dead zone equation are two models by which the effects of this phenomenon can be predicted in a reach length. These have been applied by researchers in an effort to quantify the longitudinal dispersion due to surcharged manholes.

Chapter 3

Experimental Procedures

3.1 Introduction

The longitudinal dispersion due to surcharged manholes was determined by means of a series of laboratory experiments. Important aspects of the mixing that were specifically investigated were the determination of the effects of extreme high surcharges and of step heights between the inlet and outlet pipes. In addition, visual analysis of the flow mechanisms within the manhole was undertaken. Measurements of the head loss caused by the manhole structure were also obtained.

Previous work relating to longitudinal dispersion in manholes undertaken by Guymer and O'Brien (1995, 2000), Guymer *et al* (1996, 1998) and O'Brien (2000) was completed to surcharges of approximately 300mm. The results presented from these experiments revealed trends that were not fully defined over this surcharge range. The addition of step heights between the upstream and downstream pipes at the manhole was felt to add to the necessity of examining high surcharge levels. Ultimately, the maximum surcharges possible were restricted by the size of the laboratory to approximately 1250mm, equivalent to over 14 pipe diameters above the downstream pipe soffit. Although surcharges as high as those considered for these experiments may be uncommon, it was felt to be important to ensure that results were extended to a limiting surcharge level.

Differences in the elevation of sewer pipes at manholes are a common occurrence since sewer pipe levels and gradients are dictated by hydraulic, economic and ground topology considerations (Bartlett, 1970). The maximum step height that was considered within the laboratory test schedule was two times greater than the pipe diameter. This was similar to previous studies examining head loss. For step heights greater than approximately 600mm, regardless of pipe diameter, a back drop manhole is required to avoid sewer flow splashing unnecessarily within the chamber. Therefore the laboratory tests encompass the step height to pipe diameter ratios expected for sewer pipes of diameter 300mm or greater.

Experimental work utilising soluble tracer measuring devices positioned either side of the manhole was only capable of providing measurements of the effects of the flow conditions within the manhole. The use of laser lightsheet technology allowed a study of these actual conditions inside the chamber and provided further information for the interpretation of the other laboratory data.

3.2 Laboratory system

3.2.1 General arrangement

A laboratory system (Figure 3.1) was constructed for the purpose of examining longitudinal dispersion due to surcharged manholes. The apparatus consisted of a re-circulating water supply that was pumped from a storage sump to a constant head tank and gravity fed through the test apparatus

before returning to the sump. The manhole that was used throughout the course of this research was a 388mm internal diameter circular design, and is fully described in the following section. The upstream supply pipe was over 20 metres in length, with a straight section immediately prior to the manhole 3.0 metres long. The downstream straight section after the manhole was 2.7 metres long. The delivery pipes, representing the sewer pipes, were constructed from 88mm internal diameter perspex and the upstream and downstream pipework was set at a zero slope. A valve attached to the upstream delivery pipe controlled flow rates through the manhole of between 0.0 and 8.0 litres per second. Flow rates were monitored by means of a 30° V-notch weir located upstream of the sump. The calibration equation for the weir is given below (Equation [3.1]).

$$Q = \frac{8}{15} C_d \tan\left(\frac{\vartheta}{2}\right) H^{5/2} \sqrt{2g} \qquad [3.1]$$

where C_d is the coefficient of discharge, in this case 0.597, θ is the V-notch angle and H is the head of water over the weir.

The header tank was kept at a constant head by a pump that delivered water from the sump and a bell mouth overflow positioned within the header tank returned the overspill to the sump. Positioned at the end of the exit pipe from the manhole was a surcharge control system. This consisted of a cylindrical tower of diameter 600mm, within which there was a height adjustable circular weir. This device was used to alter the water surface level in the manhole at any given flow rate.

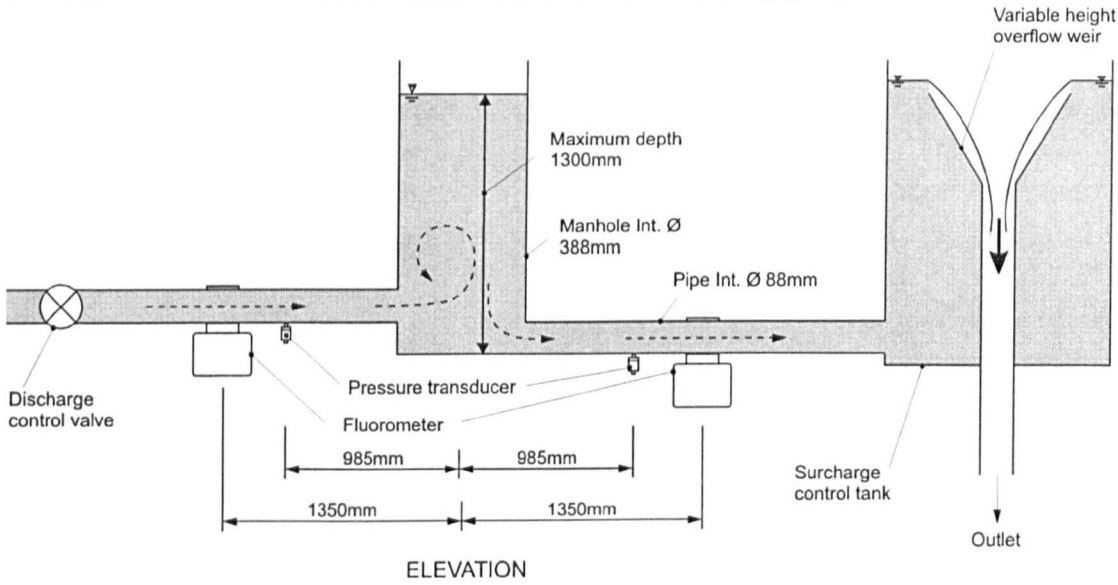

Figure 3.1 Schematic arrangement of laboratory apparatus.

3.2.2 Manhole details

The manhole used for the experiments was a 388mm internal diameter circular manhole constructed from clear perspex. The surcharge height to be tested was varied by means of the weir within the surcharge control tower. This weir had a metal support pole that was drilled at 100mm intervals. These holes allowed a metal pin to be inserted to fix the surcharge control weir at regular and repeatable heights. A maximum water depth of approximately 1300mm was available, giving a safety freeboard of 200mm from the top of the manhole.

The upstream and downstream pipes were aligned longitudinally and in the zero step height configuration the pipe inverts were set level with the base of the manhole chamber. An aluminium plate that was used to connect the pipes to the manhole could be adapted to allow the upstream pipe to enter the manhole at different heights. Figure 3.2 shows the laboratory manhole with a 1.5D step. The step height configurations that were tested were between 0.0 and 2.0 pipe diameters, in 0.5 pipe diameter increments. For each step height the upstream delivery pipe was raised on adjustable metal supports to retain the stability of the apparatus. The manhole with a 1.5 pipe diameter step height was tested with and without a benching arrangement in the manhole base. A diagram of the benching configuration is provided in Figure 3.3. The design had a half pipe diameter base, which was angled between the inverts of the delivery pipes. Vertical side walls to the channel were raised to the level of the upstream pipe soffit, and the benching platform was sloped upwards at an angle of 1 in 12 towards the manhole walls.

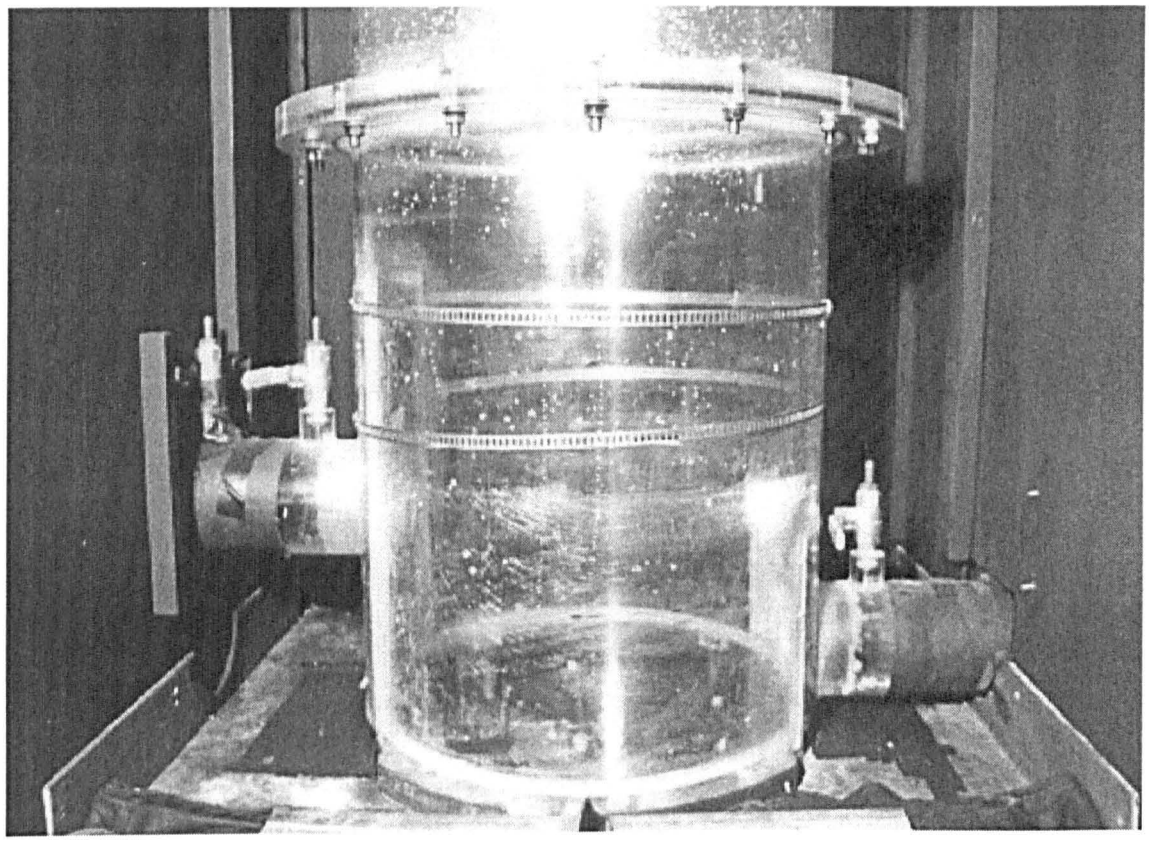

Figure 3.2 Laboratory manhole with 1.5D step height.

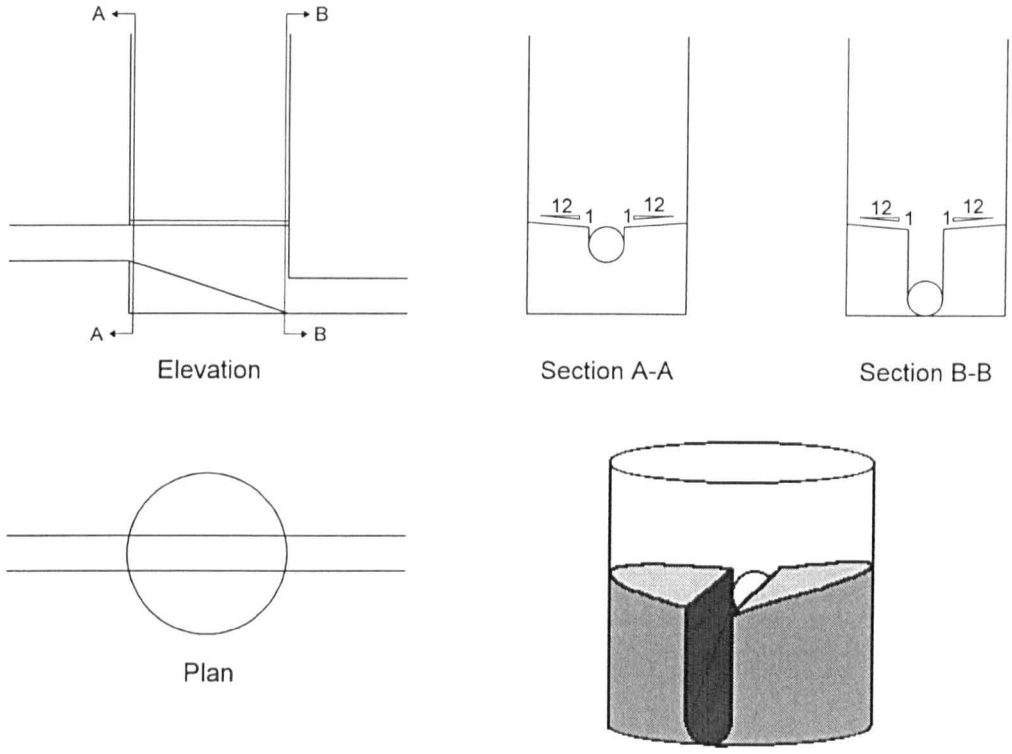

Figure 3.3 Benching arrangement for 1.5D step manhole.

3.3 Instrumentation

3.3.1 Instrumentation for head loss

Two methods were used to measure the head loss that occurred as flow passed through the manhole chamber. The first method was the use of electronic pressure transducers attached to the delivery pipes. A second system employing a series of 23 pressure tappings along the length of the delivery pipes was fitted so that the pattern of head loss along the entire laboratory pipe lengths could be determined.

The pressure transducers were attached to the invert of the pipe upstream and downstream of the manhole, at a distance of 0.985 metres from the centre line. A 2mm diameter hole was drilled through the pipe and a strong adhesive was used to attach a perspex mount that held the pressure transducer in place. The arrangement was such that the water flowing through the manhole delivery pipes was in contact with the transducer pressure sensor. Each transducer was capable of measuring static water pressures of between 0.0 and 2.0 metres.

A possible source of error for these single point pressure measurements was highlighted by Archer *et al* (1978). Their studies of head loss with a similar manhole configuration concluded that the hydraulic grade line in the pipe exiting the manhole was not necessarily of a constant linear gradient. Indeed, for as far as 70 pipe diameters downstream of the manhole the hydraulic grade line was measured by Archer *et al* as being asymptotic to the hydraulic grade line for a straight pipe. Therefore if, as with previous researchers, the hydraulic grade line was linearly extrapolated from the single measurement point to the centre of the manhole to calculate the head loss due to the manhole there could be some error in the calculation (Figure 3.4).

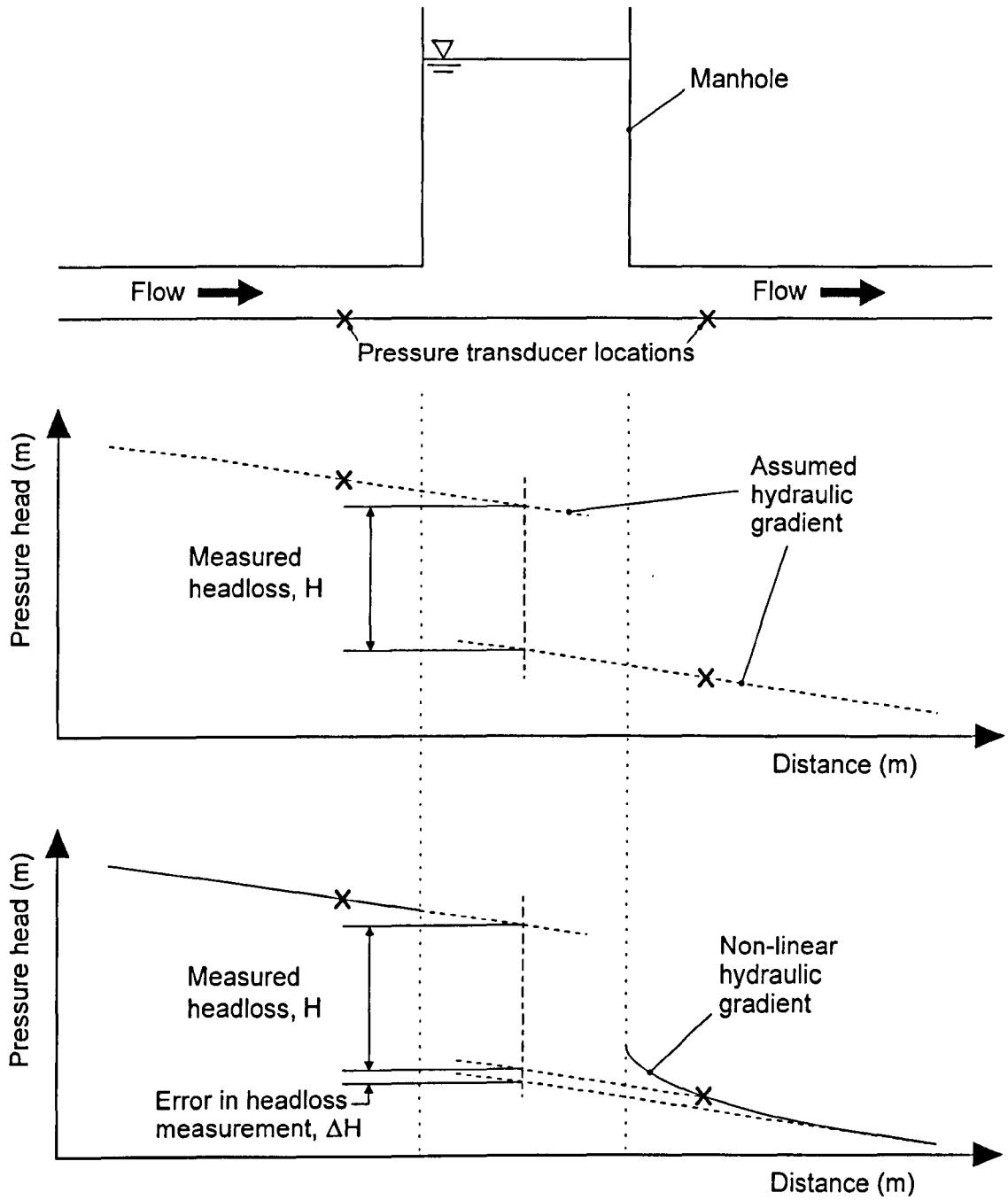

Figure 3.4 Potential source of error in head loss measurement.

In an attempt to examine the profile of the hydraulic grade line in the upstream and downstream pipe lengths, 23 piezometer tappings were made at intervals along the pipe. Each pressure tapping consisted of a 2mm hole drilled in the pipe soffit over which was attached a circular perspex mount. Lever operated valves were then fixed to the mounts allowing individual pressure tappings to be switched on and off. From the valve a length of flexible plastic pipe of diameter 8mm led to a rack containing glass piezometer tubes of the same diameter and a measuring scale. Pressure tappings with valves attached are shown located on the pipe sections in Figure 3.2.

3.3.2 Instrumentation for longitudinal dispersion

The determination of coefficients describing travel time and longitudinal dispersion requires a measurement of temporal concentration profiles at two sites. It was decided to use fluorescent dye as a tracer for this purpose. This choice was primarily governed by the experience and equipment held by the Civil and Structural Engineering department at the University of Sheffield regarding these materials. Fluorescent tracers have the advantages of being well conserved between measuring locations, relatively inexpensive and can be detected with high accuracy by non-intrusive means.

Fluorometric dye concentration measurements were obtained using two Turner Series 10 fluorometers, one positioned 1.35 metres upstream of the manhole centre line and the other at the same distance downstream. In normal operation these fluorometers are used to measure dye concentrations in either a discrete test tube sample or in a 12mm diameter through flow pipe arrangement. A fluorometer measures the concentration of a fluorescent dye tracer by emitting light from a steady light source. This excites any fluorescent particles present and the light emitted from them is of a different wavelength to the original source. Filters block the source light, allowing only the light reflected from the fluorescent particles to pass to a photomultiplier, which converts the amount of light received to an electrical voltage signal. The intensity of light emitted by the fluorescent particles is directly proportional to the concentration of these particles within the measuring volume. Hence the voltage output from the fluorometer can be calibrated to the concentration of fluorescent material present in the sample. Rhodamine WT was selected as the fluorescent dye to use. This dye was developed specifically for tracer studies and is resistant to absorption, detectable in low concentrations, readily available and economic (Smart and Laidlaw, 1977).

Using the normal operation mode for the work in the laboratory manhole test facility was not considered appropriate since this would require a sampling system that intruded into the flow. Interrupting the flow with even a small diameter sampling tube positioned within the delivery pipe system would have an effect on the local flow patterns and the dispersion of the tracer dye. For this reason an adapter device was developed by a previous researcher (O'Brien, 2000) that allowed the whole of the 88mm internal diameter clear perspex pipe to be used as a through flow arrangement. A light tight metal housing, holding a series of aligned mirrors, was fitted to the fluorometer, and this unit diverted the light path from its original route in such a way as to allow the dye concentrations over the entire pipe cross section to be measured (Figure 3.5). The adapter also housed the filters necessary for operation. Each fluorometer was located beneath the pipe section and the attached adapter was positioned in place around the pipe (Figure 3.6). Accurate fluorometer measurements required that no extraneous light reached the fluorometer photomultiplier. For this reason the entire laboratory apparatus was sealed from daylight by the use of lightproof material.

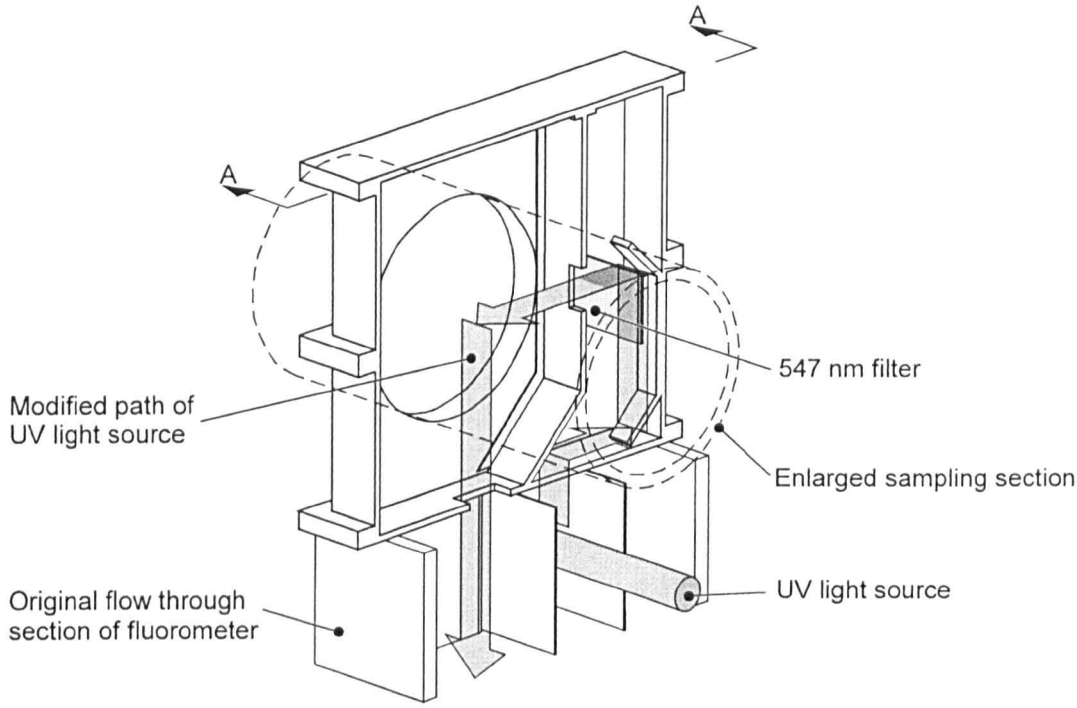

Figure 3.5 Diagram of fluorometer adapter (O'Brien, 2000).

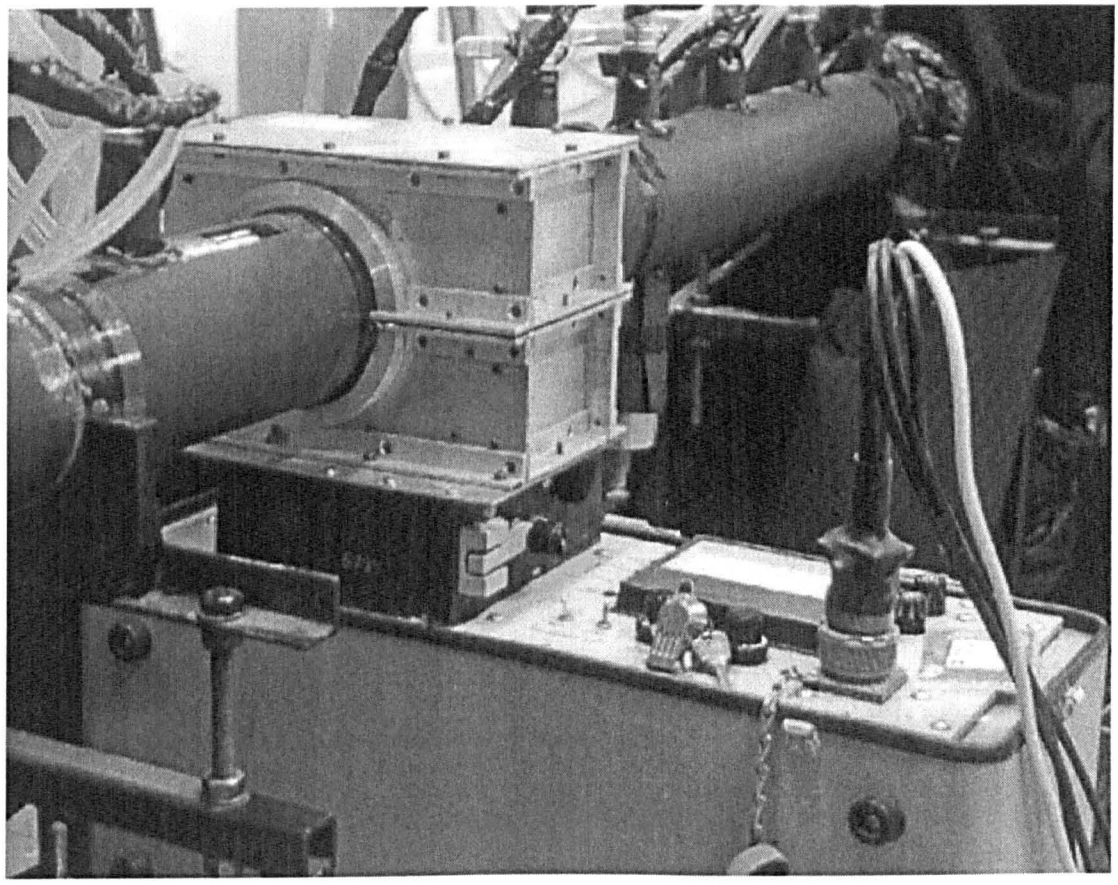

Figure 3.6 Fluorometer and adapter fitted in position on manhole pipeline.

3.3.3 Data logging instrumentation

Data from the measuring devices giving an electronic output was gathered by logging the output on a Cambridge Electronic Design (CED) 1401 data logger unit, used in conjunction with Spike2 software (Cambridge Electronic Design, 1990). This equipment allowed a selection of logging rates and data collection intervals for up to 16 channels, or input devices. Preliminary laboratory tests demonstrated that under certain flow conditions it could take over six minutes for a dye injection to completely pass the downstream fluorometer. It was therefore decided to log each injection test for ten minutes. This ensured all dye from a previous injection would have passed through the system and also gave allowance for a constant background concentration reading before and after the passage of the dye.

The data logging rate was set to 26.0417 Hertz. A feature of the logging software that was used for the experimental testing was that the total available data rate of 1kHz was shared between the required waveform channels. It was therefore not always possible to set integer data collection rates. The selected logging rate was chosen as being capable of well defining the shape of the concentration profile at all flow rates with the additional advantage of allowing an entire 10 minute logged file to be held on a Microsoft Excel 5.0 spreadsheet.

3.4 Calibration

The measurement instrumentation was calibrated as described in the following sections both before and after each schedule of tests undertaken at a particular step height configuration. The results were combined to give a calibration equation for the appropriate tests.

3.4.1 Calibration of pressure transducers

The pressure transducers were calibrated by filling the manhole and neighbouring pipework to a series of static water levels. A metal scale was permanently attached to the side of the manhole so that the water depth could be determined by a visual measurement. The electronic voltage output from the pressure transducers was recorded on the CED 1401 data logger at 26.04 Hertz for one minute and the mean value used. A linear regression was applied to the relationship between the water depth in the manhole system and the voltage output given by the pressure transducers and gave a high quality fit to the data. The results of an example calibration are shown in Figure 3.7.

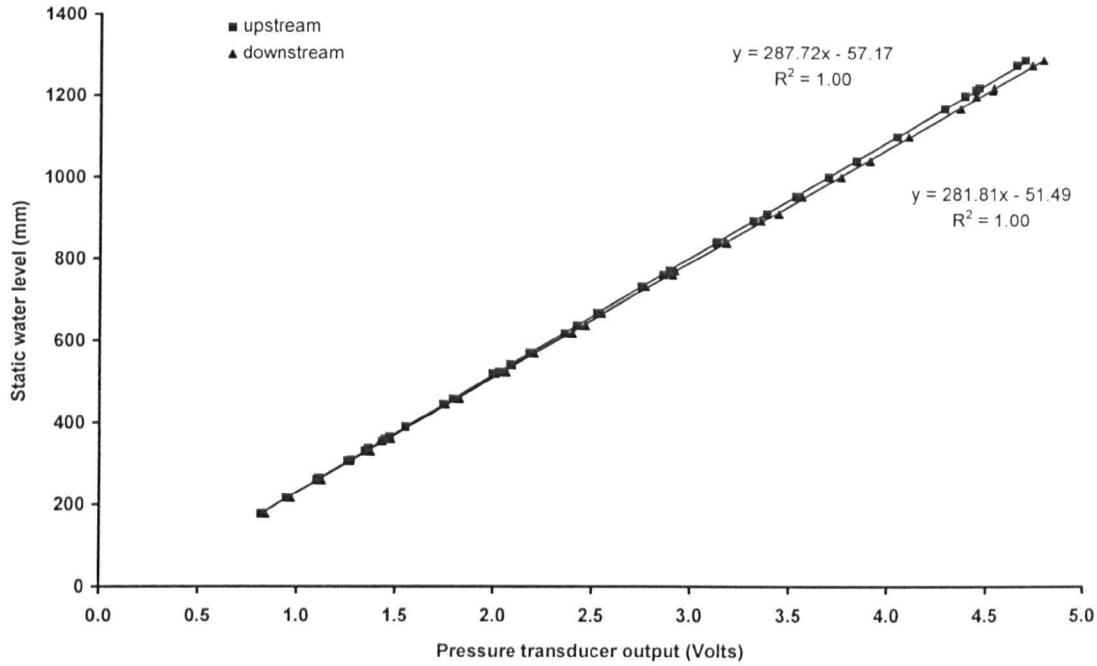

Figure 3.7 Example calibration lines for pressure transducers.

3.4.2 Calibration of fluorometers

Calibration of the fluorometers was achieved with them in-situ on the laboratory manhole apparatus. The manhole and surrounding pipework were blacked out with lightproof material. The upstream delivery pipe was detached from the main water supply system a distance of 3.5 metres from the manhole centreline. A metal plate that included an adapter for the attachment of a length of plastic pipe was fitted at this location. This pipe and a small water pump were used to join the upstream delivery pipe to the downstream surcharge control chamber. Thus a complete flow circuit was achieved with a volume much less than the system as a whole, since the sump and header tank volumes were bypassed. This calibration circuit was filled with a known quantity of water that could be re-circulated by means of the small pump (Figure 3.8).

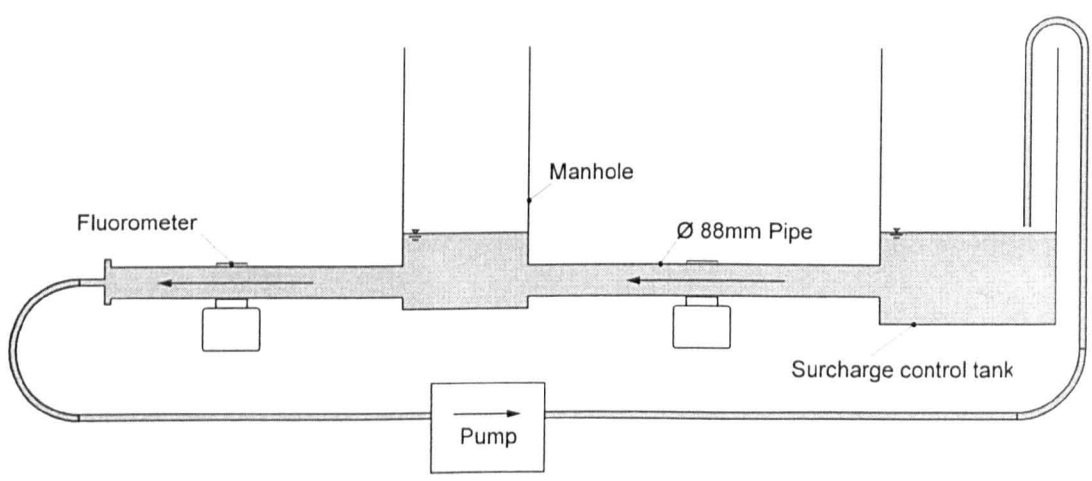

Figure 3.8 Diagram of fluorometer calibration flow circuit.

Measured quantities of Rhodamine WT dye were added, and the system allowed to re-circulate until fully mixed. The time taken for full and complete mixing to be achieved was calculated by a test procedure whereby fluorometer readings were recorded every five minutes, noting the time beyond which both fluorometers gave constant readings. For each calibration concentration the fluorometer output was logged at 26.04 Hertz for one minute and the mean value used. The dye concentration recorded at each time interval was adjusted for the temperature of the water using the equation given by Smart and Laidlaw (1977) for Rhodamine WT dye. This was necessary because the small pump and the room temperature caused a gradual increase in the temperature of the water in the calibration volume.

An example of the calibration results is shown in Figure 3.9. Although it was possible to use the fluorometers on different sensitivity scales, the tracer experiments were completed entirely on a single scale. This simplified calibration and testing, and also prevented the measuring devices from automatically switching sensitivity during any of the experiments.

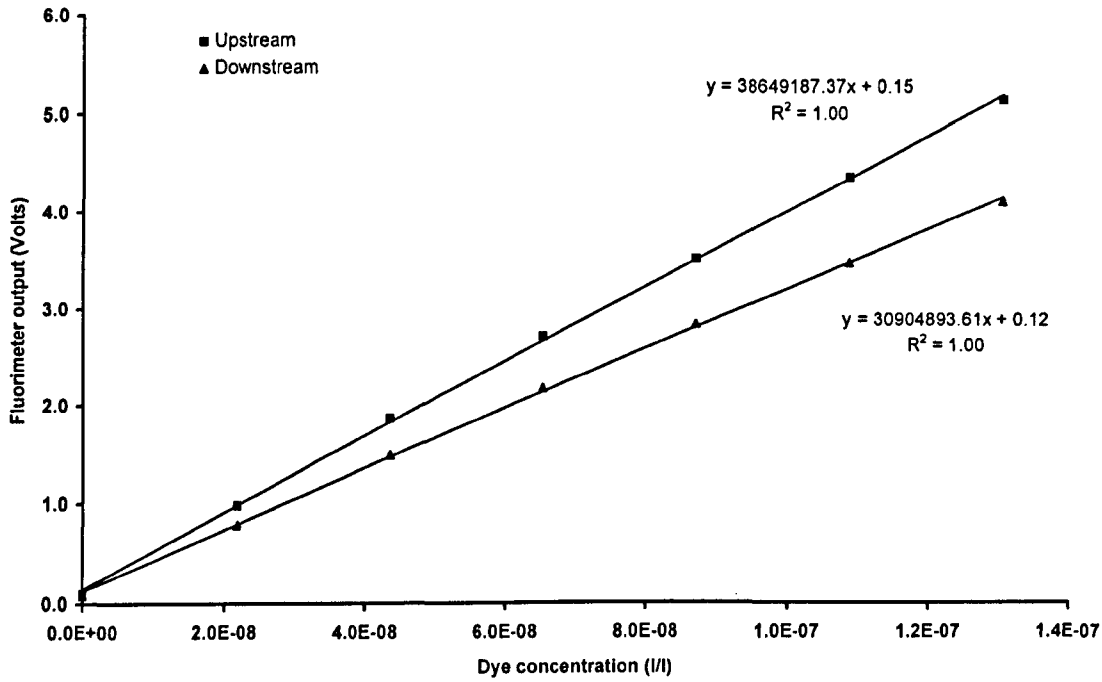

Figure 3.9 Example of calibration for fluorometers (temperature adjusted to 15° Celsius).

Calibration tests using the fluorometer with the adapter fixed in place around the pipe demonstrated that the maximum dye concentration that could be measured accurately was reduced by almost 90 percent from the normal flow through mode (O'Brien, 2000). This was due to the source light intensity being spread over a greater measuring volume. It was still possible to obtain a linear response from the device over a suitable working range, up to 8×10^{-7} litres of dye to litres of water. The fluorometer adapters were assumed to enable measurements of a cross sectional average tracer concentration, although the exact illumination pattern through the pipe was uncertain. Also, flow conditions at the manhole exit may have caused an uneven spread of dye over the downstream cross section. However, the arrangement was superior to any intrusive method on a small scale facility.

3.5 Test preparation

The discharge for a particular test was controlled by a valve that was positioned on the upstream pipe. A rotational scale was attached to the valve so that the degree of rotation could be measured. Unfortunately this valve and scale could not be relied upon to give repeatable flow conditions with sufficient accuracy. This was due to the variations in pressure head difference between the constant head tank and the surcharge levels in the manhole requiring slight adjustments in the valve position to obtain the same flow rate. For this reason the discharge for each test was measured by the V-notch weir and the valve scale was used for guidance only. A limit of 2 percent variation of the measured discharge value from the required value was imposed.

Any adjustments made to the surcharge or discharge required a period of time to allow the system to settle to steady flow conditions. A short test whereby flow rates were measured at one minute intervals after an alteration was used to establish that it took twenty minutes for the flow to settle to a new setting. Flow rates of between 1.0 and 8.0 litres per second were used for the laboratory tests. This was the practical limit of the system. Discharges of less than 1.0 litres per second could not be accurately measured by the V-notch weir and the system was not capable of flow rates much greater than 8.0 litres per second.

3.6 Test procedure

A single test condition of flow rate and surcharge level was established and time given for steady flow conditions to be achieved. For each individual test approximately 25ml of Rhodamine WT fluorescent dye tracer was injected into the upstream delivery pipe, 10.5 metres prior to the manhole, using a manual syringe. The start of data logging and the introduction of the dye were adjusted appropriately to ensure that the first arrival time of the dye at the upstream fluorometer occurred approximately one minute after the start of the logging. In this way a clear period of 30 seconds could be used at the start of the data file to establish the background concentration and the upstream and downstream concentration profiles were recorded in their entirety.

Each dye tracer test for a flow rate and surcharge condition was conducted five times, reduced to three times for the benched manhole tests. This was a suitable number to reduce the effects of any anomalies within an individual test resulting from the manual injection procedure, whilst still giving a practical time scale for the test schedule to be completed. The process of repeating the experiments also allowed the reliability and consistency of the data collection and analysis methods to be assessed. The output from the pressure transducers was recorded for the ten minute duration of an individual test and the mean value was entered into the calibration equation to give the pressure head at that location.

Some previous researchers (Marsalek and Greck, 1988; Kusuda and Arao, 1996) have highlighted the possible errors in taking piezometer readings due to level oscillations. These are caused by rapid pressure fluctuations that occur during observation. In order to reduce the impact of this effect on the final results the high and low point of individual manometers was read three times during any given flow rate and surcharge combination. The average value of the six measurements (three high and three low) was taken as the piezometric pressure head for that location. If there were any air bubbles present in the piezometer system these were allowed to flow out of the flexible tubing before it was attached to the glass piezometer tubes and readings were taken. The flexible rubber tubing

allowed stubborn bubbles to be moved along the pipework by squeezing the pipe upstream of the bubble. The piezometer levels were regularly checked to ensure that they were constant for any given static head in the manhole.

3.7 Test Schedule

The same manhole and pipework was used for all tests in the laboratory schedule, and all used an in line arrangement of the upstream and downstream delivery pipes. The effects of a step height between the upstream and downstream pipes were studied with five step height arrangements in equal steps from 0.0 to 2.0 times the diameter of the pipes (i.e. 0 - 176mm). For each geometrical set-up, a complete range of surcharge and discharge combinations were studied. Surcharge heights up to 1250mm above the downstream pipe soffit were considered, with the lowest surcharge values being governed by the geometry and flow rate, and the 100mm spacing of the overflow weir height adjustment.

The complete set of manhole configurations and flow conditions that have been analysed is presented in Table 3.1. Given that each test configuration was repeated a number of times, almost 2000 individual ten minute periods of data collection were completed.

Step height = 0.0 D, no benching		
Discharge, Q (l/s)	Surcharge range (mm)	Number of tests
1.0	28 - 1127	12
2.0	-	-
3.0	149 - 1148	10
4.0	-	-
5.0	-	-
6.0	207 - 1195	11
7.0	-	-
8.0	168 - 1241	12
Total number of tests		45

Step height = 0.5 D, no benching		
Discharge, Q (l/s)	Surcharge range (mm)	Number of tests
1.0	125 - 1130	11
2.0	138 - 1143	11
3.0	155 - 1162	12
4.0	176 - 1183	12
5.0	203 - 1209	12
6.0	249 - 1242	12
7.0	281 - 1176	11
8.0	322 - 1118	10
Total number of tests		91

Step height = 1.0 D, no benching		
Discharge, Q (l/s)	Surcharge range (mm)	Number of tests
1.0	133 - 1129	11
2.0	151 - 1145	11
3.0	171 - 1169	11
4.0	196 - 1196	11
5.0	146 - 1231	12
6.0	182 - 1170	11
7.0	218 - 1211	11
8.0	282 - 1163	10
Total number of tests		88

Step height = 1.5 D, no benching		
Discharge, Q (l/s)	Surcharge range (mm)	Number of tests
1.0	225 - 831	7
2.0	143 - 846	8
3.0	162 - 869	8
4.0	190 - 896	8
5.0	141 - 931	9
6.0	189 - 975	9
7.0	218 - 1021	9
8.0	278 - 1076	9
Total number of tests		67

Step height = 1.5 D, with benching		
Discharge, Q (l/s)	Surcharge range (mm)	Number of tests
1.0	230 - 731	6
2.0	-	-
3.0	160 - 761	7
4.0	-	-
5.0	-	-
6.0	142 - 841	8
7.0	-	-
8.0	218 - 815	7
Total number of tests		28

Step height = 2.0 D, no benching		
Discharge, Q (l/s)	Surcharge range (mm)	Number of tests
1.0	226 - 1133	10
2.0	242 - 1147	10
3.0	265 - 1069	9
4.0	195 - 1098	10
5.0	231 - 1133	10
6.0	188 - 1174	11
7.0	225 - 1119	10
8.0	274 - 1176	10
Total number of tests		80

Table 3.1 Summary of laboratory tests.

3.8 Laser light sheet visualisation

Visualisation of the mixing within the manhole was achieved using a Laser Induced Fluorescence (LIF) technique developed by Guymer and Harry (1996). The beam from a 300mW Argon-Ion laser was directed to scan rapidly by means of a rotating hexagonal mirror and a parabolic mirror, collectively known as a light sheet generator. This created a parallel sheet of light 500mm wide and only approximately 2mm deep. An angled mirror was positioned beneath the manhole so that the lightsheet illuminated essentially a two-dimensional plane of fluid along the manhole centreline, parallel with the main flow direction (Figure 2.13). The LIF technique required a fluorescent dye to be excited by the energy from the laser light beam, which is emitted over a narrow wavelength band. The excited dye particles fluoresce and emit light of a different wavelength to the laser light with an intensity proportional to the dye concentration. The emitted light was recorded using a sVHS video camera and a high quality recorder. A filter placed in front of the camera lens was used to eliminate the wavelengths of the original laser light and thus leave only the light emitted by the fluorescent tracer. A total blackout of extraneous light was required for this to be successful and was achieved by constructing a blackened hardboard cover over the manhole and surrounding area. A computer combined with digital image processing hardware and software was used to analyse the video tape and convert the image brightness into values of greyness within the range of 0 to 255. The average greyscale values for selected locations within the image area were used in conjunction with calibration measurements to determine the tracer concentrations at specified time intervals.

Unfortunately, under the laboratory conditions for the study of mixing in manholes it was discovered that the laser used was not sufficiently powerful to obtain a well defined resolution of the tracer dye concentration. When the technique had been used previously by Guymer and Harry (1996) the lightsheet generated had been only 150mm in length. Increasing the lightsheet length to 500mm by means of a different parabolic mirror had the effect of spreading the laser power and thus reducing the concentration resolution that was attainable.

However, the technique allowed some qualitative observations of the mixing processes to be made. Images of the tracer dye passing through the surcharged manhole chamber were obtained by using the digitally captured video images and also a 35mm still camera. In the case of the still camera shutter speeds in the region of 0.5 seconds were required to obtain correct exposure and thus the images obtained were effectively an average of the dye flow over the exposure time period.

In addition, further understanding of the flow structures in the manhole was achieved by constantly injecting small diameter polystyrene beads into the flow. The beads were highlighted by the laser lightsheet as they passed through it and reflected the laser light. Using a time lapse method where the camera shutter was held open for an extended length of time enabled the path of the beads to be captured on film with the still camera. A pattern of the flow structure was produced since there were many beads passing through the laser lightsheet in the recorded period of time.

Chapter 4

Experimental Results

4.1 Introduction

The primary aim of the experimental work was to determine the effect of a step height between the inlet and outlet pipes of a circular sewer manhole on the longitudinal dispersion of a solute. Further considerations were the effects of surcharges up to heights significantly greater than had been examined previously, and head loss measurements to establish any possible relationships between the head loss and the transport of a solute through a manhole chamber. Furthermore, Laser Induced Fluorescence (LIF) techniques have been used to enable visual studies to be made of the mixing and retention effects of the manhole and the flow patterns present within it.

The experimental work completed in the laboratory produced raw data that was processed and interpreted to provide results for the head loss, travel time and longitudinal dispersion characteristics of the manhole configurations tested. This chapter explains the methods that were applied to the data collected and presents the results from the manhole step height experiments.

4.2 Processing of laboratory data

Head loss across the manhole was measured using pressure transducers fitted to the delivery pipes upstream and downstream of the manhole. The average of 10 minutes of logging the pressure transducer output at 26.04 Hertz was used to determine the pressure at both transducer locations. A time averaged transducer output value was converted using the calibration equations into pressure head in metres. The difference between the readings for the upstream and downstream transducers gave the head loss between these two points. This measured head loss was a combination of the effects of the manhole and the lengths of pipe either side. The pressure loss due to pipe friction was determined from the results of experiments conducted on a straight length of similar pipe with no manhole present (Guymer and O'Brien, 2000). These results allowed the hydraulic grade line to be extrapolated from the transducer locations to the centre line of the manhole. The vertical difference between the hydraulic grade lines at this central location is the head loss caused by the manhole, over and above the effects of a pipe of length equal to the manhole diameter. This process was completed for the five repeat tests that were conducted for a particular geometry at a given flow rate. The final head loss value for a test condition was taken as the average of the results from the five repeats.

4.3 Optimisation of travel time and longitudinal dispersion coefficients

The longitudinal dispersion due to the manhole was determined by means of analysing the measured upstream and downstream temporal concentration profiles of a fluorescent dye introduced into the

experimental system. This process required determination of the centroid time, $\bar{t}_i$, temporal variance, $\sigma_{t(i)}^2$, and the first arrival time t_i' of the tracer at each site i. The longitudinal dispersion was then initially quantified by calculating the standard longitudinal dispersion coefficients. For the advection dispersion equation (Equation [2.14]) these are the travel time, $\bar{t}$, equal to ($\bar{t}_d$ - $\bar{t}_u$) and the dispersion coefficient, K, (Equation [2.17]). In the case of the aggregated dead zone equation (Equation [2.25]) the required coefficients are the travel time as for the advection dispersion equation and the reach time delay, τ, (t_d' - t_u'). However, downstream concentration predictions made using these standard coefficients were often a poor representation of the effects of the manhole.

A process of optimisation applied to the determination of the coefficients for a longitudinal dispersion model was used to significantly improve the quality of concentration profiles predicted by the models. The measured upstream data was applied as the input to either the advection dispersion equation or a first order aggregated dead zone model. The model coefficients were varied within a suitable range and for each case the longitudinal dispersion equation was applied to the upstream data. For each variation of coefficients the downstream data and prediction were compared to estimate the effects of the changes. Continued adjustment of the coefficients for each model resulted in significant improvements in the ability of the predictions to match the observed downstream data. This procedure was the foundation for the method of optimisation that was incorporated into a computer program.

4.3.1 Data preparation

A pair of FORTRAN software programs were developed and written to facilitate the analysis of the laboratory data and to calculate standard and optimised longitudinal dispersion coefficients. The first of these programs was written to prepare the data for analysis by the second.

The premise behind the formulation of the optimisation software was that it should have the potential to provide analysis for data from a wide range of sources. Although for the work described here it would be used to analyse data collected at two fixed sampling stations the program would be more versatile if it was also applicable to other users. It was therefore decided to have the data required by the analysis software input as individual upstream and downstream data files each containing the time in uniform steps and the measured concentration of the tracer, rather than a single file containing both upstream and downstream data. This broadened the applicability of the software, such that it was used by Guymer *et al* (1999) for analysing data from a laboratory channel where results were required between different combinations of measuring stations.

The data preparation program was written to convert the experimental data logged with the Spike2 data logging software (Cambridge Electronic Design, 1990) into two files suitable for using as upstream and downstream input data to the analysis and optimisation program. An example of the data collected from the upstream and downstream fluorometers is presented in Figure 4.1. For convenience of presentation, the full time scale of the data has been omitted. The voltage output values were calibrated and temperature corrected to give the tracer concentration. It was found that the background concentration of dye within the system tended to increase gradually with time as volumes of dye were added to the re-circulating water volume. A linear variation in background readings was assumed between the mean value of the first 30 seconds of logging and the mean value of the final 30 seconds. This was subtracted from the profiles.

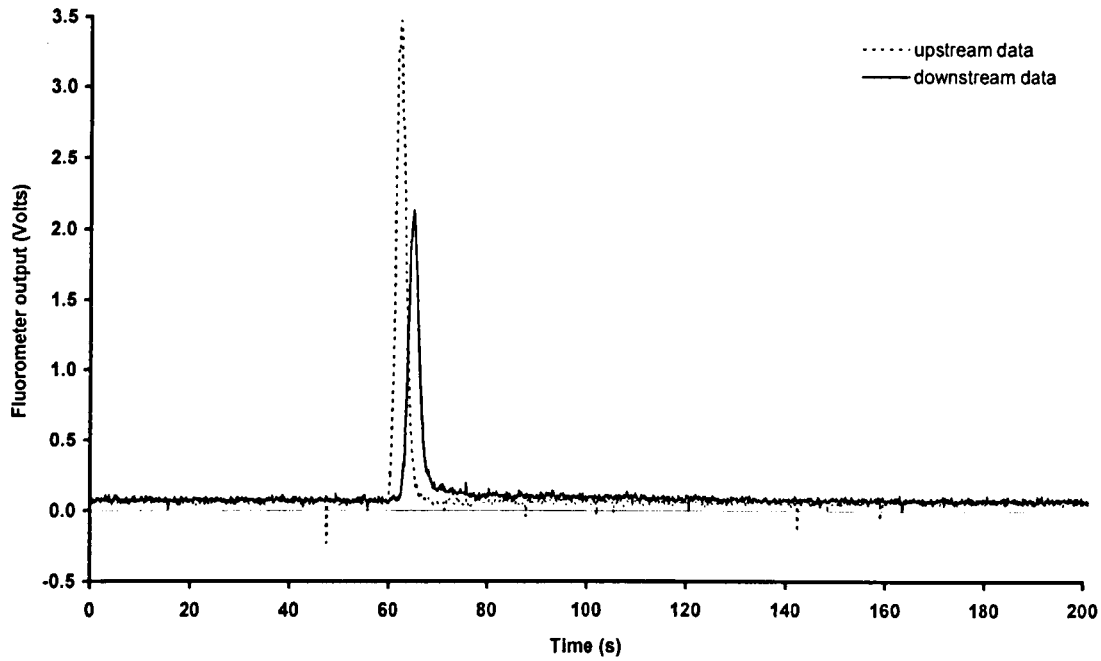

Figure 4.1 Example of manhole dye tracer data collected by upstream and downstream fluorometers (388mm manhole, no step, Q = 6.0l/s, surcharge = 402mm).

Operation of the analysis program revealed that the number of data points in the tracer concentration profiles was too great for the optimisation procedure to run at a reasonable speed. It was therefore decided to reduce the number of data points by sampling the data and so effectively increasing the time step. A sensitivity analysis was completed to ensure that sampling the data had no significant effect on the longitudinal dispersion results. Figure 4.2 shows the results of this analysis. The variation of the ADE and ADZ coefficients with the rate of sampling the data is shown. This variation was checked for both the maximum and minimum discharge, but the results are presented solely for the maximum discharge. This is the more critical case because it has the least number of data points to define the tracer profiles, since the tracer cloud passes the fluorometer in less time. Predominantly there is little variation in the coefficients for effective sampling rates greater than approximately 1.0 Hertz. However, the values for the ADE optimised travel time do tend to continue a gradual decrease in value as the effective sampling rate increases. For this reason the effective rate of sampling chosen was 6.51 Hertz, where all optimised coefficients had settled to almost constant values. This sample rate was equivalent to a data time step of 0.1536 seconds and meant selecting one in every four data points from the original logged file. With this process the operational speed of the software became acceptable. This data sampling procedure was written into the software that prepared the data for analysis.

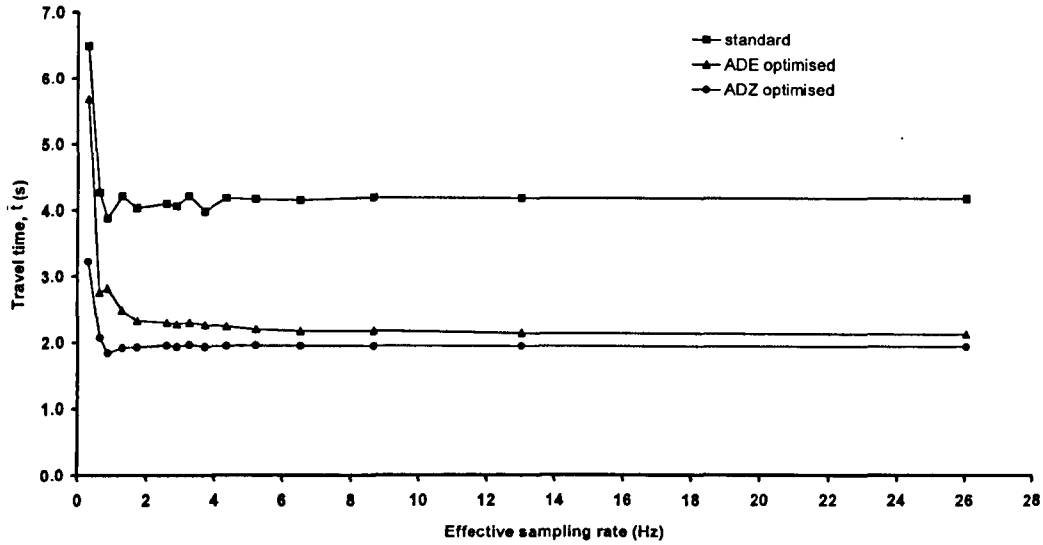

Figure 4.2a Variation of travel time with effective sampling rate.

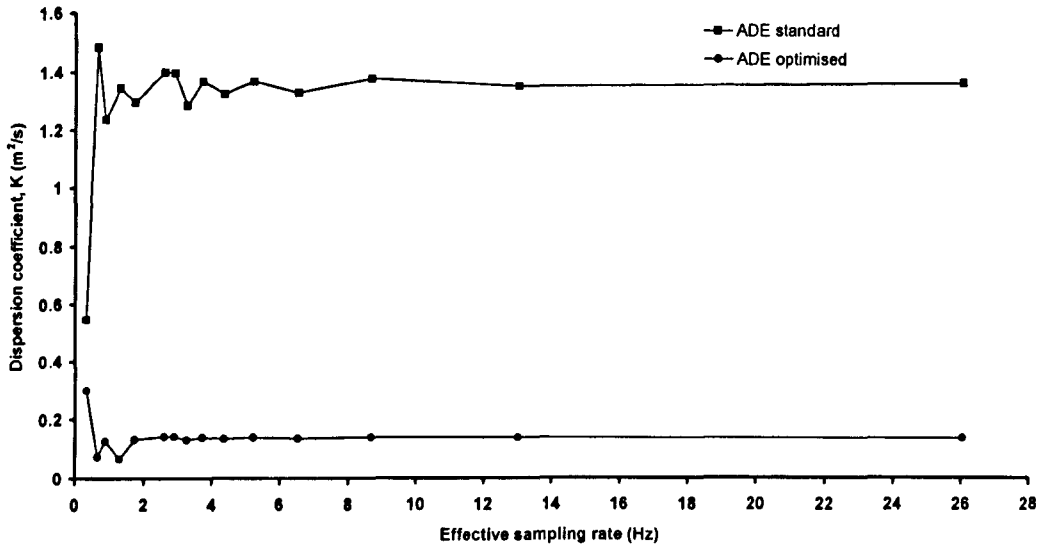

Figure 4.2b Variation of dispersion coefficient with effective sampling rate.

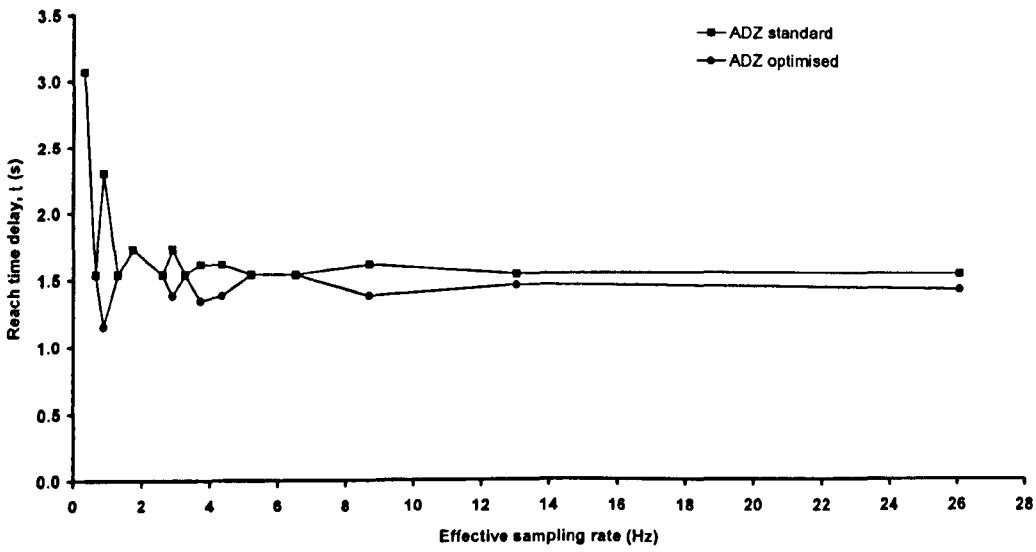

Figure 4.2c Variation of reach time delay with effective sampling rate.

Figure 4.2 Sensitivity analysis for rate of sampling data.

At this stage the requirement for the analysis of the data was that the upstream and downstream profiles needed to be extracted from the entire data recording. This required the determination of the start and end points of each profile. The start point is the time at which tracer from the injection is considered to have first been registered by the fluorometer and the end point is the time at which the last of the tracer cloud has passed the fluorometer. There are several problems to be overcome with this procedure. Firstly, there is a degree of noise associated with the recorded fluorometric data which causes difficulties in establishing an exact time location where the dye concentration is no longer greater than the background concentration. This noise appeared to be unavoidable and was attributed to electrical interference within the fluorometers themselves (O'Brien, 2000). Secondly, a feature of longitudinal dispersion where dead zones are involved is the long tail length of very low concentrations at the end of each profile. This compounds the difficulty in determining the measured end point for the trace from the downstream fluorometer.

Traditional methods of longitudinal dispersion analysis using the advection dispersion equation require the variance of the profiles to be measured and hence the calculation of second moments about the profile centroid is required. Whilst the concentration values for the tail length are very small, they are located at a considerable distance from the centroid and therefore have a profound effect on the second moments. Thus the analysis results are highly sensitive to the chosen time location for the end of the profile, and often the result is an overprediction of the dispersion. Previous researchers (Guymer and O'Brien, 1995; Guymer *et al*, 1996, 1998) have tried several different approaches designed to determine a consistent profile cut off location for all measured profiles. Unfortunately these techniques did not give a high degree of reliability in overcoming the difficulties that were encountered due to the noise on the profile recordings. An analysis procedure was required that would be less sensitive to the actual cut off times on a particular profile. For this reason a process by which the longitudinal dispersion coefficients were optimised to give the best fit to the measured data was used.

The requirement that the analysis method should have a very low sensitivity to the profile start and end points meant that the cut off points could be determined with a simple approach. Working outwards from the peak concentration, the cut off point was selected as the time when 10 consecutive data points were less than one percent of the peak value for that particular profile (Figure 4.3). The number of consecutive points and the percentage cut off were variables that could easily be changed in the program to give suitable start and end points for data from other sources.

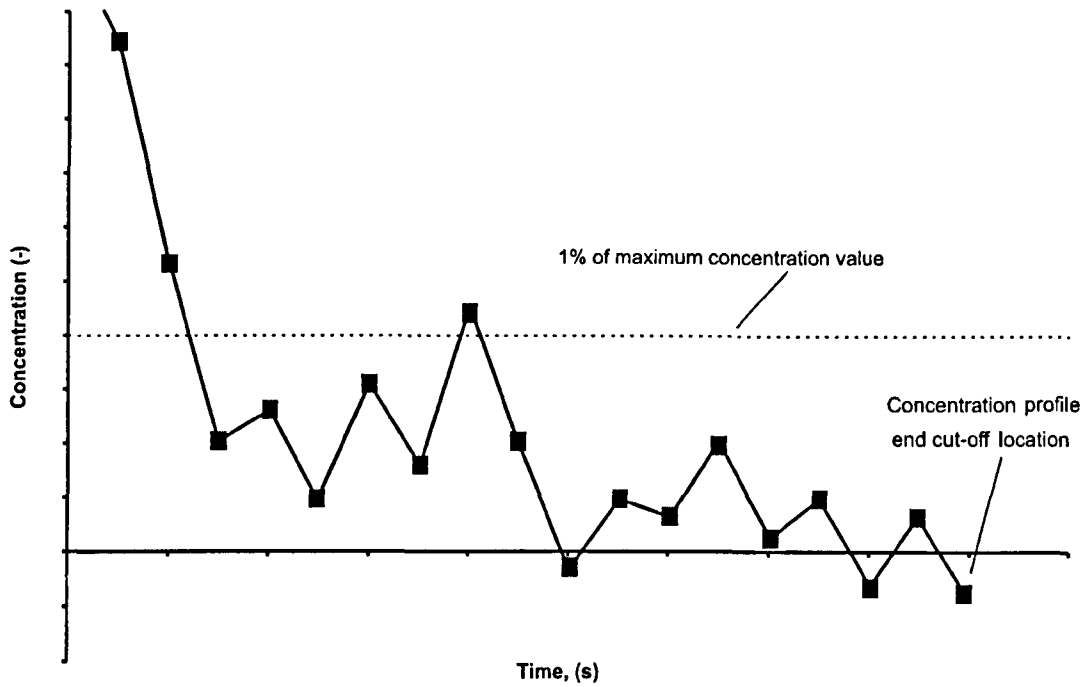

Figure 4.3 Location of temporal concentration profile start and end points.

The sensitivity of the cut off procedure to different percentage values of the peak concentration was examined (Figure 4.4). It was determined that the longitudinal dispersion coefficients calculated in a standard manner directly from the upstream and downstream profiles were highly sensitive to the tracer profile cut off percentage, and hence the cut off location. This is an example of the difficulties faced by earlier researchers in finding a reliable method for extracting the profiles from the raw data. However, using an optimisation procedure for determining the longitudinal dispersion coefficients greatly reduces their sensitivity to the selected start and end points of the tracer profiles. In the case of travel time, there is almost no variation in optimised value for cut off percentages between 0.02 and 10 percent. There is a slight variation for the dispersion coefficient and reach time delay values where small cut off percentages were used. For this reason a low value of 1.0 percent of the peak was selected for the cut off. A value any less than this tended to result in difficulties with the optimisation process being applied due to the noise associated with the data collected.

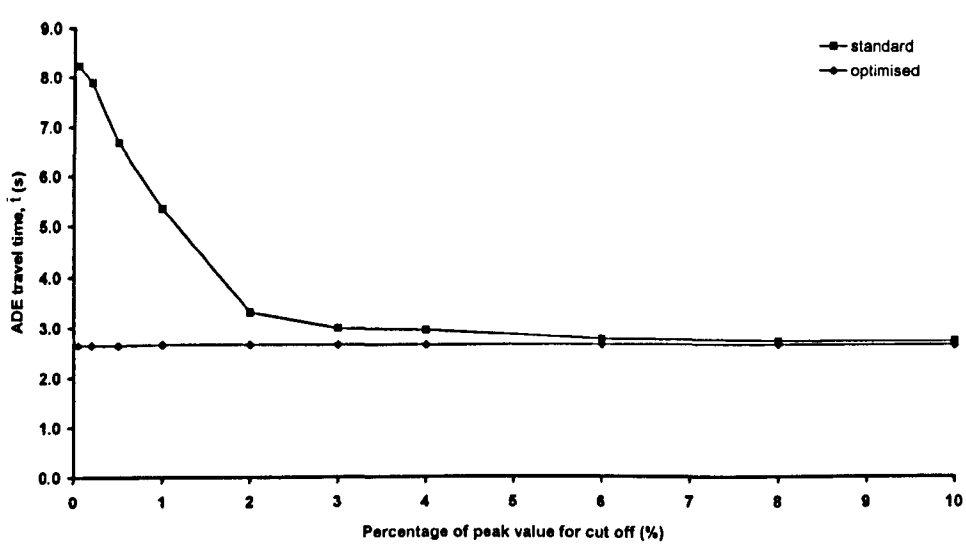

Figure 4.4a Variation of ADE travel time with percentage of peak value for cut off.

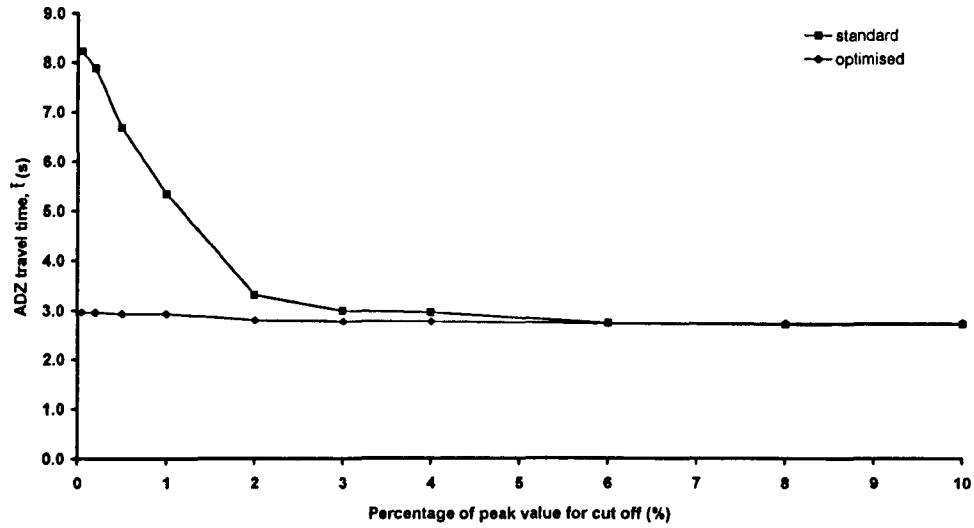

Figure 4.4b Variation of ADZ travel time with percentage of peak value for cut off.

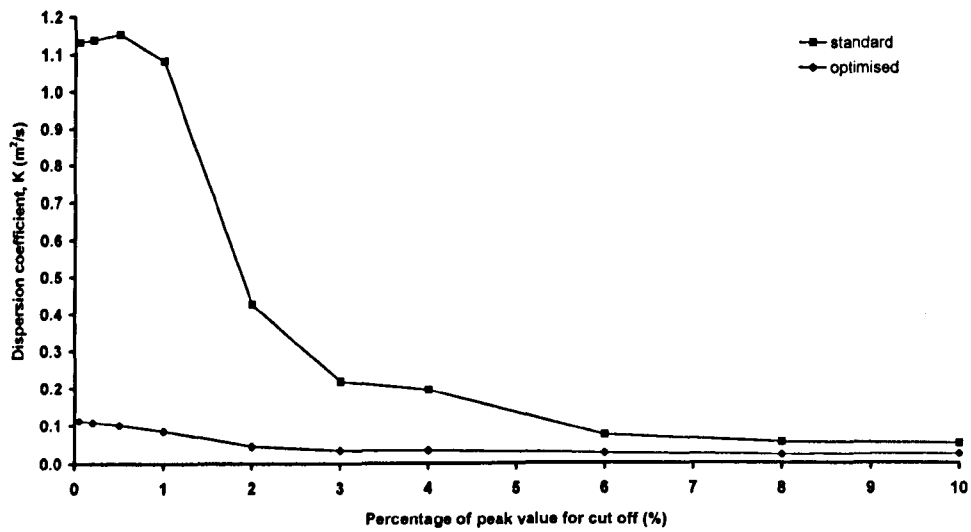

Figure 4.4c Variation of ADE dispersion coefficient with percentage of peak value for cut off.

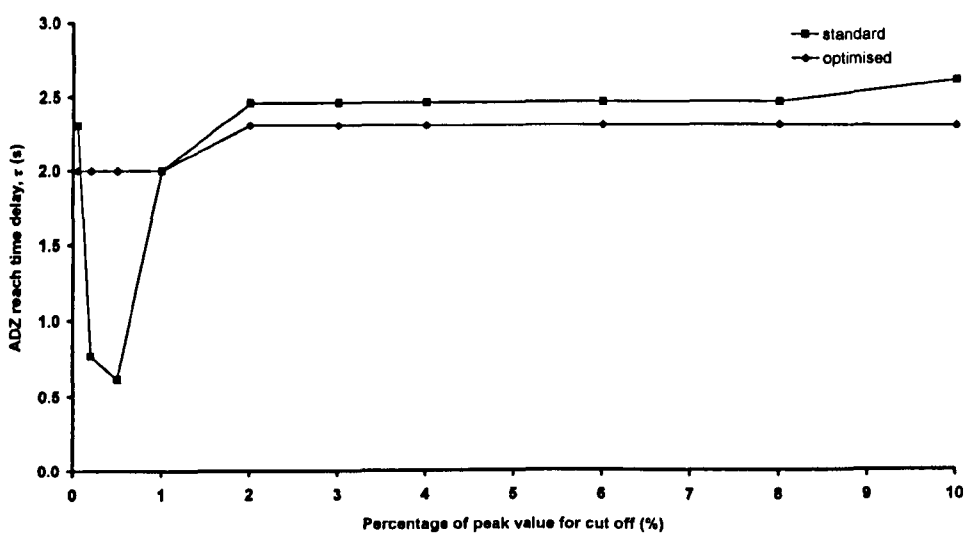

Figure 4.4d Variation of ADZ reach time delay with percentage of peak value for cut off.

Figure 4.4 Sensitivity for profile cut off determination.

An output file was created for both the upstream and downstream locations. Each of these contained data for time and respective concentration values. These data were held in the appropriate format for application into the data analysis program described in the following section.

The data in Figure 4.5, Figure 4.6 and Figure 4.7 show temporal concentration profiles that are fully prepared for the analysis program. Three test combinations of high and low surcharge, maximum and minimum discharge and step height variation are presented. The general shape of the profiles is broadly similar for all of the zero step height manhole tests completed. One of the most obvious features of the profiles is the long tail of low concentration that exists on the downstream profile. This is a common feature of dead zone effects where the dye that mixes with the storage volume is only gradually released back into the main flow after the bulk of the tracer cloud has passed. The introduction of a step height has altered the downstream profile shape that has been recorded. The mass of tracer passing directly to the outlet is reduced considerably and therefore a correspondingly greater proportion is delayed in the storage volume. This causes increased dispersion resulting in a greatly reduced maximum concentration value and a profile tail consisting of a significant proportion of the tracer mass (Figure 4.7).

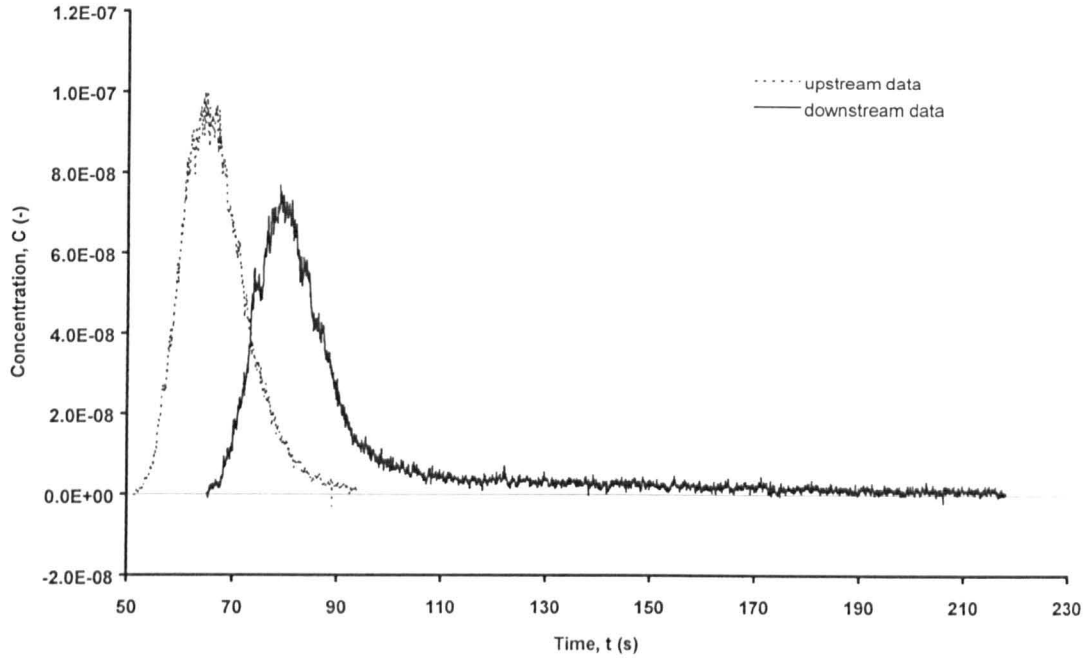

Figure 4.5a Q = 1.0 l/s, surcharge = 127mm

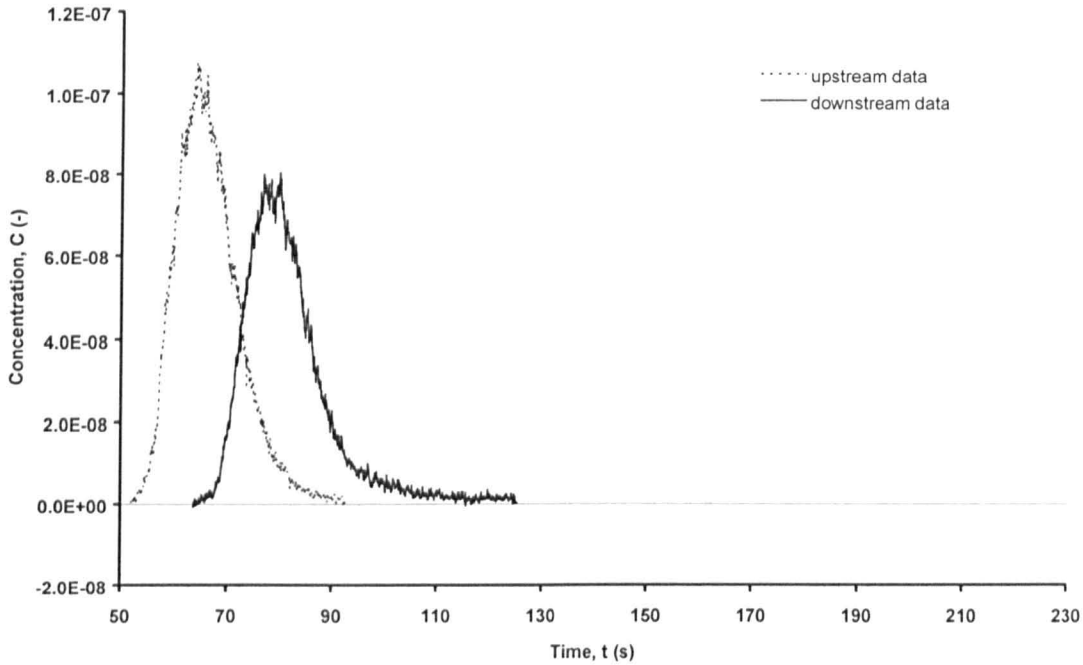

Figure 4.5b Q = 1.0 l/s, surcharge = 1031mm

Figure 4.5 Examples of tracer temporal concentration profiles for variations in surcharge at low discharge (388mm unbenched manhole with no step).

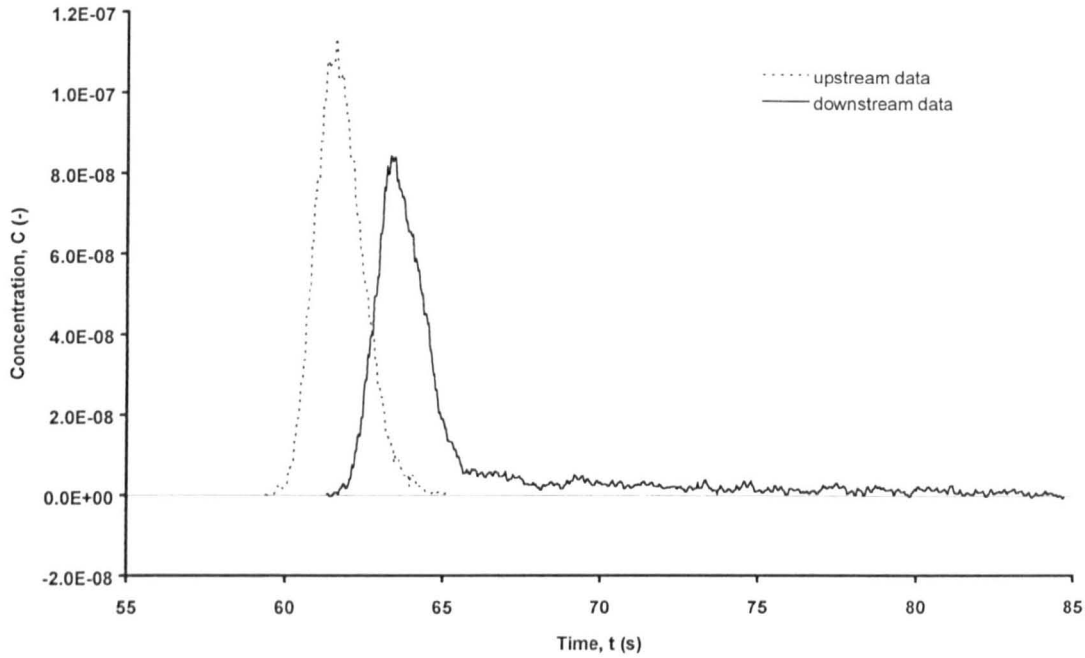

Figure 4.6a Q = 8.0 l/s, surcharge = 168mm

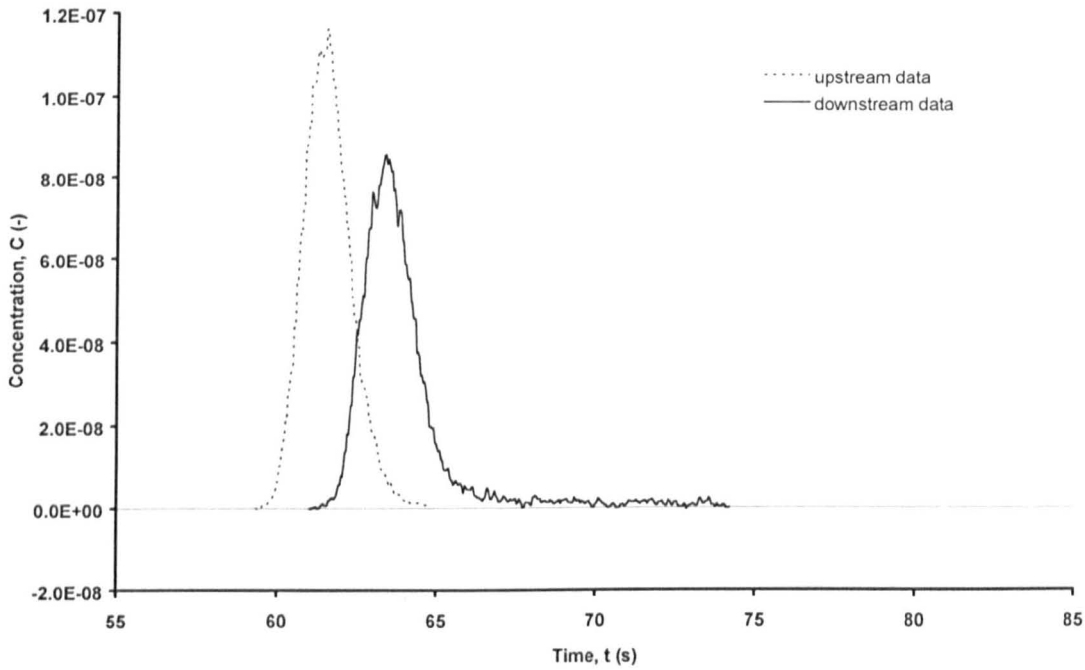

Figure 4.6b Q = 8.0 l/s, surcharge = 1045mm

Figure 4.6 Examples of tracer temporal concentration profiles for variations in surcharge at high discharge (388mm unbenched manhole with no step).

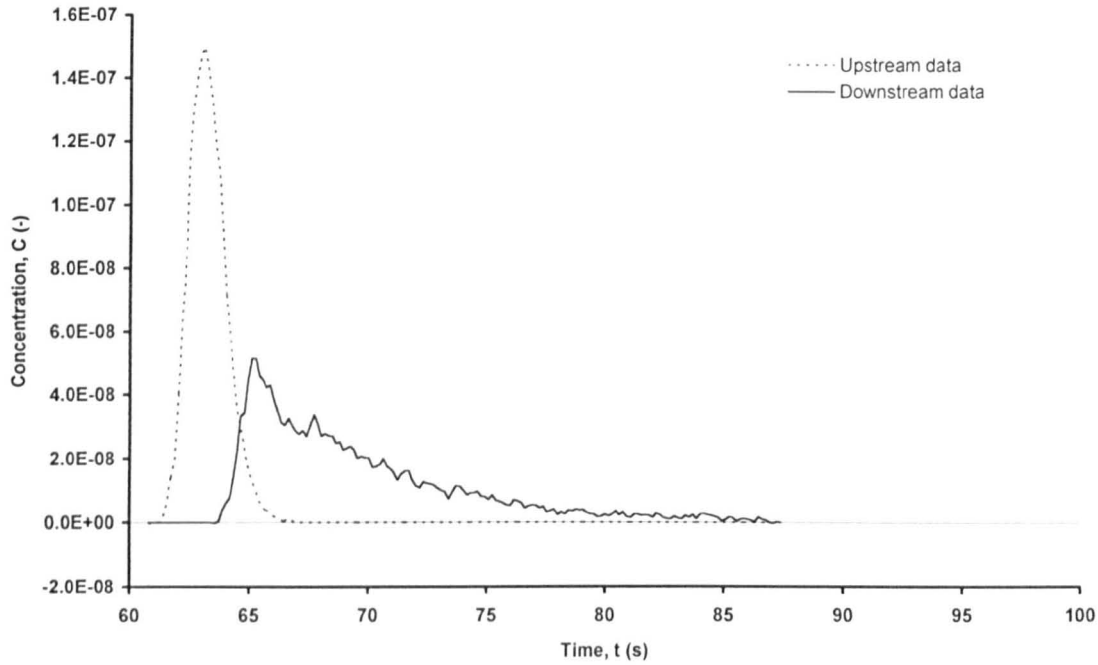

Figure 4.7a Q = 8.0 l/s, surcharge = 278mm

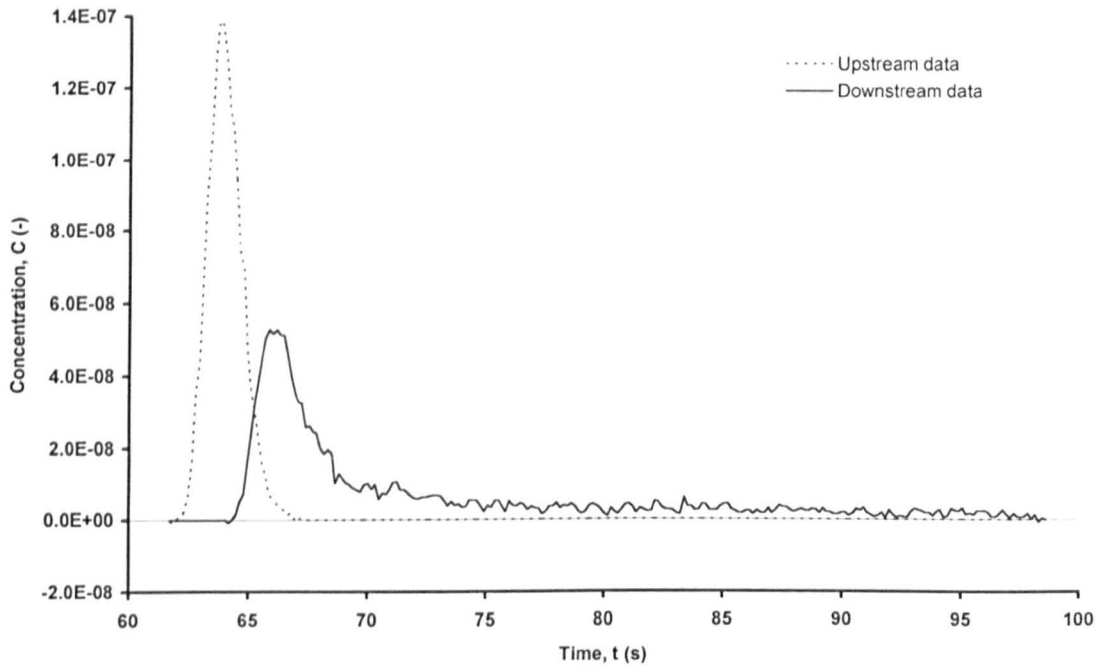

Figure 4.7b Q = 8.0 l/s, surcharge = 1076mm

Figure 4.7 Examples of tracer temporal concentration profiles for variations in surcharge at high discharge (388mm unbenched manhole with 1.5D step).

4.3.2 Data optimisation

Preliminary calculations within the main analysis program ascertained the start and end times of each distribution, and then calculated their area, centroid time and variance. In order that a fair assessment of the longitudinal dispersion modelling equations could be made it was necessary to balance the tracer mass measured at the upstream and downstream locations. This procedure assumed that the tracer was conservative and that the entire tracer mass measured upstream was also measured by the downstream fluorometer. Although this was rarely the case, recovery ratios were generally good and in the region of 90 to 95 percent. Also, the simplest forms of the longitudinal dispersion models assume conservation of the tracer and so it would be inappropriate to compare model predictions that are fully mass balanced with the upstream data to downstream profiles that are not. To achieve mass balance the downstream data points were each multiplied by a mass balance factor calculated from the upstream tracer mass divided by the downstream tracer mass (Equation [4.1]). Since the discharge was equal at the two measurement locations the mass balance factor could be determined from the ratio of the areas under the temporal concentration profiles.

$$B = \frac{Q_u \int_{t=-\infty}^{\infty} C_u dt}{Q_d \int_{t=-\infty}^{\infty} C_d dt} = \frac{\int_{t=-\infty}^{\infty} C_u dt}{\int_{t=-\infty}^{\infty} C_d dt} \qquad [4.1]$$

where B is the mass balance factor.

Adjusting the downstream concentration values in such a way meant deviating from the calibration equation for the downstream fluorometer. However, the calibration was still important to check for a linear response to the tracer concentrations and to ensure that tracer tests were conducted within the calibrated concentration range.

The FORTRAN analysis program calculated the standard and optimised ADE and ADZ coefficients from a given pair of temporal concentration distributions. These are the coefficients that are employed by the advection dispersion equation and the aggregated dead zone method for predicting longitudinal dispersion. The premise behind the software was to make it broad enough to operate with data collected from a wide range of sources, such as laboratory data with very small reach lengths and time steps to field conditions where these values would generally be much greater. This resulted in a program primarily designed for data collected in the laboratory manhole apparatus but with minor changes to the code was sufficiently versatile to calculate results from a variety of data sources.

The calculations of area, centroid and variance were used to determine the standard coefficients for the equations to be calculated. Hence values for centroid travel time, $\bar{t}$, dispersion coefficient, K and reach time delay, τ, were calculated at this stage.

The ADE and ADZ equations (Equation [2.14] and Equation [2.25]) were then used in combination with these standard coefficients in order to produce downstream predictions of concentration profiles from the upstream data. A measure of the goodness of fit (Young *et al*, 1980) between the profiles and the actual data, R_t^2, (Equation [2.38]) was calculated.

For the ADE and ADZ equations the optimisation procedure was very similar and was included

together in the same piece of software. The program performed a sequence of refined searches through combinations of parameters, travel time and dispersion coefficient values for the ADE model, and travel time and time delay values for the ADZ equation, to determine the pair that gave the best fit downstream concentration profile, indicated by the maximum R_t^2 value. A matrix system was used to significantly reduce the number of calculations required to reach the best fit solution. An 11 by 11 matrix was constructed, where the rows were headed by varying values of dispersion or time delay, and the columns were associated with travel times. For each combination of model parameters a downstream profile was predicted from the upstream data using the ADE or ADZ equation in the same way as the standard profiles were created. The R_t^2 value for this prediction was calculated, and assigned to the appropriate cell of the matrix. A total of 121 combinations were required to fill the matrix.

The software initialised a maximum and minimum value for the travel time, time delay and dispersion coefficient parameters at the side of the matrix, and calculated the step size and hence the intermediate values along the matrix boundary. This initial range for the first matrix could easily be altered within the program, and the best option depended upon the actual data. The settings shown in Table 4.1 were found to be appropriate for the laboratory manhole data. The optimisation procedure operated most efficiently if boundary values for the first matrix had a range for each coefficient extending between zero and approximately two times the expected final result. In this way a pair of coefficients likely to yield the best fit prediction represented a cell close to the centre of the first matrix. This generally resulted in the refining procedure locating the optimised results most swiftly. Obviously the expected optimised coefficient value, for example for the travel time, would be different at different flow rates. The most universal set up for the first matrix was thus to use the worst case results for the 1.0 litres per second tests and therefore the matrix would encompass the results for other test discharges.

	Minimum	Maximum
Travel time	0.0 s	30.0 s
Dispersion coefficient	0.0 m^2/s	2.0 m^2/s
Time delay	0.0 s	30.0 s (approximately)

Table 4.1 Boundary settings for first optimisation matrix calculation.

In the discrete form of the ADZ model (Equation [2.25]) it is only possible to apply values of the time delay, τ, that are multiples of the data time step. The program had to ensure that all time delay values used along the matrix boundary were exact multiples of the time step. Therefore the maximum time delay for the initial matrix was set at approximately 30.0 seconds but it was increased or decreased as necessary to ensure that the time delay steps along the matrix boundary all fitted the criteria imposed.

At this stage the contents of the calculated optimisation matrix were examined and the combination of coefficients that gave the prediction with the best fit to the downstream data, represented by the cell with the greatest R_t^2 value assigned to it, were determined. A new matrix was created by the software that 'zoomed in' towards the best fit coefficients. Where the cell representing the best fit coefficients was not on an edge of the matrix a new matrix could be generated whose boundaries were defined by the coefficients immediately either side of the best fit values. This refining procedure

is illustrated in Figure 4.8. However, if the maximum R_t^2 was calculated to be on an edge of the matrix then there was the possibility that a better downstream profile prediction might be achieved with coefficients out of the range of the current matrix. Therefore, in this case, a new matrix was generated which did not 'zoom in' further but had boundary coefficient values adjusted so as to translate the matrix and establish a maximum R_t^2 value within the new boundaries.

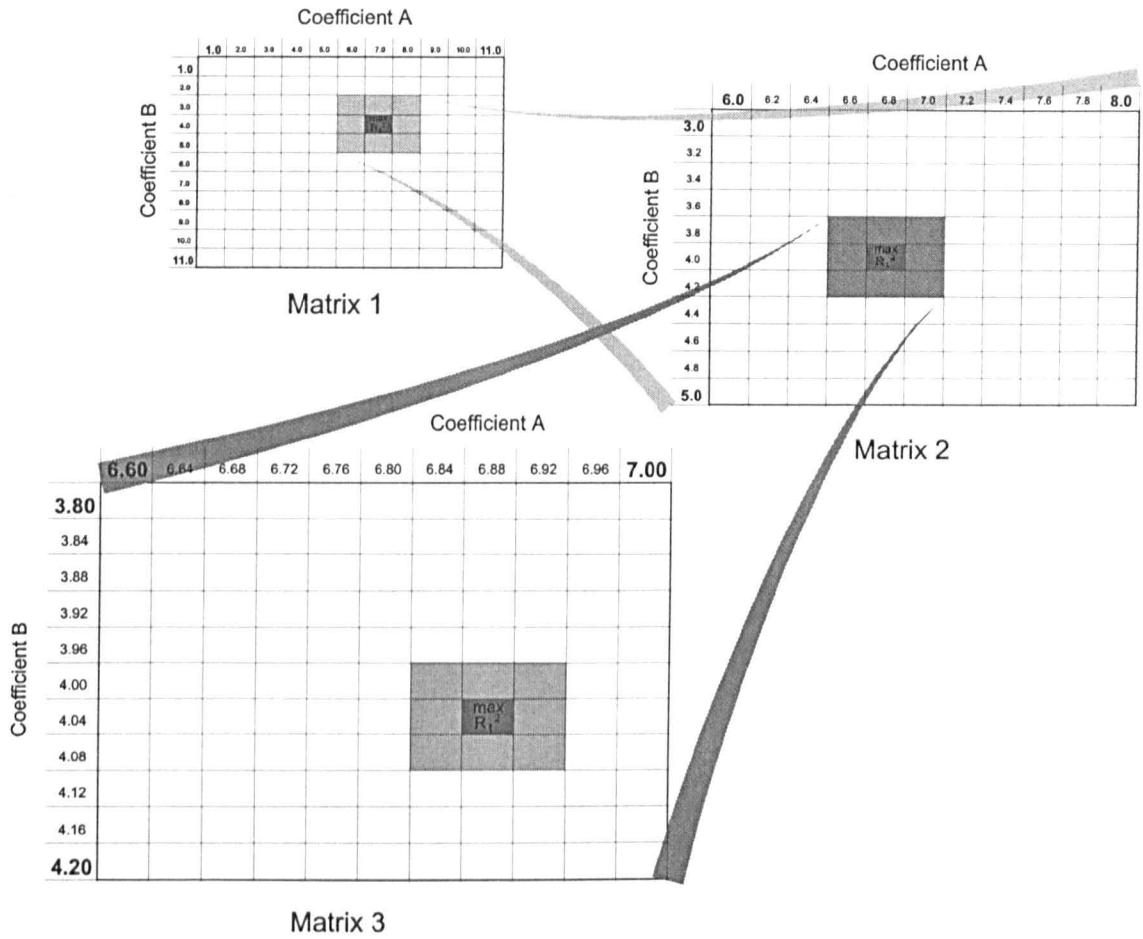

Figure 4.8 Representation of the matrix optimisation procedure.

The process of producing a new matrix was repeated until a predetermined final resolution was attained. This was done by checking the step sizes between coefficients along the matrix edge each time a new matrix was generated and when these were reduced to certain minimum values for the coefficients the ultimate best fit prediction was said to have been found.

In a similar way to the definition of the first matrix range, the ultimate resolution values could be adjusted within the program depending on requirements from the data analysis. Default settings are given in Table 4.2. These values were determined by examining the output from some sample test results used during the construction of the software. It was found that the benched manhole results produced the minimum travel time values, close to 1.0 seconds, and dispersion coefficient values, approximately $0.01 m^2/s$. The ultimate resolution of the matrix analysis was therefore set to one percent of these values, giving a good level of accuracy and reasonable processing times. In the case of the reach time delay, if the step size between the values along the matrix became less than the data time step it was set as equal to the data time step, and the final resolution for time delay was said to have been reached.

Coefficient	Ultimate resolution
Travel time steps	0.01 s
Dispersion coefficient steps	0.0001 m^2/s
Time delay steps	data time step (Δt)

Table 4.2 Ultimate resolution values for matrix boundary coefficients.

For the optimisation technique to be reliable it was essential to verify that there was a unique pair of parameters that gave the best fit of the prediction to the measured data. It was confirmed by the work of Antonopoulos (1997) and preliminary studies that there was only a single best fit combination of parameters for a given data set. This was determined by examining the R_t^2 values over the entire matrix and ensuring that there was only one peak value. Figure 4.9 displays the results for this procedure using laboratory manhole data and the ADZ model. The base of each chart in the figure is composed of the travel time and time delay values used in the matrix. The three-dimensional surface represents the R_t^2 values for each travel time and time delay combination on the base. It is clear in Figure 4.9a that there is a single peak in the R_t^2 values given by the parameter combination that produces an ADZ model prediction with the best fit to the data. Figure 4.9b presents the results under the circumstances where the matrix is at the ultimate resolution. The time delay scale, governed by the time step at which the data was recorded, spans a greater range than the travel time scale. This explains the shape of the three-dimensional surface, whose curvature is considerably more pronounced in one direction than the other. However, there is a single maximum value of R_t^2, in this case given by a travel time of 3.0 seconds and a reach time delay of 2.073 seconds.

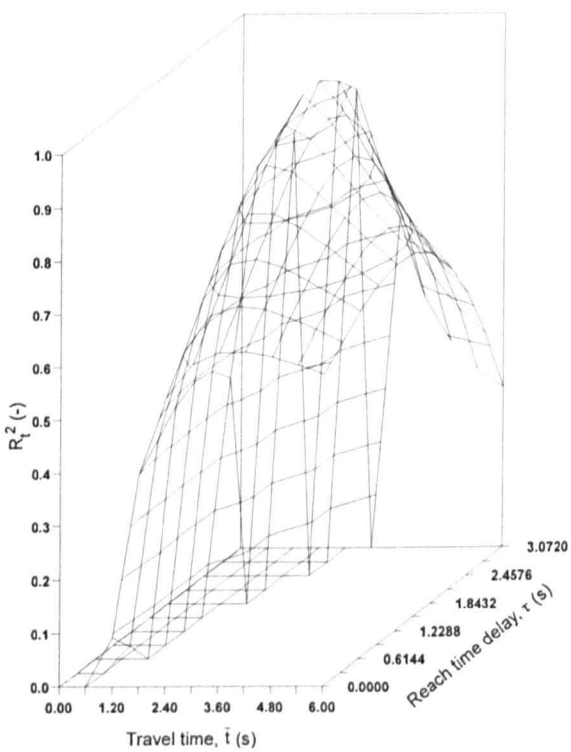

Figure 4.9a

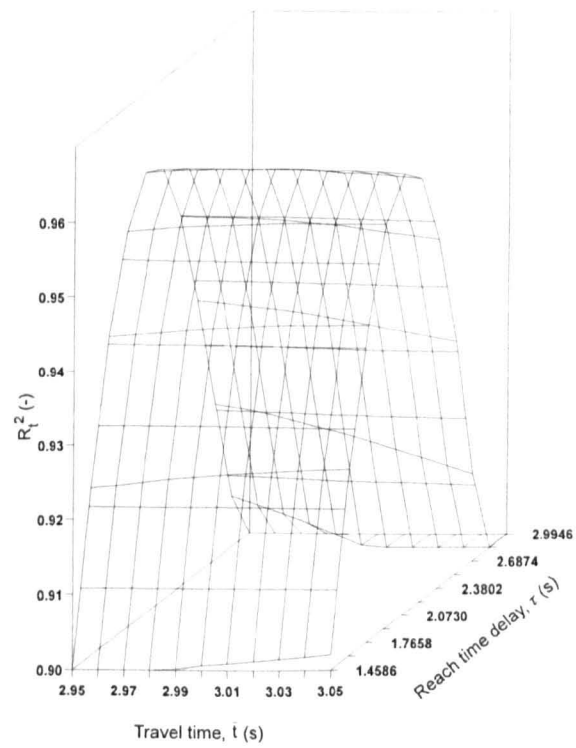

Figure 4.9b

Figure 4.9 3-D surface representation of matrix optimisation results.

When the optimisation procedures had been completed an output file was created. Information written to the output file included the data filenames, measuring station distance and mass balance factor. All the standard and optimised coefficients were given, along with the R_t^2 values for each case. Also, the full data sets for time and concentration were output, enabling the upstream data, downstream data, and standard and optimised predictions to be compared.

Figure 4.10 and Figure 4.11 provide a comparison between the downstream temporal concentration profiles predicted from measured upstream data using standard methods and optimisation. It is clear that the standard predictions made with the ADE and ADZ models give a very poor representation of the measured data. In both cases the dispersion is considerably overestimated, predicting a peak concentration well below the measured value. The justification for optimising the coefficients is clear. The optimisation procedure used has significantly improved the accuracy and reliability of the longitudinal dispersion predictions. With optimised coefficients, both of the models demonstrate a good capability to describe the measured downstream profiles. The peak value and time of occurrence is well represented. Although the full tail effect fails to be reproduced, the optimised predictions successfully account for the majority of the tracer mass.

The variation of the results over the repeat tests was examined (Figure 4.12). The optimisation process was found to be essential in order to obtain reliable and consistent results. This is most clearly demonstrated by the dispersion coefficient results (Figure 4.12b) where the spread of the data for the repeat tests is considerably reduced when optimisation is used. The data in the figure show that determining the dispersion coefficient by a standard procedure using the variance of the upstream and downstream profiles (Equation [2.17]) is inappropriate where a long tail of low concentration distorts the calculation. Similar problems are apparent with the other coefficients. The close grouping of the optimised data suggests that the process can yield consistent results regardless of potential anomalies in the manual injection of tracer or the data measurement and preparation.

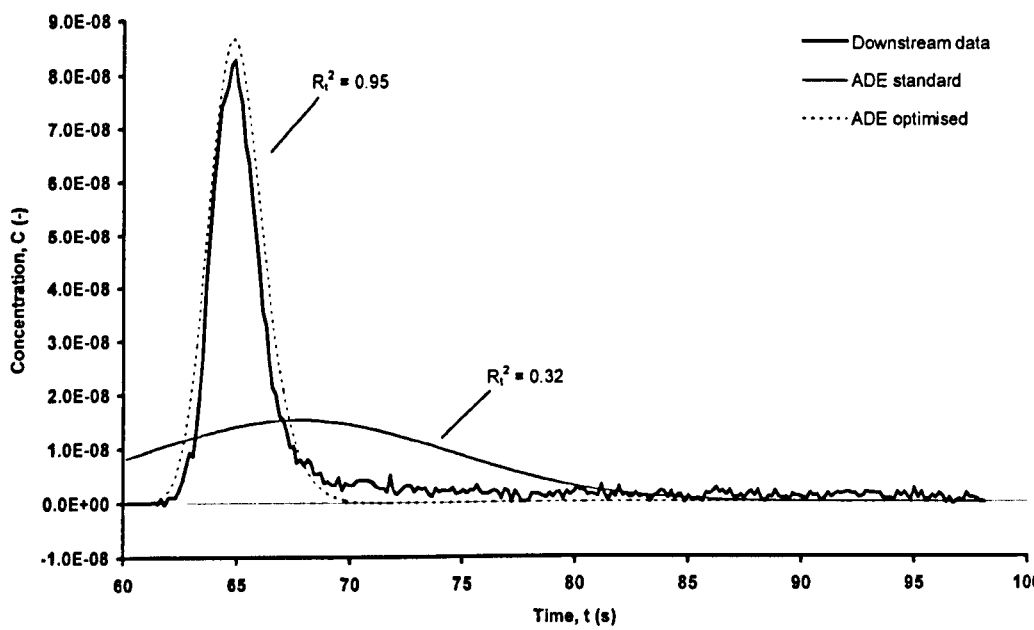

Figure 4.10 Measured downstream temporal concentration profile with ADE predictions. (388mm manhole with no step, Q = 6.0l/s, surcharge = 402mm).

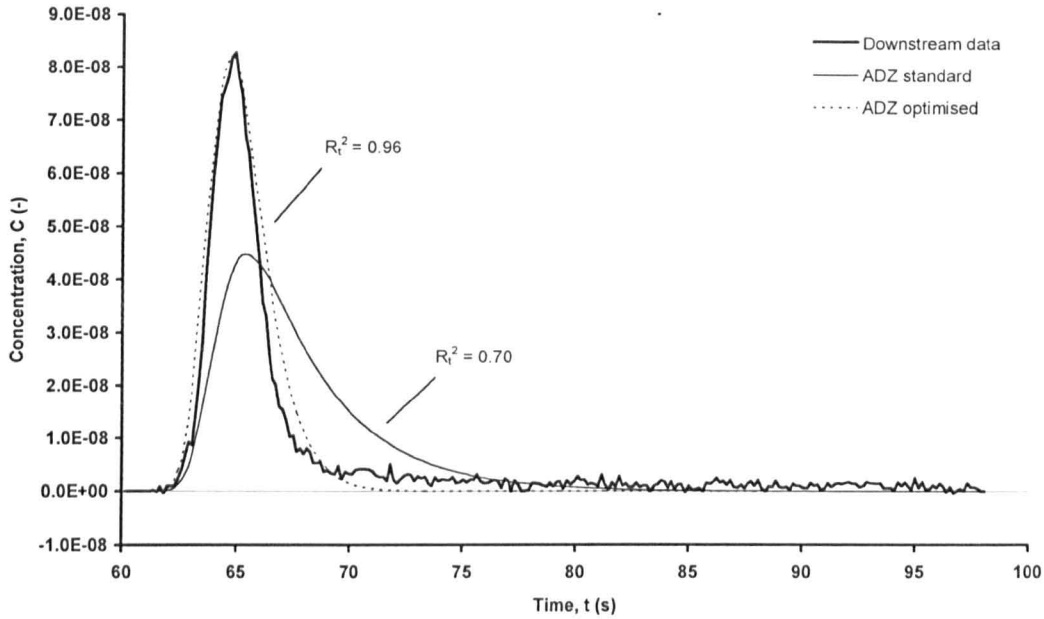

Figure 4.11 Measured downstream temporal concentration profile with ADZ predictions (388mm manhole with no step, Q = 6.0l/s, surcharge = 402mm).

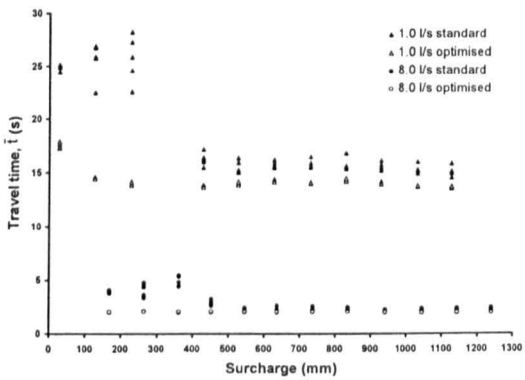

Figure 4.12a ADE travel time

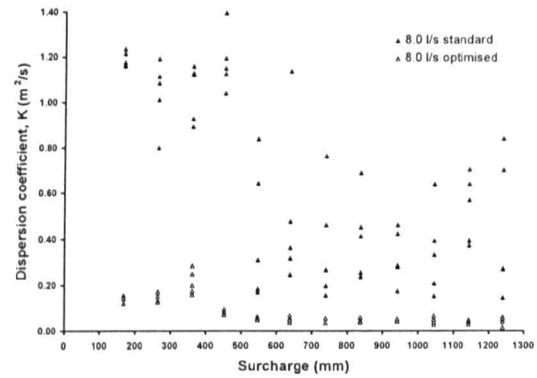

Figure 4.12b Dispersion coefficient

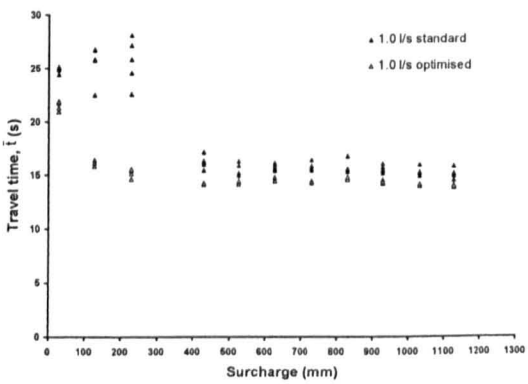

Figure 4.12c ADZ travel time

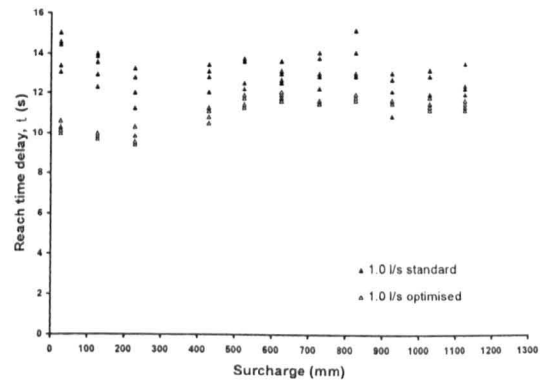

Figure 4.12d Reach time delay

Figure 4.12 Longitudinal dispersion coefficients from 5 repeat tests with standard and optimised analysis (388mm manhole with no step).

4.4 Laboratory results

4.4.1 Flow regimes

Throughout the laboratory test procedures a description of the flow regime present in the manhole for each combination of discharge, surcharge and geometry conditions was recorded. It became appropriate to use 5 different descriptions, numbered 1 to 5 and described below.

1 Very calm conditions. Difficult to discern movement.
2 Slight surface movement with small surface ripples present.
3 Surface movement obvious. At the downstream side of the manhole a distortion of the water surface which rises above the general water surface level is noticeable.
4 Movement is rapid and rather chaotic. The surface is broken at times with small whirls causing bubbles to appear on the surface and occasionally in the flow volume.
5 Vigorous movement. The downstream surface distortion is a steeply formed wave, causing the surface to be continuously broken. Bubbles and whirls almost continuously on the surface and within the manhole volume.

The photographs in Figure 4.13 to Figure 4.17 show these flow conditions. The circulation regimes were affected by several factors such as the flow rate, the surcharge level, the step height and the presence of benching. Figure 4.18 and Figure 4.19 show a record of the circulation regime descriptions for different surcharge levels and discharges at two step height conditions. It can be seen that the degree of vigorous movement of the water in the manhole increases as the flow rate increases. Where the surcharge is greater, it appears that the extra volume of water acts to damp out the surface fluctuations. The presence of a step height causes the incoming flow to impact on the downstream wall of the chamber. This gives rise to more severe flow conditions in comparison with the zero step case.

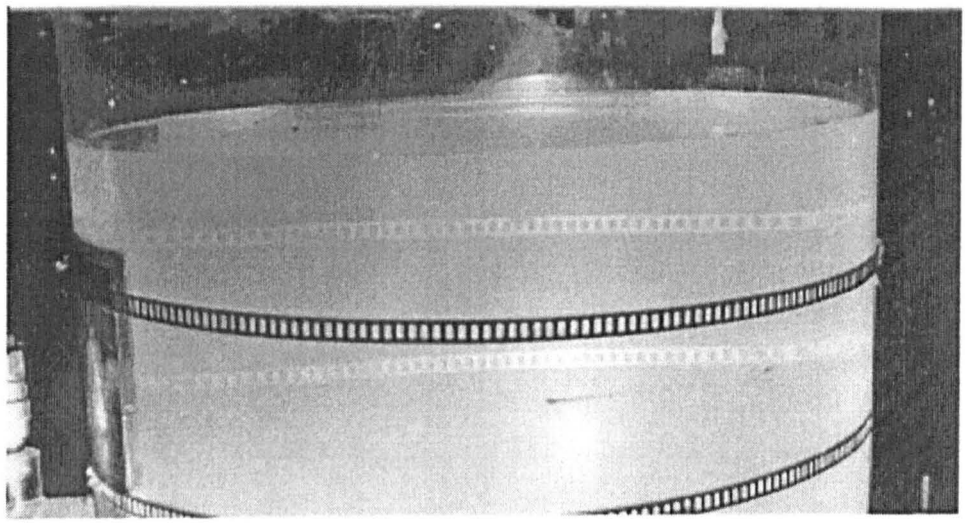

Figure 4.13 Flow condition 1.

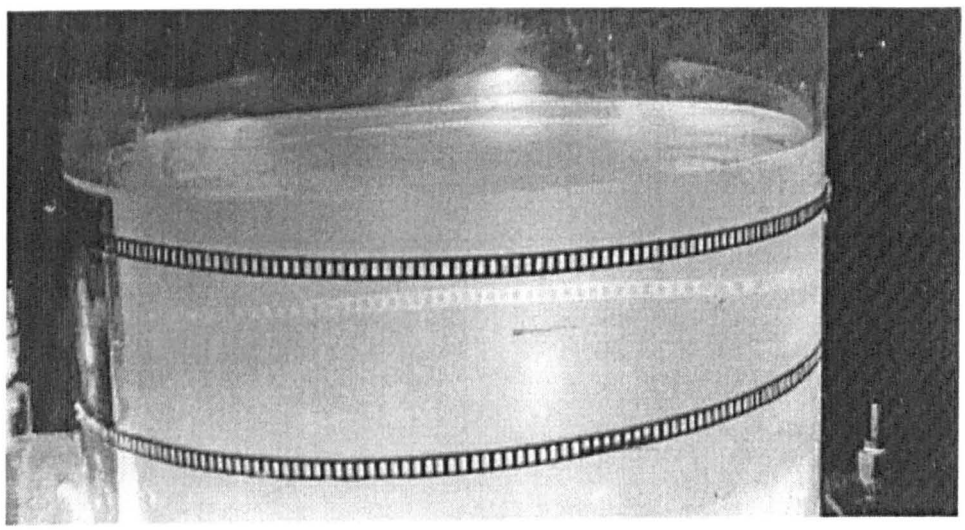

Figure 4.14 Flow condition 2.

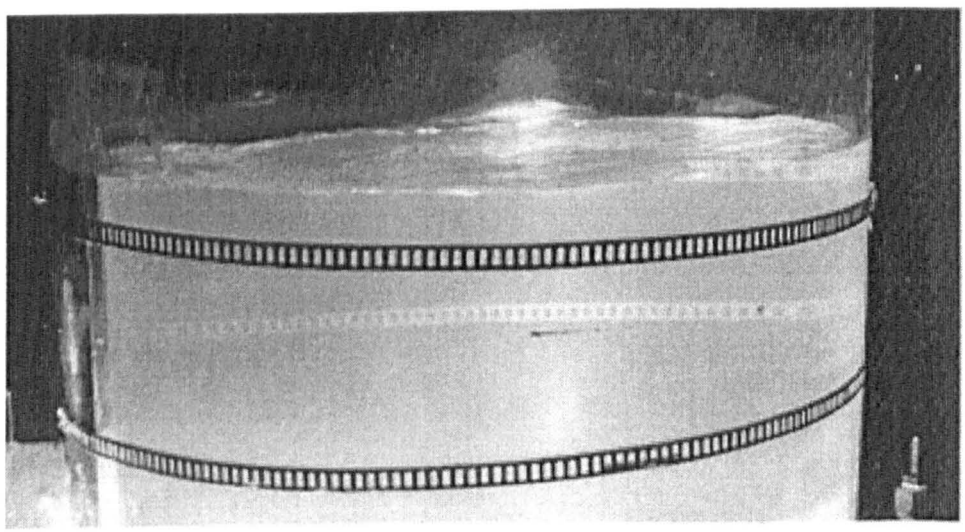

Figure 4.15 Flow condition 3.

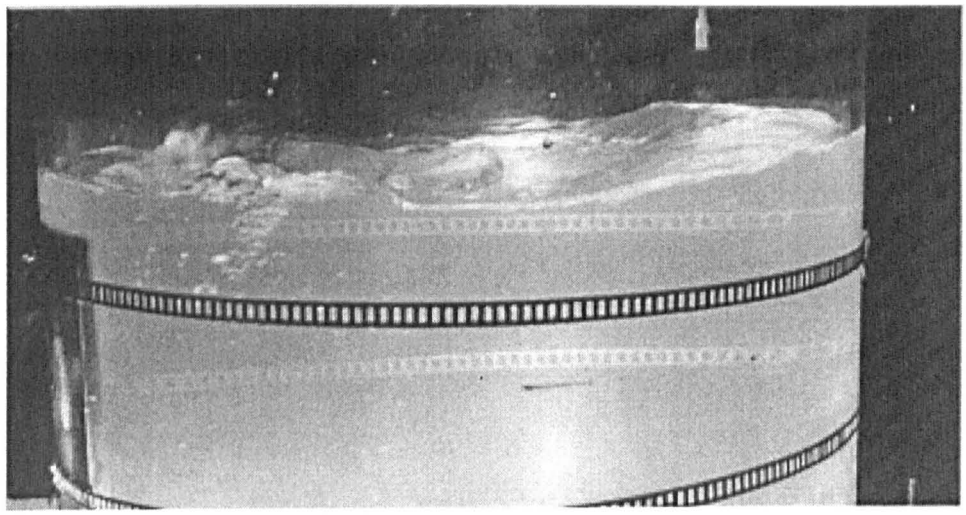

Figure 4.16 Flow condition 4.

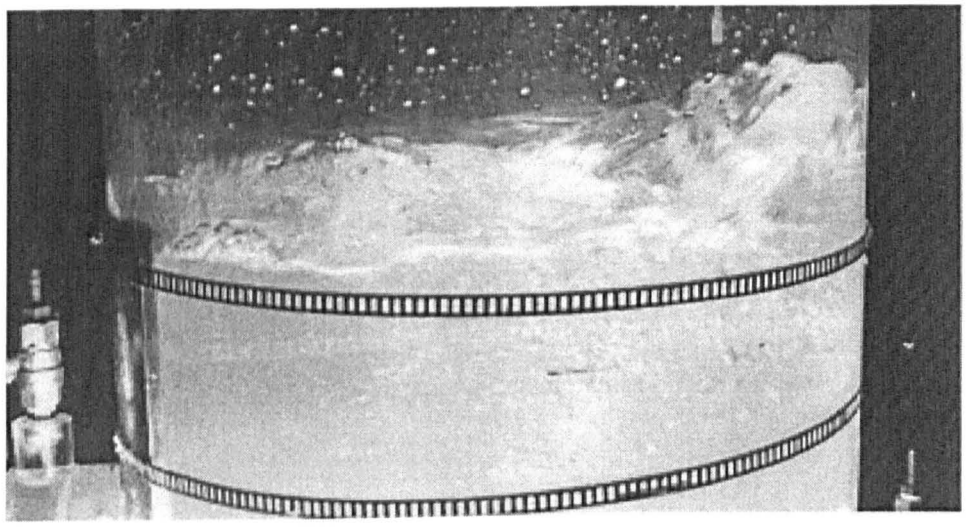

Figure 4.17 Flow condition 5.

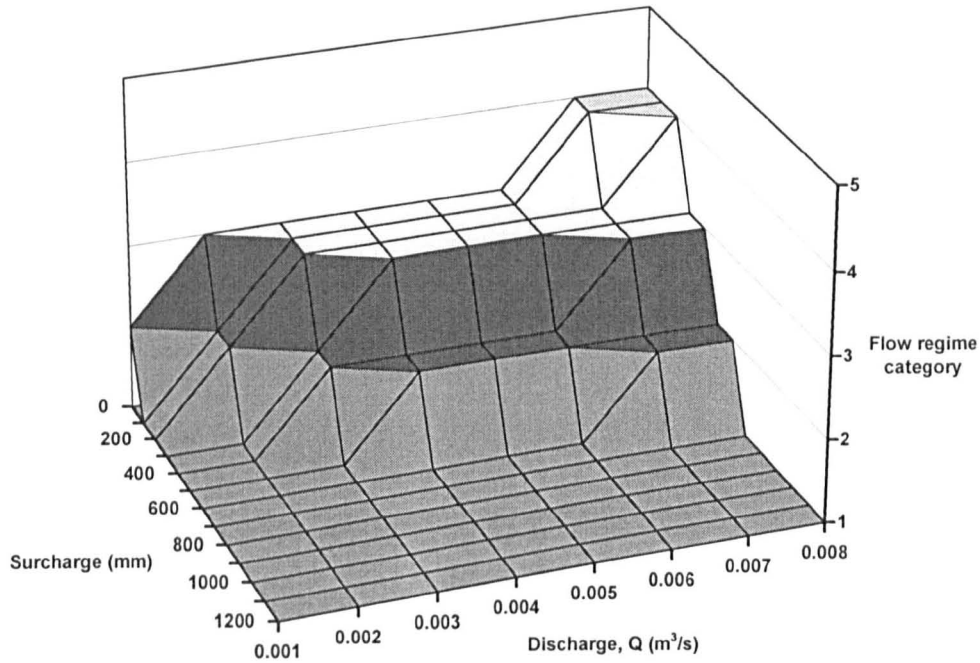

Figure 4.18 Flow condition variation with surcharge and discharge (step=0.0D).

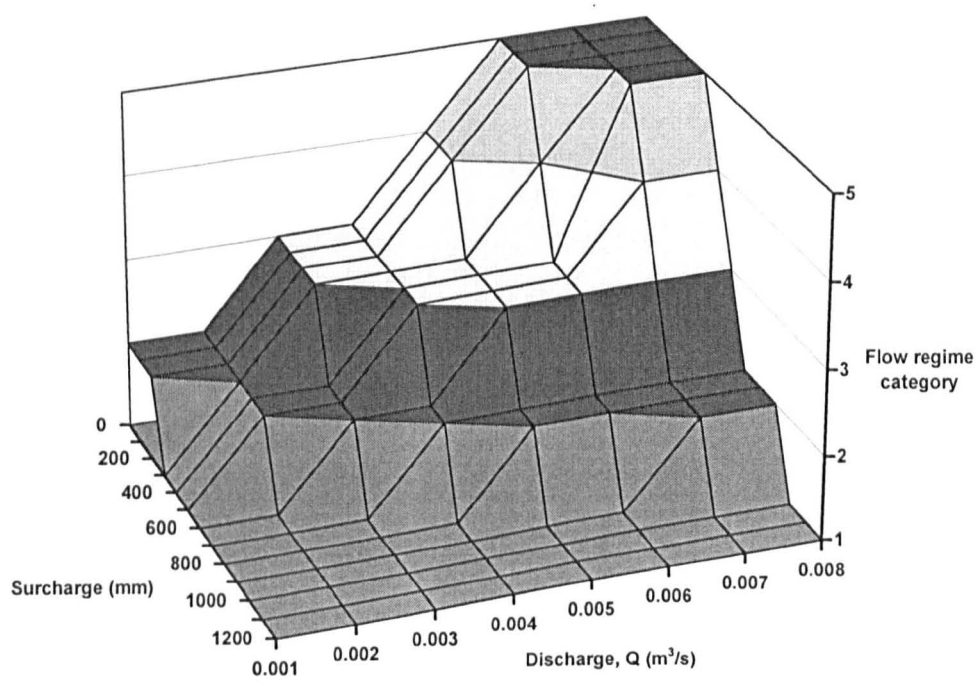

Figure 4.19 Flow condition variation with surcharge and discharge (step=2.0D).

4.4.2 Head loss results

Results are presented in Figure 4.20 for the variation of the head loss with surcharge for the 388mm manhole at all tested step heights. The data in the figure show the head loss at the different flow rates that were tested. In general the head loss that occurs due to the manhole is almost independent of surcharge over the range tested.

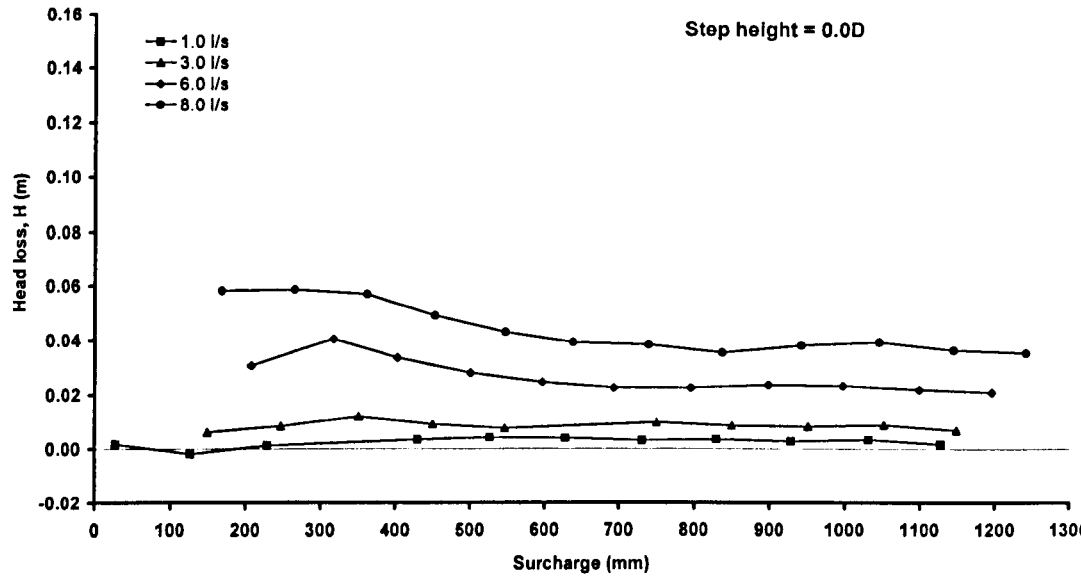

Figure 4.20a

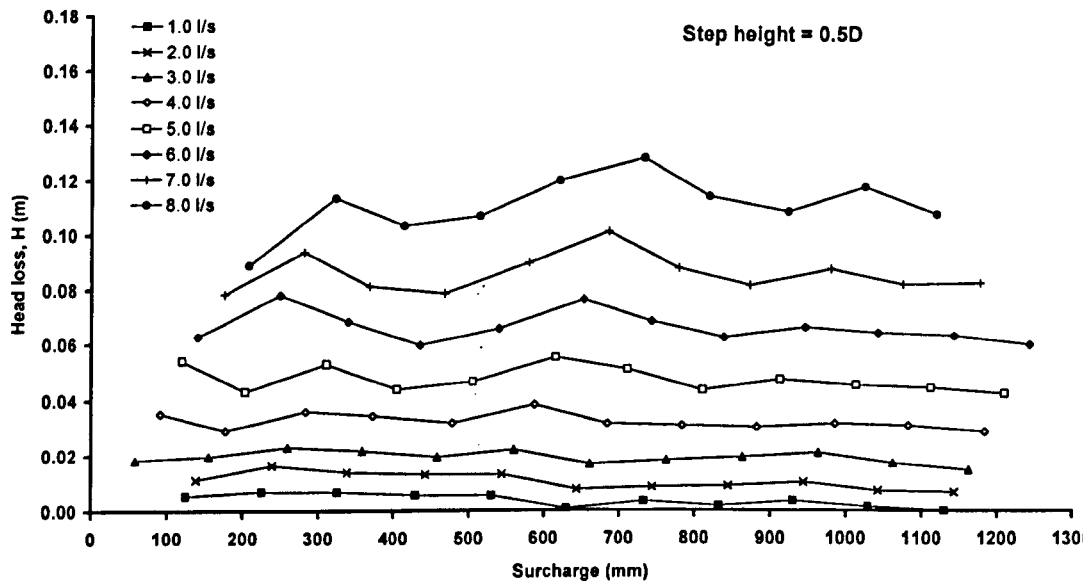

Figure 4.20b

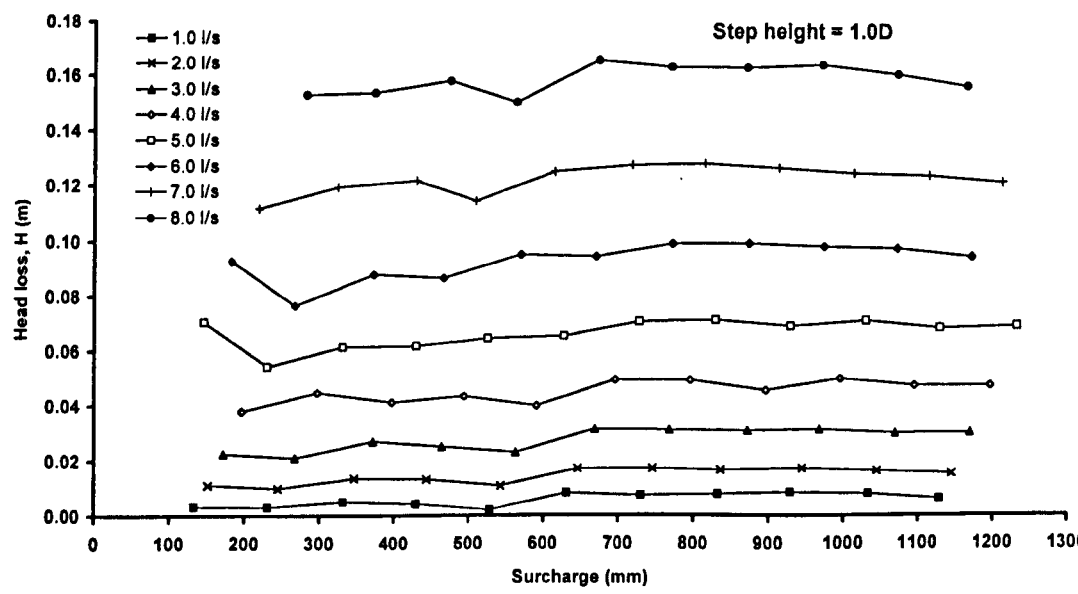

Figure 4.20c

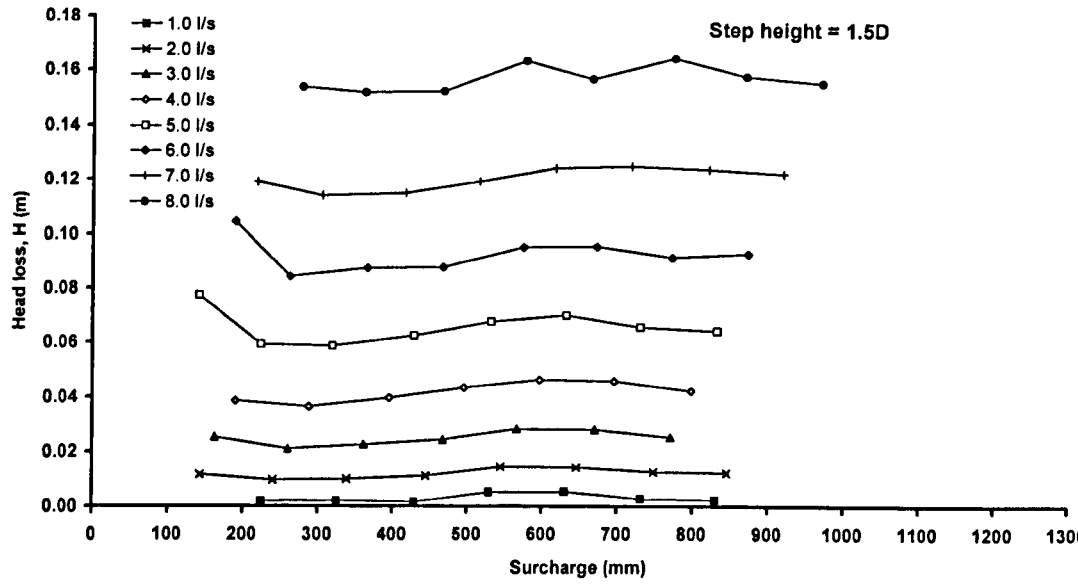

Figure 4.20d

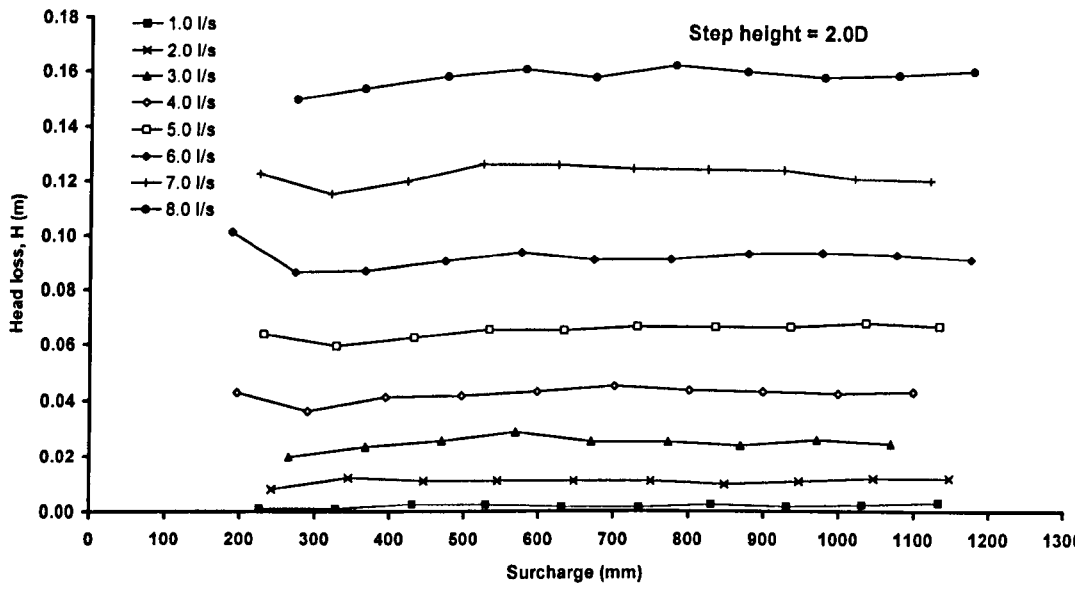

Figure 4.20e

Figure 4.20 Variation of head loss with surcharge (388mm unbenched manhole).

In common with the flow of fluid through a pipe, the head loss is greater at greater discharges. Averaging the head loss values across the surcharge range allows the relationship between the head loss and the velocity head to be determined (Figure 4.21). In all cases there is a good linear fit showing that the head loss can be well represented by such a relationship. An increase in step height causes a considerable increase in head loss for step heights between 0.0 and 1.0 pipe diameters. From the 0.0 to 0.5 pipe diameter step height there is an increase in head loss of approximately 2.5 times. Increasing the step further, to 1.0 pipe diameters, results in a lesser increase in head loss. Any step height variation above 1.0 pipe diameters appears to have no significant influence on the head loss values.

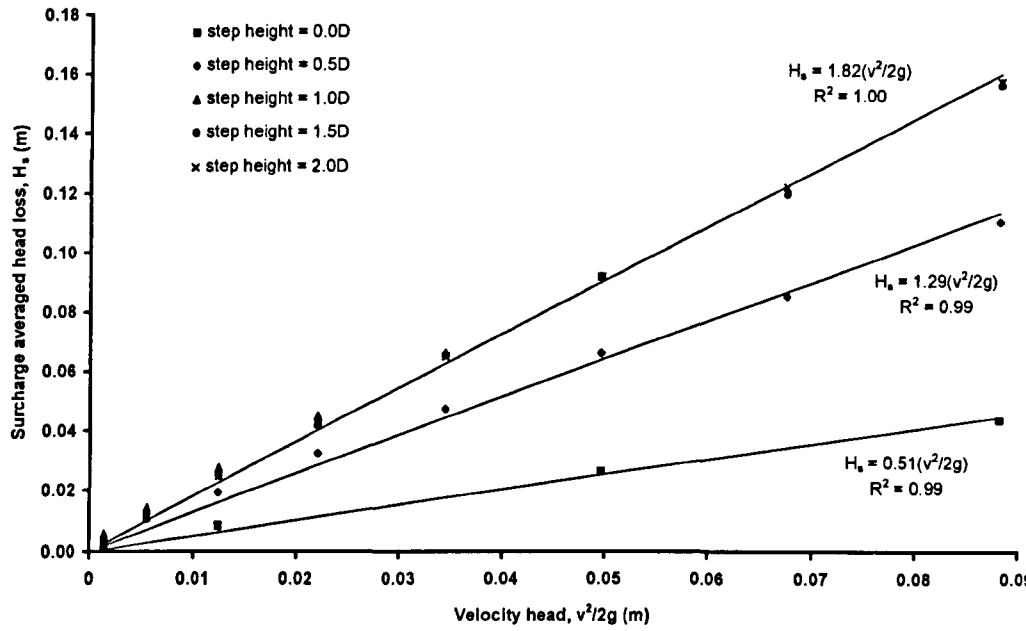

Figure 4.21 Variation of surcharge averaged head loss with velocity head (388mm unbenched manhole).

	0.0D		0.5D		1.0D		1.5D		2.0D	
$v^2/2g$ (m)	mean	s.d.	mean	s.d.	mean	s.d.	mean	s.d.	mean	s.d.
0.0014	0.0024	0.0017	0.0038	0.0023	0.0058	0.0022	0.0031	0.0014	0.0021	0.0007
0.0055	-	-	0.0107	0.0030	0.0143	0.0026	0.0120	0.0016	0.0111	0.0012
0.0124	0.0085	0.0016	0.0194	0.0023	0.0274	0.0037	0.0249	0.0025	0.0247	0.0022
0.0220	-	-	0.0324	0.0029	0.0449	0.0038	0.0418	0.0035	0.0423	0.0022
0.0344	-	-	0.0475	0.0045	0.0663	0.0049	0.0656	0.0057	0.0652	0.0025
0.0496	0.0266	0.0058	0.0664	0.0055	0.0924	0.0063	0.0924	0.0059	0.0922	0.0038
0.0675	-	-	0.0859	0.0067	0.1216	0.0048	0.1204	0.0040	0.1227	0.0033
0.0882	0.0440	0.0088	0.1109	0.0100	0.1581	0.0048	0.1571	0.0045	0.1582	0.0037

Table 4.3 Mean and standard deviation values for surcharge averaged head loss, H_s.

The piezometer measurements at locations along the manhole supply pipes were intended to provide a longitudinal section of the pressure along the pipe length. It proved difficult to obtain reliable readings from the manometers due to the turbulent flow causing pressure fluctuations, which caused excessive rise and fall in the piezometer measuring tubes. Also, the pressure tapping pipe work was required to be kept scrupulously clean and air free and this proved difficult to achieve consistently during the extensive laboratory testing period. Although it is not possible to have full confidence in the piezometer pressure values, results are presented for one case to provide an indication of the pressure profiles obtained (Figure 4.22).

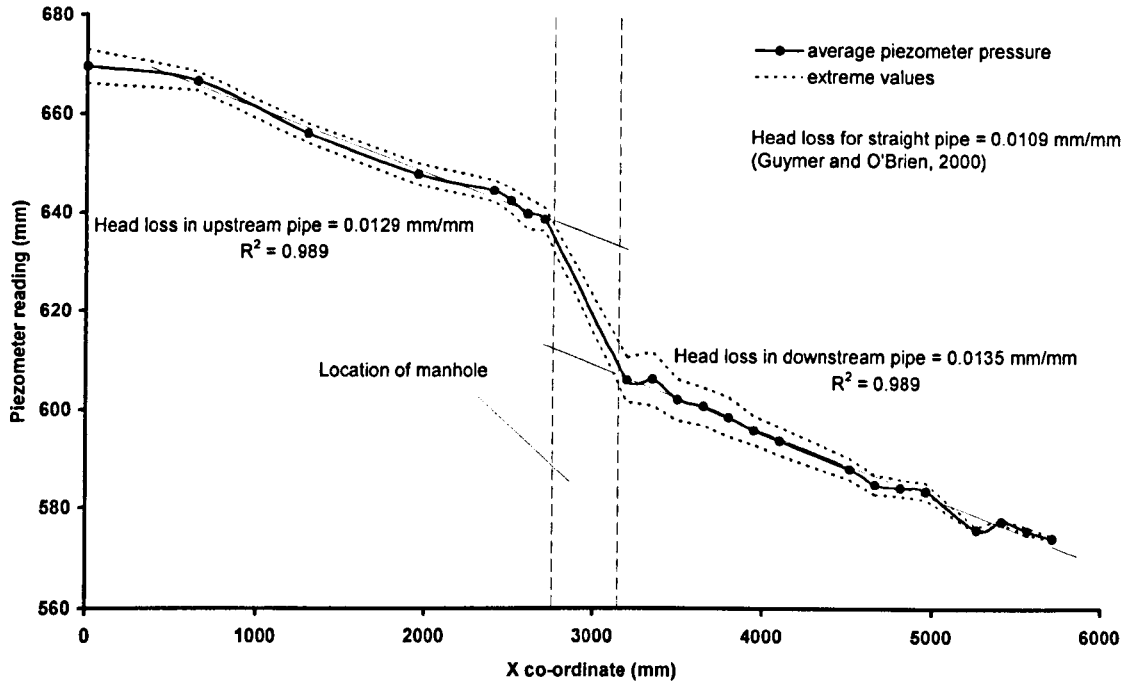

Figure 4.22 Sample results from piezometer readings (388mm unbenched manhole, Q = 6.0l/s, surcharge = 402mm).

The pressure profile from the piezometer measurements has a general shape similar to that obtained from the numerical model of Asztély and Lyngfelt (1996). In the central sections of the pipe lengths either side of the manhole the data shows almost constant head loss as the distance along the pipe increases. However, as with Asztély and Lyngfelt there appears to be an additional pressure drop immediately prior to the manhole inlet. This is attributed to the re-circulation occurring in the chamber compressing the incoming jet, thereby causing an increase in the velocity in this section of the pipe and an associated reduction in pressure. This phenomenon has not been observed by any previous laboratory researchers due to the fact that it occurs too close to the manhole to be detected by their pressure measurement devices. It has therefore been left out of the theoretical models produced. In addition, both the numerical analysis and the laboratory manometer profile highlight the effects of the vena contracta that develops in the pipe exiting the manhole, where the pressure recovers slightly before settling to the uniform pipe flow head loss. The piezometer results were not refined enough to provide confirmation of the asymptotic downstream hydraulic grade line described by Archer *et al* (1978).

4.4.3 ADE results

The two parameters required to predict longitudinal dispersion with the ADE model are travel time and dispersion coefficient. These coefficients have been determined from the data analysis and optimisation procedure.

The variation of the results for the travel time with respect to surcharge for the 388mm internal diameter circular manhole are presented in Figure 4.23. It is clear that the travel time for the zero step manhole is almost independent of the surcharge level. The only variation of any significance is for the lowest surcharge measurement at the least flow rate where the travel time value is slightly higher than the almost constant value above this surcharge. With the inclusion of a step height the results demonstrate a similar trend with a maximum value at lower surcharge levels and then a

reduction in the travel time to a value that remains constant at further increases of surcharge. The level of surcharge at which the travel times attain a constant value appears to increase with increasing step height.

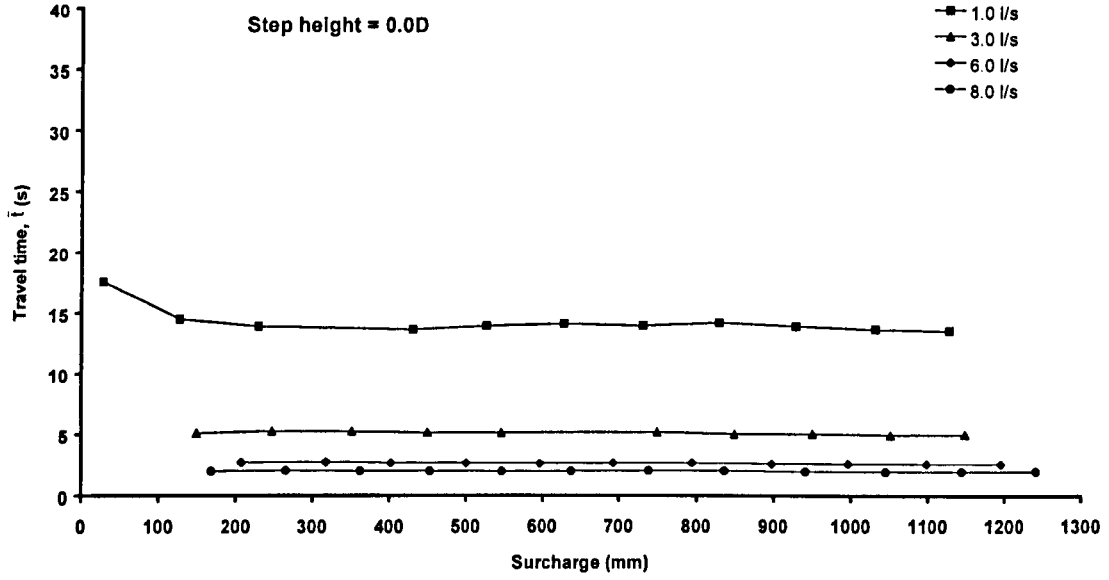

Figure 4.23a

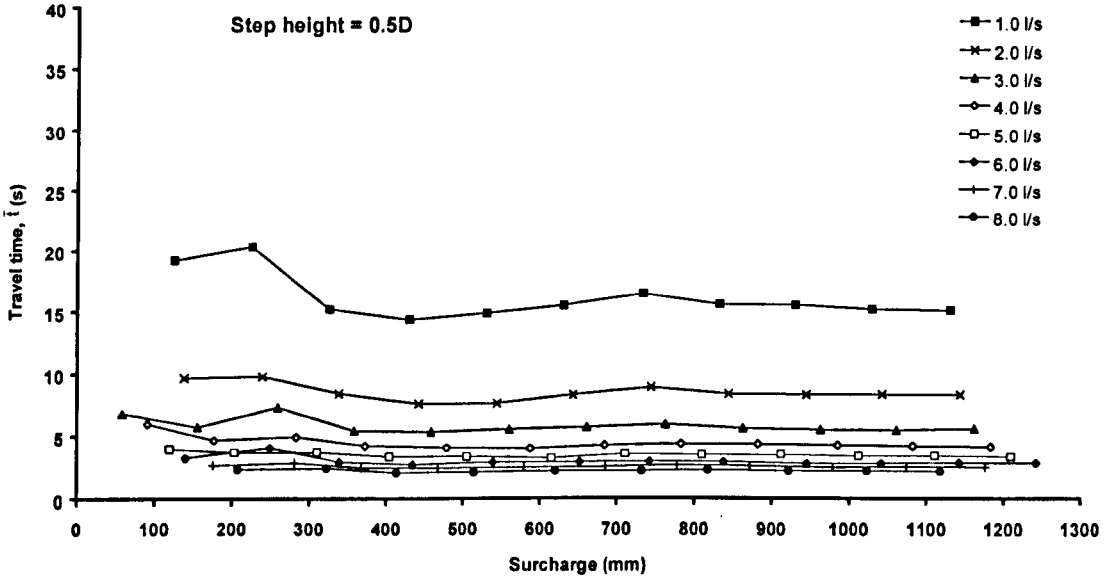

Figure 4.23b

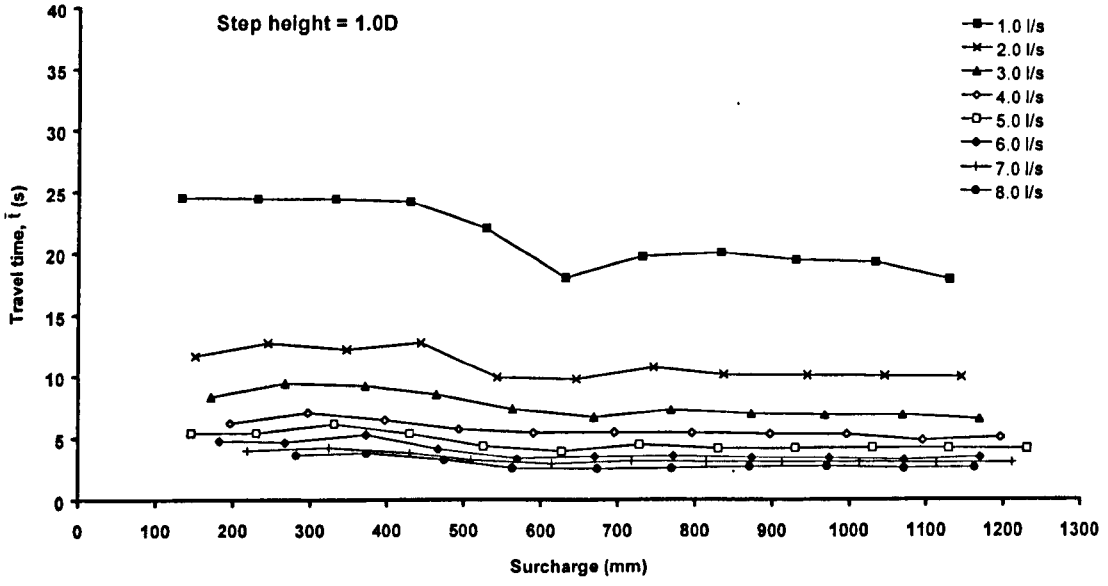

Figure 4.23c

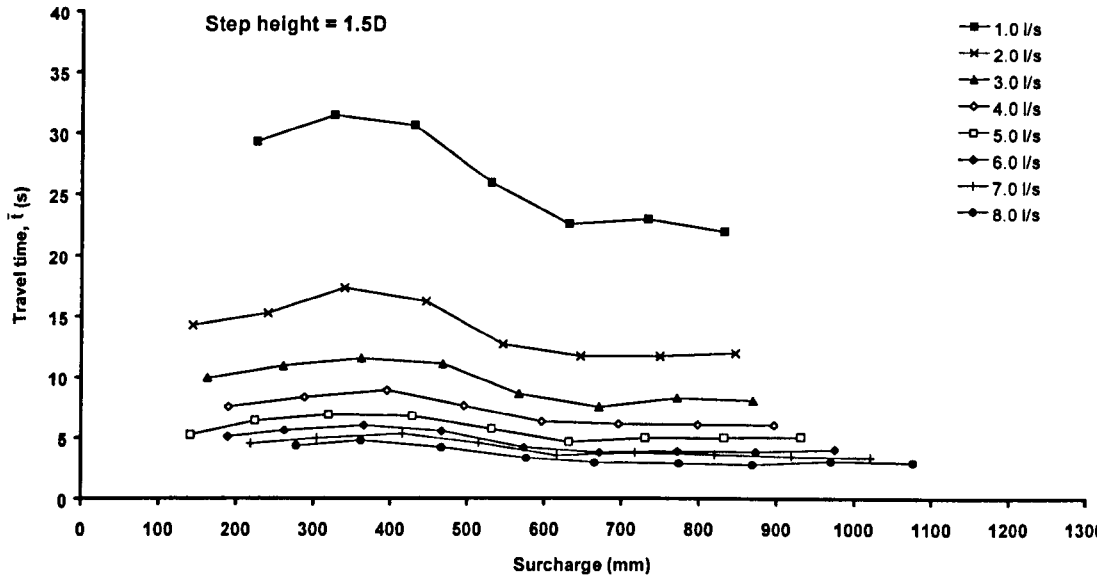

Figure 4.23d

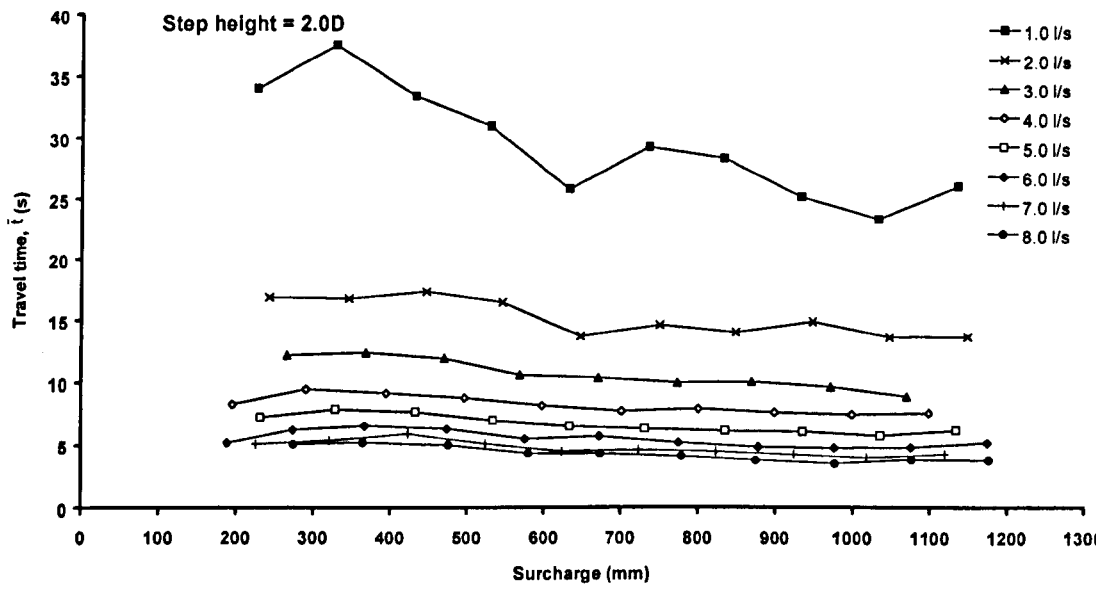

Figure 4.23e

Figure 4.23 Variation of ADE travel time with surcharge (388mm unbenched manhole).

The travel time coefficient is influenced greatly by the discharge through the system. If the values for travel time are assumed constant through the surcharge range then it is possible to investigate the discharge effect. The data in Figure 4.24 show the trend for the variation of surcharge averaged travel time with discharge. It can be seen that there is an almost uniform increase in ADE travel time with step height for any given discharge.

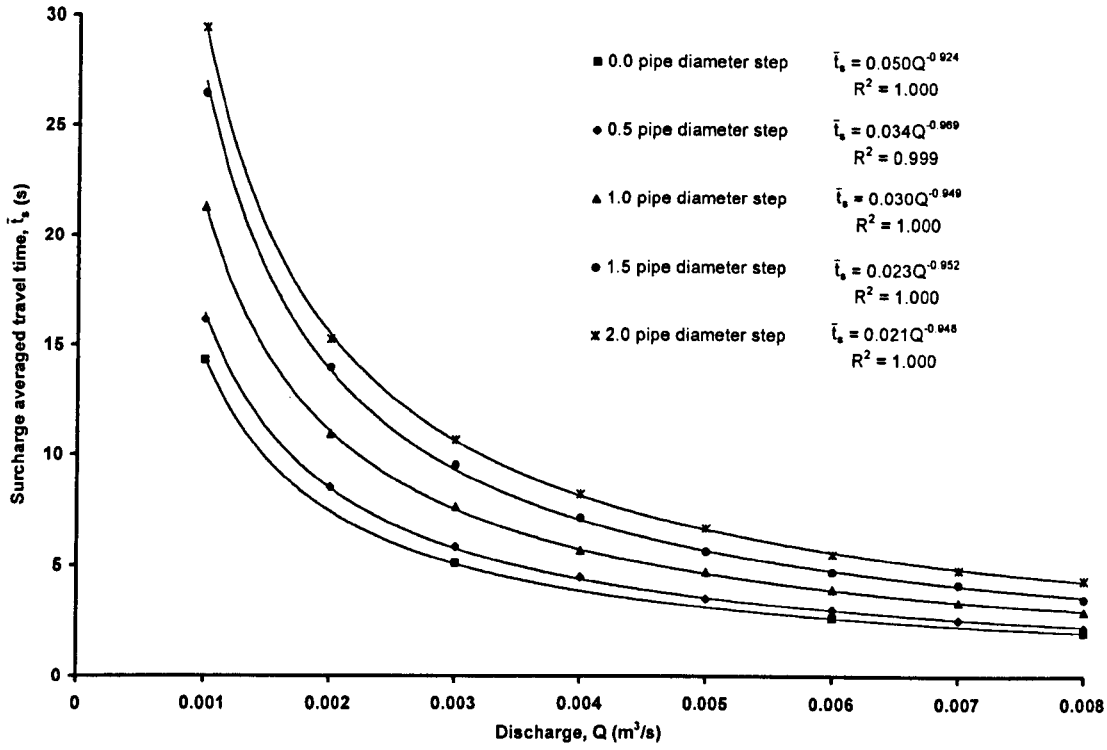

Figure 4.24 Variation of surcharge averaged ADE travel time with discharge.

	0.0D		0.5D		1.0D		1.5D		2.0D	
Q (l/s)	mean	s.d.	mean	s.d.	mean	s.d.	mean	s.d.	mean	s.d.
1.0	14.304	1.067	16.145	1.793	21.266	2.578	26.446	3.742	29.436	4.275
2.0	-	-	8.524	0.669	10.942	1.140	13.927	2.054	15.240	1.416
3.0	5.105	0.099	5.846	0.593	7.643	1.002	9.526	1.448	10.687	1.157
4.0	-	-	4.476	0.526	5.679	0.622	7.146	1.055	8.218	0.661
5.0	-	-	3.516	0.200	4.699	0.673	5.650	0.785	6.682	0.682
6.0	2.634	0.044	3.004	0.353	3.934	0.663	4.701	0.816	5.517	0.586
7.0	-	-	2.565	0.120	3.357	0.440	4.168	0.668	4.797	0.553
8.0	1.987	0.028	2.220	0.105	2.916	0.449	3.507	0.698	4.343	0.564

Table 4.4 Mean and standard deviation values for surcharge averaged ADE travel time, $\bar{t}_s$.

The results for the variation of dispersion coefficient with surcharge are given in Figure 4.25. The data shown in this figure demonstrate quite distinct features. In the zero step height case, at surcharges below approximately 500mm there is some variability in the dispersion coefficient values. As the surcharge increases above the minimum there is a tendency for the dispersion coefficient value to also increase, attaining a maximum value at a surcharge of approximately 300mm. Further increases in the surcharge result in the dispersion coefficient values swiftly reducing until becoming an almost constant value for surcharges greater than 500mm. A similar pattern is followed less distinctly by the data for the 0.5 pipe diameter step. However, for greater step height conditions the peak dispersion coefficient values occur at significantly higher surcharge levels. The 2.0 pipe diameter step geometry demonstrates a peak at surcharges in the region of 800mm.

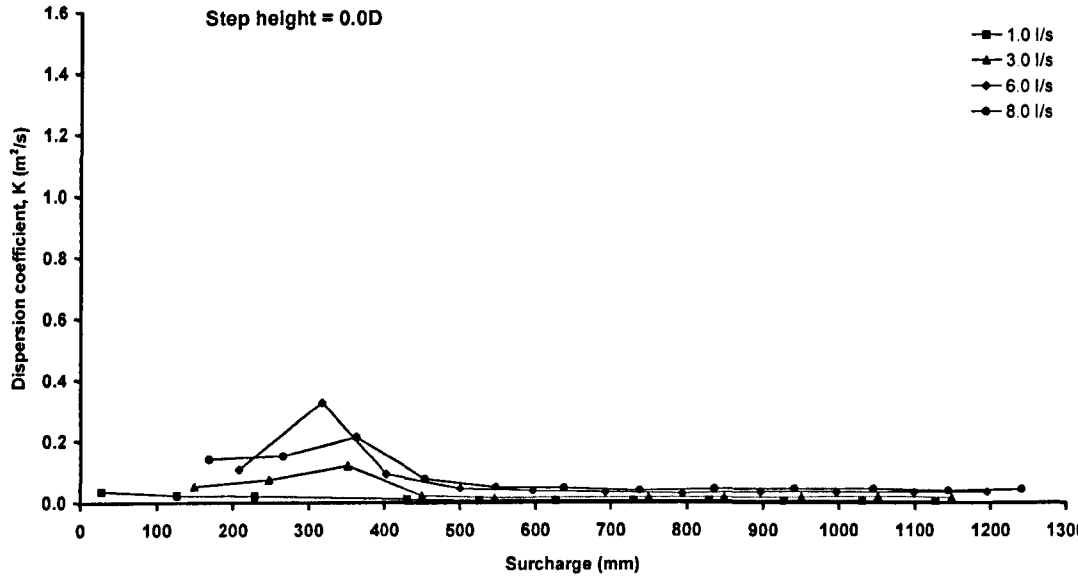

Figure 4.25a

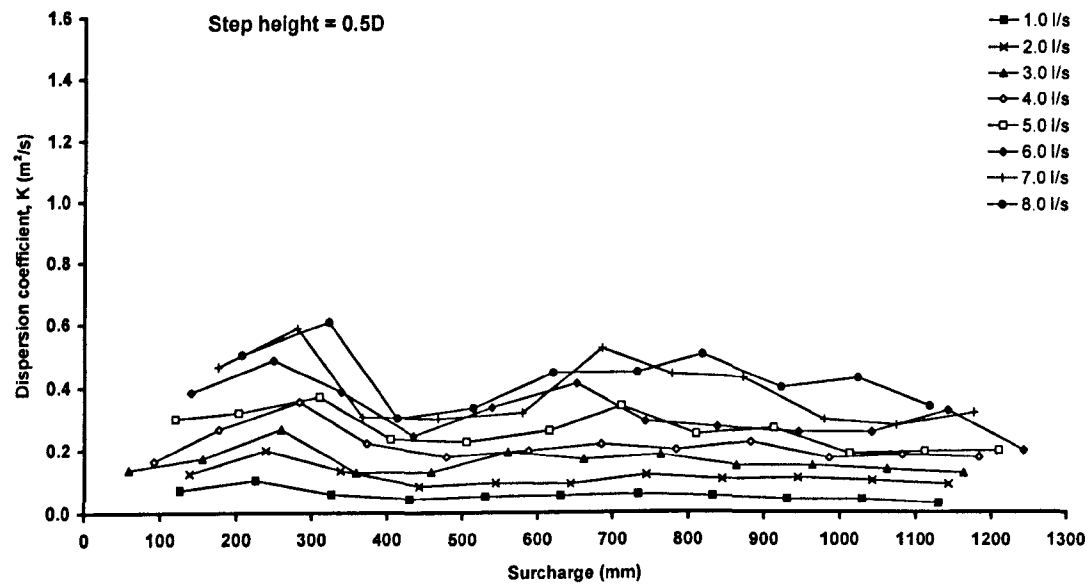

Figure 4.25b

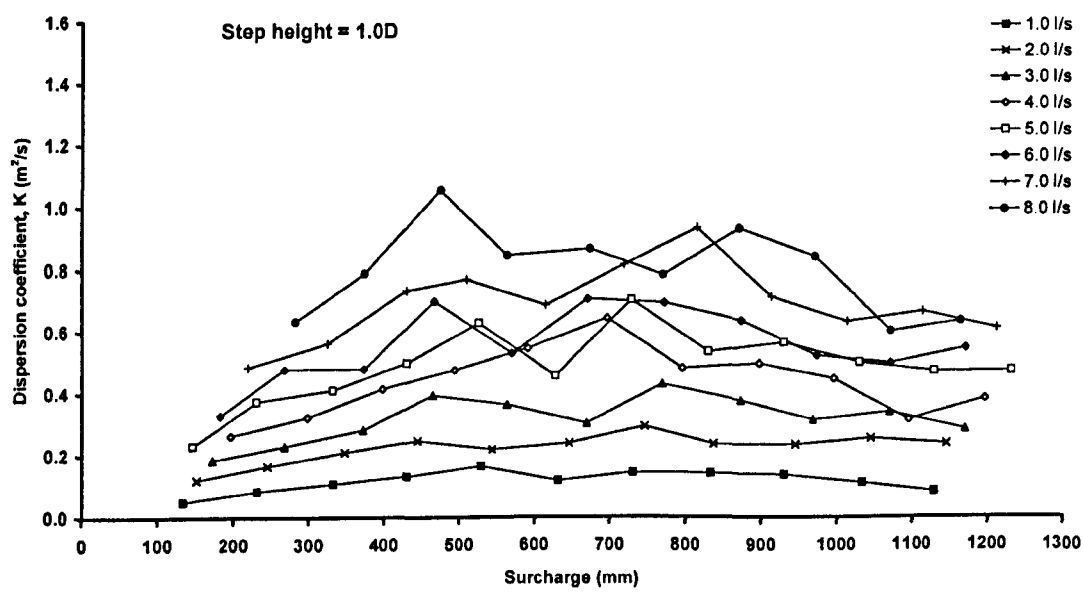

Figure 4.25c

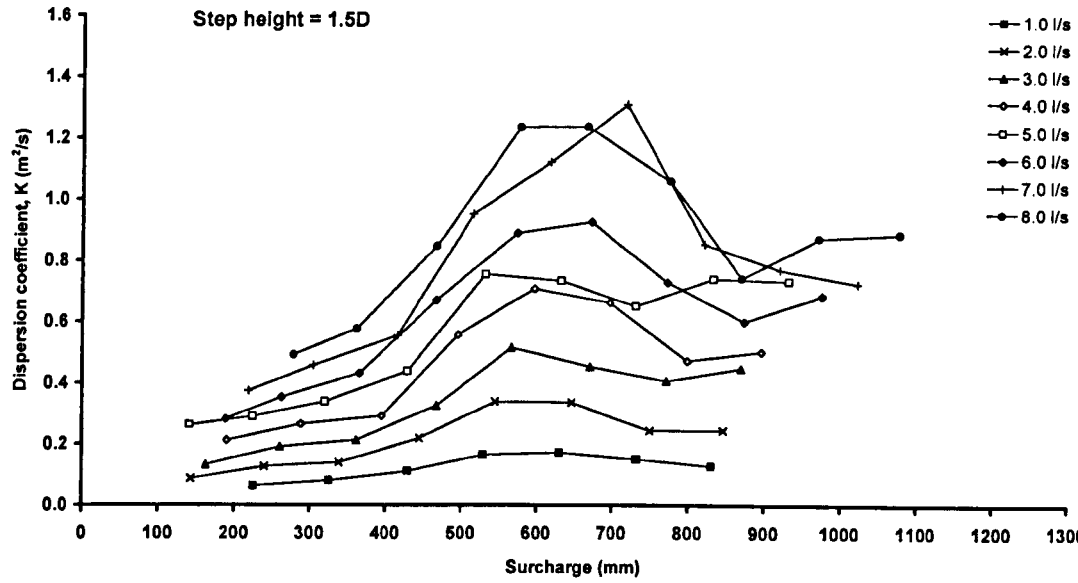

Figure 4.25d

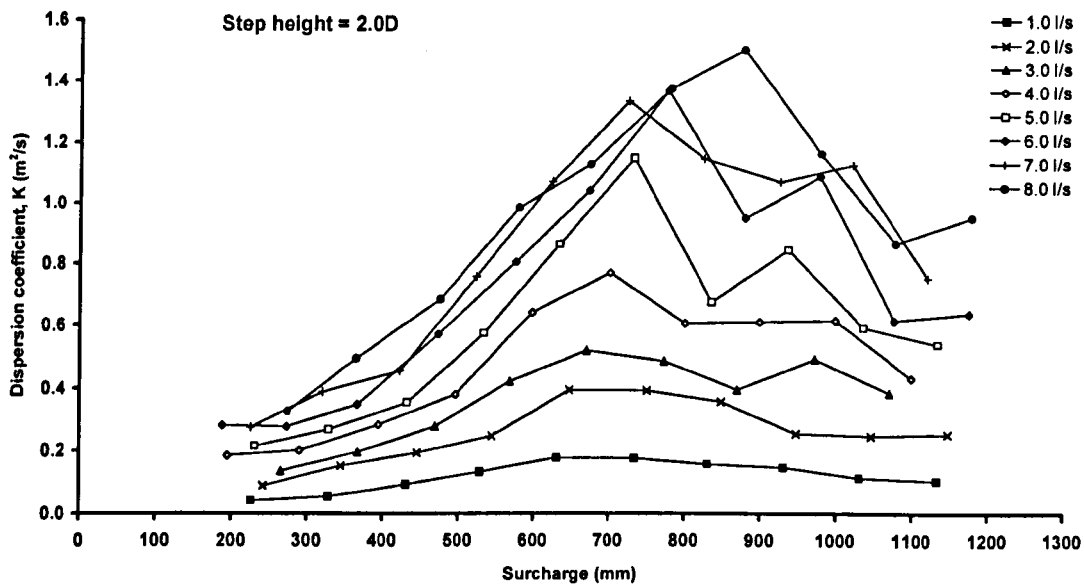

Figure 4.25e

Figure 4.25 Variation of dispersion coefficient with surcharge (388mm unbenched manhole).

In some of the step height cases there is undoubtedly considerable variation of dispersion coefficient with surcharge. However, as a means of determining the effect of step height upon the dispersion coefficient, the values have been averaged across the surcharge range (Figure 4.26). A linear relationship between the surcharge averaged longitudinal dispersion coefficient and the discharge has been assumed. This has been fitted to the data and through the origin. For the zero step height manhole, the surcharge averaged dispersion coefficient has a value of 11.0Qm^2/s. This is over three times greater than the value of 3.3Qm^2/s determined for a straight length of pipe (Guymer and O'Brien, 2000). There are further increases in dispersion as the step height increases, and a step height of 1.0 pipe diameters gives rise to dispersion coefficients over nine times greater than no step. Increases in step height above 1.0 pipe diameters cause smaller increases in the dispersion coefficient.

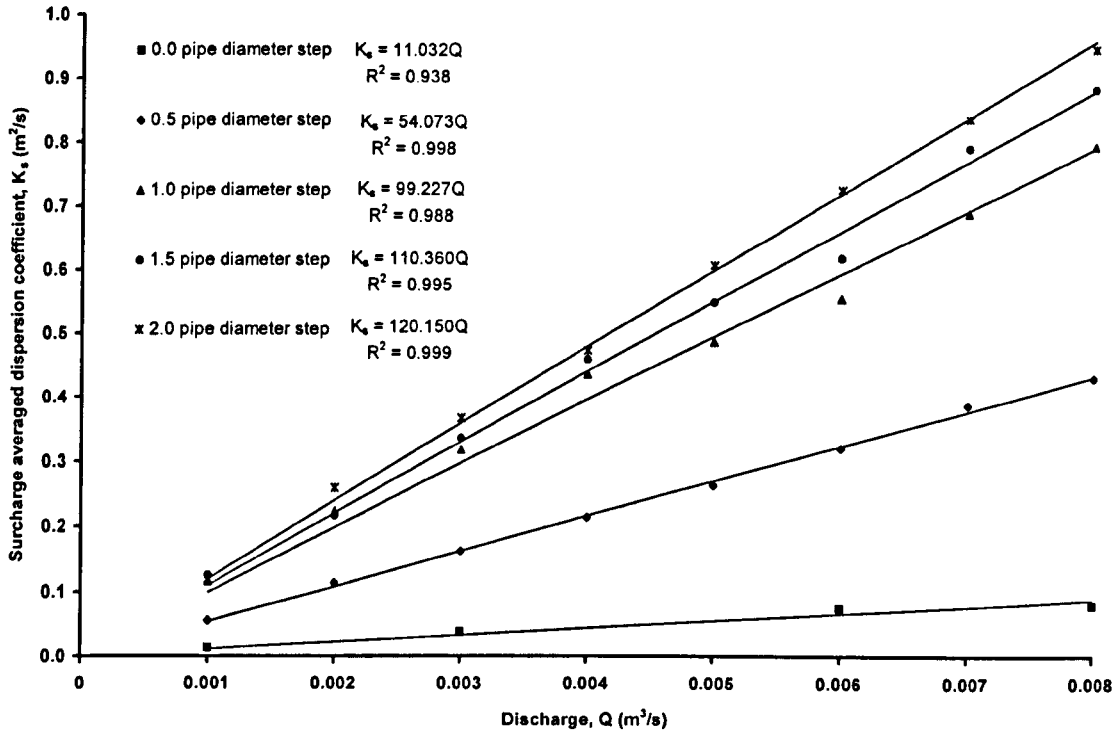

Figure 4.26 Variation of surcharge averaged dispersion coefficient with discharge.

	0.0D		0.5D		1.0D		1.5D		2.0D	
Q (l/s)	mean	s.d.	mean	s.d.	mean	s.d.	mean	s.d.	mean	s.d.
1.0	0.013	0.009	0.056	0.019	0.116	0.031	0.125	0.039	0.120	0.045
2.0	-	-	0.114	0.031	0.224	0.044	0.217	0.088	0.259	0.095
3.0	0.038	0.033	0.162	0.039	0.319	0.069	0.336	0.134	0.368	0.128
4.0	-	-	0.214	0.051	0.436	0.105	0.460	0.175	0.474	0.195
5.0	-	-	0.263	0.057	0.488	0.115	0.785	0.202	0.609	0.276
6.0	0.075	0.084	0.321	0.079	0.556	0.111	0.620	0.213	0.728	0.342
7.0	-	-	0.388	0.101	0.691	0.116	0.793	0.290	0.839	0.349
8.0	0.080	0.055	0.431	0.088	0.796	0.135	0.886	0.248	0.949	0.353

Table 4.5 Mean and standard deviation values for surcharge averaged dispersion coefficient, K_s.

The effect of benching upon the ADE parameters for longitudinal dispersion through the manhole is shown in Figure 4.27 and Figure 4.28. The travel time values for the ADE analysis are approximately halved by the presence of benching. Also, any variation in the travel time values with changes in surcharge level are eliminated. The comparison with dispersion coefficient values is even more marked. In the case of the benching design tested, the dispersion coefficient values have been reduced to a minor fraction of those for the unbenched case. Only at surcharges less than approximately 400mm is there any increase in the dispersion coefficient above the almost constant value of approximately 0.01metres squared per second for greater surcharges.

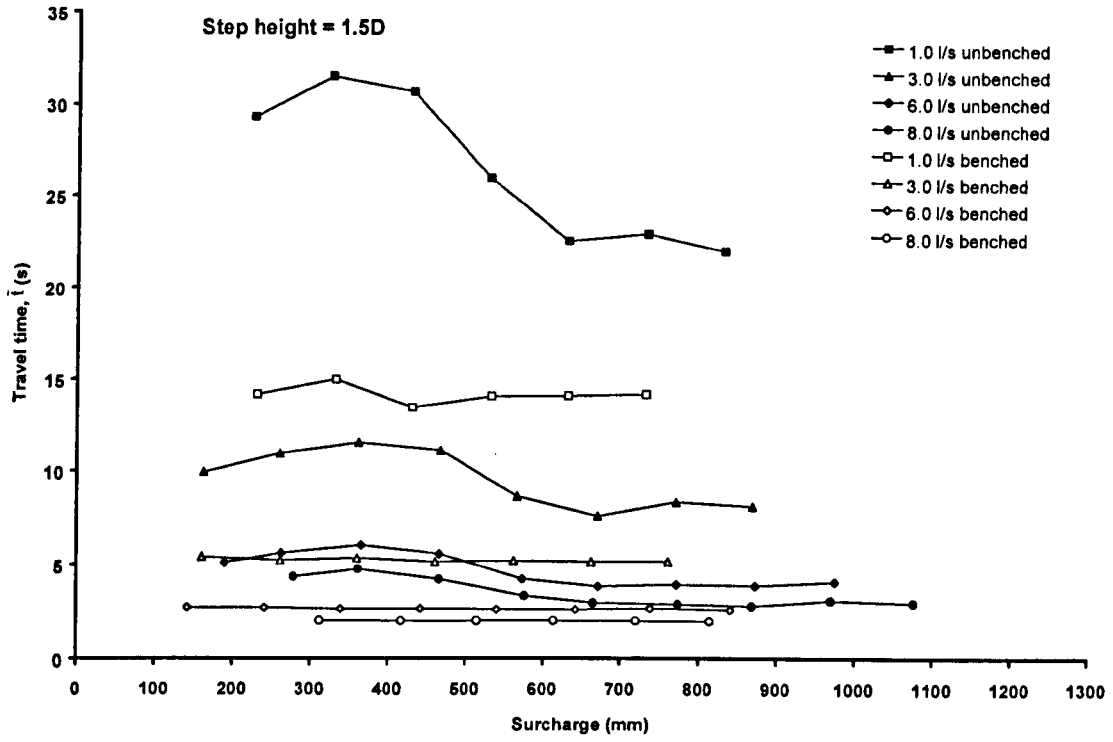

Figure 4.27 Comparison of travel time for benched and unbenched manholes.

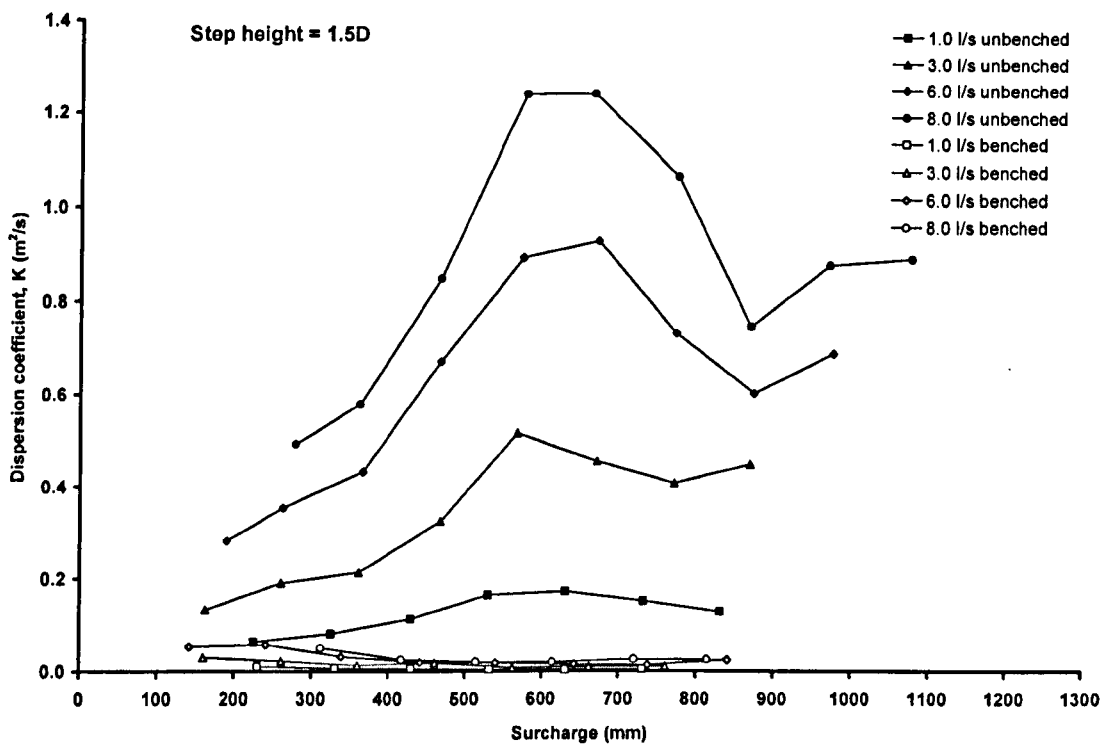

Figure 4.28 Comparison of dispersion coefficient for benched and unbenched manholes.

Averaging these ADE coefficient values over the surcharge range tested provides the relationship between them and the discharge. The results presented in Figure 4.29 highlight the reduction in travel time that the presence of benching in the manhole causes. As a comparison, travel time values for a straight length of pipe (Guymer and O'Brien, 2000) are included in the figure. The benching arrangement was a deep channel with a half pipe bed and this has clearly guided the flow towards

the outlet giving travel time results that are very similar to the straight pipe values. Figure 4.30 shows the comparison of benched and unbenched dispersion coefficient results in relation to the discharge. It can be seen that the provision of benching causes a huge reduction in the dispersion coefficient values and gives results very similar to those for a straight pipe. Therefore, whilst the dispersion analysis provided by Taylor (1954) assuming constant cross section is not strictly valid for a surcharged manhole, it is clear that this theory can provide a very good approximation of longitudinal dispersion for benched manholes, regardless of surcharge or step height conditions.

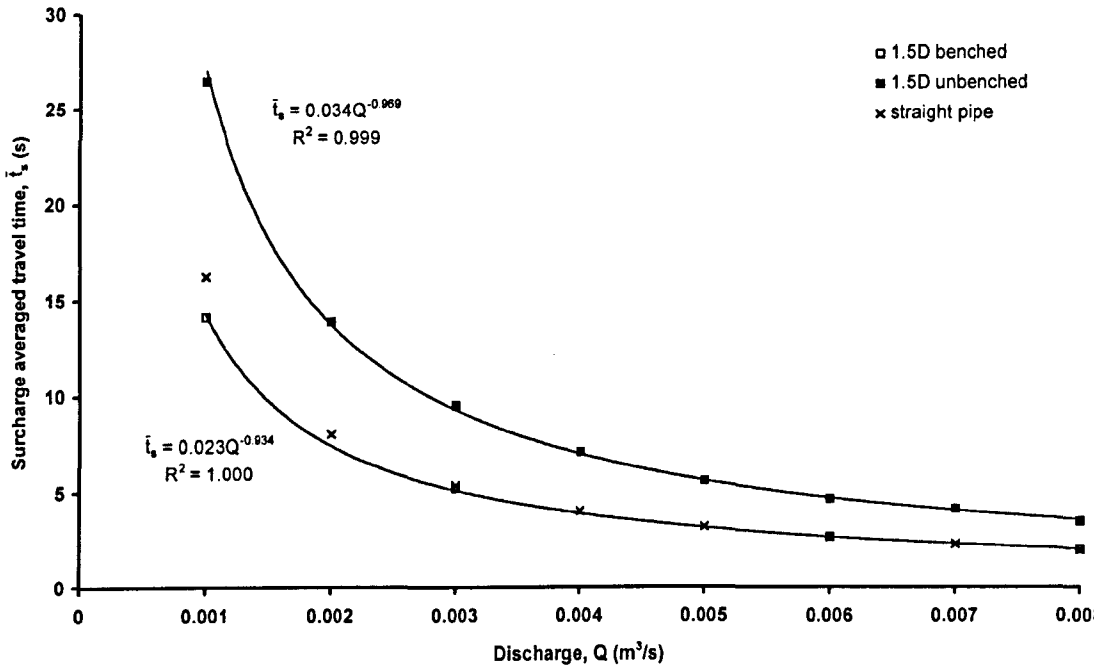

Figure 4.29 Comparison of variation of surcharge averaged ADE travel time with discharge for benched and unbenched manholes and straight pipe (pipe data from Guymer and O'Brien, 2000).

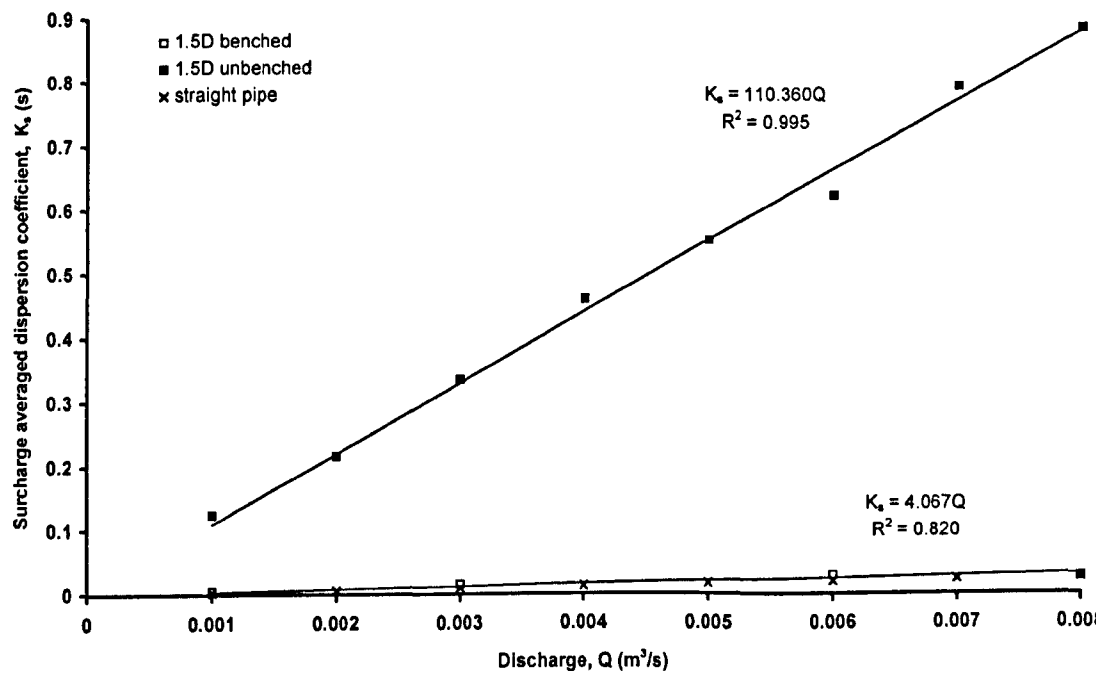

Figure 4.30 Comparison of variation of surcharge averaged dispersion coefficient with discharge for benched and unbenched manholes and straight pipe (pipe data from Guymer and O'Brien, 2000).

	1.5D unbenched				1.5D benched			
	$\bar{t}_s$		K_s		$\bar{t}_s$		K_s	
Q (l/s)	mean	s.d.	mean	s.d.	mean	s.d.	mean	s.d.
1.0	26.446	3.742	0.125	0.039	14.162	0.487	0.006	0.002
2.0	13.927	2.054	0.217	0.088	-	-	-	-
3.0	9.526	1.448	0.336	0.134	5.233	0.100	0.016	0.007
4.0	7.146	1.055	0.460	0.175	-	-	-	-
5.0	5.650	0.785	0.785	0.202	-	-	-	-
6.0	4.701	0.816	0.620	0.213	2.683	0.039	0.029	0.016
7.0	4.168	0.668	0.793	0.290	-	-	-	-
8.0	3.507	0.698	0.886	0.248	2.029	0.014	0.027	0.010

Table 4.6 Comparison of benched and unbenched manhole mean and standard deviation values for surcharge averaged ADE parameters.

4.4.4 ADZ results

The measured upstream and downstream temporal concentration profiles were used to establish the parameters for the ADZ equation to give the best prediction of the data. These parameters are the travel time and the time delay, both measured in seconds.

Figure 4.31 presents the variation of the ADZ travel time with surcharge level for all tested discharges. There appears to be little variation of travel time with surcharge in the range considered, although at step heights of 0.5 pipe diameters or lower there is a slight trend for the travel time to be greater at lower surcharges. It can be observed that there is an increase in travel time for a given discharge as the step height increases.

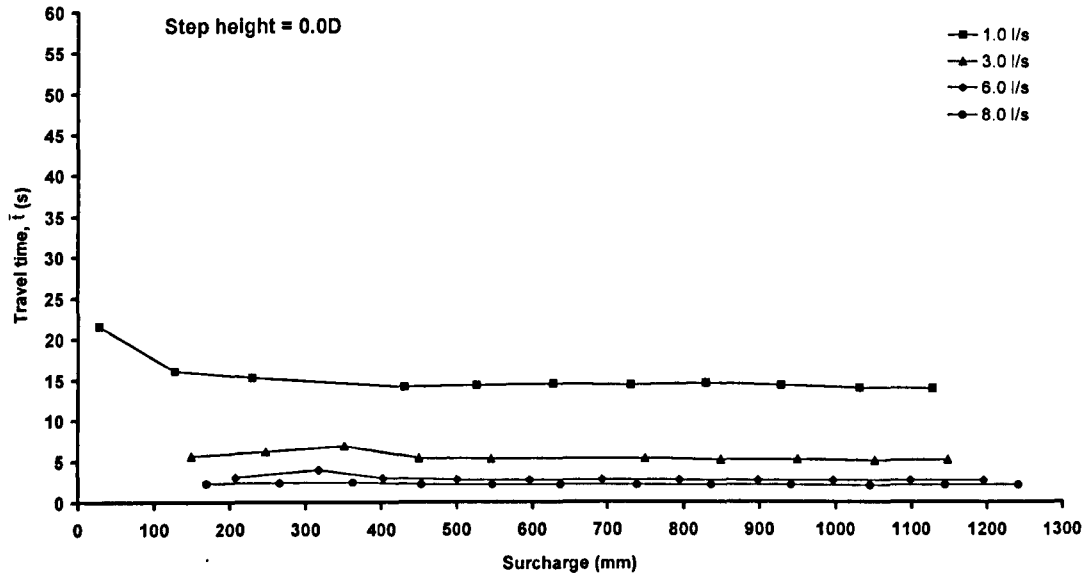

Figure 4.31a

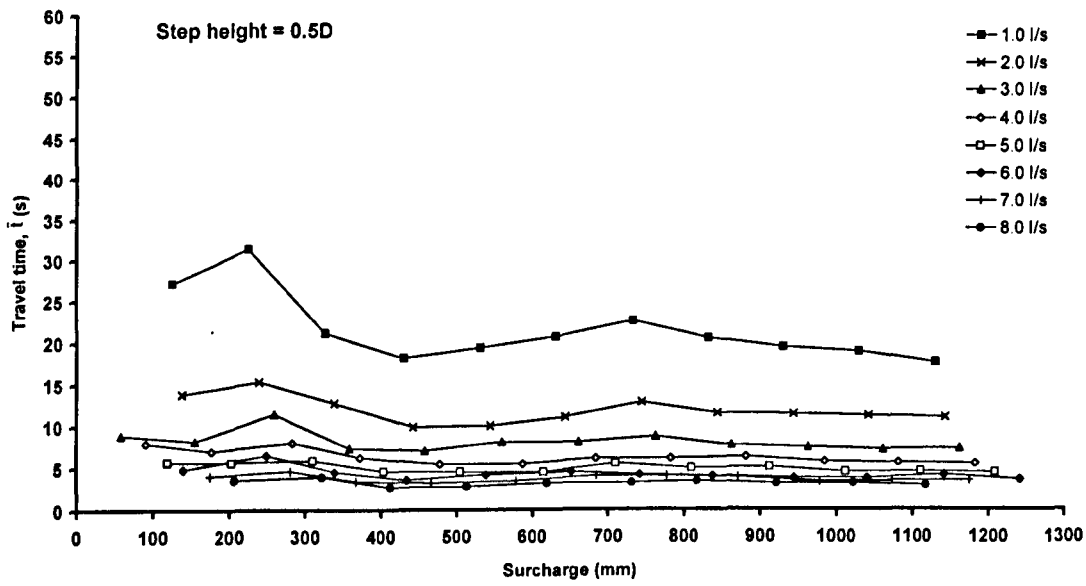

Figure 4.31b

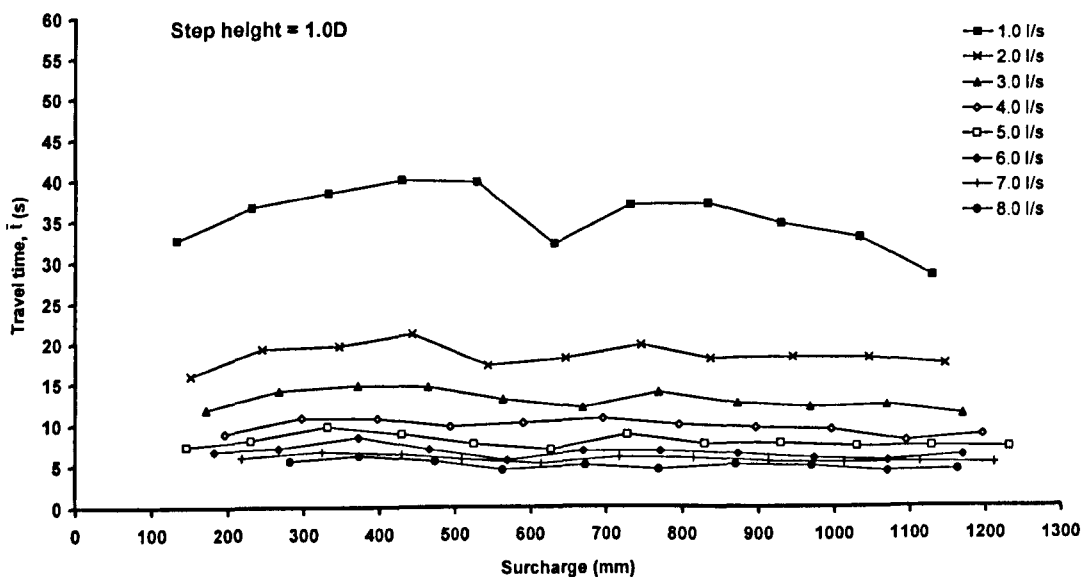

Figure 4.31c

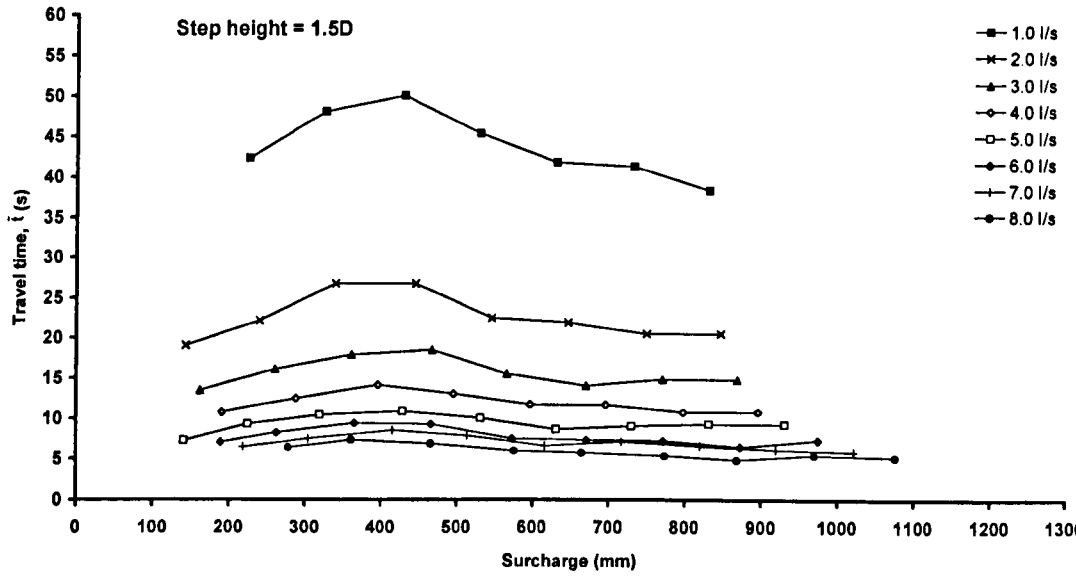

Figure 4.31d

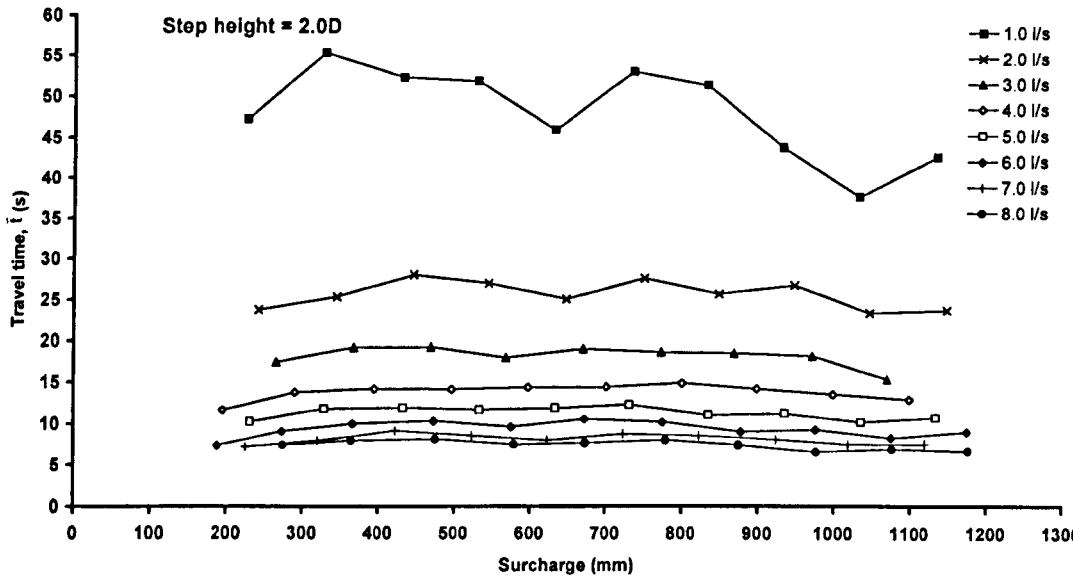

Figure 4.31e

Figure 4.31 Variation of ADZ travel time with surcharge.

The values of the reach time delay coefficients are presented in Figure 4.32. This represents the time taken for the fastest travelling dye to be transported between the measurement locations. Generally the trend is for the surcharge height to have little effect on the time delay for any given discharge with the zero step height condition. As the step height increases there becomes more variation in the time delay values through the surcharge range. Step heights of 1.0 pipe diameters or greater display a maximum time delay for the lowest measured surcharges which decreases with increasing surcharge. At surcharges of approximately 500mm or greater there is no further variation of time delay.

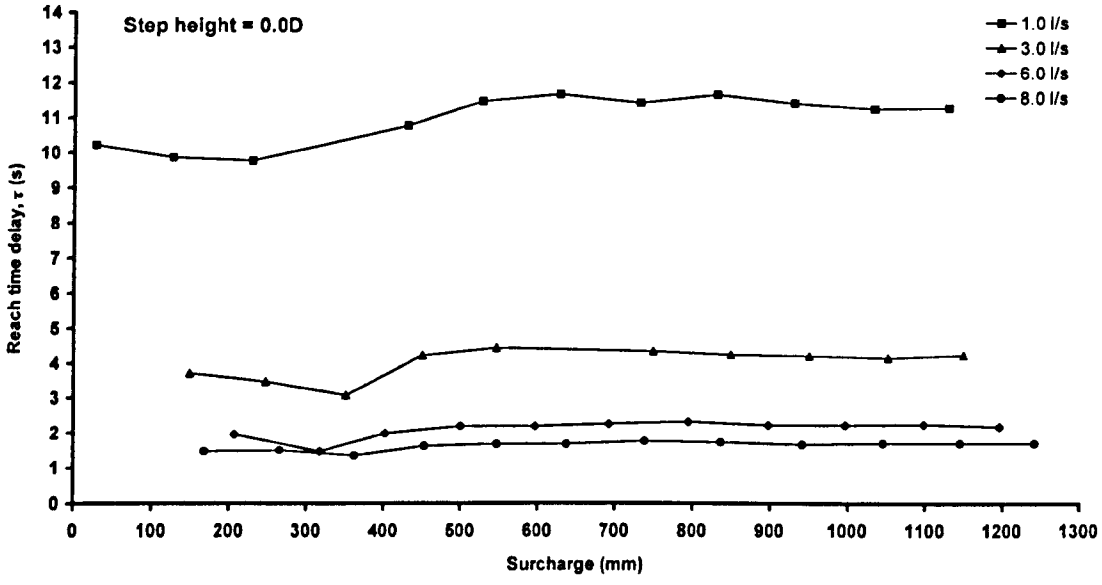

Figure 4.32a

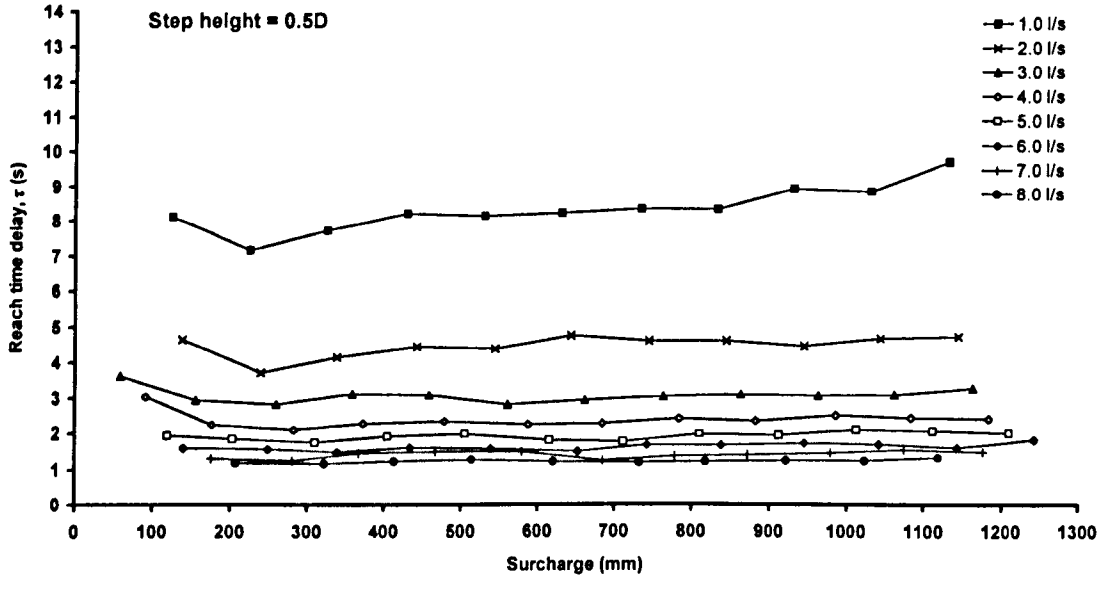

Figure 4.32b

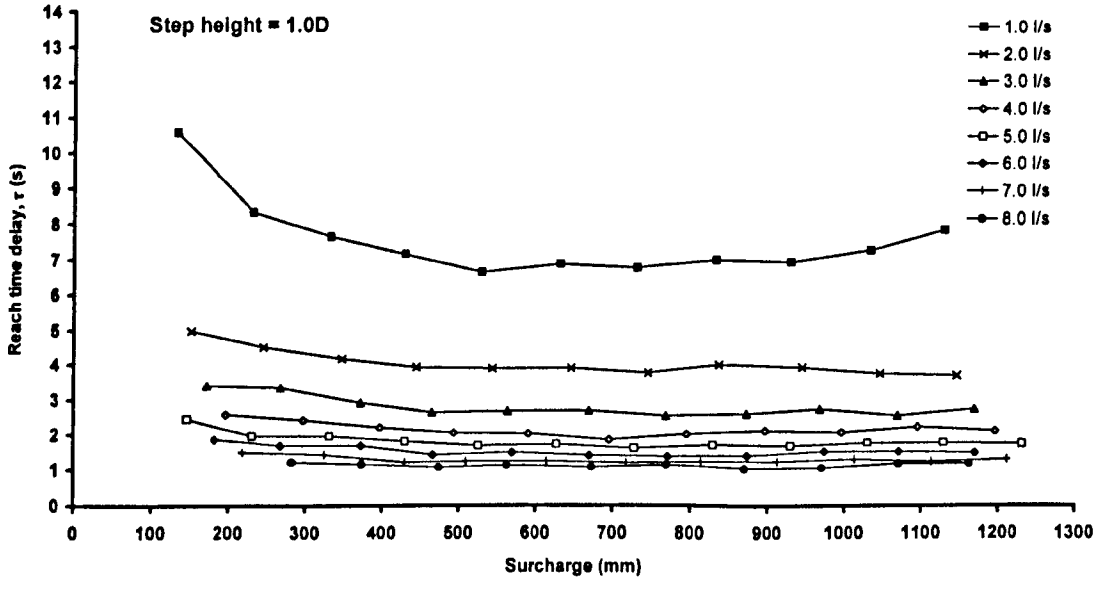

Figure 4.32c

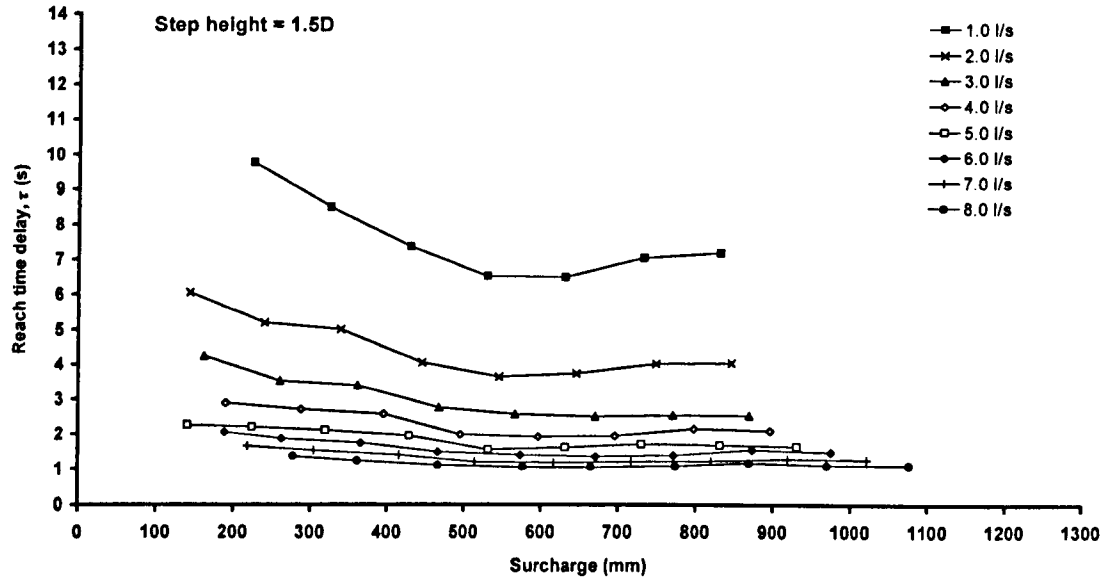

Figure 4.32d

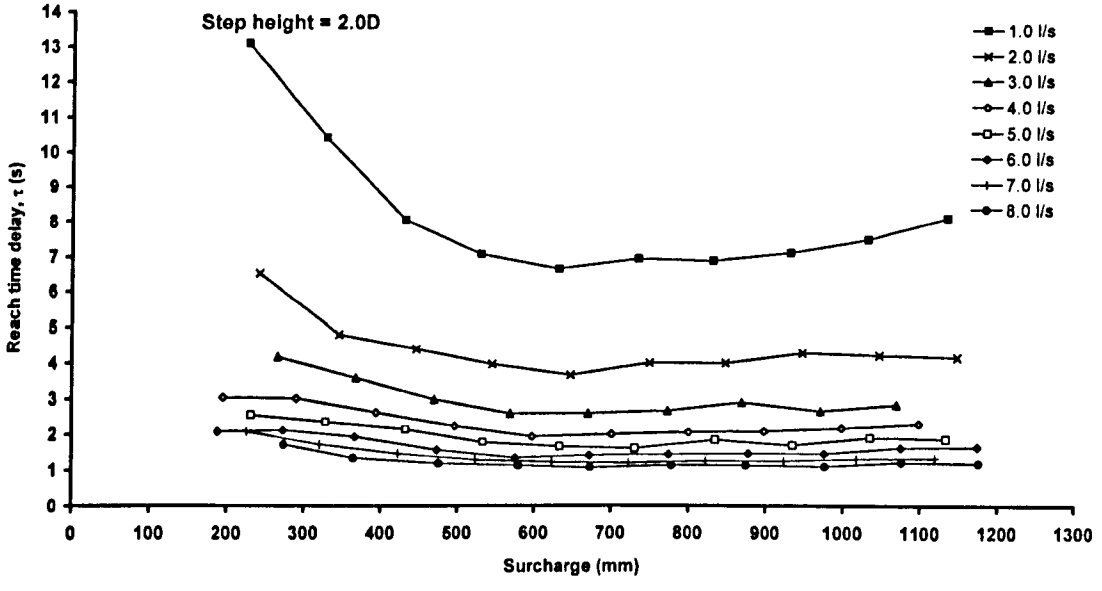

Figure 4.32e

Figure 4.32 Variation of reach time delay with surcharge.

If the travel time and time delay are considered to be independent of surcharge variations then the relationship between the ADZ time coefficients and the discharge can be determined. Figure 4.33 shows the surcharge averaged travel time values in relation to the discharge. At higher flow rates the fluid velocity is greater and hence the tracer cloud takes less time to travel between the fluorometers. The figure indicates that an increase in step height causes an increase in travel time for a particular flow rate. The increase with step height is almost uniform. All the step height conditions demonstrate travel time variations that are a high quality fit to being nearly inversely proportional to the discharge.

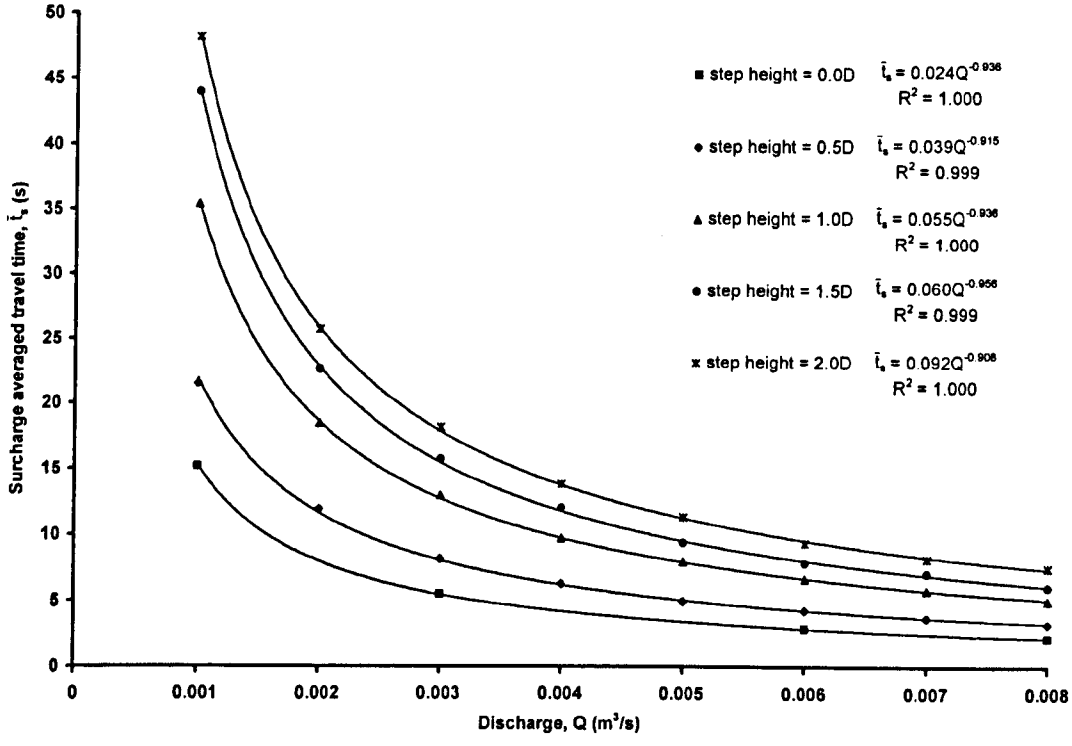

Figure 4.33 Variation of surcharge averaged ADZ travel time with discharge.

	0.0D		0.5D		1.0D		1.5D		2.0D	
Q (l/s)	mean	s.d.	mean	s.d.	mean	s.d.	mean	s.d.	mean	s.d.
1.0	15.199	2.093	21.503	3.988	35.407	3.447	44.001	3.801	48.167	5.256
2.0	-	-	11.902	1.571	18.457	1.374	22.607	2.649	25.680	1.586
3.0	5.515	0.531	8.113	1.169	12.960	1.667	15.728	1.655	18.156	1.118
4.0	-	-	6.249	0.864	9.709	0.866	11.985	1.143	13.832	0.883
5.0	-	-	4.959	0.525	7.918	0.796	9.382	0.986	11.322	0.690
6.0	2.887	0.345	4.291	0.757	6.617	0.778	7.819	0.920	9.336	0.912
7.0	-	-	3.716	0.410	5.774	0.462	7.028	0.791	8.125	0.593
8.0	2.153	0.120	3.211	0.352	5.028	0.572	5.992	0.769	7.443	0.500

Table 4.7 Mean and standard deviation values for surcharge averaged ADZ travel time, $\bar{t}_s$.

The reach time delay calculated with the optimised ADZ analysis varies with the discharge applied through the system in a similar manner to the travel time. (Figure 4.34). Although the manhole acts as a dead zone there is clearly a portion of the tracer cloud that bypasses it entirely and thus travels between the measurement locations with the maximum velocity of flow. It is apparent that increases in the step height above 0.5 pipe diameters causes very little change in the time delay for a given discharge. The only marked difference is for the case where there is no step height. Under these circumstances the time delay is greater than for the manhole conditions where a step height is present. It is therefore observed that the introduction of a step height between the inlet and outlet pipes at the manhole junction actually results in an increase in the maximum velocity of flow through the system at a particular discharge.

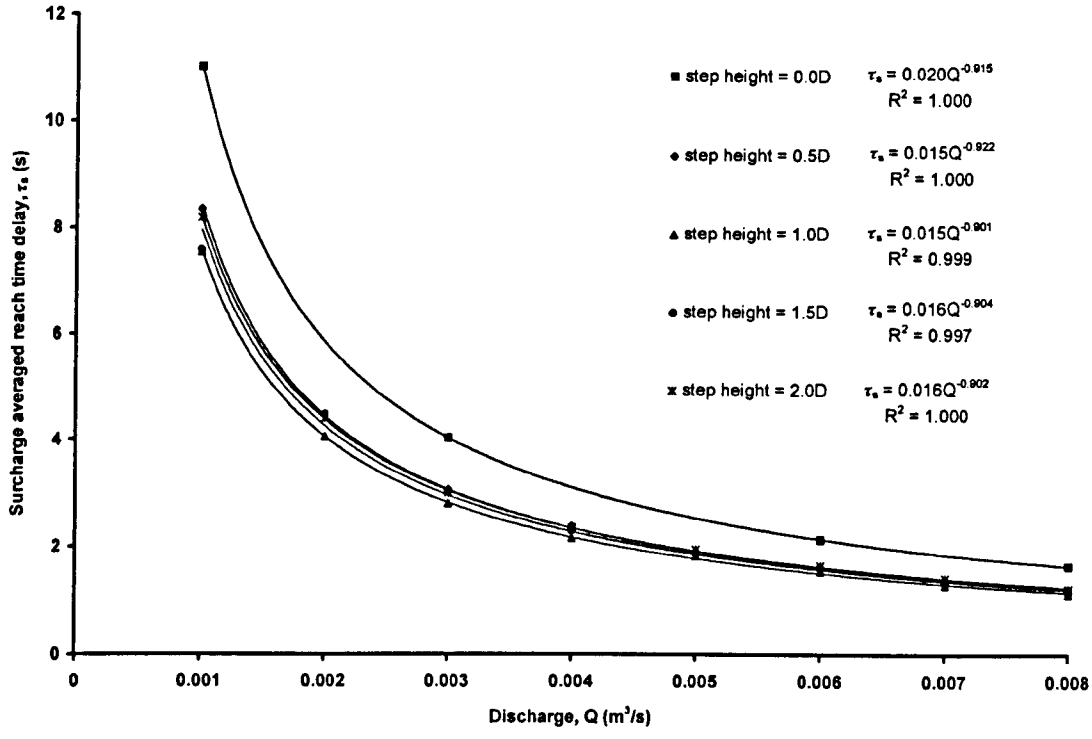

Figure 4.34 Variation of surcharge averaged reach time delay with discharge.

	0.0D		0.5D		1.0D		1.5D		2.0D	
Q (l/s)	mean	s.d.	mean	s.d.	mean	s.d.	mean	s.d.	mean	s.d.
1.0	11.009	0.695	8.348	0.641	7.535	1.091	7.570	1.089	8.187	1.936
2.0	-	-	4.449	0.283	4.052	0.362	4.474	0.793	4.393	0.762
3.0	4.027	0.429	3.062	0.208	2.798	0.293	3.018	0.597	2.990	0.516
4.0	-	-	2.378	0.224	2.156	0.196	2.296	0.348	2.347	0.384
5.0	-	-	1.915	0.108	1.825	0.217	1.871	0.258	1.942	0.299
6.0	2.131	0.234	1.618	0.093	1.544	0.143	1.608	0.222	1.651	0.261
7.0	-	-	1.399	0.094	1.299	0.091	1.348	0.149	1.419	0.266
8.0	1.644	0.125	1.020	0.044	1.134	0.061	1.167	0.094	1.229	0.180

Table 4.8 Mean and standard deviation values for surcharge averaged reach time delay, τ_s.

The effect of the presence of benching in the manhole on the ADZ time coefficients is shown in the following figures. The variation of the travel time with surcharge for the benched and unbenched 1.5 pipe diameter step height manholes is shown in Figure 4.35. The provision of a benching arrangement has caused a significant reduction in the travel time values to approximately 35 percent of the values for the unbenched manhole. There is also less variation in travel time with surcharge for the benched manhole condition. In a similar manner the reach time delay values are compared in Figure 4.36. In this case the results are somewhat different. The presence of benching actually causes an increase of up to 100 percent in the time delay values above the unbenched results. Thus the presence of benching causes the maximum flow velocity in the system to be less than without benching for any given flow rate.

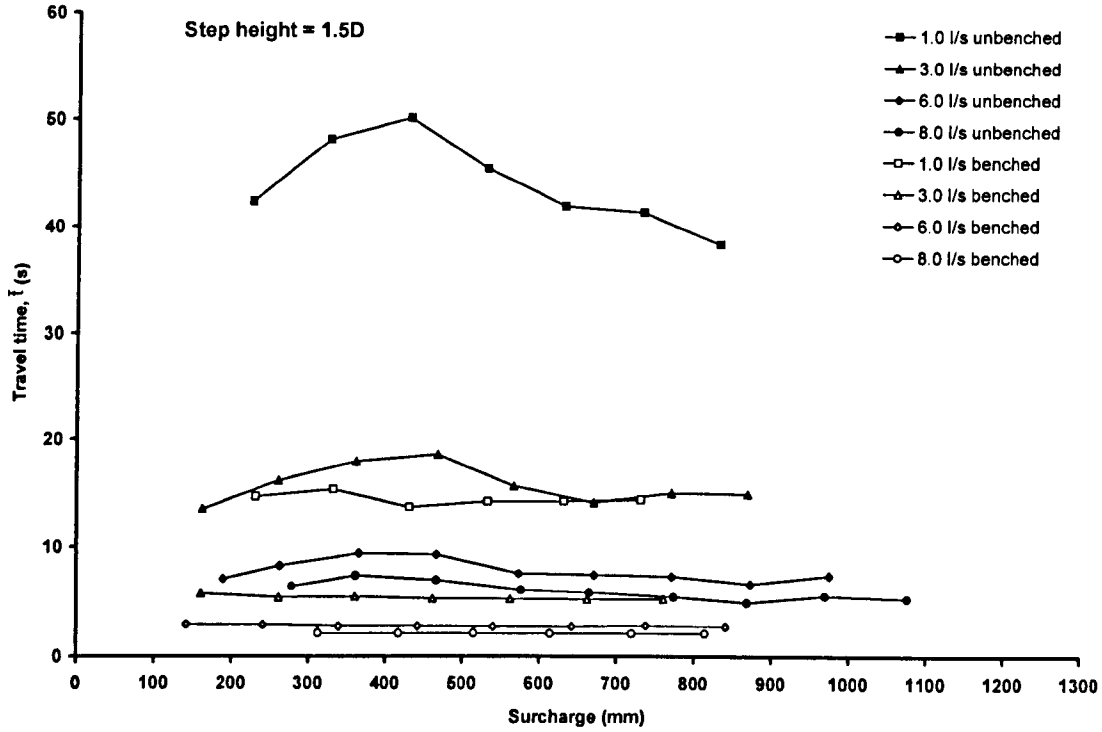

Figure 4.35 Comparison of variation of ADZ travel time with surcharge for benched and unbenched manholes.

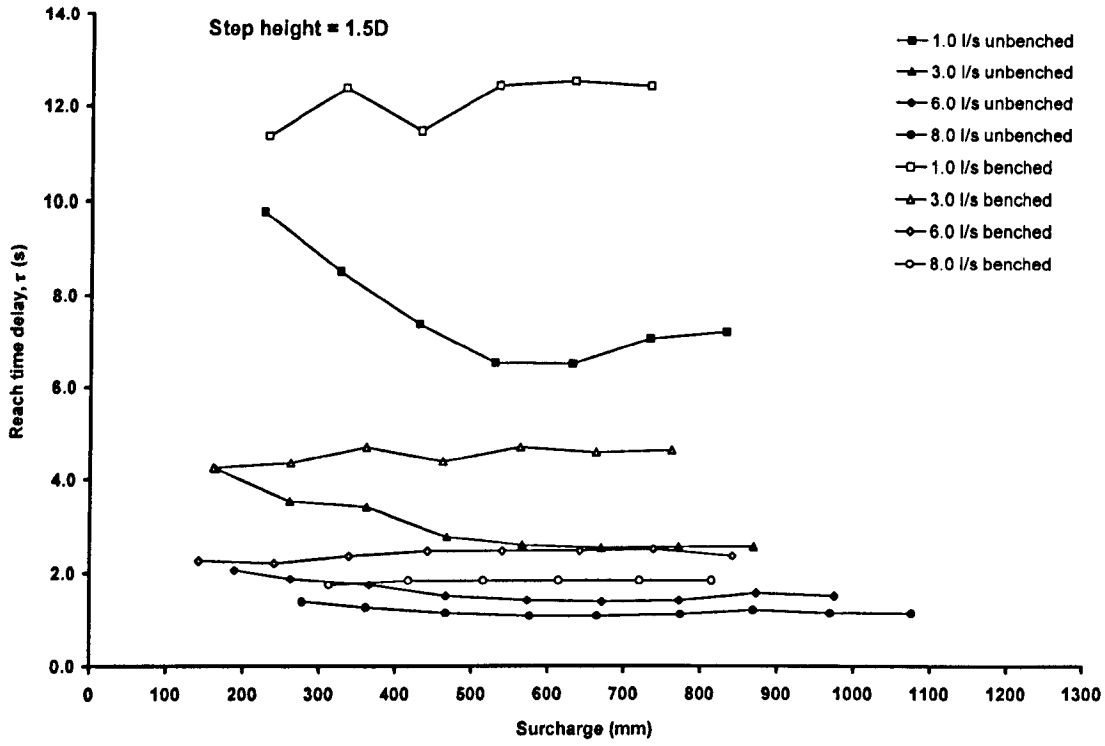

Figure 4.36 Comparison of variation of reach time delay with surcharge for benched and unbenched manholes.

Averaging the ADZ time coefficient values over the surcharge range tested provides the relationship between the time coefficient and the discharge. In a similar manner to the ADE coefficients, the results presented in Figure 4.37 demonstrate a clear reduction in travel time caused by the presence of benching in the manhole whilst the data in Figure 4.38 provides a comparison of benched and

unbenched reach time delay results in relation to the discharge. ADZ model coefficients for a straight length of pipe (Guymer and O'Brien, 2000) are also included in the figures. In both cases, the benching gives coefficients that are very similar to the straight pipe values. Friction between the passing jet and the boundary edges of the benching are clearly slowing the peak velocity, such that the reach time delay increases with benching in place. The reach time delay for the benched manhole is slightly less than that for the straight pipe. This difference can be explained by the all encompassing nature of the pipe walls, which have greater contact with the passing flow and therefore apply additional friction effects.

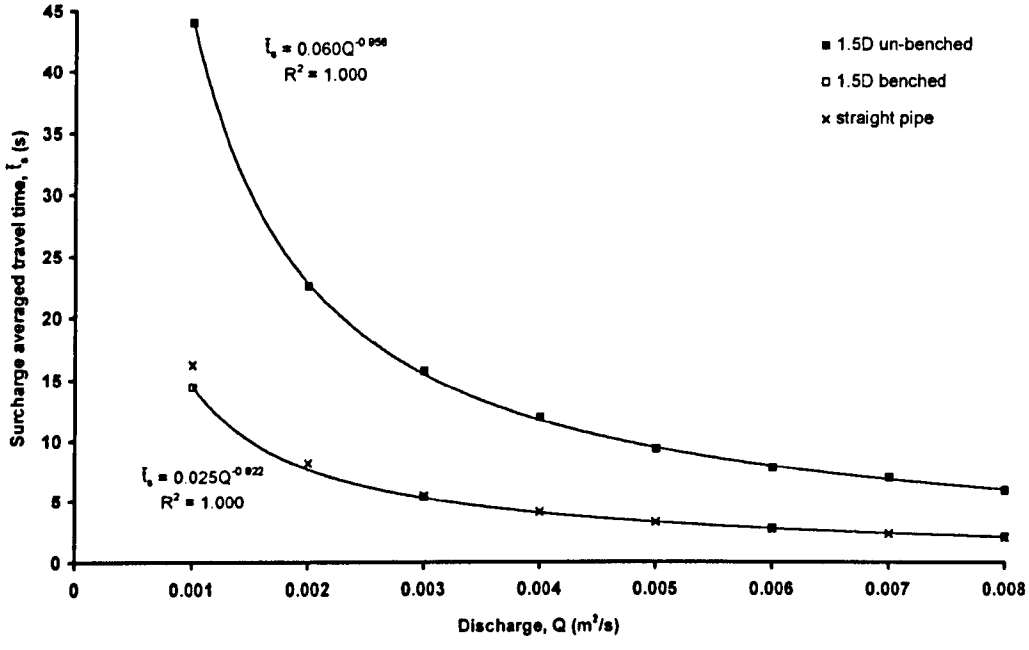

Figure 4.37 Comparison of variation of ADZ surcharge averaged travel time with discharge for benched and unbenched manholes and straight pipe (pipe data from Guymer and O'Brien, 2000).

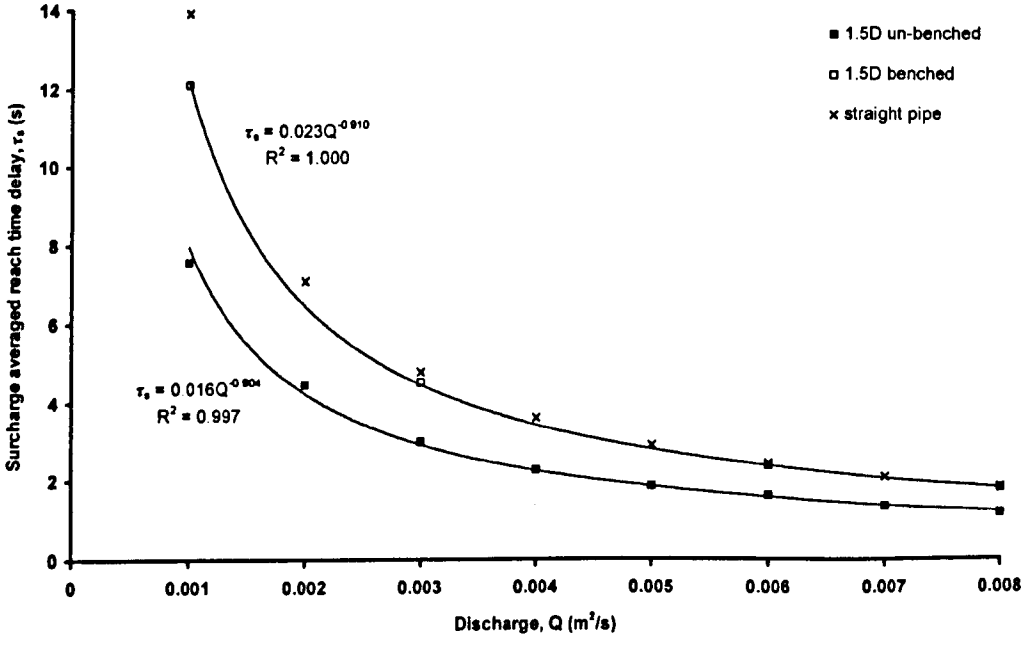

Figure 4.38 Comparison of variation of surcharge averaged reach time delay with discharge for benched and unbenched manholes and straight pipe (pipe data from Guymer and O'Brien, 2000).

	1.5D unbenched				1.5D benched			
	$\bar{t}_s$		τ_s		$\bar{t}_s$		τ_s	
Q (l/s)	mean	s.d.	mean	s.d.	mean	s.d.	mean	s.d.
1.0	44.001	3.801	7.570	1.089	14.421	0.495	12.109	0.492
2.0	22.607	2.649	4.474	0.793	-	-	-	-
3.0	15.728	1.655	3.018	0.597	5.391	0.157	4.528	0.175
4.0	11.985	1.143	2.296	0.348	-	-	-	-
5.0	9.382	0.986	1.871	0.258	-	-	-	-
6.0	7.819	0.920	1.608	0.222	2.797	0.073	2.381	0.102
7.0	7.028	0.791	1.348	0.149	-	-	-	-
8.0	5.992	0.769	1.167	0.094	2.115	0.024	1.826	0.038

Table 4.9 Comparison of benched and unbenched manhole mean and standard deviation values for surcharge averaged ADZ parameters.

4.4.5 Laser imaging

The following images in Figure 4.39, Figure 4.40 and Figure 4.41 were obtained by means of a 35mm still camera used in conjunction with a laser light sheet illuminating the central plane of the manhole. Shutter speeds in the region of 0.5 seconds were required to obtain the correct exposure. This leads to the images effectively representing the tracer movements averaged over a short time. The results of this technique are presented to show the passage of a short injection of fluorescent tracer through a manhole with no step between the inlet and outlet (Figure 4.39). The first image shows the tracer soon after having initially entered the manhole from the left. This clearly reveals a narrowing jet with at least some portion of the tracer passing directly to the outlet pipe. In Figure 4.39b, more of the tracer mass is present and some has begun to travel up and backwards within the surcharge volume. Once all the tracer has entered the manhole a jet of clear water is observed (Figure 4.39c). This jet slowly re-entrains the tracer from the volume above it and carries it into the outlet pipe. In addition, Figure 4.39d provides an indication of flow velocities by means of the reflection of light from many neutrally buoyant particles travelling with the flow. This indicates the lower comparative velocities in the surcharge volume re-circulation.

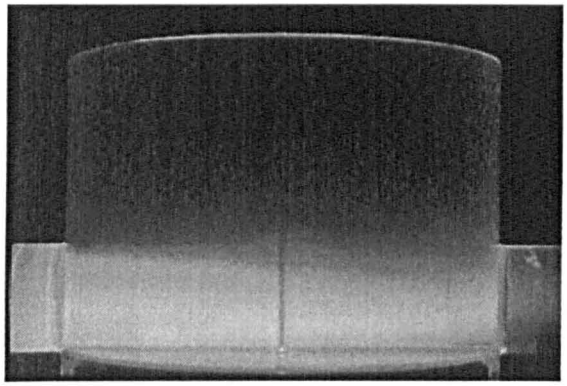

Figure 4.39a

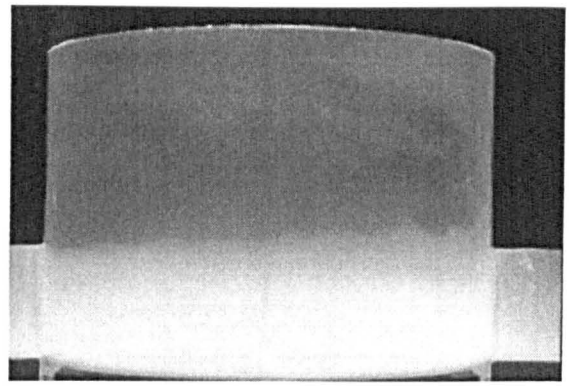

Figure 4.39b

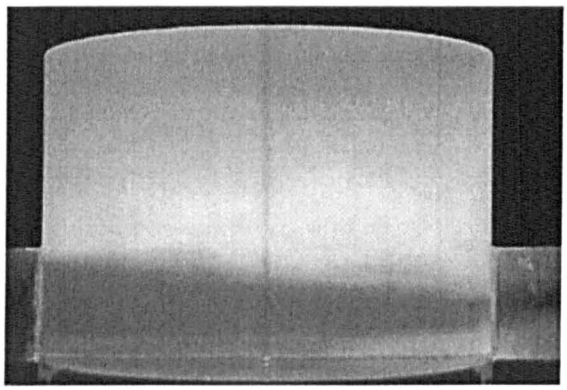

Figure 4.39c

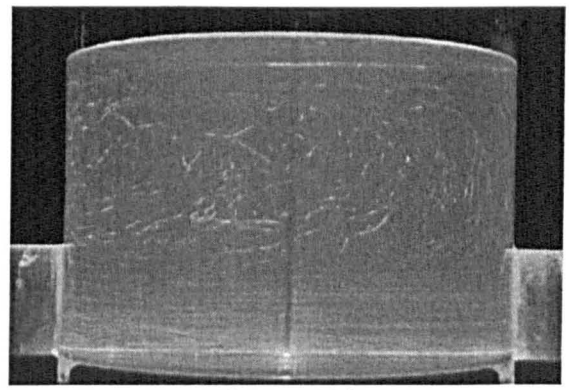

Figure 4.39d

Figure 4.39 Passage of tracer and particles through unbenched manhole with no step (Q = 1.5l/s, surcharge = 150mm).

The images in Figure 4.40 were obtained from a 1.5D step manhole at a relatively low surcharge. As before, the images show the jet of tracer entering the manhole from the left. In this case, the jet appears to be slightly distorted and tends to dip towards the outlet pipe (Figure 4.40b). In this way, as before, at least some quantity of the tracer mass passes directly through the manhole. Also, the impact of the tracer jet on the back wall of the manhole can be seen to force tracer up into the surcharged region of the chamber. The clear jet of water appears to be compressed from both above and below, though the effect is stronger from above suggesting that this region has a more powerful re-circulation effect.

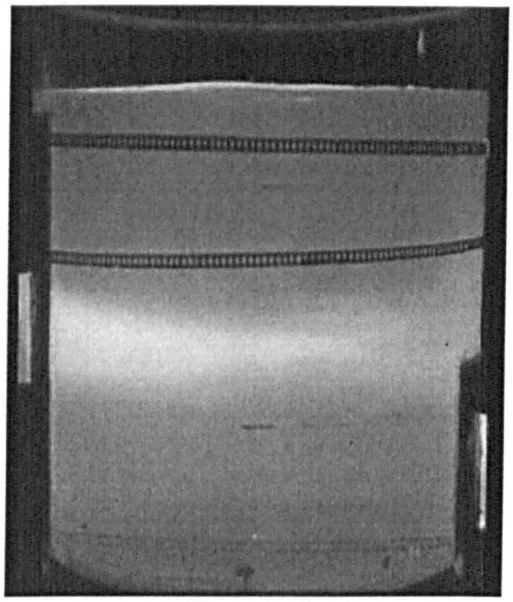

Figure 4.40a

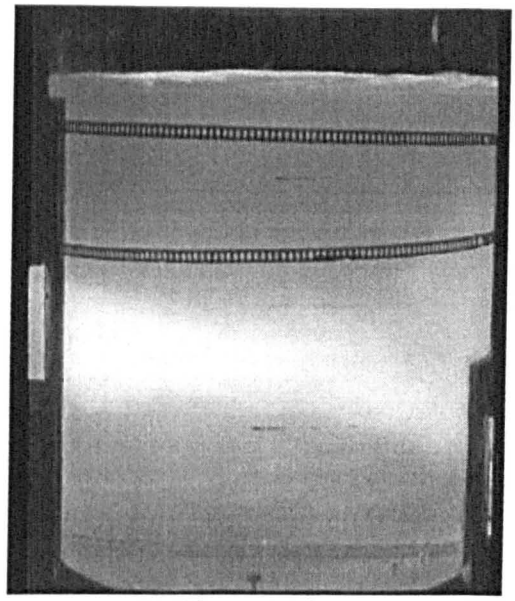

Figure 4.40b

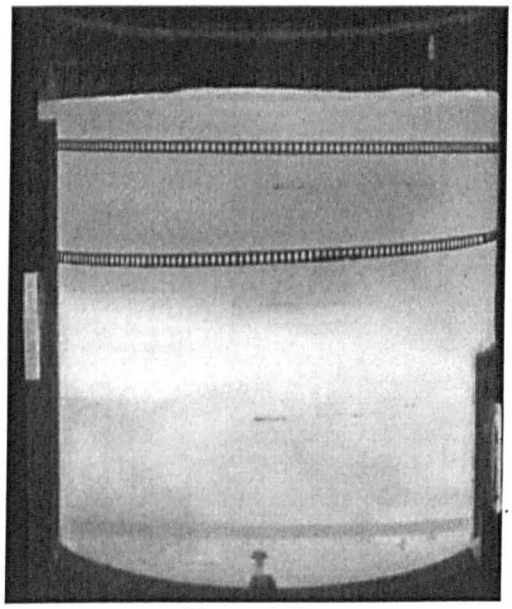

Figure 4.40c

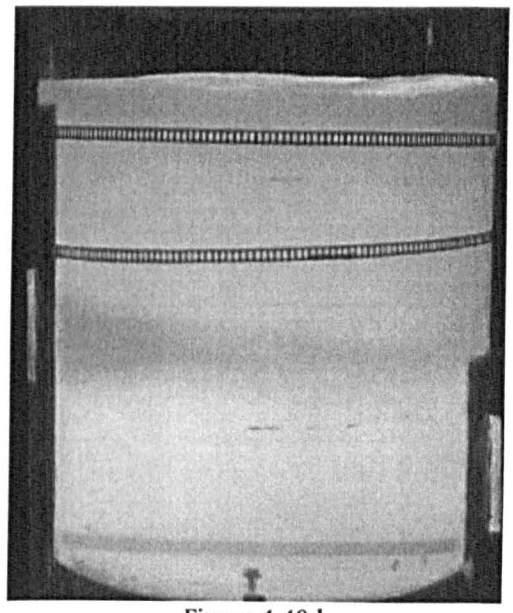

Figure 4.40d

Figure 4.40 Passage of tracer through unbenched manhole with 1.5D step at low surcharge (388mm manhole, Q = 4.0l/s, surcharge = 288mm).

The images presented in Figure 4.41 were recorded under the same flow conditions as for the previous figure except that for this case the surcharge was significantly greater. It is interesting to note from these images that the tracer injected does not appear to spread entirely throughout the surcharge volume. It must be remembered that some reduction in light intensity at upper levels will be apparent due to attenuation of the laser light sheet by the tracer lower down. However, there is a defined edge to the tracer cloud in the upper volume rather than a gradual loss of intensity and this implies a limit for the spread of the tracer. This demonstrates that the assumption of full, instantaneous mixing is not appropriate under these circumstances.

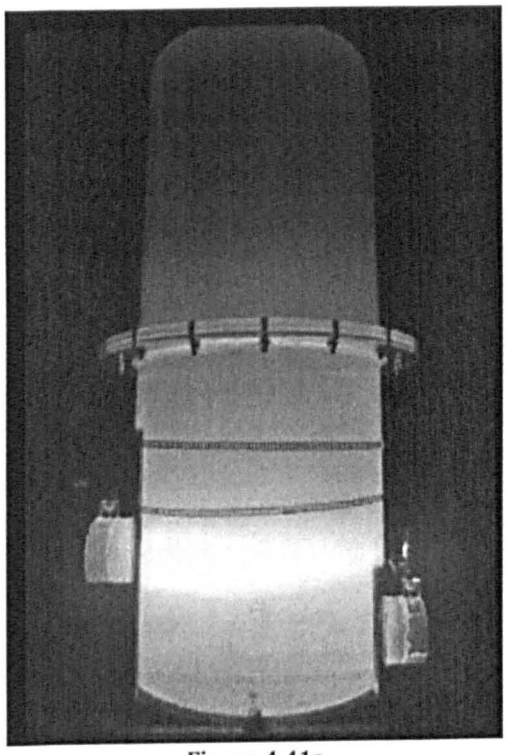

Figure 4.41a

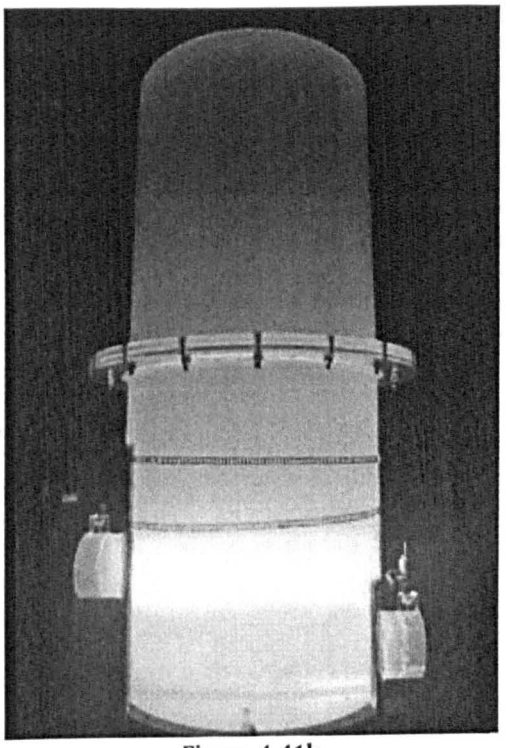

Figure 4.41b

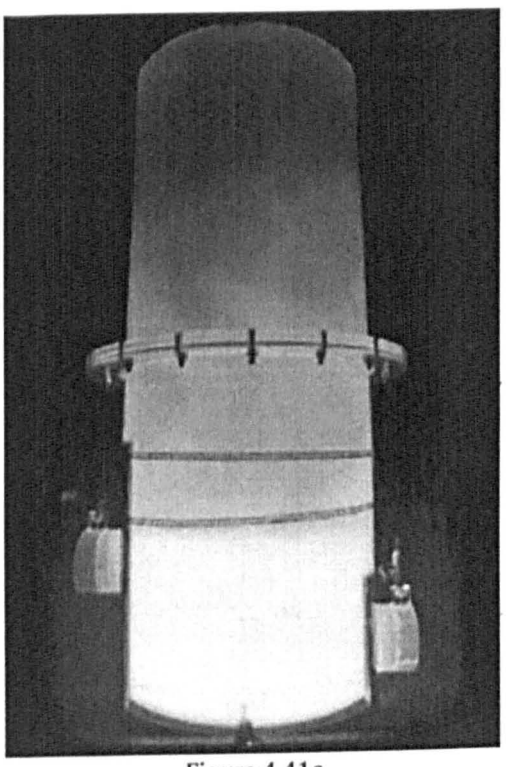

Figure 4.41c

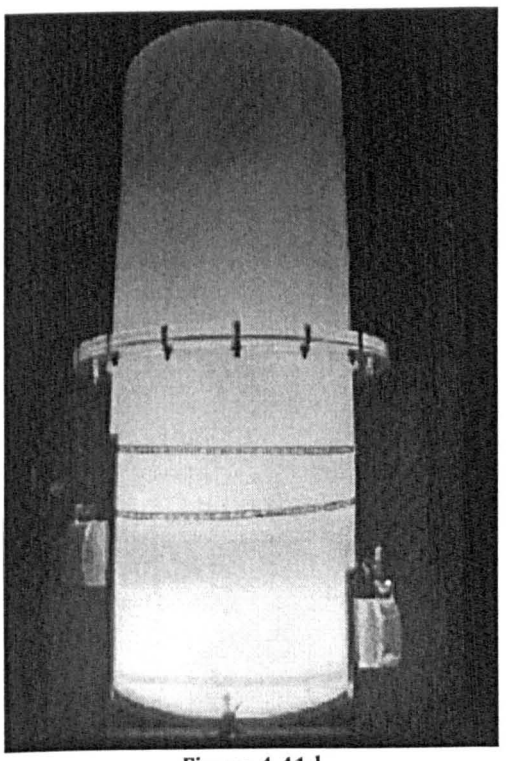

Figure 4.41d

Figure 4.41 Passage of tracer through unbenched manhole with 1.5D step at high surcharge (388mm manhole, Q = 4.0l/s, surcharge = 798mm).

Chapter 5

Discussion

5.1 Introduction

This chapter provides discussion and interpretation of the results presented previously for longitudinal dispersion and head loss due to a stepped, surcharged manhole. In addition, further results are presented for a range of manhole diameters. These data were collected by O'Brien (2000) using similar laboratory procedures to those outlined in Chapter 3. All the data from these tests have been thoroughly re-analysed using the optimisation techniques described. The range of experiments that were undertaken and analysed for the investigation of manhole diameter variations is provided in section 5.3. This gave considerable extra results from which to draw conclusions on the effects of manholes on longitudinal dispersion. Also, there was an opportunity to make a direct comparison between results obtained for a manhole of almost identical dimensions, thus giving extra confidence in the laboratory and analysis methods.

5.2 Head loss

5.2.1 Comparison of head loss results with other researchers

It has proved convenient to consider the head loss coefficient (Equation [2.1]) as a measure of the head loss due to a manhole. This eliminates the effect of the flow velocity on the results. The values of the head loss coefficient for the manhole configurations tested are presented in Table 5.1.

Step height	Head loss coefficient (K_H)
0.0 D	0.51
0.5 D	1.29
1.0 D	1.83
1.5 D	1.81
2.0 D	1.82

Table 5.1 Head loss coefficients.

Bo Pedersen and Mark (1990) present shape factors for different manholes, which allow the prediction of a head loss coefficient for a manhole of a given diameter. Their theory and experimental work revealed that for a particular manhole design there was a unique relationship between the head loss coefficient and the ratio of manhole to pipe diameter. In the case of the zero step height and unbenched condition the shape factor was determined by means of plotting the head loss results from previous researchers against the diameter ratio of the manhole concerned. A linear regression with a gradient of 0.12 was determined, and hence they proposed that $K_H=0.12(D_m/D)$. Bo Pedersen and Mark were limited by the available data to manholes with a diameter ratio less than or

equal to 4.0. However, for the work in this thesis the zero step manhole, which has a diameter ratio of 4.41, gave a predicted value of 0.53 for K_H, using the appropriate shape factor. This is very close to the experimental result of 0.51. Since the relationship developed by Bo Pedersen and Mark (1990) was developed from the experimental work of a number of researchers there is good confidence that the results from the present study are concurrent with much of the previous recognised manhole head loss research.

The head loss results for the manholes with step height variations also compare favourably with results of Kusuda and Arao (1996). Their experiments with equal diameter inlet and outlet pipes demonstrate the same pattern where the loss coefficient becomes almost constant for step heights of in the region of 1.0 to 1.5 pipe diameters or greater. This constant loss coefficient value is approximately 2.0, which is close to the value of 1.8 for the work presented here (Figure 5.1). The results from only one manhole to pipe diameter ratio from Kusuda and Arao (1996) are shown since they found that it was not a significant factor on head loss for stepped manholes.

As the step height increases between 0.0 and approximately 1.0 pipe diameters the head loss increases. It has previously been demonstrated that the reduction of the diffusion zone volume of the submerged jet, for instance by the restraining presence of benching, leads to a reduction in the head loss (Marsalek, 1984; Johnston and Volker, 1990) and this is the basis for the jet theory approach to predicting manhole head losses considered by Bo Pedersen and Mark (1990). This is discussed in more detail in section 5.8.

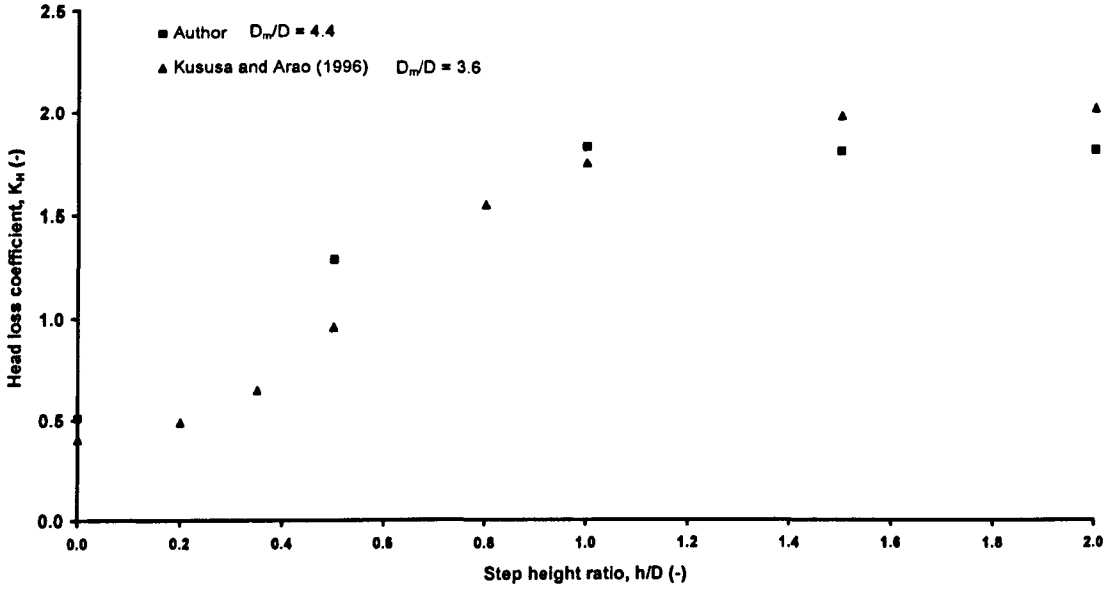

Figure 5.1 Comparison of head loss coefficient with Kusuda and Arao (1996).

5.3 Re-analysis of manhole diameter data

In addition to the laboratory tests for stepped manholes outlined in section 3.7, considerable data from previous research conducted by O'Brien (2000) were re-analysed with the optimisation procedure developed for this present work. This enabled consideration of the effect of variations in the surcharged manhole diameter on the longitudinal dispersion. The manhole diameters tested were 400, 500, 600 and 800mm giving D_m/D ratios of 4.41, 5.68, 6.82 and 9.10 respectively. Steady flow

discharges in the range of 1.0 to 8.7 litres per second were used. All manholes were without a step height condition or benching and the surcharge range tested was up to a maximum of approximately 300mm above the pipe soffits. O'Brien also provided data for re-analysis from tests conducted on a straight length of pipe with no manhole present. Test procedures were similar to those detailed for the investigation into the effect of step heights and high surcharges. Two of the differences were that data was logged at almost 167 Hertz and a different method of data preparation was used. This involved determining the start and end points of the upstream and downstream temporal concentration profiles by working away from the peak value and establishing the location of the first negative value either side of the peak. Five repeat tests for a given flow rate and surcharge combination were recorded. The profiles of the five tests were then superimposed onto each other by temporally shifting the profiles until the times of occurrence of the peak concentration values were aligned. Thus the final upstream and downstream profiles were a merged average of the five tests. To eliminate the effects of the noise on the concentration profiles the data were processed using a mathematical smoothing filter, a process described in more detail by O'Brien (2000).

To enable a direct comparison to be made between the manhole diameter and the step height results it was necessary to keep the analysis procedure similar. For this reason the manhole diameter data were sampled at a rate that gave a time step value as near as possible to that for the step height analysis. The original tracer concentration profiles were logged at 166.67 Hertz, giving a time step value of 0.006 seconds. A data sample rate of 1 in 25 was applied, thereby giving a time step of 0.15 seconds, close to the stepped manhole data which were analysed with a time step of 0.1536 seconds.

The full schedule for the laboratory tests completed by O'Brien is summarised in Table 5.2. Each manhole was circular with no step height or benching.

Manhole diameter (mm)	Discharge range (l/s)	Surcharge range (mm)	Number of tests
Straight pipe	2.1 - 10.3	n/a	7
400	1.0 - 7.6	7-282	95
500	1.0 - 7.5	10-268	60
600	0.9 - 8.7	27-309	95
800	1.0 - 6.1	27-332	23
		Total number of tests	280

Table 5.2 Summary of manhole diameter tests completed by O'Brien (2000).

The work of O'Brien (2000) included longitudinal dispersion data for a length of straight pipe. The measured head loss was used in conjunction with Equation [2.15] proposed by Taylor (1954) to determine a theoretical value for the dispersion coefficient of 3.6Qm^2/s. The standard analysis method applied to the laboratory data gave a dispersion coefficient for the pipe of 8.0Qm^2/s. However, the optimisation of the ADE coefficients resulted in the value of K being determined as 3.3Qm^2/s, thus further improving confidence in the procedure.

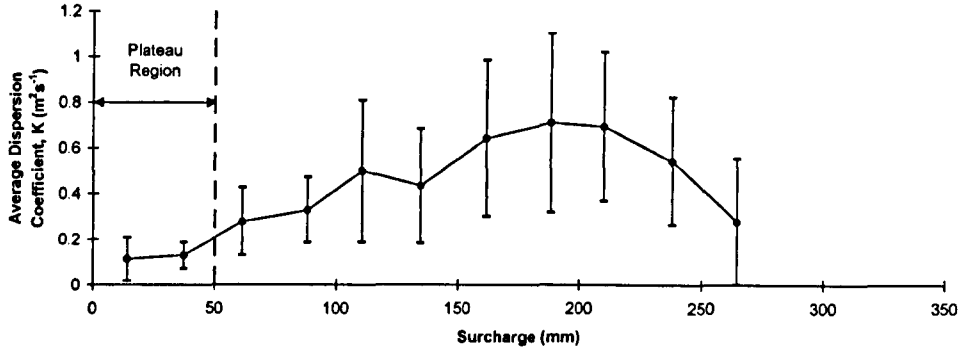

Figure 5.2a 400mm diameter manhole

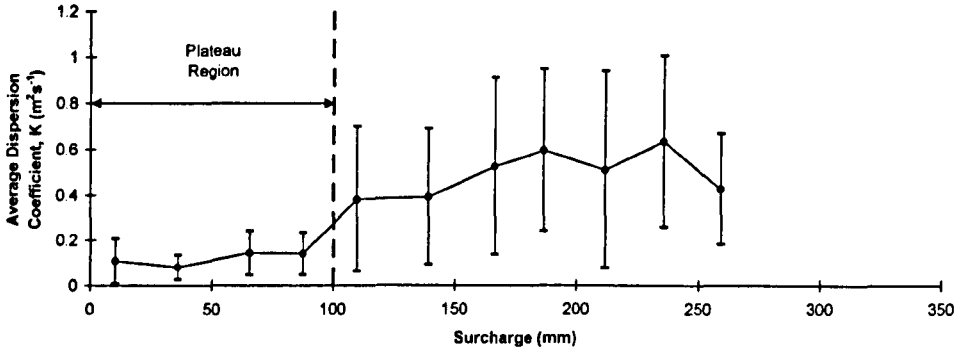

Figure 5.2b 500mm diameter manhole

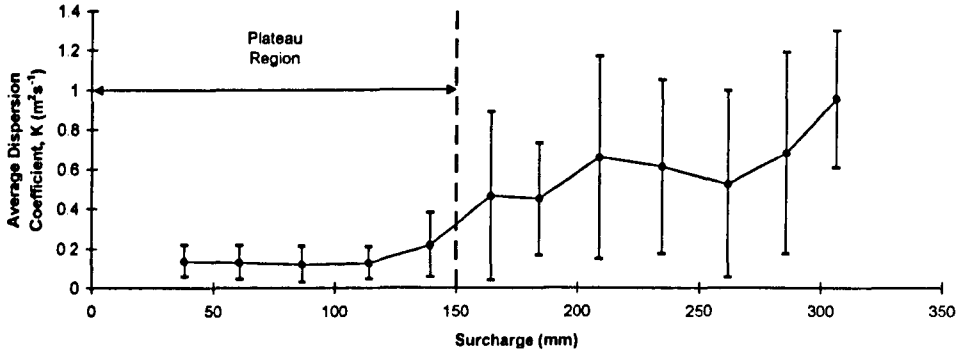

Figure 5.2c 600mm diameter manhole

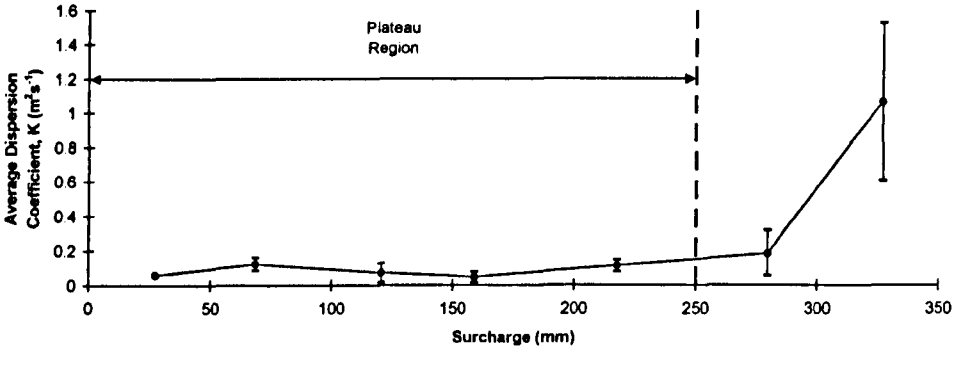

Figure 5.2d 800mm diameter manhole

Figure 5.2 Variation of discharge averaged dispersion coefficient with surcharge determined with standard ADE procedure (O'Brien, 2000).

The earlier work of O'Brien (2000) for longitudinal dispersion in manholes with varying diameter was originally analysed using a standard procedure to determine the coefficients for the ADE and ADZ models. One of the reasons for the present work examining the effects of high surcharge levels was because of the recorded trend in the variation of dispersion coefficient with surcharge. These data demonstrated a tendency for there to be a plateau region of low dispersion coefficient at low surcharges, and this was followed by significant increase and variation in dispersion coefficient values as the surcharge was increased above a certain level, dictated by the manhole diameter (Figure 5.2). The experimental investigation in this current study was designed to obtain data that could be used to clarify the trends for dispersion coefficient at higher surcharge levels. In fact, the re-analysis of data gathered by O'Brien using an optimisation procedure resulted in somewhat different trends for the variation of dispersion coefficient with surcharge.

5.4 ADE longitudinal dispersion

Figure 5.3 and Figure 5.4 present a combination of the results of the author's laboratory investigation and the re-analysis of a similar manhole design used by O'Brien (2000). There is generally good agreement between the results, which indicates that the data manipulation and smoothing process employed by O'Brien does not adversely affect the final coefficients. Including these extra results from the laboratory tests completed by O'Brien has allowed a more comprehensive study of the effect of surcharge on the ADE coefficients determined, with increased detail in the low surcharge region, which previous head loss research has highlighted as a significant area.

A comparison of the ADE travel time results from the present study and the data provided for a 400mm diameter manhole is shown in Figure 5.3. The general trend for any flow rate where a low enough surcharge was achievable is for there to be a rapid increase in travel time to a maximum value as the surcharge increases between a value of zero and approximately 40mm. Further increases in surcharge result in the travel time decreasing and for surcharges of approximately 150mm or greater the travel time is almost constant.

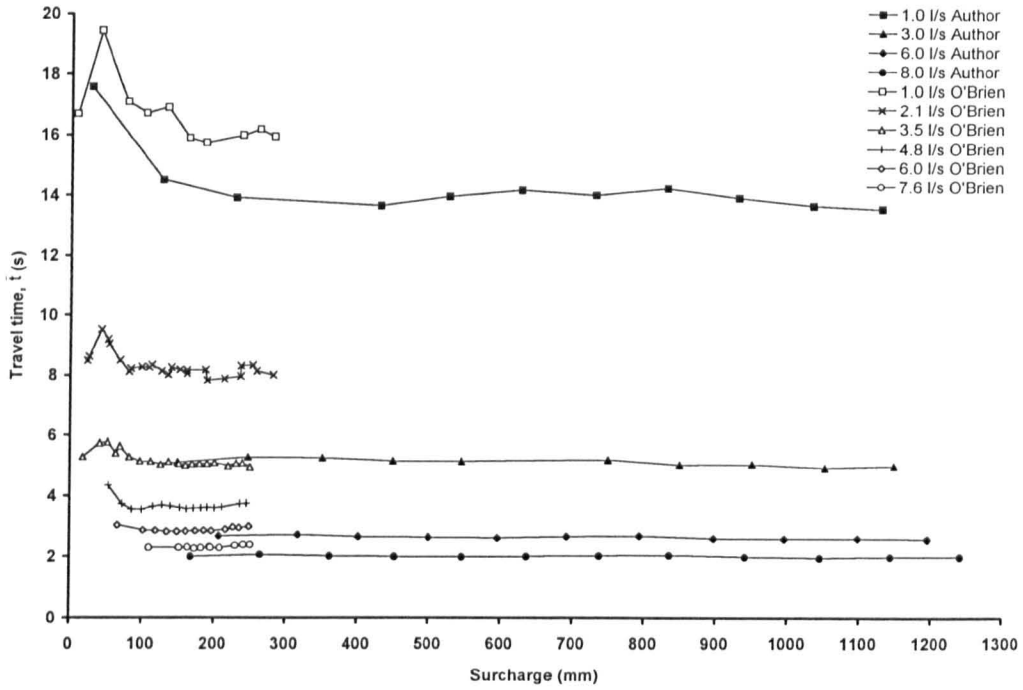

Figure 5.3 Comparison of ADE travel time data from Author and O'Brien (≈388mm unbenched manhole with no step).

The comparison of dispersion coefficient data for similar manholes is shown in Figure 5.4. The data in this figure provide a clear case for the need to extend the work of O'Brien to greater surcharge depths. Although there is some scatter in the data for surcharges less than 300mm there are trends evident. Between surcharge values of zero and approximately 200mm the dispersion coefficient for any discharge tends to reduce, before increasing again to a maximum as the surcharge reaches approximately 350mm. Further increases in the surcharge result in a significant reduction in the dispersion coefficient, which is then almost constant for any surcharge greater than approximately 500mm. The constant dispersion coefficient value that is measured for the higher surcharges is in the region of 10-20 percent of the maximum dispersion coefficient for the same discharge.

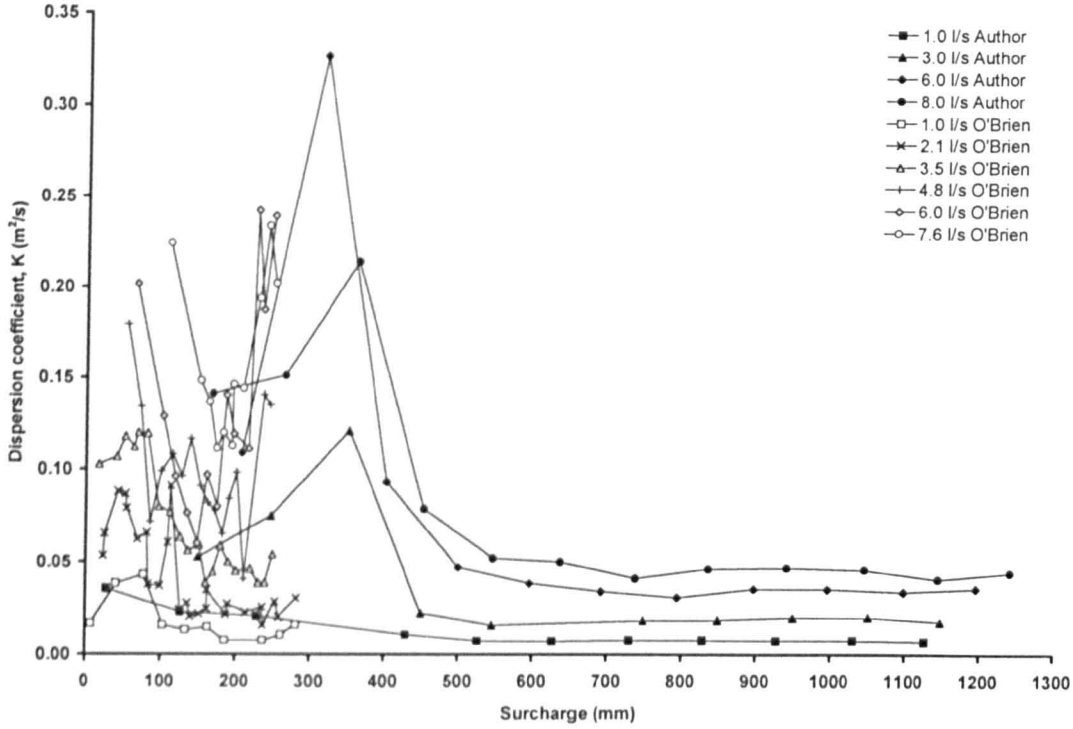

Figure 5.4 Comparison of dispersion coefficient data from Author and O'Brien (≈388mm unbenched manhole with no step).

The variation of travel time with surcharge for different manhole diameters displays some very clear trends. The results of the re-analysis of the data collected by O'Brien are presented in Figure 5.5. For a particular discharge the travel time increases with surcharge in an approximately linear fashion to a maximum value at a certain surcharge that increases with increasing manhole diameter. There is then a sudden drop in travel time after the maximum value and then no further variation with increasing surcharge. It has been observed that there is a particular surcharge level for each manhole diameter where the travel time coefficient becomes almost constant, and an approximate surcharge level for this, based on averaging the upper and lower limits for different discharges, has been marked on the figures. The peak travel time value increases as the manhole diameter increases. This is most noticeable between the 400mm and 500mm diameters, and the increase is much less between the larger manholes.

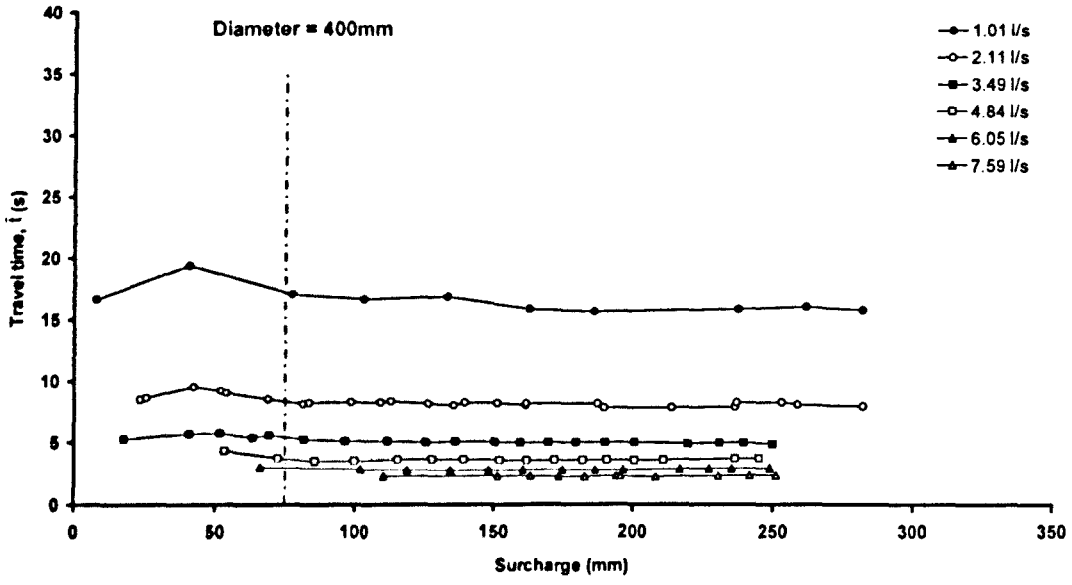

Figure 5.5a

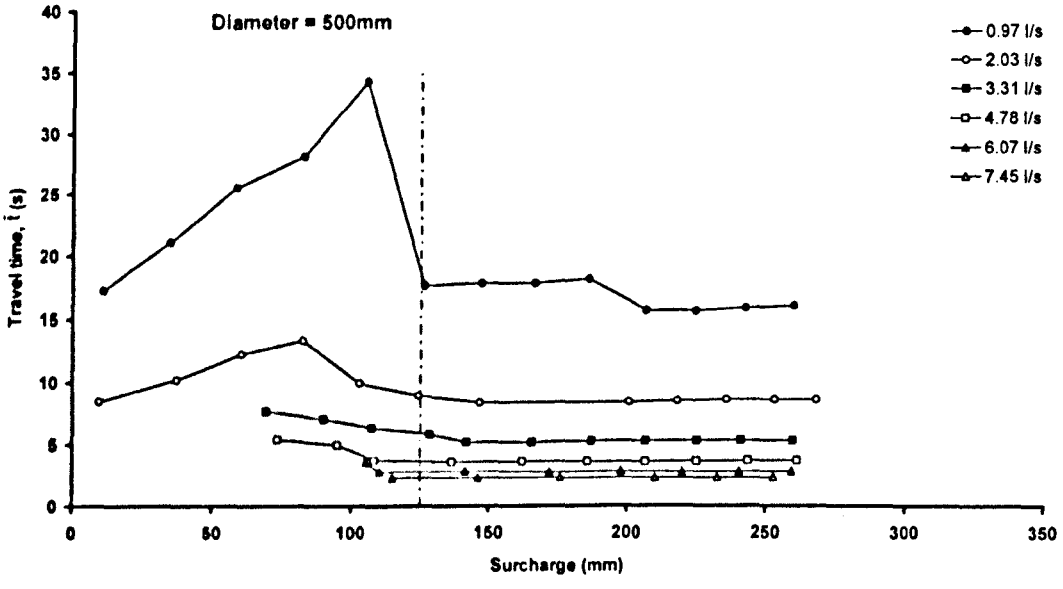

Figure 5.5b

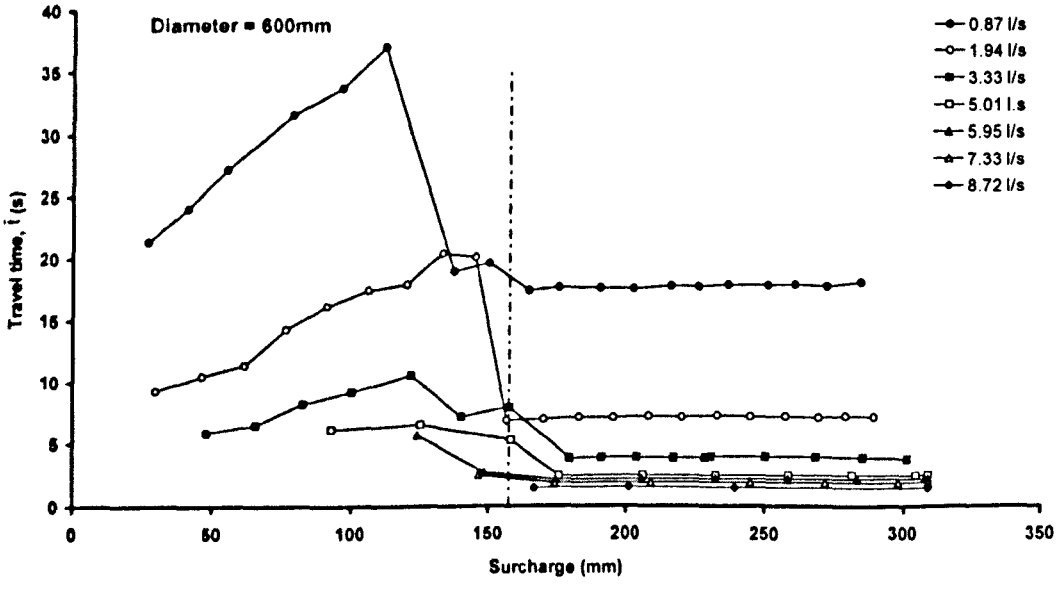

Figure 5.5c

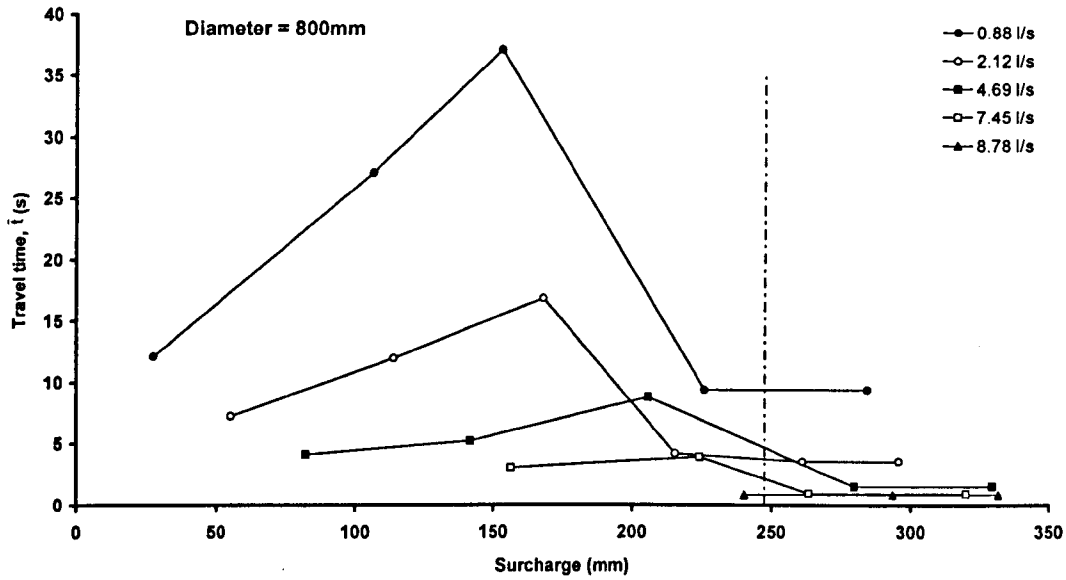

Figure 5.5d

Figure 5.5 Variation of ADE travel time with surcharge for manhole diameters.

It would be very beneficial to be able to predict this travel time surcharge threshold for different diameters. Figure 5.6 presents the data for threshold level as a function of the manhole diameter with error bars included to represent the extremes of the surcharge threshold for different discharges. Over the range of manholes that has been tested there is an extremely good linear relationship. Therefore, it should be possible to obtain a reliable estimate of the surcharge level above which ADE travel time values will be constant for a solute passing through the manhole for any manhole within this range.

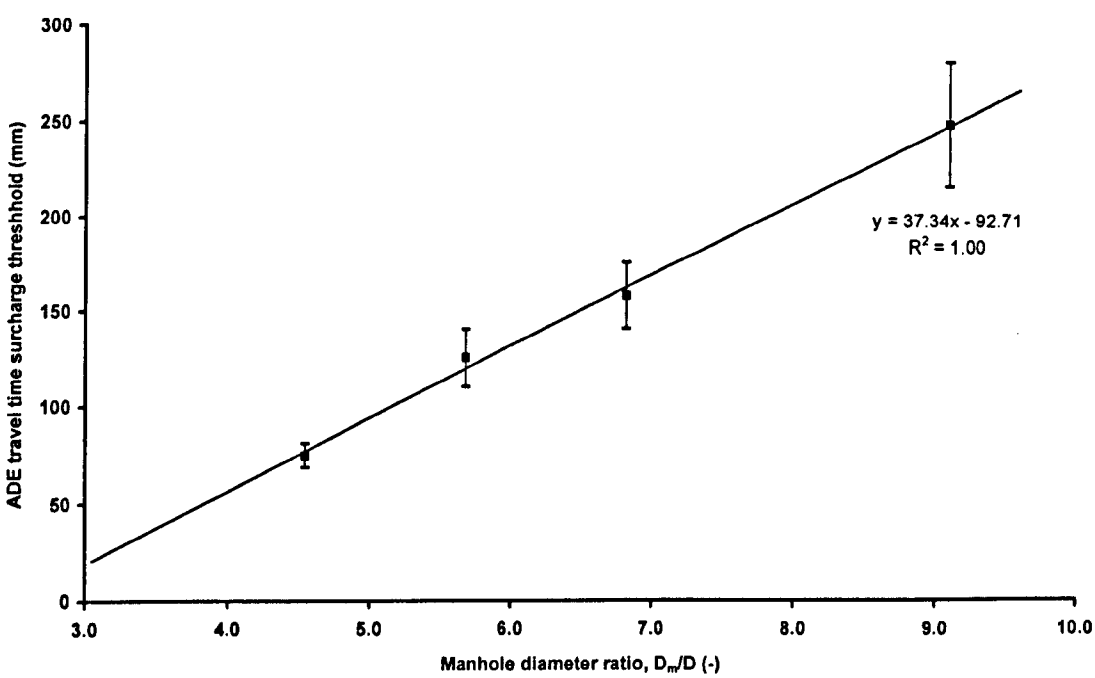

Figure 5.6 Variation of ADE travel time threshold surcharge with manhole diameter.

Trends for the dispersion coefficient are less clear for different manhole diameters (Figure 5.7). The 400mm diameter manhole demonstrates two peak dispersion coefficient values, one at the very low surcharges and one in the region of the greatest surcharges tested in this case. This pattern is more obvious in Figure 5.4 where the manhole diameter re-analysis results are combined with data from the present study to provide a more complete picture. With the 500mm manhole the trends are similar but it would appear that the maximum surcharge levels tested are not great enough to include the second peak in the dispersion coefficient, potentially associated with the transition from predominantly horizontal to vertical re-circulation patterns. This suggests that a transition such as this would be caused by the volume of water in the manhole attaining a certain aspect ratio in relation to the manhole diameter. This theory is supported by the results from the 600mm diameter manhole, although these data have a somewhat increased scatter making the trends less discernible. Again it would appear that the possible occurrence of a second peak in the dispersion coefficient values cannot be validated without results from experiments at greater surcharges. There is a lack of data for the 800mm diameter manhole, which makes it difficult to draw any satisfying conclusions regarding the effect of surcharge on the dispersion coefficient in this case (Figure 5.7). In addition, the figure is somewhat distorted by the presence of an extreme data point for the 7.45 litres per second results. The original temporal concentration profiles supplied were thoroughly examined for the cause of this high dispersion coefficient value. Whilst the profiles did reveal unusually high dispersion in comparison to those for similar conditions, there was insufficient evidence to confirm that the data was actually unreliable and the data point has therefore remained included in the results.

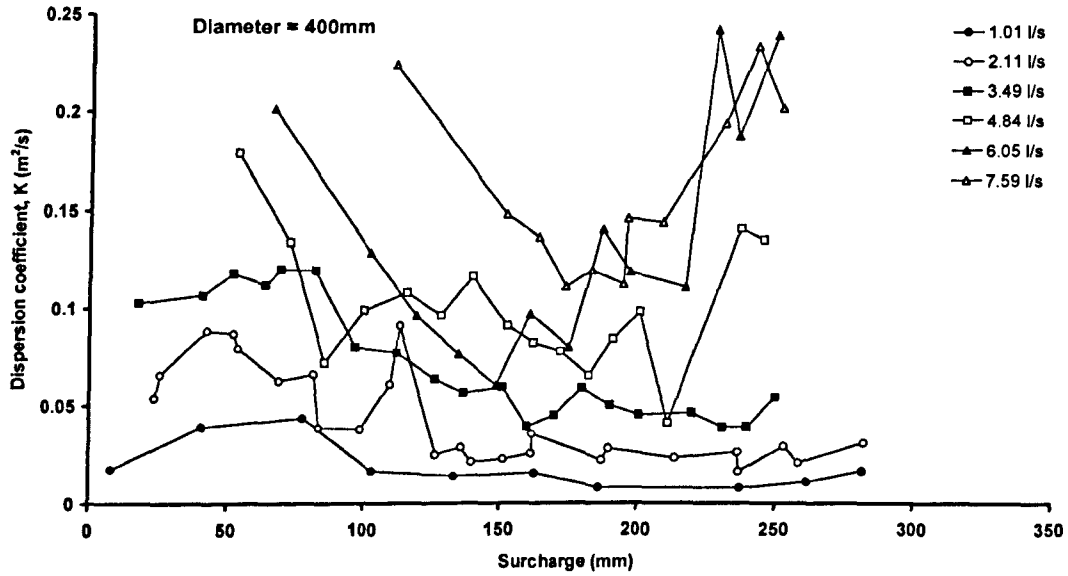

Figure 5.7a

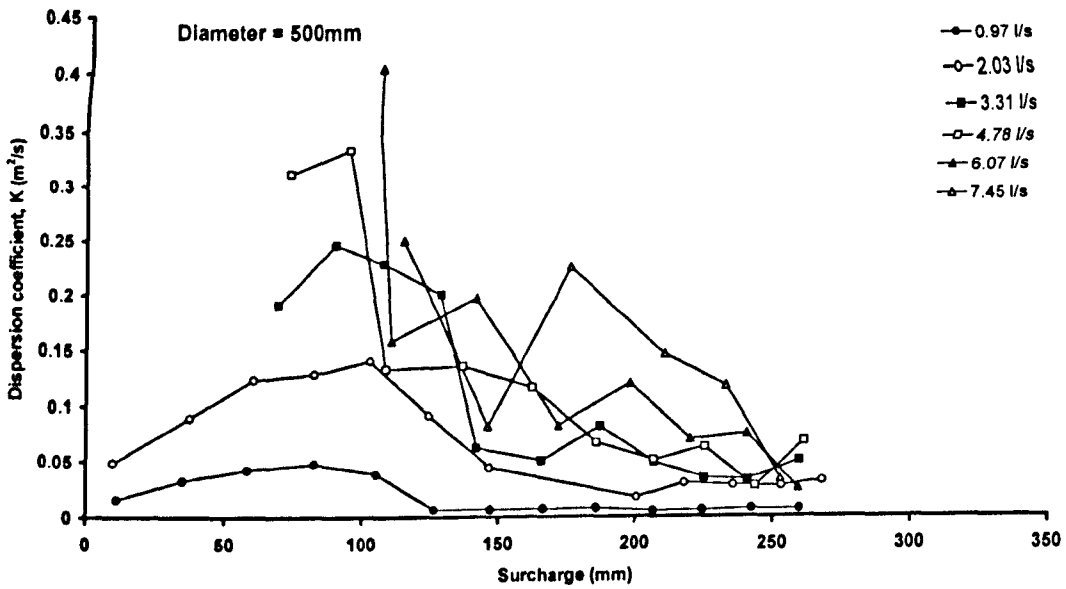

Figure 5.7b

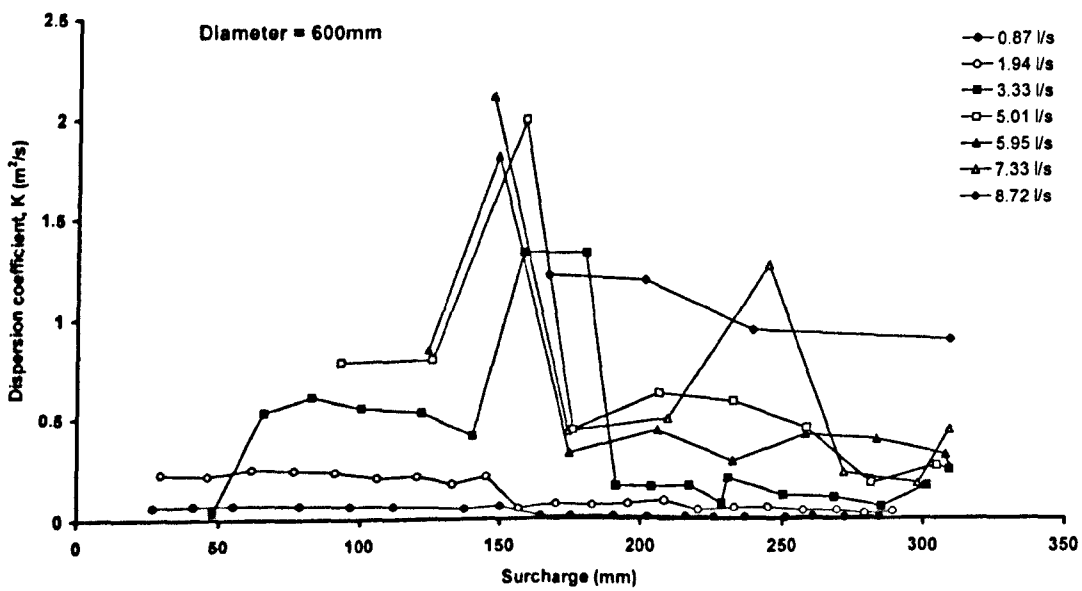

Figure 5.7c

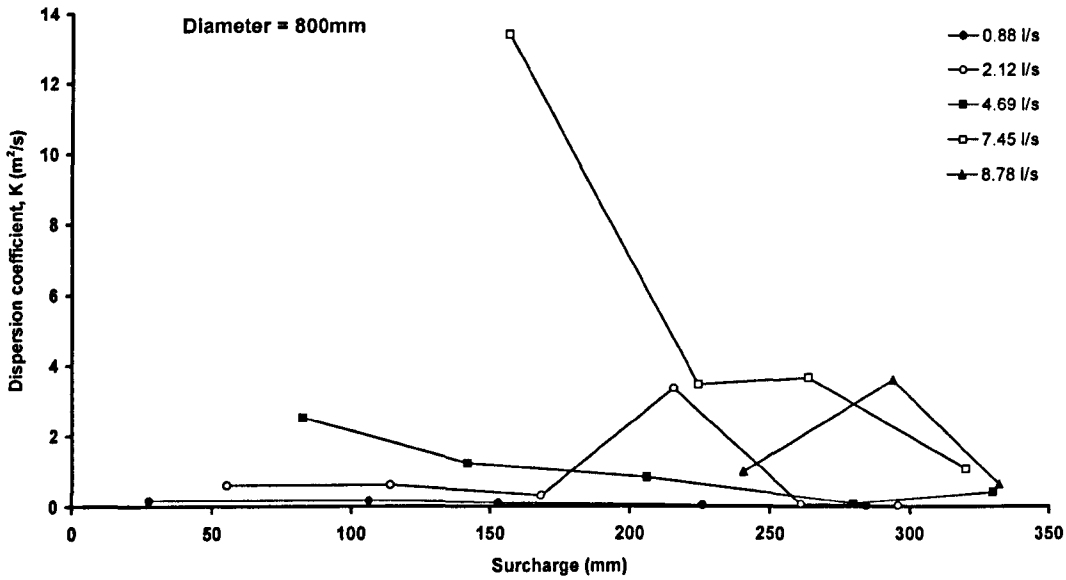

Figure 5.7d

Figure 5.7 Variation of dispersion coefficient with surcharge for manhole diameters.

5.5 ADZ longitudinal dispersion

Figure 5.8 presents a comparison of the ADZ travel time data obtained from the laboratory 388mm diameter straight through manhole with the results for the 400mm manhole studied by O'Brien (2000). It can be seen that the results for the same flow rate and surcharge combination are similar and thus there is confidence that the method of concentration profile averaging and smoothing employed by O'Brien does not affect the ADZ optimised results unduly. The data show a peak travel time value at a surcharge of approximately 50mm for those flow rates that could be tested at these low surcharges. The travel time then decreases as surcharge increases further before rising to another peak at approximately 350mm. Surcharges greater than approximately 450mm have no further effect on the travel time, which remains almost constant for a given discharge up to the maximum surcharge. This is a very similar trend to that displayed by the dispersion coefficient with the ADE analysis. If it is assumed that the reach time delay is a function of the velocity profile only, then the travel time component of the ADZ equation is the part that gives a measure of the longitudinal dispersion, and reflects the presence or otherwise of a long tail on the downstream tracer profile. Thus the variation of travel time with surcharge appears to reflect the trends displayed by the dispersion coefficient.

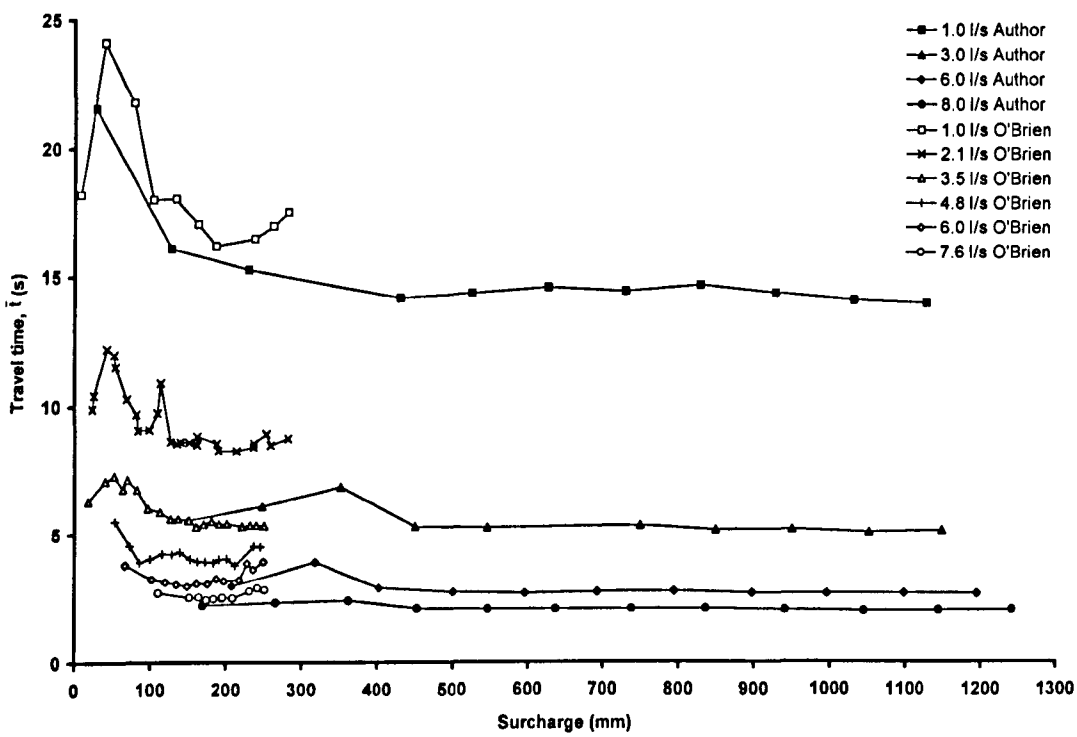

Figure 5.8 Comparison of travel time data from Author and O'Brien (≈388mm unbenched manhole with no step).

The comparison of the reach time delay variation with surcharge between the current laboratory results and the re-analysis of the data collected by O'Brien is presented in Figure 5.9. There is generally good agreement between the two sets of results, although there is a degree of scatter for the results from O'Brien's data at lower discharges. Predominantly the time delay values are independent of surcharge and the discharge has a far greater influence over the results.

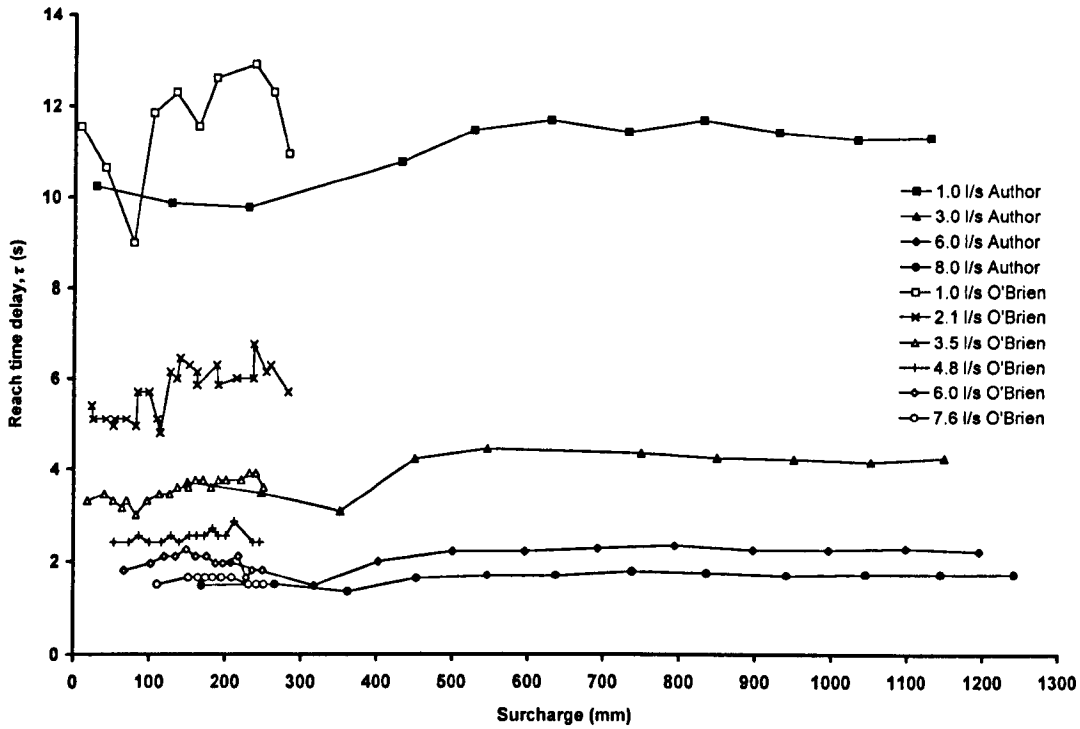

Figure 5.9 Comparison of time delay data from Author and O'Brien (≈388mm unbenched manhole with no step).

The variation of ADZ travel time with surcharge for different manhole diameters has been evaluated after re-analysis of the data collected by O'Brien (Figure 5.10). The travel time increases sharply with surcharge in an approximately linear fashion to a maximum value at a surcharge that appears to be dictated by the manhole diameter. Further increases in surcharge result in a sudden drop in travel time and then no further variation with increasing surcharge. Again this pattern highlights a particular surcharge level for each manhole diameter where the travel time coefficient suddenly reduces and becomes almost constant. The upper and lower limits for this threshold for different discharges have been averaged and the resulting mean threshold surcharge has been marked on the figures. The peak travel time value increases by a factor of approximately two between the 400mm and 500mm diameters and continues to increase to a lesser extent between the results from the larger manholes.

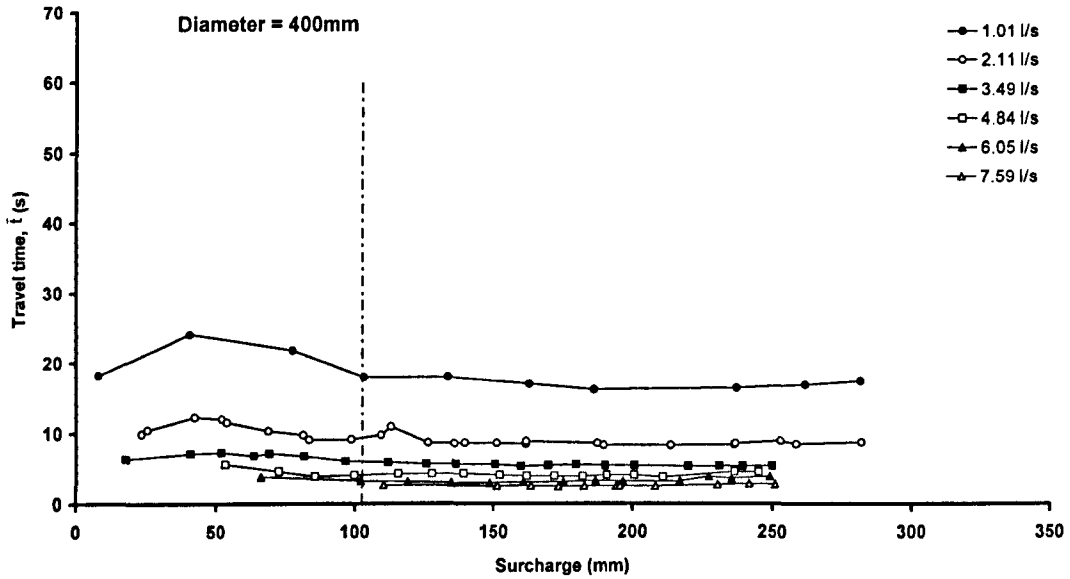

Figure 5.10a

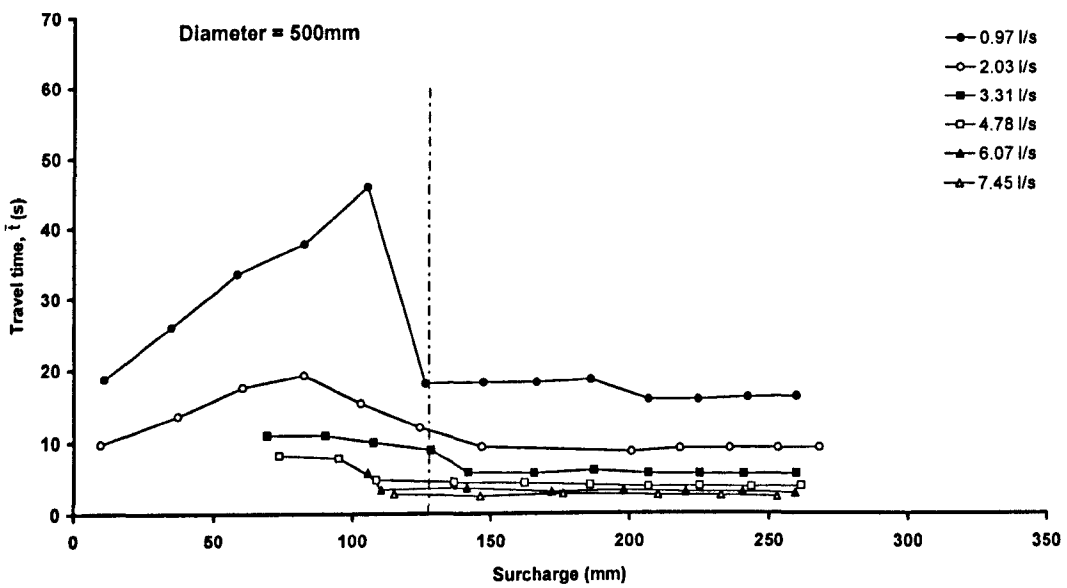

Figure 5.10b

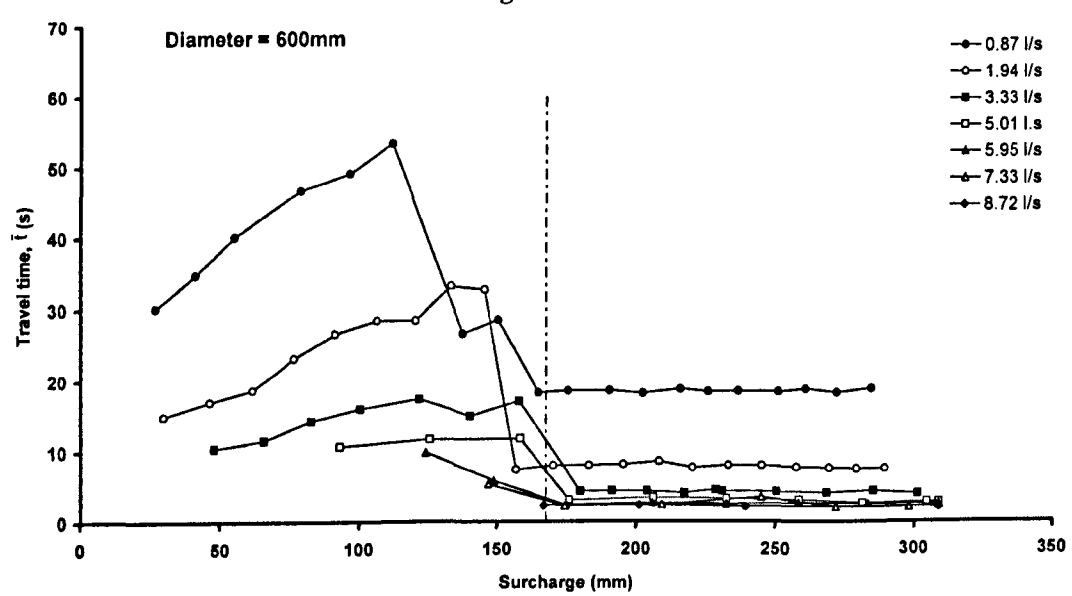

Figure 5.10c

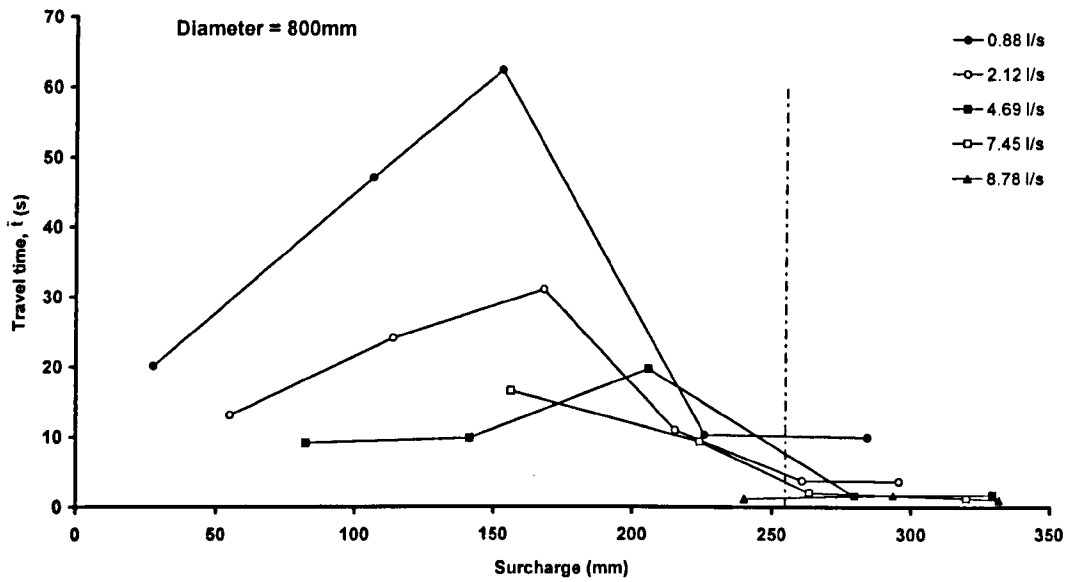

Figure 5.10d

Figure 5.10 Variation of travel time with surcharge.

In a similar manner to the ADE travel time, it appears possible to be able to predict the surcharge threshold for the ADZ travel time coefficient as a function of the manhole diameter. Again, error bars are used to mark extreme threshold values from different discharges. There is a good linear relationship between the manhole diameter and the surcharge threshold over the range of manholes that have been tested.

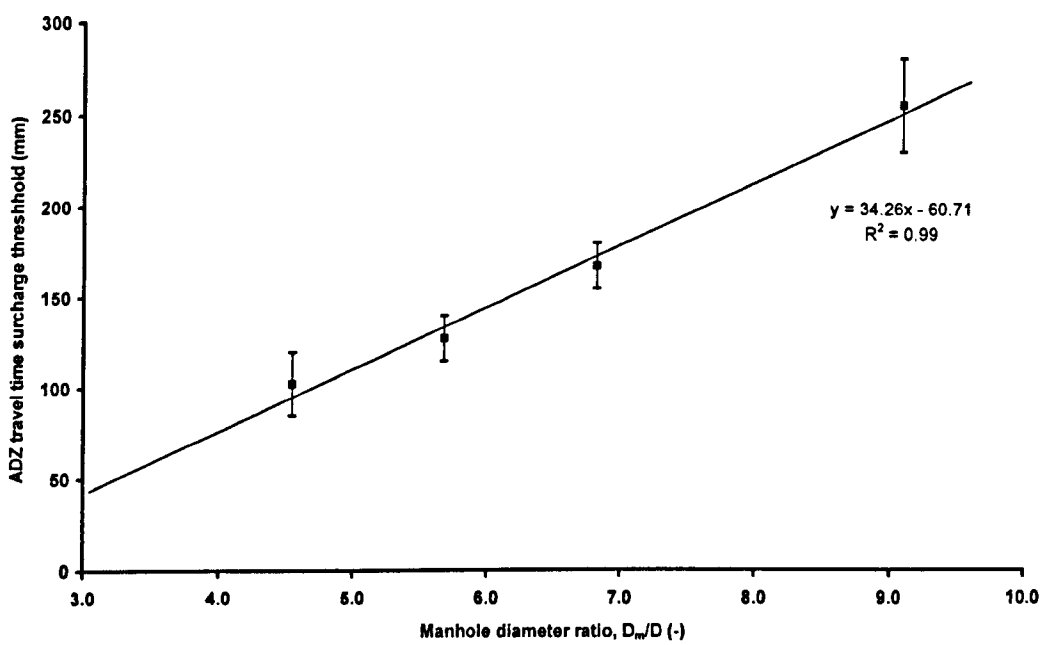

Figure 5.11 ADZ travel time threshold.

The response of the ADZ reach time delay values to variations in surcharge and manhole diameter (Figure 5.12) reflect the same theory as applies to the stepped manhole cases. It is assumed that at least some fraction of the tracer injected passes directly through to the downstream pipe. Therefore the time delay is largely independent of the surcharge level.

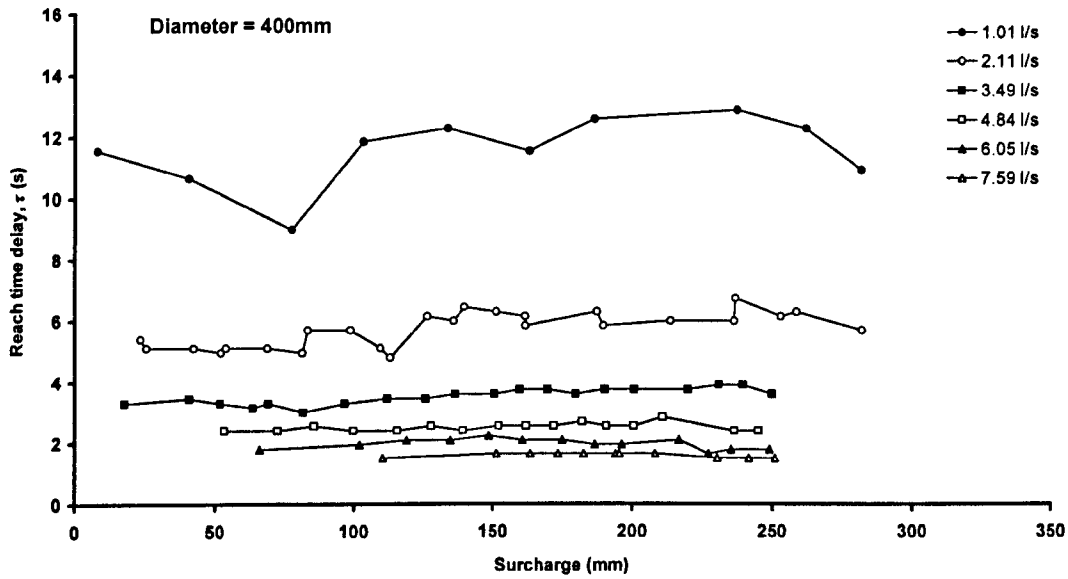

Figure 5.12a

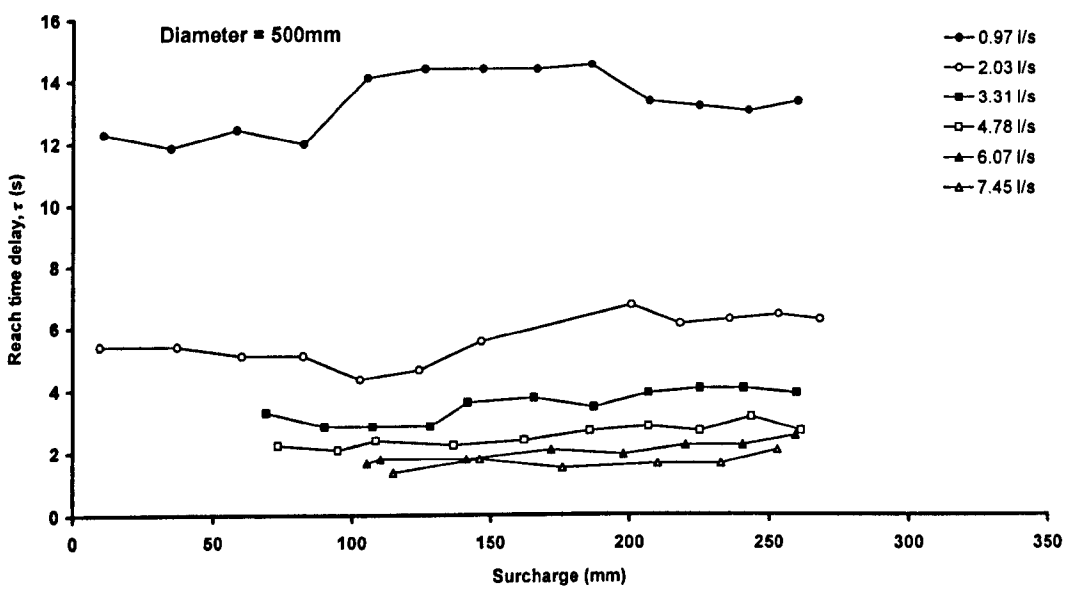

Figure 5.12b

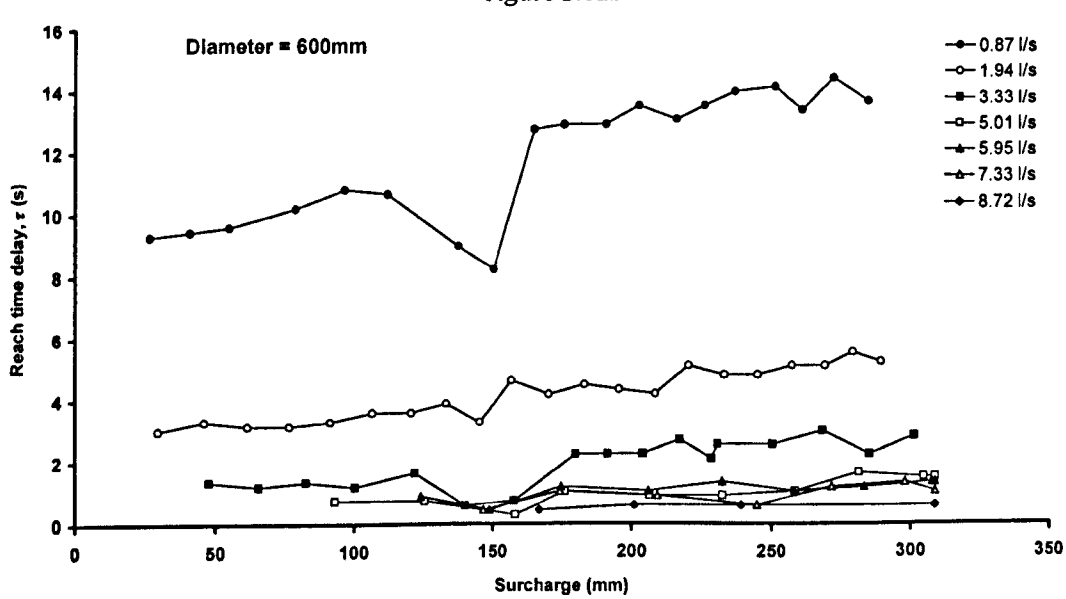

Figure 5.12c

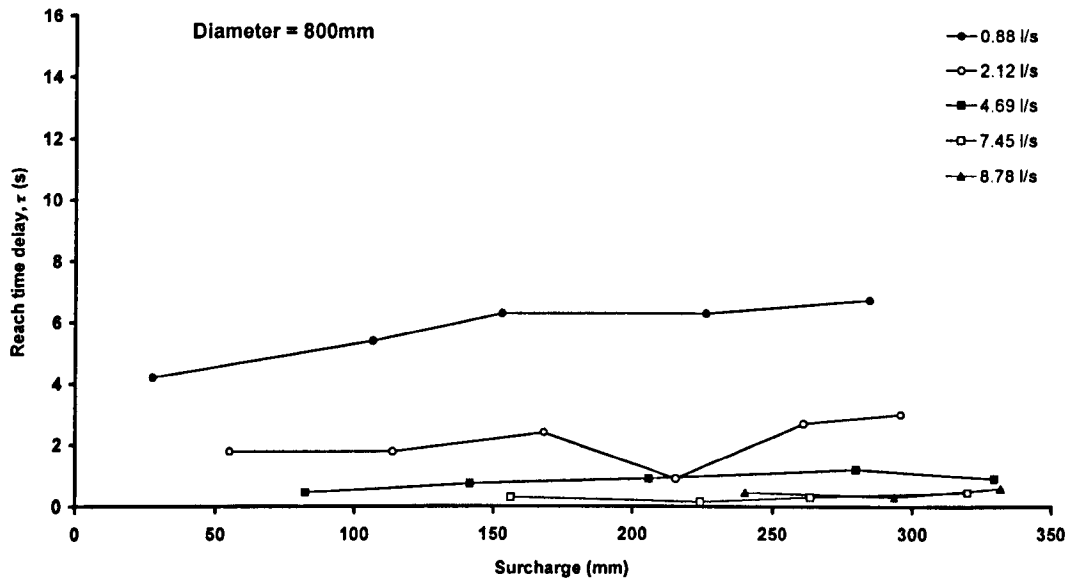

Figure 5.12d

Figure 5.12 Variation of time delay with surcharge.

There is considerable variation in the ADZ travel time values at low surcharges. Therefore, in order to examine the effect of discharge on the travel times for the different manhole diameters only travel times for surcharges greater than the surcharge threshold for the particular manhole have been considered. The data presented in Figure 5.13 illustrate that for manholes with a surcharge above the threshold value the travel time will be very similar to that for a straight pipe, regardless of the manhole diameter. The 800mm diameter manhole varies from this pattern slightly. However, the relationship for this case is defined by very few data points and therefore must be treated with caution. Error bars represent one standard deviation about the mean value.

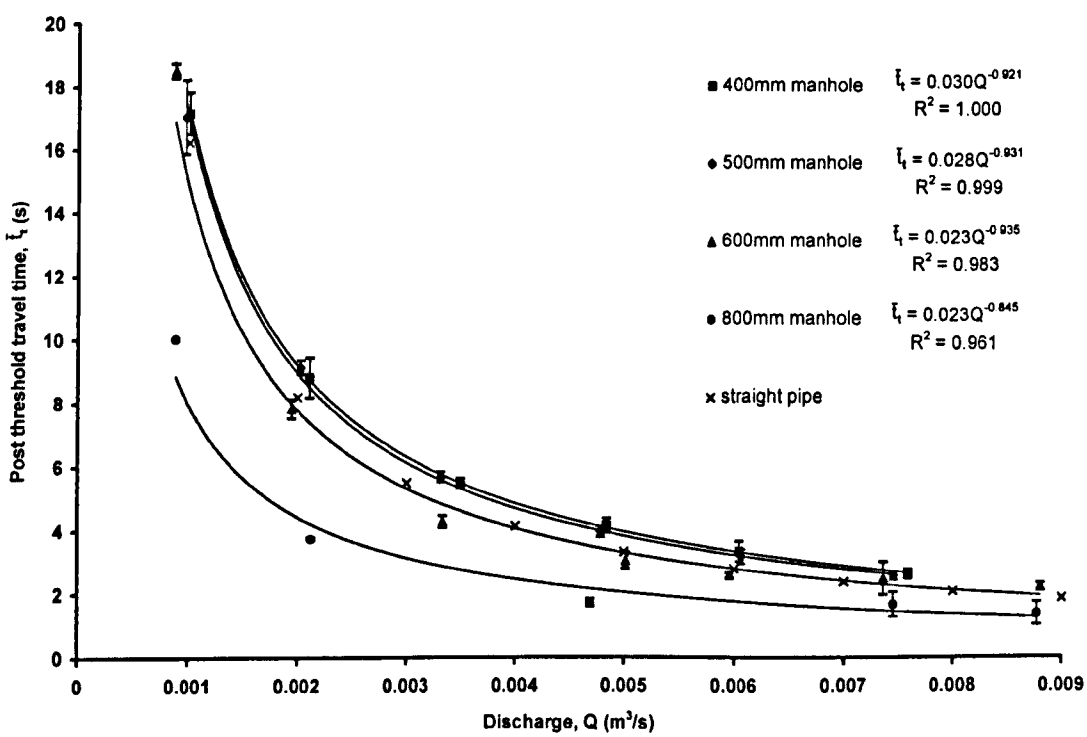

Figure 5.13 Variation of ADZ post threshold travel time with discharge for manhole diameters.

The level of surcharge has little effect on the reach time delay, the time difference between the first arrival of the tracer at the upstream and downstream measuring locations. The effect of discharge is shown by the data in Figure 5.14. Error bars are included to show one standard deviation either side of the surcharge average. These data indicate that there is generally a good fit to an inverse power law. The fastest travelling fraction of the tracer is transported between the fluorometer locations more rapidly than it would be by flow through a straight pipe. This implies that the maximum flow velocity through the system is increased by the presence of a manhole. Examination of images of the jet flow through the manhole has revealed that re-circulation patterns cause a narrowing of the incoming jet which gives rise to a related increase in velocity. In addition, the jet in the manhole is free of some of the pipe friction effects and therefore the maximum velocity is likely to be increased.

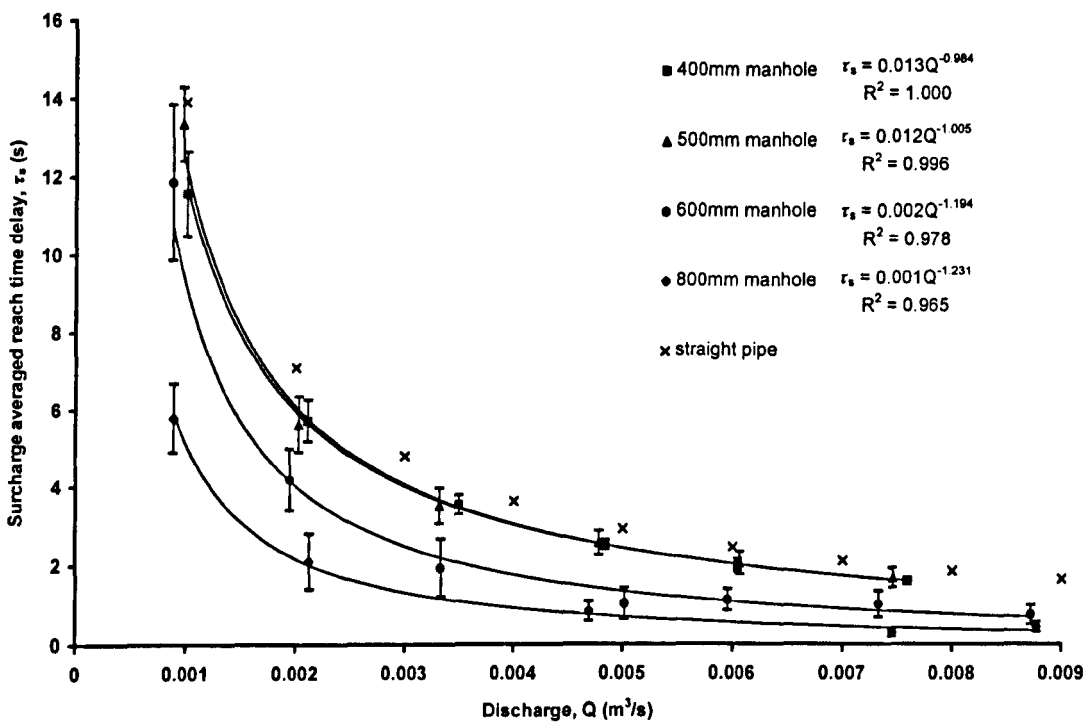

Figure 5.14 Variation of surcharge averaged reach time delay with discharge for manhole diameters.

5.5.1 Equivalent pipe length analysis

A simple procedure for incorporating longitudinal dispersion due to surcharged manholes into the processes of sewer water quality modelling software would be to represent the manhole by an equivalent length of pipe. The work of Guymer and O'Brien (2000) presented data for flow through a length of straight pipe between the fluorometer locations. This gave equations for the tracer cloud mean travel time and the reach time delay with respect to the discharge through the pipe. These were in good agreement with theoretical values. The ratio of the measured travel time between the fluorometers and through the manhole to the straight pipe travel time over the same distance gives the equivalent number of pipes (Equation [5.1]).

$$P_t = \frac{\bar{t}_m}{\bar{t}_p} \qquad [5.1]$$

where P_t= travel time equivalent number of pipes, $\bar{t}_m$ = measured travel time with manhole in position and $\bar{t}_p$ = straight pipe travel time.

In a similar way the equivalent pipe time delay is given by

$$P_\tau = \frac{\tau_m}{\tau_p} \qquad [5.2]$$

where P_τ= time delay equivalent number of pipes, τ_m= measured time delay with manhole in position and τ_p= straight pipe time delay.

Thus a value greater than unity for the equivalent pipes implies that the centroid or leading edge of the tracer cloud travels slower through the manhole than it would be expected to through a straight length of pipe. Conversely, a value less than unity means that the presence of the manhole causes an increase in average or maximum speed over that of pipe flow.

The results from analysing the manhole tracer studies have highlighted the problem with applying an equivalent pipe length method for application in a sewer model. The nature of flow through a surcharged manhole results in the leading edge of the tracer cloud travelling faster through the length of the system than it would through a straight pipe. At the same time, the surcharged volume in the manhole retains a proportion of the tracer mass and releases it only gradually. This causes the centroid of the tracer to travel slower through the manhole system than through a straight pipe. Therefore there is no single equivalent pipe length that can be used to represent the manhole in terms of both the travel time, $\bar{t}$, and the reach time delay, τ, simultaneously. For this reason the longitudinal dispersion due to manholes in sewers is required to be modelled individually at the junctions with coefficients appropriate to the particular manhole, rather than employing a pipe length with pipe coefficients to represent the manhole.

5.6 Flow patterns

The longitudinal dispersion results presented for stepped manholes and variations in diameter need to be examined with regard to the flow patterns and re-circulation profiles observed in the surcharged chamber. There appears to be a strong correlation between the flow regime observed and the measured dispersion results. The images obtained using the vertical laser lightsheet provide increased insight into the flow regimes within the manhole. This technique has provided a first look at the mixing processes that are present in stepped manholes, and whilst not giving a quantitative analysis, useful understanding has been gained. The incoming jet is noticeably compressed by the re-circulation of the flow. It is also possible to see how a proportion of the tracer passes directly to the outlet pipe. The step height case shows the tracer highlighting how the jet impacts on the downstream face of the manhole. In the extreme high surcharge case the tracer has failed to reach the very upper levels of the surcharge volume, even after a considerable period of time. It would appear that the nature of the re-circulations within the manhole prevent full mixing from occurring.

In the case of the straight through manholes, it is assumed that at the lowest surcharge levels the flow patterns are predominantly horizontal, since there is a restricted volume above the incoming jet to allow re-circulations in a vertical plane. For a given discharge at low surcharges under approximately 100mm, the flow conditions in the manhole were observed to produce more vigorous motion and re-circulation than at higher surcharges. Included in these patterns at higher flow rates were a steep standing wave at the downstream wall and small whirls forming on the free surface.

Under these circumstances, the dispersion was measured as being greater than that occurring once the surcharge had risen slightly higher. This is attributed to the motion encouraging more tracer to be forced out of the main through flow and into these strong re-circulation regimes, thus causing greater longitudinal dispersion.

As the surcharge increases flow patterns are damped slightly, and whilst the system is likely to remain structured in the horizontal plane, less tracer mass is released out of the main flow and the dispersion coefficient reduces. However, when the water depth reaches a particular level, which in this case is a little less then the manhole diameter, it may be considered that the re-circulation pattern alters from predominantly horizontal to a regime with a significant vertical re-circulation element. Hence it is postulated that for lower surcharges, flow from the incoming jet which does not pass directly to the outlet tends to return to the inlet region in a horizontal plane. At higher surcharges at least some portion of the returning flow passes back towards the inlet in a vertical plane. This circumstance causes an increase in solute dispersion due to the greater mixing opportunities and the larger dead zone volume. Further increases in surcharge result in a significant reduction in the longitudinal dispersion. At these surcharges the flow pattern for all discharges was recorded as being very calm. It is therefore surmised that this flow regime results in much smaller quantities of tracer being released from the submerged jet into the surrounding surcharge volume. Under these circumstances the travel time and dispersion effects of the surcharged manhole are remarkably similar to those for a straight pipe.

There is an increase in the longitudinal dispersion that occurs if there is a step height between the inlet and outlet. The increase in step from 0.0D to 1.0D causes the most significant rises in the dispersion. Further step height increases result in little additional dispersion effects. With the presence of a step height there is greater contact between the submerged jet and the surrounding volume resulting in a greater transfer of tracer to the dead zone regions through the entrainment process.

Manholes with benching in place cause considerably less longitudinal dispersion than their unbenched counterparts. This reduction is due to the benching restricting the volume of the submerged jet available for interaction with the surrounding volume. As such, the specific geometry of the benching, such as half pipe or full pipe depth, will determine the amount by which the dispersion is reduced. In the case tested, with a 1.5D step manhole and a deep benching channel, the response of the manhole to the tracer experiments was very similar to that of a straight pipe.

5.7 Dispersive fraction

As a means of further understanding the mixing processes occurring in the manhole it is worth considering the dispersive fraction of the system. This has been used by previous ADZ model users (Young and Wallis, 1996; Wallis *et al*, 1989a, 1989b) as a measure of the proportion of the total reach volume that is responsible for dispersion. In many cases for laboratory channels, man made large scale channels and natural rivers the dispersive fraction has been found to be almost independent of discharge. The value for the dispersive fraction appears to well reflect the dead zone features of a particular reach such that higher dispersive fraction values occur for the natural channel shapes where more dead zone and mixing activity can be expected. Indeed there has been an interest in classifying flow conditions through the dispersive fraction from a broad range of research studies, an

example of which is the work of Lancaster and Hildrew (1993). They investigated the feasibility of using the dispersive fraction results from an ADZ analysis as a method for quantifying areas in a stream that remain quiescent even during high discharge events. They had hypothesised that the abundance of these features was related to the availability of refuge areas for macroinvertebrates. They discovered that the dispersive fraction did not vary with discharge in any of the streams examined, and was indeed related to the refuge availability. Therefore, the different streams could be broadly categorised in terms of dispersive processes by means of the dispersive fraction.

There is no method as yet for predicting the dispersive fraction of a reach without completing tracer measurements. Part of the problem here is that there are many mixing conditions that are difficult to measure. For instance, a natural river is likely to have dead zone effects along the banks and also along the riverbed caused by rocks, pebbles and vegetation as well as the general channel shape. The ADZ model simply lumps these conditions together as one effective dead zone. With so many variables it would be difficult to single out the longitudinal dispersion effects caused by individual dead zone elements, especially along the channel bed where measurements would be difficult to obtain.

The circumstances for a surcharged manhole chamber are very different. The size and geometry can be measured in detail with a high degree of accuracy and there is only a single, principal dead zone element. Under these circumstances the dispersive fraction parameter can be considered a very powerful coefficient, and there is a possibility that its value for a particular manhole could be predicted without the need for tracer dispersion experiments once a range of laboratory studies have been completed.

Figure 5.15 presents the data for the variation of the dispersive fraction with respect to the surcharge level in the manhole for the 388mm manhole for all step heights. Each data point is the average of the values from the five repeat tests completed. Since the time delay at a given discharge is almost independent of surcharge the dispersive fraction follows the trends of the travel time parameter. Considering the cases where the step height is equal or greater to 1.0 pipe diameters (Figure 5.15c, d and e) the dispersive fraction variations are very similar. The minimum value for the dispersive fraction occurs at the lowest surcharges and increases slightly with surcharge until the water level reaches a surcharge of approximately 400mm. At greater water depths, the dispersive fraction remains almost constant at a value of approximately 0.8. This suggests that any increase in step height above 1.0 pipe diameters causes no increase in the mixing volume. The pattern for step heights less than 1.0 pipe diameters is somewhat different. In these cases the values of dispersive fraction rise to a maximum in the lower surcharge region before dropping again to reach an almost constant value at surcharges over approximately 400mm. These constant values are much reduced from the values at higher step heights, being approximately 0.6 for the 0.5 pipe diameter step and 0.2 for the case with no step. This suggests that the physical boundaries of the manhole, which restrict the incoming jet, cause a reduced volume of mixing activity in the turbulent regions surrounding the jet core.

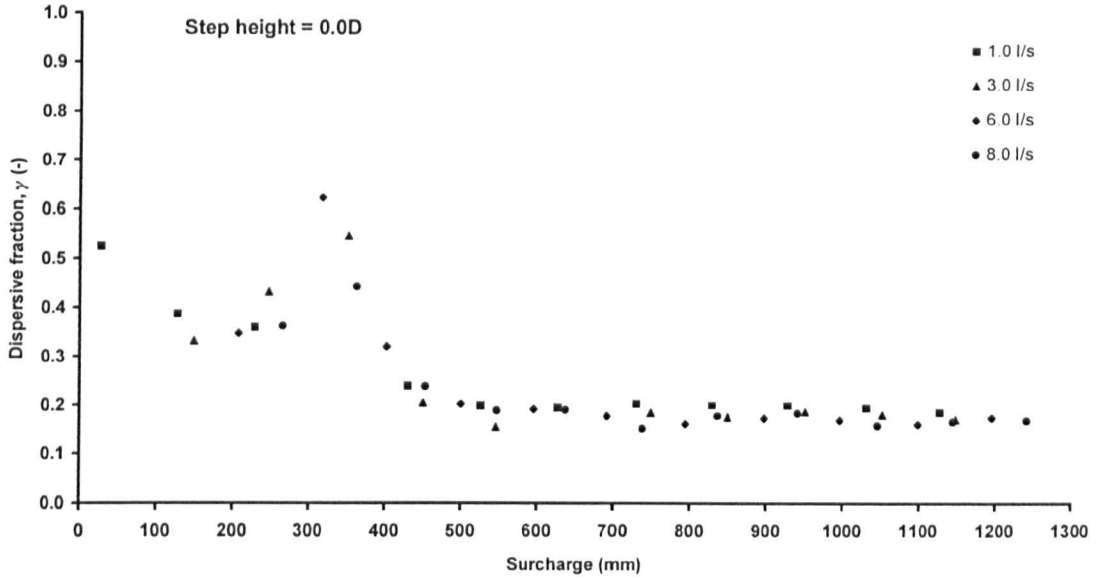

Figure 5.15a

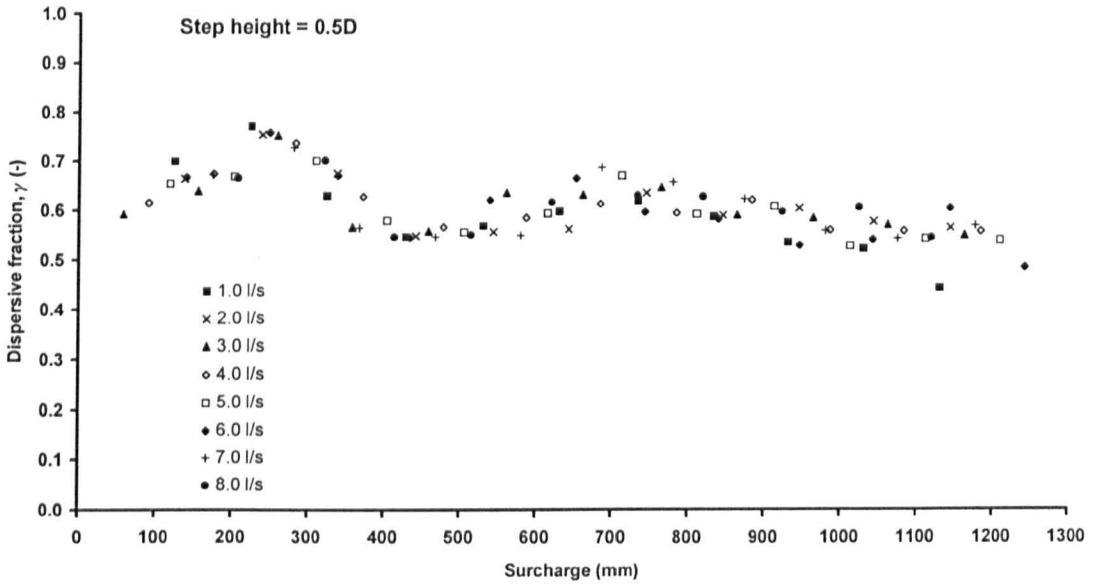

Figure 5.15b

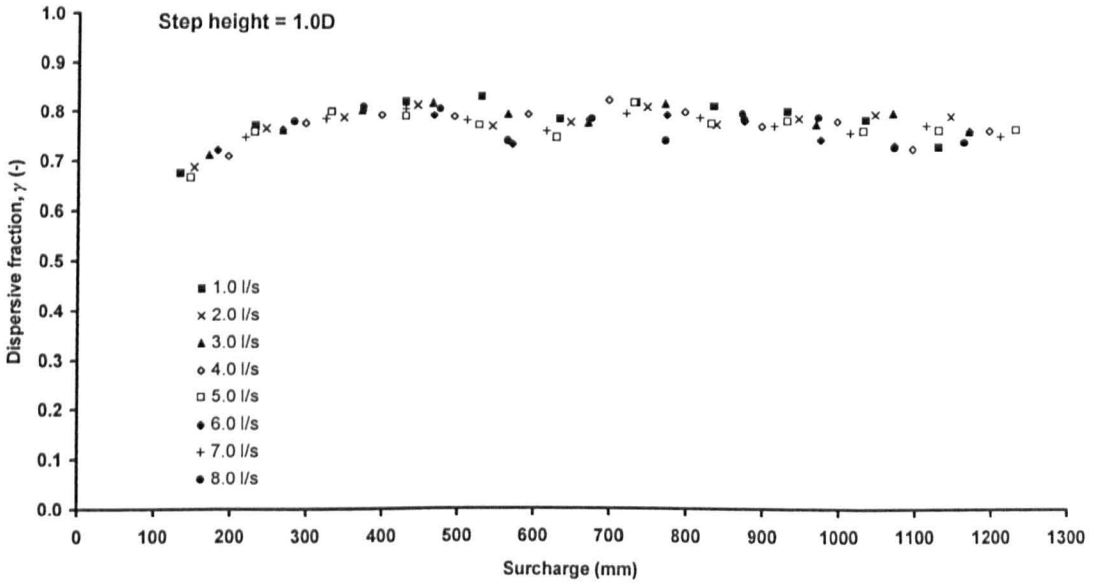

Figure 5.15c

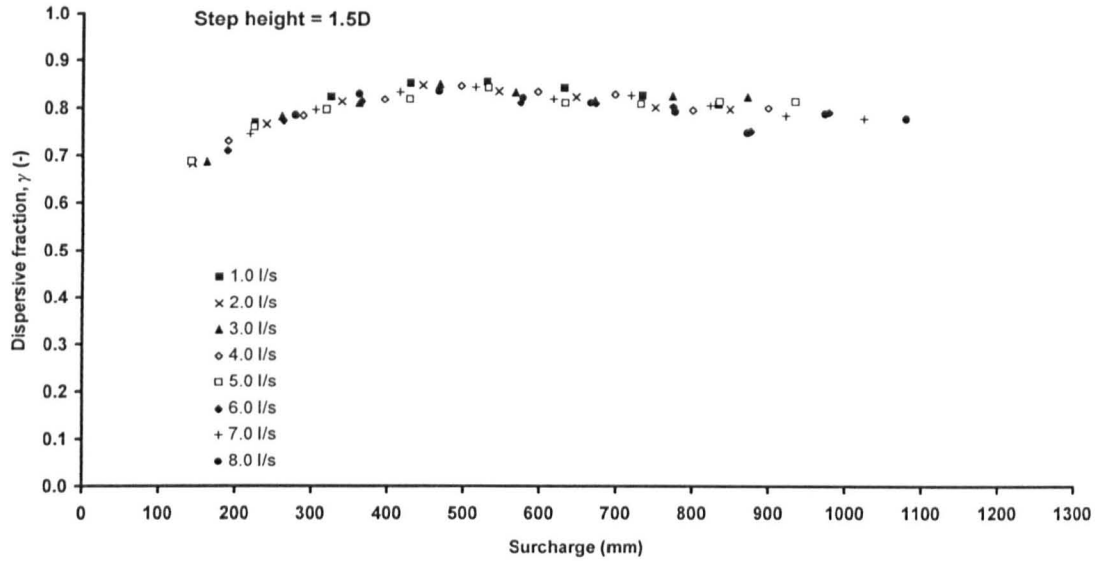

Figure 5.15d

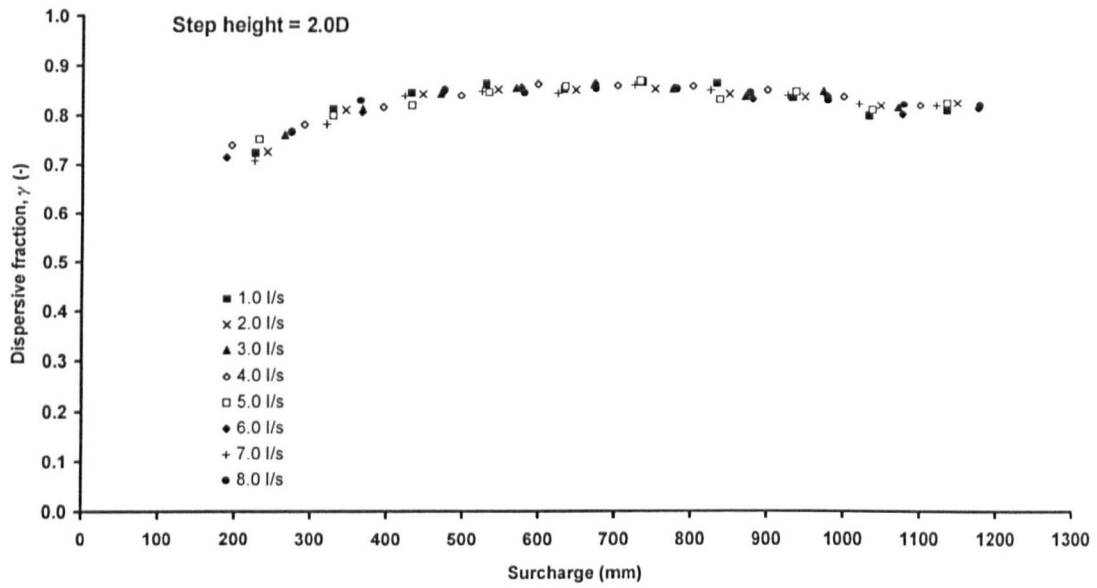

Figure 5.15e

Figure 5.15 Variation of dispersive fraction with surcharge.

The theory that boundaries to the incoming jet significantly restrict the volume of fluid responsible for dispersion is further enhanced by considering the measurements from the 1.5 pipe diameter step case with benching fitted in the manhole base (Figure 5.16). Here the trend for the dispersive fraction variation with surcharge is similar to the lower step conditions, where there is a maximum value at lower surcharges reducing to a constant value of approximately 0.1 when the surcharge increases over the region of 500mm. This implies that the presence of benching in a manhole has a considerable impact on reducing the volume of the surcharged manhole that is responsible for dispersing the passing tracer.

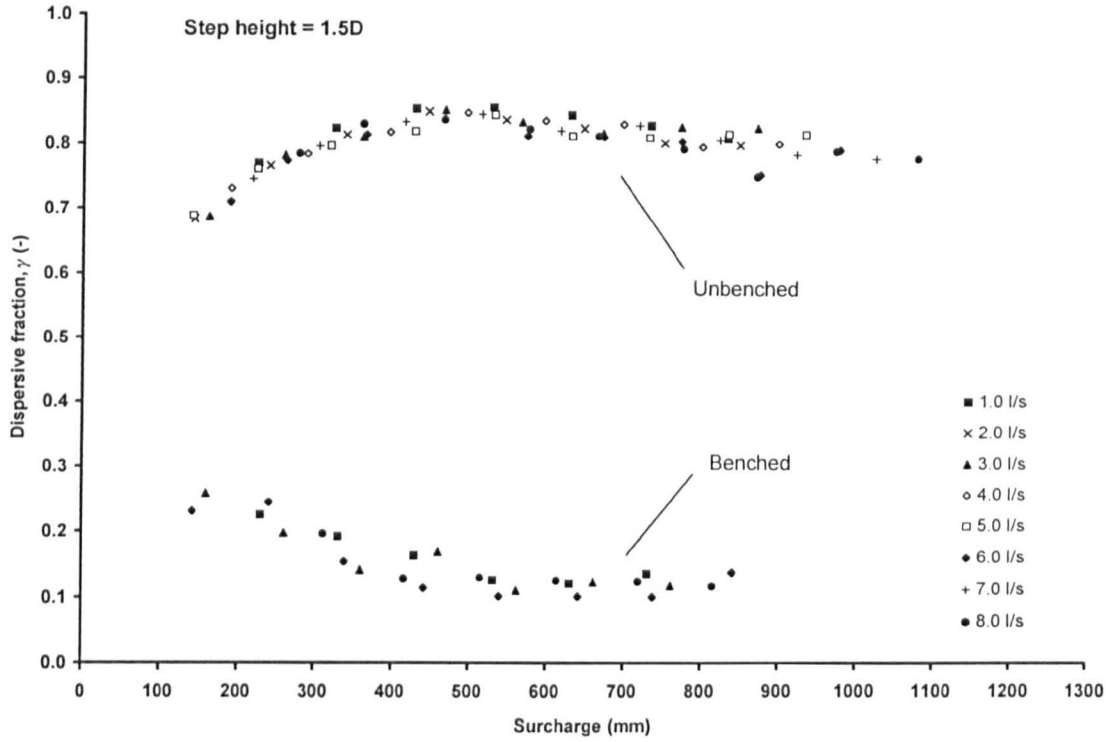

Figure 5.16 Comparison of dispersive fraction data for benched and unbenched-benched manholes.

It can be clearly observed that the flow rate for a particular manhole geometry has no significant effect on the dispersive fraction. This is in line with other researchers considering the dispersive fraction of river reaches. The average values of the dispersive fraction for the whole surcharge range at each discharge are presented in Figure 5.17. Error bars are shown, representing plus and minus one standard deviation of the averaged value. For clarity, only example error bars are added to a selection of the data for step heights equal to or greater than 1.0 pipe diameters. As can be seen, the dispersive fraction for any discharge over the range considered appears to be constant. This implies that the dispersive fraction of the manhole volume can be determined with tracer tests conducted at only a single discharge.

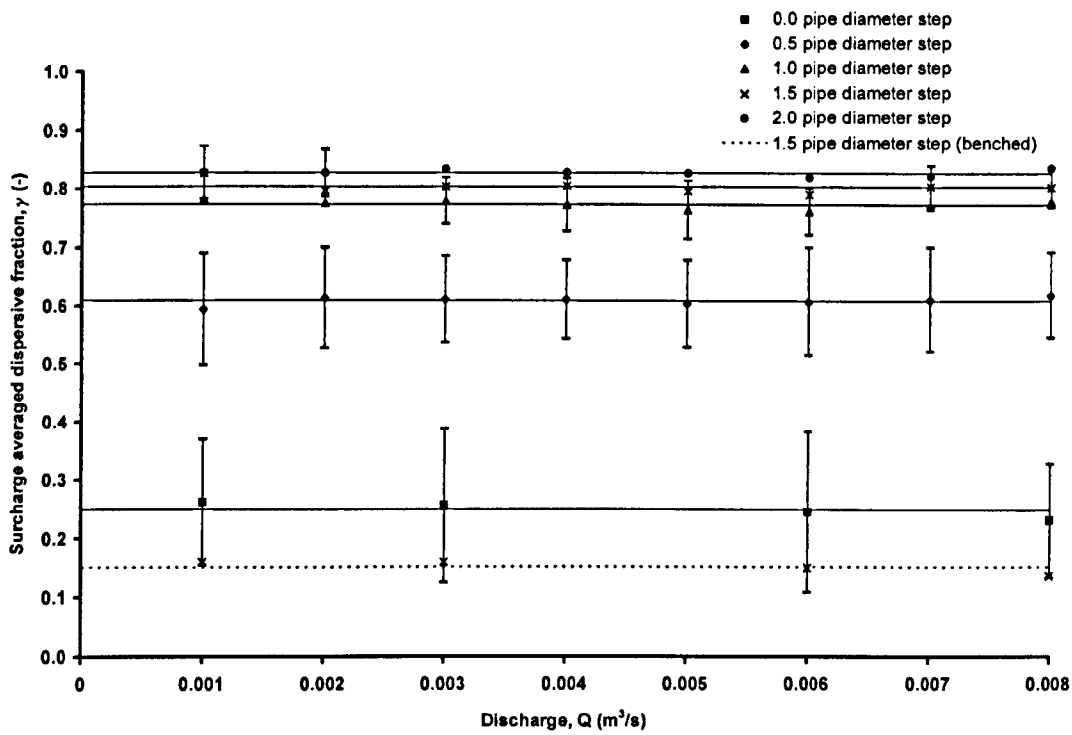

Figure 5.17 Variation of dispersive fraction with discharge.

A summary of the surcharge and discharge averaged dispersive fraction results for the stepped manholes with and without benching is shown in Table 5.3. This indicates that increasing the step height causes an increase in dispersive fraction. The effect is most pronounced between a zero step and a 0.5 pipe diameter step where the dispersive fraction increases from 0.249 to 0.609. A further 0.5 pipe diameter step increase causes the dispersive fraction value to rise to 0.774 after which extra step height increases have a greatly reduced effect on the increase in dispersive fraction. With benching in place the 1.5 pipe diameter step condition has a dispersive fraction less than that for the unbenched zero step configuration.

	Surcharge averaged dispersive fraction, γ_s (-)	
Step height	Unbenched	Benched
0.0D	0.249	-
0.5D	0.609	-
1.0D	0.774	-
1.5D	0.804	0.151
2.0D	0.828	-

Table 5.3 Surcharge averaged dispersive fraction values.

5.8 Relationship between head loss and ADZ parameters

Bo Pedersen and Mark (1990) proposed that the head losses in surcharged manholes with straight through flow could be best represented by an approach based on submerged jet theory. They divide the head loss coefficient, K_H, into the contributions made by the entrance energy loss (as the jet

enters the manhole) and the exit loss (as flow continues into the downstream pipe).

Earlier work by Albertson *et al* (1950) provides extensive mathematical definitions for the mean flow patterns of fully submerged jets. During the process of flow establishment, immediately after exiting the orifice, the jet is described as a combination of a central core section where the velocity is constant and equal to that of the inlet pipe. Surrounding this core is a diffusion region with an approximate rate of expansion of 1 in 5 (Figure 5.18). The velocity profile in this region is given by a Gaussian normal probability function. The flow is considered to have become fully established at a distance x from the orifice, where x/D = 6.2. At this point, the eddies in the diffusion region surrounding the central core meet at the centre line. These are convenient nominal designations, since the true nature of the flow pattern makes it impossible to precisely define the regions concerned.

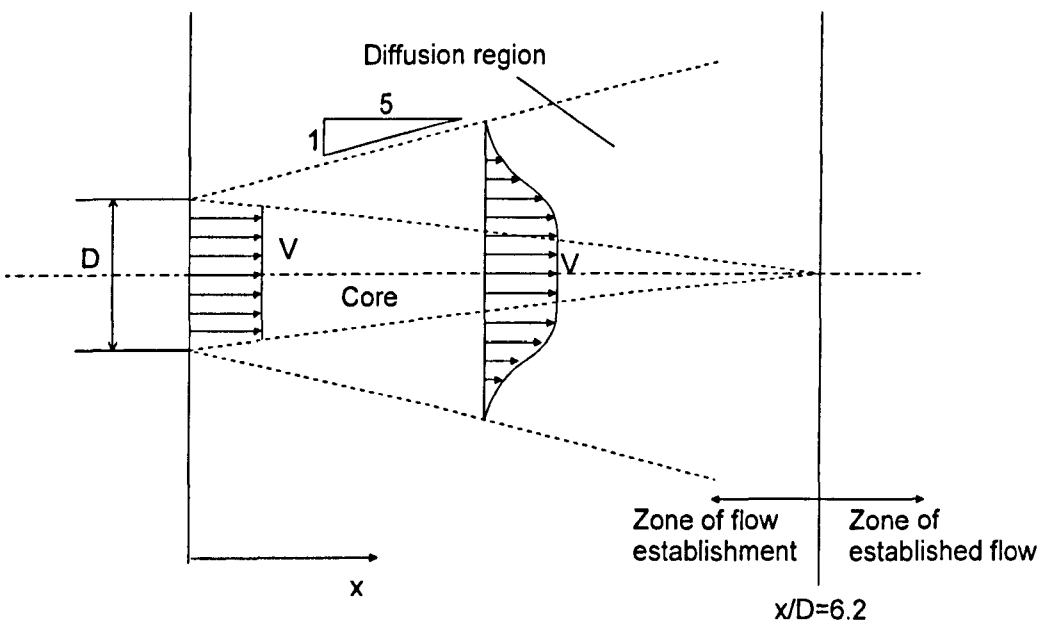

Figure 5.18 Velocity distribution and diffusion region in a circular free jet (Albertson *et al*, 1950)

There is a pronounced velocity discontinuity as the jet enters the manhole and this causes a lateral mixing process. Fluid within the surrounding manhole volume is entrained within the jet and thus the discharge in the manhole increases to a value greater than that in the inlet pipe. Prior to the jet reaching the outlet this extra discharge is rejected back into the manhole volume. This discharge gain and loss mechanism is directly related to the entrance head loss (Bo Pedersen and Mark, 1990). The exit head loss is caused by the expansion of the flow downstream of the vena contracta in the downstream pipe. This exit loss will be similar for cases with the same discharge and manhole diameter.

Therefore, the head loss for similar manholes at a particular discharge is primarily a function of the size of the diffusion region, which is exchanging energy with the surrounding fluid. From this assumption it is possible to relate the head loss coefficients that have been established for the stepped manholes to this diffusion region.

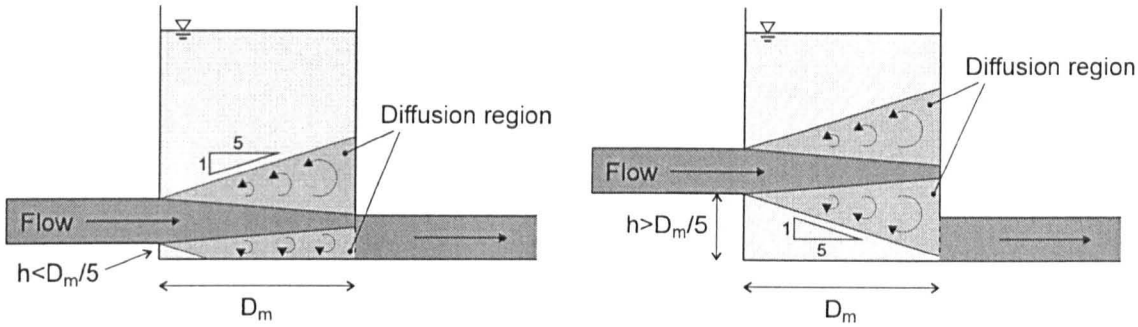

Figure 5.19a Step height less than $D_m/5$

Figure 5.19b Step height greater than $D_m/5$

Figure 5.19 The effect of step height on the volume of jet diffusion region.

Assuming the approximate jet expansion rate of 1 in 5 (Albertson *et al*, 1950), it can be determined that the diffusive region of the submerged jet will be unaffected by contact with the manhole base at step heights of greater than $D_m/5$, or approximately 78mm in the case of the 388mm manhole (Figure 5.19). Once the jet becomes free of the manhole base, any further step height increases will result in no further increase in the volume of the jet diffusion region, and therefore there is no further increase in the head loss coefficient. This theory is supported by the head loss coefficient results for the stepped manhole. This local diffusion and entrainment pattern of a submerged jet will be altered by proximity to longitudinal boundaries such as the free surface of the manhole base (Albertson *et al*, 1950) and therefore, at low surcharges it can be expected that results for head loss and dispersion will differ from higher surcharges, as has been found to be the case.

Benching designs can be included in these considerations by assuming that the entrainment and rejection zones are restricted to areas not encompassed by the physical boundaries of the benching. Thus a half pipe shaped benching configuration has half the entrance head loss of an unbounded jet entry. In fact, the proposed entrance loss value for this circumstance is likely to be slightly less than half of the unbounded jet because it reduces the tendency of the jet to oscillate (Bo Pedersen and Mark, 1990).

Computer simulation models have the ability to make reliable predictions for the hydraulics within a sewer system. This involves modelling the pressure and head losses throughout the network. Therefore, if a relationship between the head loss and longitudinal dispersion parameters could be determined it would be possible for a computer model to simulate the longitudinal dispersion of a solute passing through a manhole from the head loss coefficient calculated at that chamber. It can be considered that the dispersion region of a submerged jet entering a manhole, which is responsible for much of the head loss that occurs, is also responsible for the mixing of tracer into the dead zone region. The dispersive fraction from the aggregated dead zone model is a measure of the proportion of the reach volume that is involved in the dispersion of a tracer. Therefore the relationship between the dispersive fraction and the head loss coefficient has been examined.

Figure 5.20 shows the variation of the dispersive fraction averaged over the surcharge range with the head loss coefficient for the stepped manhole configurations. A linear regression fits this data well, suggesting that the head loss and dispersive fraction are directly related and both reflect the proportions of the diffusion region of the submerged jet. The head loss for the benched manhole was determined from the shape factors provided by Bo Pedersen and Mark (1990). In addition, results from the manhole diameter variations have been included in the figure. A regression fitted with these

data included does not provide such a good measure of fit. However, these data were made available by O'Brien (2000) who conceded that the head loss measurements recorded for the manhole diameter variations were in some doubt, due to difficulties with the pressure transducers deviating from the calibrations and possible impurities such as sediment affecting the measurements. It is therefore proposed to disregard these data and suggest that the dispersive fraction can be well estimated from the head loss coefficient. The linear regression concurs well with the results from a straight length of pipe, where the head loss coefficient is effectively zero and the dispersive fraction was determined as 0.13 (Guymer and O'Brien, 2000). This is an attractive result, since if the reach time delay is known, or estimated from the maximum velocity through the reach, and the head loss coefficient is accurately predicted by the computer model then the ADZ model can be applied to predict the longitudinal dispersion due to the manhole.

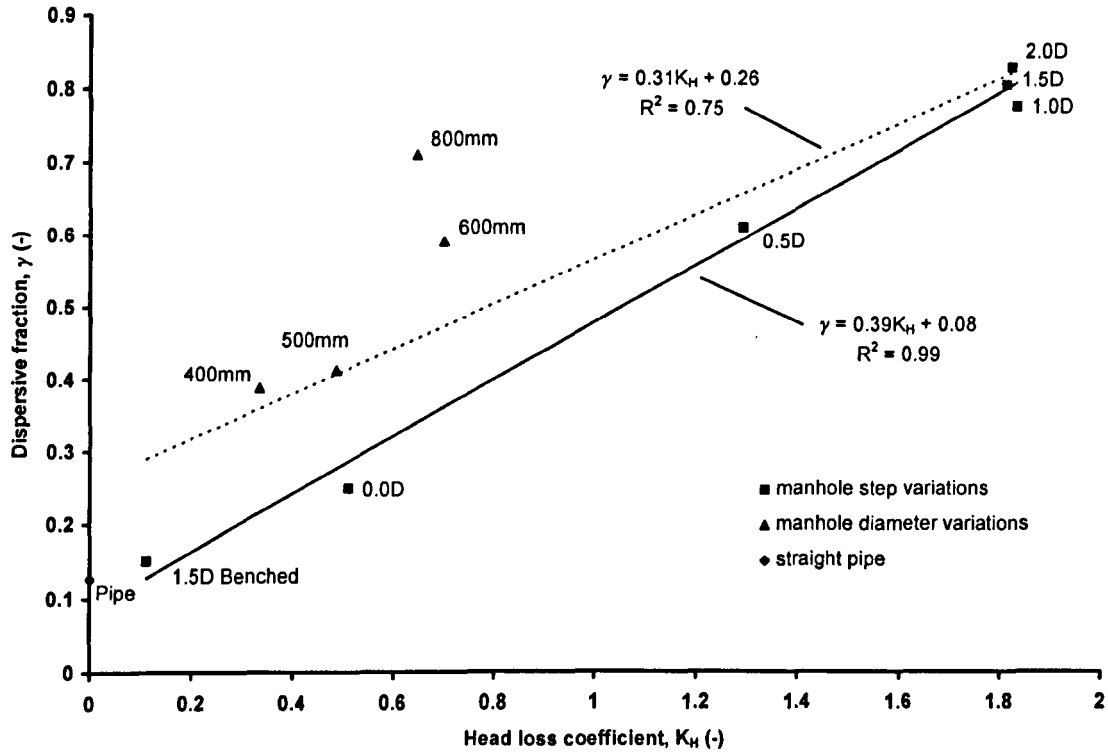

Figure 5.20 Variation of dispersive fraction with head loss coefficient.

5.9 Simulation of longitudinal dispersion in a sewer

The significance of the longitudinal dispersion due to surcharged manholes in the overall design and operation of urban drainage networks has been investigated by means of a simulation considering a small length of sewer pipeline. A total length of approximately 100 metres of 88mm diameter pipe has been considered, with a flow rate of 3.0 litres per second. This length was divided into 2.7 metre sections, thus making the longitudinal dispersion results for a straight pipe (Guymer and O'Brien, 2000) directly applicable. A Gaussian distribution of simulated tracer was applied as the input profile to the upstream end of the pipe. The experimentally derived coefficients were used in combination with the ADZ longitudinal dispersion model to simulate the transport of the tracer downstream (Figure 5.21). The upstream tracer concentration profile was used as the input to the first 2.7 metre pipe length and the predicted downstream output became the input for the next length and so on.

Simulations have also been undertaken for the conditions where the sewer length has two 388mm manholes in place. A variety of step heights and benching conditions were considered. All cases have been modelled with the ADZ model for longitudinal dispersion using the surcharge averaged experimentally derived model coefficients for the manhole type concerned. Figure 5.22 presents the downstream predictions of concentration profile for each case.

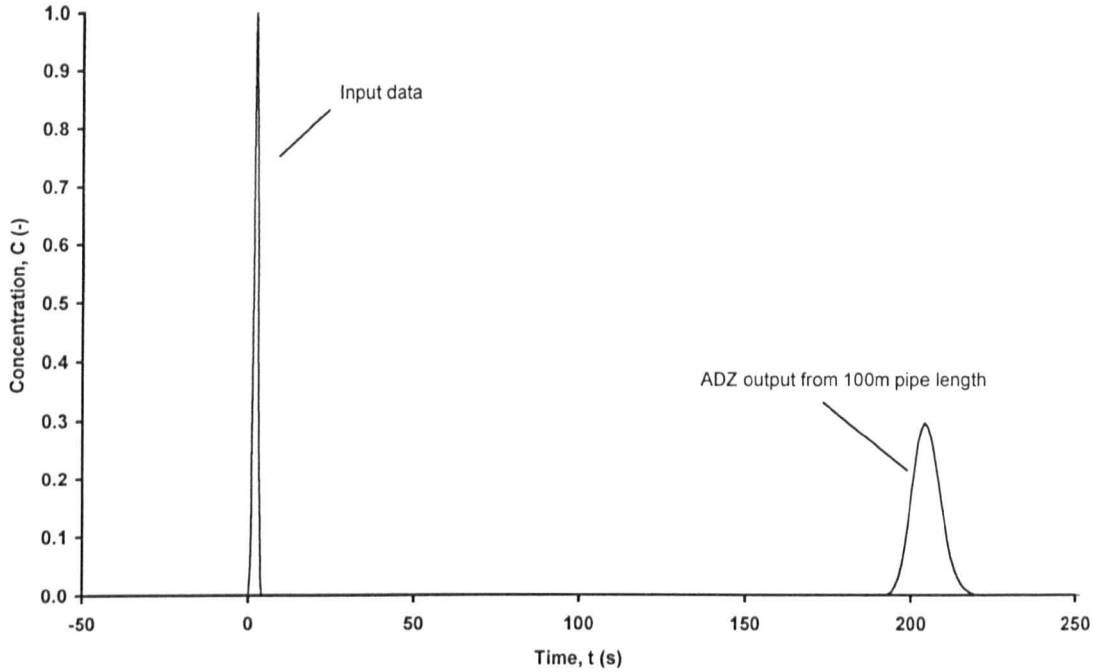

Figure 5.21 Sewer simulation input concentration profile with ADZ prediction for longitudinal dispersion due to 100 metres of pipe.

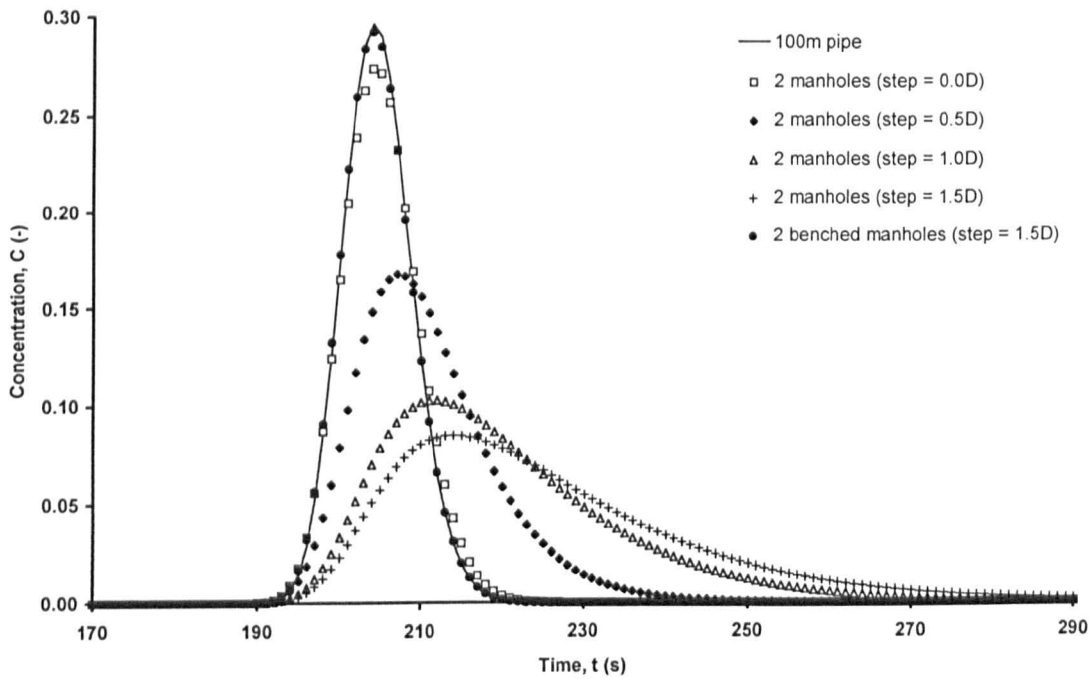

Figure 5.22 Simulation of longitudinal dispersion through 100 metres of sewer pipe.

In this simulation, it is clear that the effect of manholes on the longitudinal dispersion of solutes in sewer systems is only significant for unbenched manholes where there is a step height present. Manholes with no step, and those with a benching design channelling the flow, appear to cause little or no additional longitudinal dispersion over that of the pipe length. It is therefore likely that in many circumstances sewer quality models can operate effectively without applying special coefficients for manholes. However, this approach would have to be applied with care. In cases where the flow is poorly directed through the manhole, such as with an unbenched stepped manhole. There is potential for underestimating the longitudinal dispersion if the manholes are not taken into consideration. This may also be the case where the flow is partially obstructed in a badly maintained manhole, or where an angle between the inlet and outlet pipes prevents smooth passage of the flow. It is therefore essential to obtain high quality field data from sewers to quantify the real effects. In this way sewer modellers can gain greater assurances in their methods for simulating transport of pollutants through an urban drainage network.

Chapter 6

Numerical Modelling

6.1 The application of a CFD model

A computational fluid dynamics model uses the governing equations of fluid dynamics to establish the values of the dependent variables, such as velocity and pressure, throughout the model domain (Anderson, 1995). An analytical solution using these partial differential equations would be exact and continuous, and valid at all locations throughout the domain. However, for all but the most simple of fluid flow problems there is too great a complexity for an analytical solution to be determined in practice. In contrast, solutions found by numerical analysis are approximate and calculated only at discrete locations. Interpolation is required to find the results for locations in between the specified points.

There are various different software packages available for CFD modelling. The decision was made to use Fluent (Fluent, 1993) for this research into flow through manhole structures. This choice was encouraged by the fact that Fluent was developed at the University of Sheffield, which ensures that there is a broad field of experience in using it within the Faculty of Engineering and more specifically within the Department of Civil and Structural Engineering.

Fluent uses a control volume based, finite difference method to solve the governing equations for conservation of mass and momentum (Equation [2.40] and Equation [2.41]) and, if required, energy and chemical species conservation (Fluent, 1993). These last two equations are used for situations where the flow is not isothermal and where more than one fluid is present in the model volume respectively. Turbulent flows can be modelled using either the k-ε or the Reynolds stress turbulence model.

It is possible to simulate flows in or around structures in either two or three dimensions. The process of creating a fluid dynamics model for computer analysis and numerical solution is undertaken in a series of stages.

6.1.1 Geometry input

The physical aspects of the particular problem are required first. These include determining the number of dimensions that are appropriate and outlining the geometrical shape of the domain within which the simulation is to be conducted. The geometry is described using either a Cartesian or polar co-ordinate system. Points of primary concern are defined by co-ordinates and are then connected by means of lines or curves (Figure 6.1a). These curves form the boundaries to surfaces created between them. With the geometry input complete, it is necessary to define the boundary conditions at different locations. The main options for defining each of the individual surfaces created to form the solution domain are an inlet, an outlet, a boundary wall or as a wall of symmetry through the domain.

6.1.2 Grid generation

The system to be analysed is subdivided into a multitude of small discrete volumes, or cells, by means of a defined grid. This computational grid must be fine enough to give a good resolution of flow conditions throughout the total volume. However, an increase in the number of cells causes computational time to be greater, and ultimately there is a limit as to how many cells are available with the software. The application of a grid to the geometry begins by assigning grid point locations to the lines that bound the geometry (Figure 6.1b). This process is termed 'mapping' of the grid to the geometry. It is then possible for the software to interpolate the grid points over the surfaces (Figure 6.1c) and finally, for three-dimensional configurations, the grid points are interpolated through the interior of the domain (Figure 6.1d).

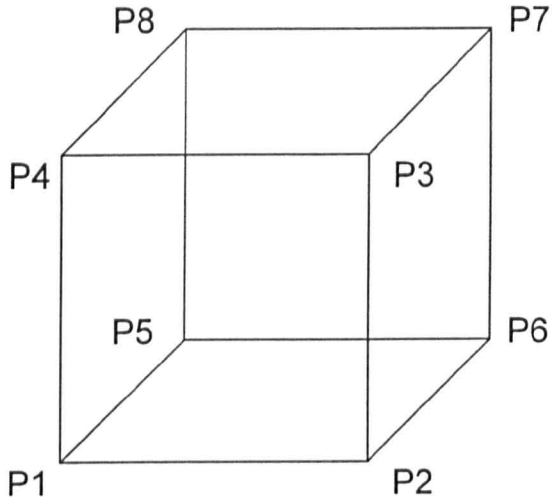

Figure 6.1a Geometry defined.

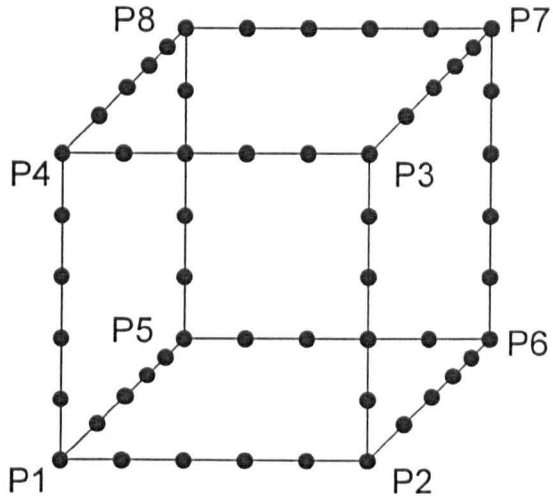

Figure 6.1b Grid points mapped to lines.

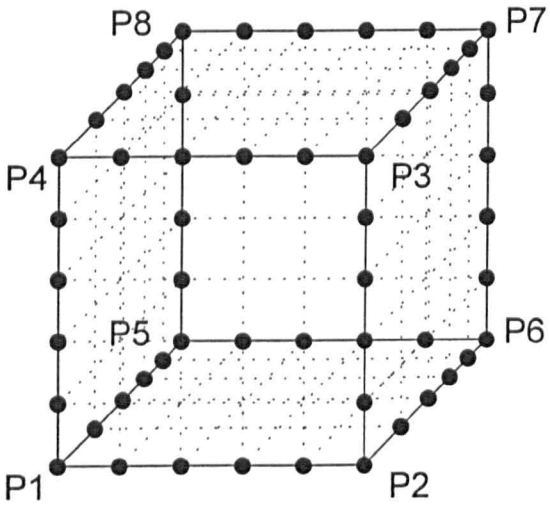

Figure 6.1c Interpolation of surface grid.

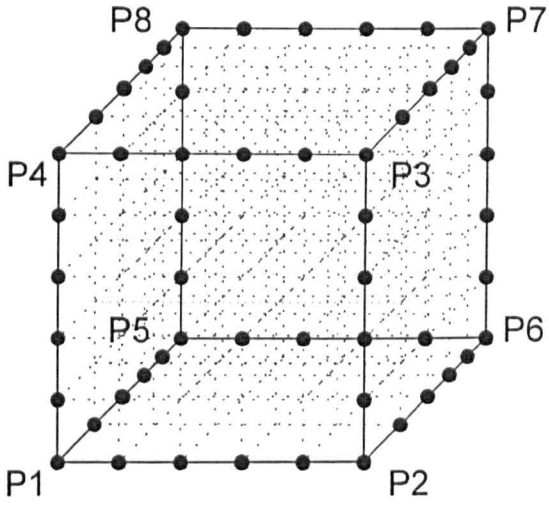

Figure 6.1d Interpolation of interior grid.

Figure 6.1 Process of CFD grid generation.

Whilst a Cartesian grid is ideal for CFD models of square edged volumes, it is often the case that the geometry boundary has more complex outlines constructed from curves. PreBFC (PreBFC, 1993), the geometry and grid generation software for Fluent, allows for a grid generation system termed Body Fitted Co-ordinates (BFC). If this system is employed, the grid co-ordinate system is moulded to

exactly fit the geometry, giving the advantage that the grid provides a more accurate representation of the shape of the domain (Figure 6.2). It is this fitted grid, rather than the geometry itself, which is used by the computer as the discretised domain for solving the governing equations.

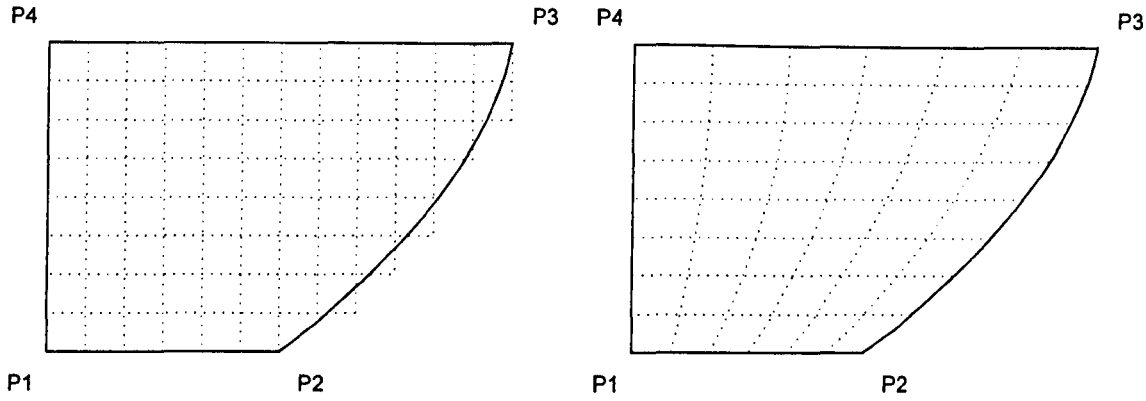

Figure 6.2a Cartesian co-ordinate grid

Figure 6.2b Body fitted co-ordinate grid

Figure 6.2 Comparison of Cartesian and body fitted co-ordinate grid systems.

6.1.3 Boundary conditions

Each cell is assigned a series of differential equations that are used to describe the fluid flow through the cell. For the majority of cells these equations can be considered appropriate. Special input requirements may be needed for certain conditions such as the inlet, where different boundary conditions will apply. It is necessary at this stage, therefore, to define inlet parameters such as velocity or pressure distribution. Similarly, specific conditions at the outlet can be described if necessary. Also, a choice of turbulence model must be made, and this will be governed by the nature of the flow simulation that is being undertaken.

6.1.4 Simulation

There are usually many unknowns within all the equations held within the cells. Furthermore, these equations are strongly coupled and must be solved simultaneously. The set of simultaneous equations is solved by an iterative process shown in Figure 6.3. Arbitrary initial conditions, except for those prescribed at the boundaries, are applied and the iterative procedure continues until the results converge to a solution that satisfies the governing equations to within the prescribed level of error. Stage 3, which considers the scalar equations, is only required for simulations of two phase flow, thermal exchange or similar.

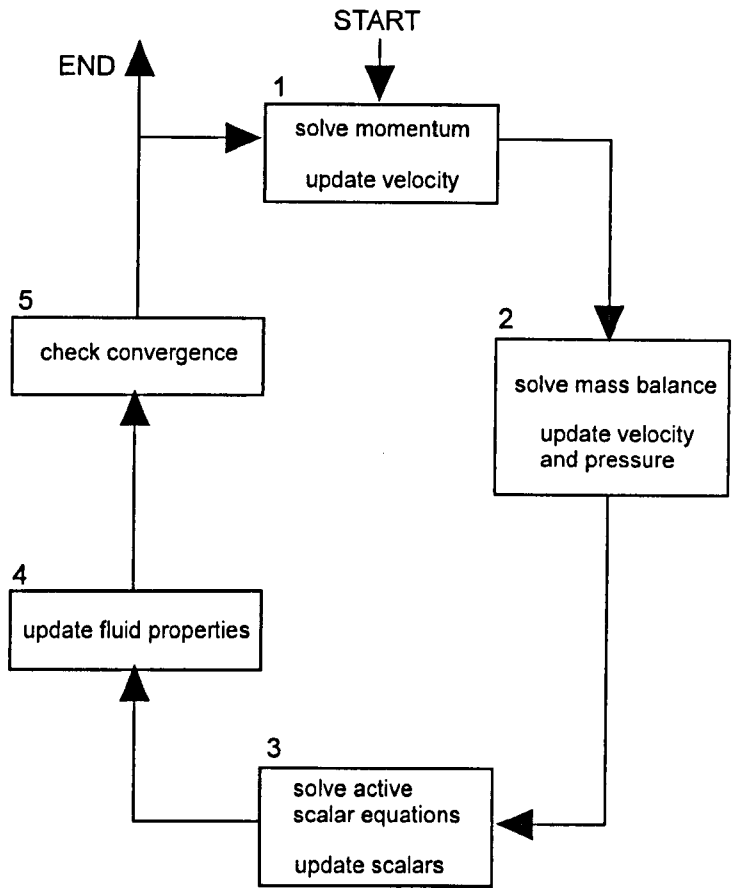

Figure 6.3 CFD model solving process.

6.2 Application of Fluent for manhole investigation

Computational Fluid Dynamics was applied to the investigation of flow through various surcharged manhole configurations. It was decided to include lengths of pipe either side of the manhole so that it would be possible to examine how the presence of a manhole structure affects the flow in the pipes immediately upstream and downstream of the chamber.

A circular manhole chamber of internal diameter 388mm was prepared, and pipe lengths of 1.15 metres and internal diameter 88mm were connected. This length of pipe was used since the model was then directly comparable to the laboratory configuration between the fluorometer locations. The standard configuration with no step height between inlet and outlet pipes and no benching fitted to the base of the manhole was simulated with two discharges. Other geometrical variations considered were the standard design incorporating benching with a full pipe depth channel, and an unbenched design with a 1.0 pipe diameter step height. A full summary of the Fluent manhole simulations completed is provided in Table 6.1.

The version of Fluent used for the study was not capable of modelling a fluid free surface. Therefore the surface of the water in the manhole was represented by means of a wall boundary. However, it was possible to cut the connection between the boundary and the adjacent cells. In this way the boundary defined no shear stress on the adjacent fluid and it therefore represented a frictionless wall. This fixed wall surface meant that it was not possible to model the broken or uneven nature of

the water surface that was especially prevalent at low surcharges. Also, the Fluent model was used to produce steady state solutions which meant that any transient features of the flow regimes such as oscillation of the incoming jet or temporary swirling motions within the manhole were not modelled.

A body fitted grid of six sided cells was arranged to fill the geometry domain (Figure 6.4). In the standard manhole case there were approximately 130,000 computational cells, and this value was increased to encompass greater surcharge levels. The grid was arranged in such a way so that a line of cells was located along the exact centreline of the pipe and manhole length. It was these cells that were analysed after a solution had been obtained to extract the pressure head loss information. In the case of the stepped manhole, the pressure readings were taken from cells located on a straight line drawn between the centres of the manhole inlet and outlet.

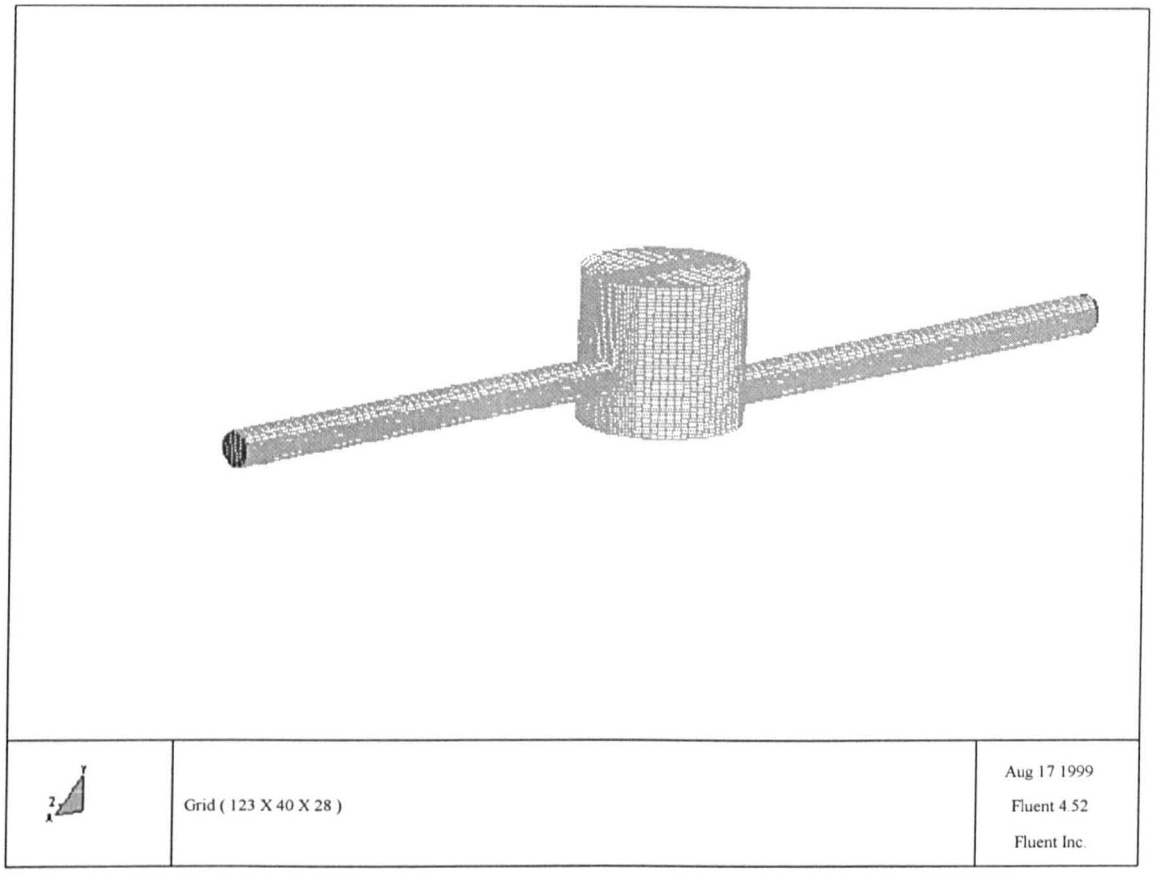

Figure 6.4 Surface grid for 388mm manhole with a step height of 1.0D.

At the inlet to the upstream pipe the velocity was set to a uniform value across the inlet plane, calculated from continuity based on the discharge to be modelled. This was a compromise in the interpretation of the turbulent pipe flow profile that would be present. However, the option of including a greater length of pipe at the upstream end of the model to allow a fully formed velocity profile to develop was deemed to require too many computational cells, thus exerting too great a demand on computer power and solution time.

The k-e turbulence model was used for the CFD testing. This has been shown to work satisfactorily with similar fluid dynamics problems (Asztély and Lyngfelt, 1996). However, any flow conditions where a strongly swirling motion developed would perhaps be more suitably modelled with the Reynolds stress turbulence model. This would most certainly be the case for conditions where the

inlet and outlet pipes were not directly aligned, but no excessive swirling motion was observed under the laboratory test circumstances.

The use of a turbulence model requires that the inlet boundary conditions applied to the model include the turbulent intensity and the characteristic length. Turbulent intensity is a measure of the magnitude of the turbulent velocity fluctuations in relation to the mean flow velocity. The characteristic length represents the maximum size of the turbulent eddies which are present in the flow. For the manhole modelling using Fluent these values were set to 5 percent and 0.088mm respectively. A value equal to the pipe diameter for the characteristic length is recommended in the Fluent user's manual (Fluent, 1993), whilst a sensitivity analysis found that between values of 5 and 15 percent the turbulent intensity was not critical in the velocity predictions.

6.3 Results

Simulations have been undertaken for a sample of conditions that can be compared with experiments conducted in the laboratory.

Step height	Benching	Surcharge (mm)	Discharge (m^3/s)
0.0D	No	172	0.001
0.0D	No	172	0.008
0.0D	Yes	172	0.001
0.0D	Yes	172	0.008
1.0D	No	272	0.001

Table 6.1 Summary of manhole CFD simulations.

6.3.1 Flow Profiles

Velocity magnitude profiles are presented in Figure 6.5, Figure 6.6 and Figure 6.7. The elevation views are a vertical section along the centreline of the manhole and pipe length. In the 0.0D step case, the plan view is a horizontal slice taken through the pipe centreline. Where a step height is present two plan views are provided, one each for the centreline of the upstream and downstream pipes.

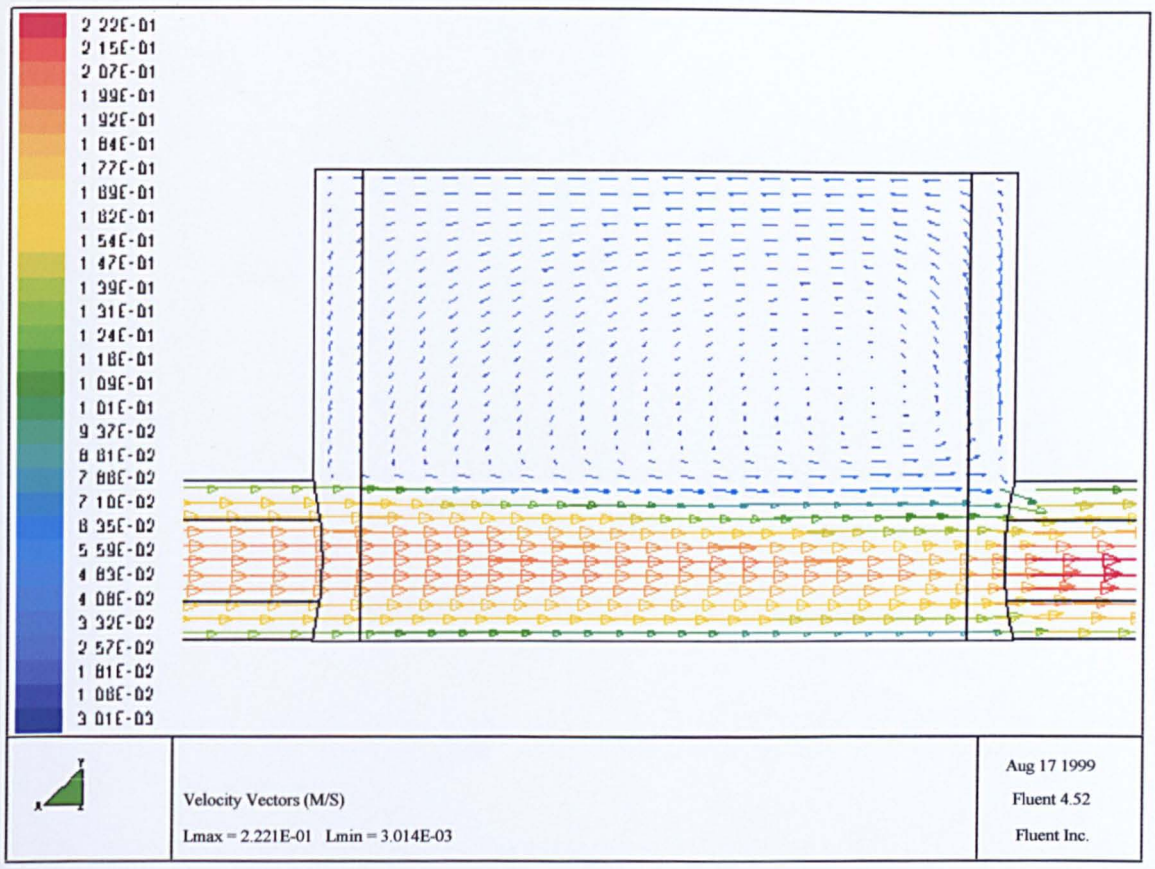

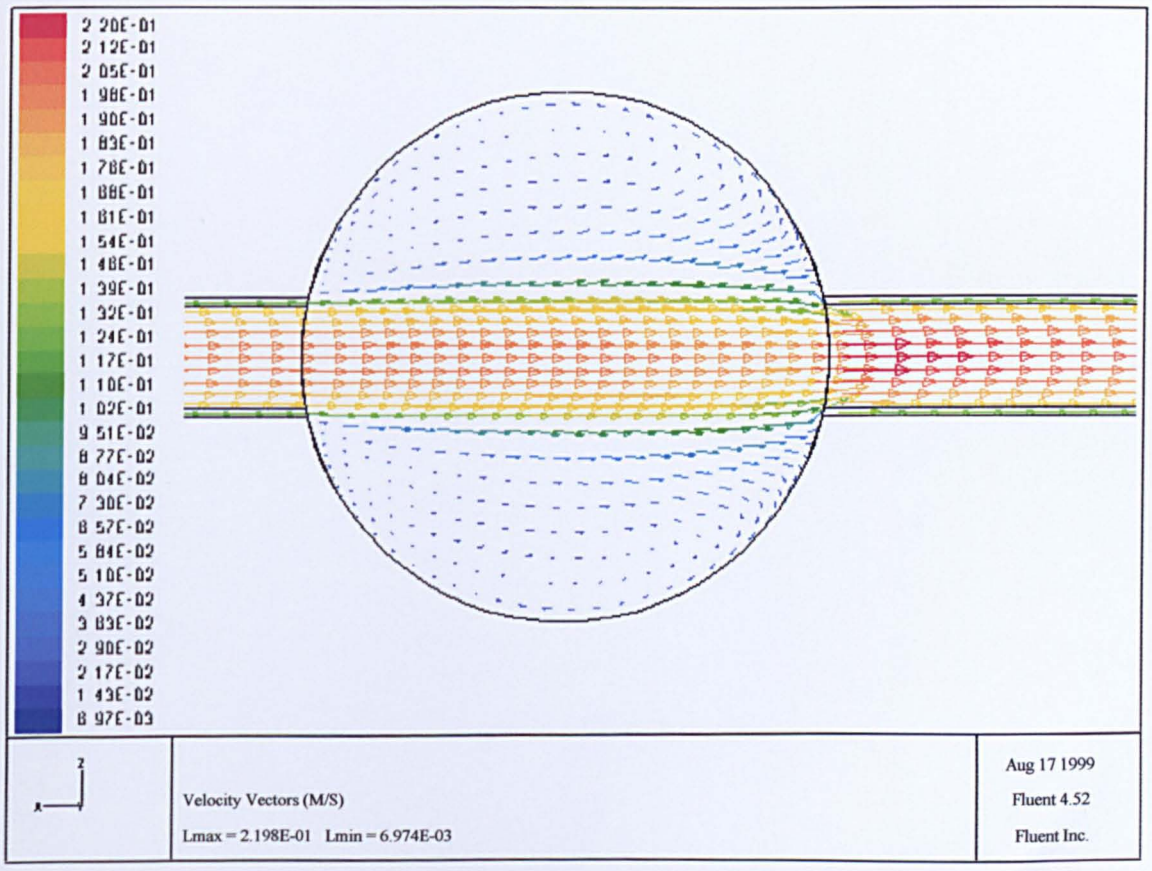

Figure 6.5 Velocity magnitude prediction (388mm unbenched manhole, step = 0.0D, Q = 1.0l/s).

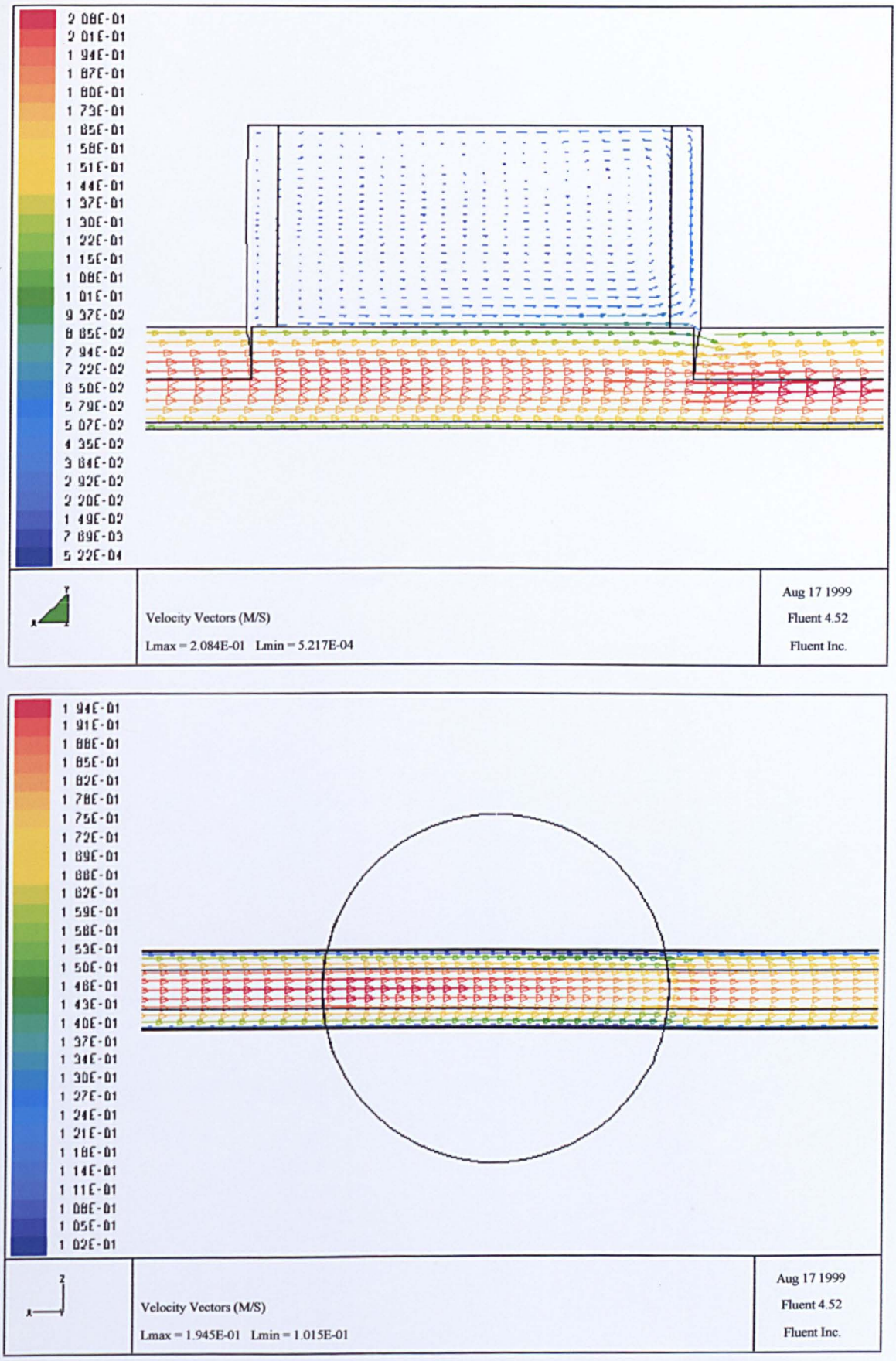

Figure 6.6 Velocity magnitude prediction (388mm benched manhole, step = 0.0D, Q = 1.0l/s).

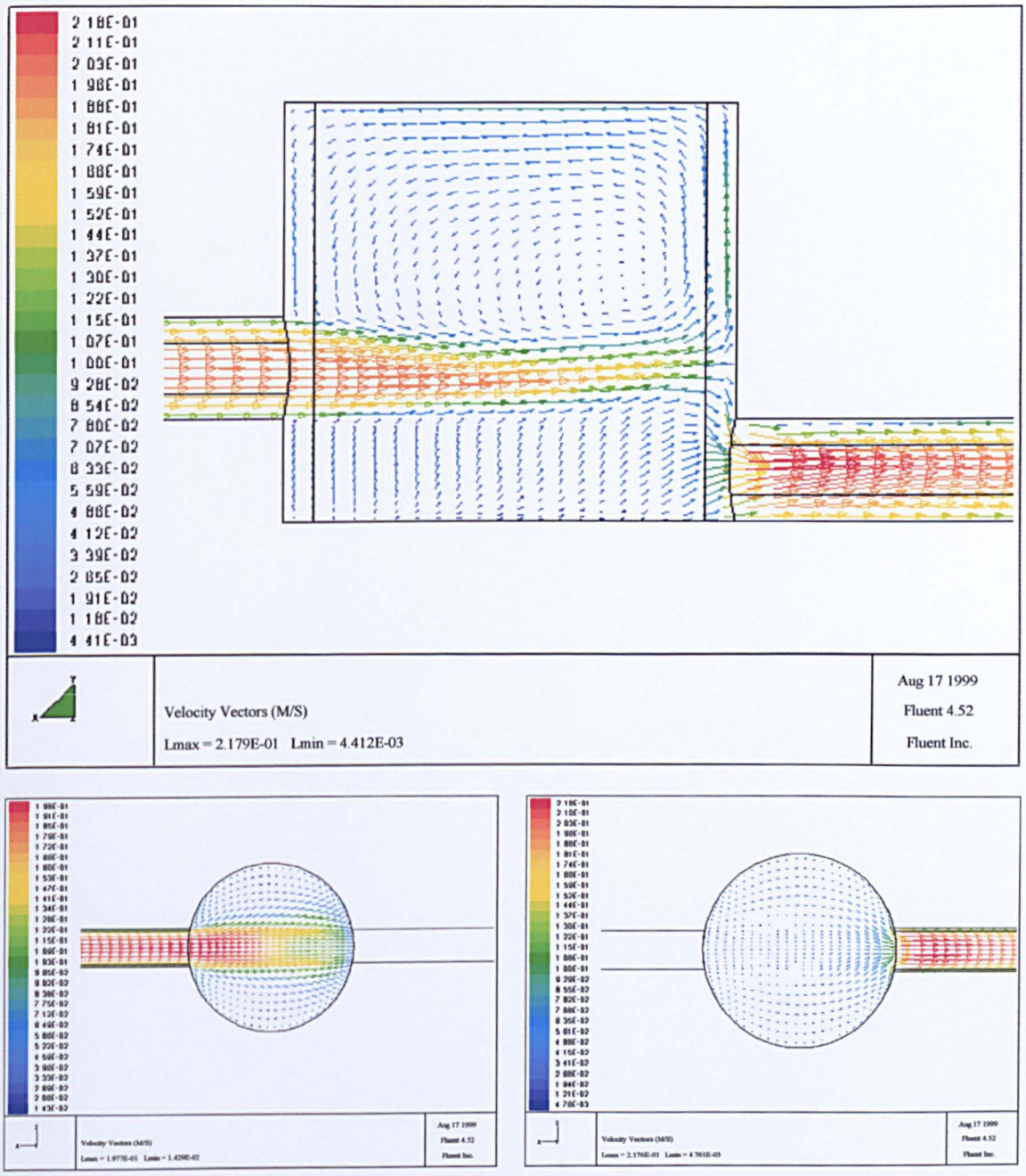

Figure 6.7 Velocity magnitude prediction (388mm unbenched manhole, step = 1.0D, Q = 1.0l/s).

The velocity magnitude predictions from the CFD analysis (Figure 6.5, Figure 6.6 and Figure 6.7) show the entrance of a jet of water into the manhole chambers. In all cases some narrowing of this jet is apparent, most obviously in the stepped manhole (Figure 6.7). The form of the jet for this manhole is similar to that observed with images using the laser light sheet (Figure 4.40). It is compressed more from above than below, and some velocity vectors close to the downstream side of the manhole can be seen to dip steeply towards the outlet pipe. This highlights how some of the injected tracer passes directly to the outlet, even with a step present. The benched manhole results (Figure 6.6) show much less compression of the jet and indeed the velocities in the surcharge volume are predicted as being less than those in the same region for the other manholes. This tends to confirm the expected result that the flow is well guided towards the outlet and there is considerably less interaction with the dead zone region above than for the other manholes. A consequence of this, however, is that the maximum jet velocity is less in comparison. This, combined with the additional friction of the benching walls, explains why the reach time delay is greater for the benched manhole than the unbenched one. The plan views of the Fluent predictions confirm the presence of re-circulations in this plane.

6.3.2 Head loss

The relative pressure along the pipe and through the manhole was determined by the CFD analysis. A central portion of the upstream and downstream pipes was used to calculate the head loss. These sections were of length 200mm, and the hydraulic grade line was extended to the centre of the manhole. The pressure head loss was then calculated from the difference between the upstream and downstream hydraulic grade lines at this point. From this value the head loss coefficient was determined.

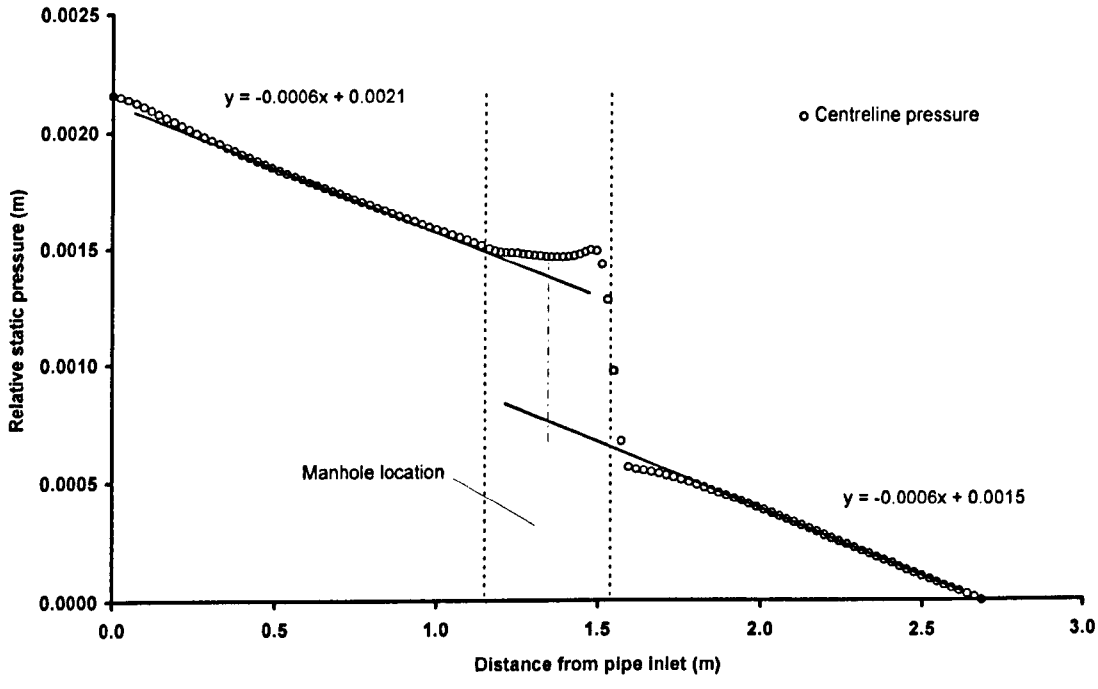

Figure 6.8 Determination of head loss due to manhole (388mm unbenched manhole, Q = 1.0l/s and step = 0.0D).

Step height	Benching	D_m/D		K_H	
		Laboratory	CFD	Laboratory	CFD
0.0D	None	4.4	4.4	0.51	0.42
0.0D	Half pipe	4.1	4.1	0.18-0.30*	0.26+
0.0D	Full pipe	4.1	4.4	0.07-0.11*	0.15
1.0D	None	4.4	4.4	1.83	1.54

* Lindvall (1984)
+ Asztély and Lyngfelt (1996)

Table 6.2 Comparison of CFD and laboratory head loss coefficients.

The comparison between the CFD and laboratory results for pressure loss coefficient reveals that the numerical modelling has a tendency to slightly underpredict the coefficient value. A potential cause of errors with the CFD solutions is the effect of boundary grid spacing on the flow conditions. As a means of describing the effects of the boundary layer in turbulent flow, Fluent assumes that the log law wall function applies in the layer of cells in contact with the geometry walls (Fluent, 1993). If this layer of cells is sized inappropriately then the prediction of the velocity profile will be inaccurate. For instance, if the boundary layer of cells is too large then the velocity profile will be underpredicted and the head loss coefficient for the pipe lengths will be greater than found in practice. Thus the hydraulic grade line for the pipes calculated by the CFD model is too steep and the corresponding prediction for the loss due to the manhole is reduced. The necessity for correctly sizing the boundary cell layer is highlighted in Figure 6.9. The Fluent user's manual (Fluent, 1993) recommends guidelines for the sizing of these boundary cells. These guidelines were adhered to in the setting up of the manhole model but due to considerations of cell numbers and distribution the boundary cell thickness at some wall locations in the pipe lengths was near to the recommended maximum limit.

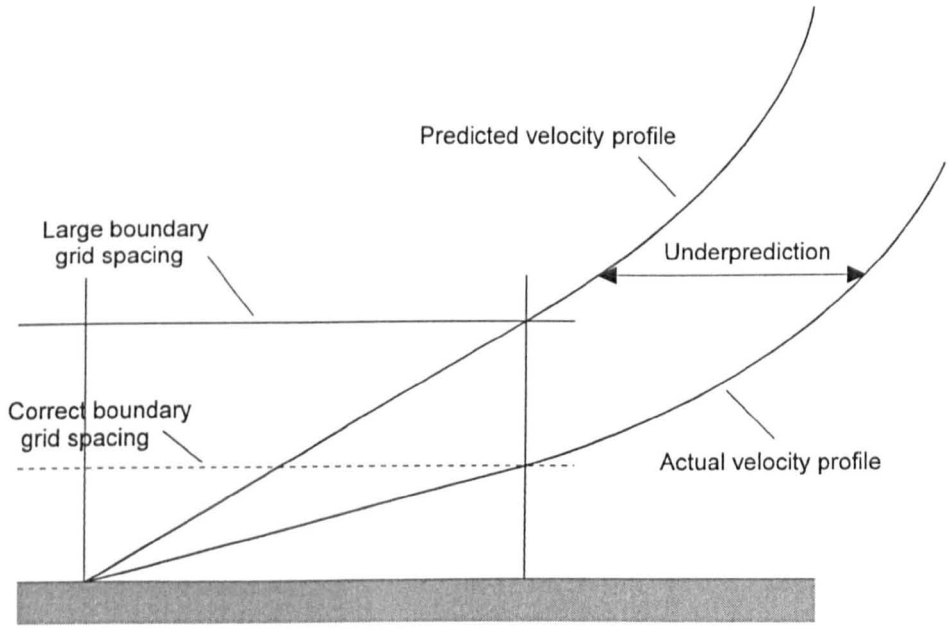

Figure 6.9 Boundary layer cell sizing.

6.3.3 Particle Image Velocimetry (PIV)

Particle Image Velocimetry (PIV) was used as a means of obtaining a complete field of flow velocities within the manhole by a non-intrusive method. An example of the flow field results obtained along the centreline of the manhole is shown in Figure 6.10. In this case, the PIV system used operated by means of a scanning laser beam highlighting particles within the flow, and images of these were captured by a digital video camera. The scanning laser caused the moving particles to be recorded as a series of white dots. Advanced computer software was then used to analyse the images and correlate the dot patterns into velocity data. Considerable difficulties were encountered with this procedure, and it was not eventually possible to obtain data of sufficient quality that could be used for the purpose of validating the CFD modelling.

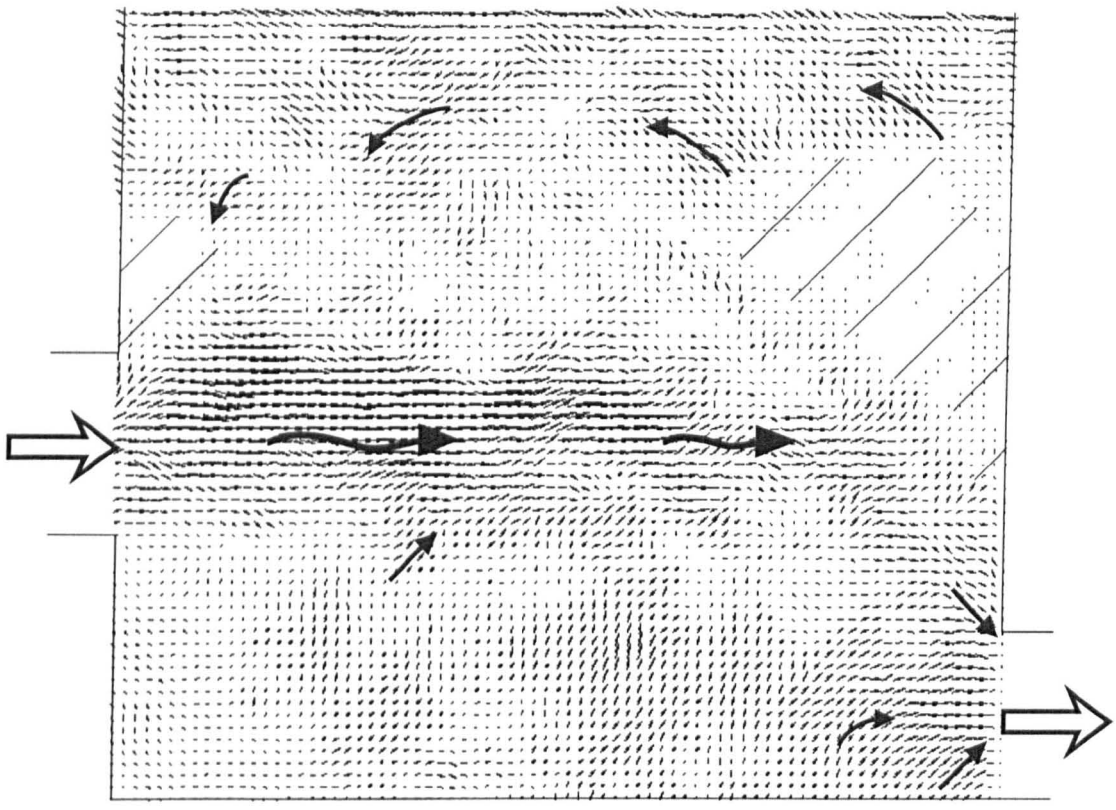

Figure 6.10 Flow patterns in manhole determined from particle image velocimetry (388mm manhole, Q = 1.0l/s, surcharge = 429mm).

Even with the use of a high powered 5W laser, the seeding particles used in the system consistently failed to provide bright images for recording. In addition, marks and bracing straps on the manhole itself precluded data from being obtained from some regions of the flow. The worst affected of these areas are marked with hash lines in the figure. The software used to process the images also proved rather unstable, and all attempts to apply a calibration scale to the measurements so as to determine quantitative velocity magnitudes resulted in the package crashing.

However, the PIV results do show similar trends in flow pattern to the CFD models. Figure 6.10 is an average of 50 images recorded over an 18 second period. Arrows summarising the main flow directions have been added to the figure. The jet entering the manhole appears to show a slight narrowing as it traverses the chamber, and also the distinct dip of a proportion of the jet towards the

outlet pipe is well represented. It is possible to observe a pattern of re-circulation across the upper portion of the figure. It should be noted that the top of the figure does not represent the water surface, since the camera was not able to be located in a position that would allow the entire surcharge volume to be imaged. Thus it is possible that the greatest re-circulating flow velocities have not been captured.

Chapter 7

Further Work

7.1 Introduction

The work presented in this thesis provides detailed results regarding the longitudinal dispersion due to surcharged manholes. Laboratory studies have investigated the effects of a step height between the inlet and outlet pipes and of extreme high surcharge conditions. Furthermore, re-analysing data for various manhole diameters using an optimisation process has allowed this extra information to be included. A preliminary approach interpreting the flow patterns in manholes has been completed using the computational fluid dynamics package Fluent. This has enabled comparisons of computed and experimentally measured pressure head loss, and also a qualitative study of flow regimes for different manhole designs. However, there are areas of further study that are necessary to enable full implementation of manhole mixing and retention effects in sewer modelling software.

7.2 Continuation of laboratory studies

The longitudinal dispersion of a solute due to surcharged manholes has been investigated for specific cases from the wide variety of possible manhole configurations. Furthermore, the possibility of a link between the head loss that occurs at a manhole junction and the longitudinal dispersion model coefficients has been proposed and investigated. Unfortunately there is a limited amount of comparable head loss and longitudinal dispersion data and thus it is not possible to extend the conclusions beyond the scope of the laboratory investigation.

The location of manholes in an urban drainage network is largely governed by topographical factors. Design requirements for manholes at every change in pipe diameter, pipe slope, pipe direction and at all pipe junctions and also at minimum spacing on straight lengths of sewer mean that a wide variety of chamber configurations are encountered in practice. In addition, alternative construction materials such as masonry or pre-cast concrete units generate manholes with different plan shapes. For this reason it is necessary to extend the laboratory studies completed so far to encompass alternative manhole configurations. The most worthwhile of these would be manholes where there is an angle between inlet and outlet pipes as opposed to the straight through design. Head loss researchers have found that this geometry causes a considerable increase in the head loss coefficient and it is anticipated that there would be a similar significant effect on the longitudinal dispersion. Other possible configurations of interest include a comparison between square and circular plan shapes and manholes where greater than two pipes connect. In all experiments it would be important to record head loss characteristics as well as the soluble tracer dispersion concentrations so that it would be possible to determine any correlation between the head loss and the coefficients for the longitudinal dispersion models.

The development of a reliable theory regarding the association of head loss and longitudinal dispersion is reliant upon increased information regarding the flow profiles and movement of tracer within the manhole itself. Whilst the use of fluorometers located upstream and downstream of the manhole provide travel time and mixing data, their use offers no direct information regarding the submerged jet and re-circulation processes within the manhole.

Laser induced fluorescence is a method by which the flow inside the manhole can be studied and analysed. This had been the original method proposed for obtaining longitudinal dispersion coefficients for the stepped manhole configurations. Unfortunately the laser employed was of insufficient power to obtain the necessary clarity of resolution of tracer concentration. Studies undertaken with a more powerful laser and high quality digital image processing equipment would enable a considerable advance in understanding the flow structures that lead to the head loss and longitudinal dispersion that occurs as flow passes through manholes. Still and video camera images clearly revealed the turbulent eddies forming part of the submerged jet as it developed inside the manhole. These eddies were observed to cause tracer to mix with the manhole volume and, once the main bulk of the tracer cloud had passed, re-entrain pockets of tracer from the areas in contact with the jet. A greater understanding of this process gained from quantitative analysis would be applicable to any work concerned with the interaction of solutes with dead zone regions and would be beneficial for the development of improved longitudinal dispersion models for manholes.

7.3 Data analysis

The optimisation of the longitudinal dispersion coefficients has been demonstrated to be crucial in determining realistic simulations for the transport of solutes through manholes. However, it should be remembered that the work presented is based on simple forms of the ADE and ADZ transport models and uses a least errors method for determining the quality of fit of a temporal concentration prediction to the measured data. Whilst this generally gives a high quality of prediction for important aspects of the profiles there may be situations where even greater levels of simulation quality are required. For instance, although the optimised predictions match the downstream data well on the rising limb and the peak time and concentration values, they are less good at representing the full length of the tail of low concentration. This is a result of the inability of these models to fully represent the shape of the downstream profile.

A method for obtaining increased quality in the model predictions would be to use higher order models. The formulation of a second order ADZ model has been outlined (Equation [2.37]) and this is effectively two first order ADZ models operating in parallel. In practical terms, the second order model represents a solute cloud passing through the manhole by two separate flow mechanisms. Thus a proportion of the solute can be said to pass straight through from the inlet to the outlet with little difference to if it was travelling through a pipe equal in length to the manhole diameter. The remainder of the solute cloud is considered to become entrained in the surcharged volume, and is only gradually released into the downstream pipe. The dead zone interactions for the two processes are very different and the results are not always described well by the first order model attempting to combine all the dead zone processes as one. With a second order application, a first order ADZ model is applied for each portion of the tracer cloud, and the result combined to give the overall effect of the manhole structure.

An example set of laboratory data was analysed using the second order model. Two coefficients, travel time and time delay, were applied to each first order model, with a further coefficient to represent the flow split between them. The measured upstream data profile was routed through the parallel model by dividing the concentration values proportionally to the required flow split. Each individual first order model was then used to process the relevant portion of the data, using the coefficients for that model. The concentration output from the two parallel models was then summed to give the predicted downstream profile (Figure 7.1).

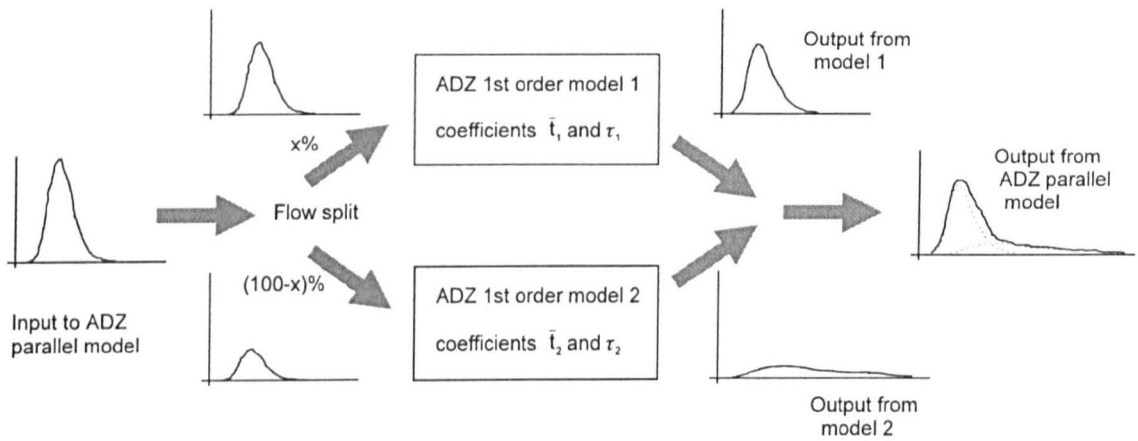

Figure 7.1 ADZ parallel model.

The coefficients for the ADZ parallel model were determined by means of an optimisation procedure in a similar manner to the first order model. In this case, there were five coefficients to be optimised, thus necessitating a 5 by 5 sided matrix to incorporate all the combinations. In most cases examined, the computer software was able to locate an optimised solution giving predictions with an extremely high quality of fit to the measured downstream concentration profiles. The combination of two ADZ models in parallel demonstrates an improved ability to represent both the peak concentration and time of occurrence as well as the long, low concentration tail effect which is a common feature of the data (Figure 7.2).

For the manhole case presented, the ADZ parallel model coefficients are provided in Table 7.1. Also shown are the travel time and time delay values for a straight length of pipe. It is clear that first order model number 1 in the parallel model uses coefficients very similar to those for a straight length of pipe. This supports the theory that a large proportion of tracer mass, in this case optimised to 76 percent, travels directly through the manhole, and a lesser mass of tracer is mixed into the surcharge volume and released slowly, thereby producing the long downstream tail effect.

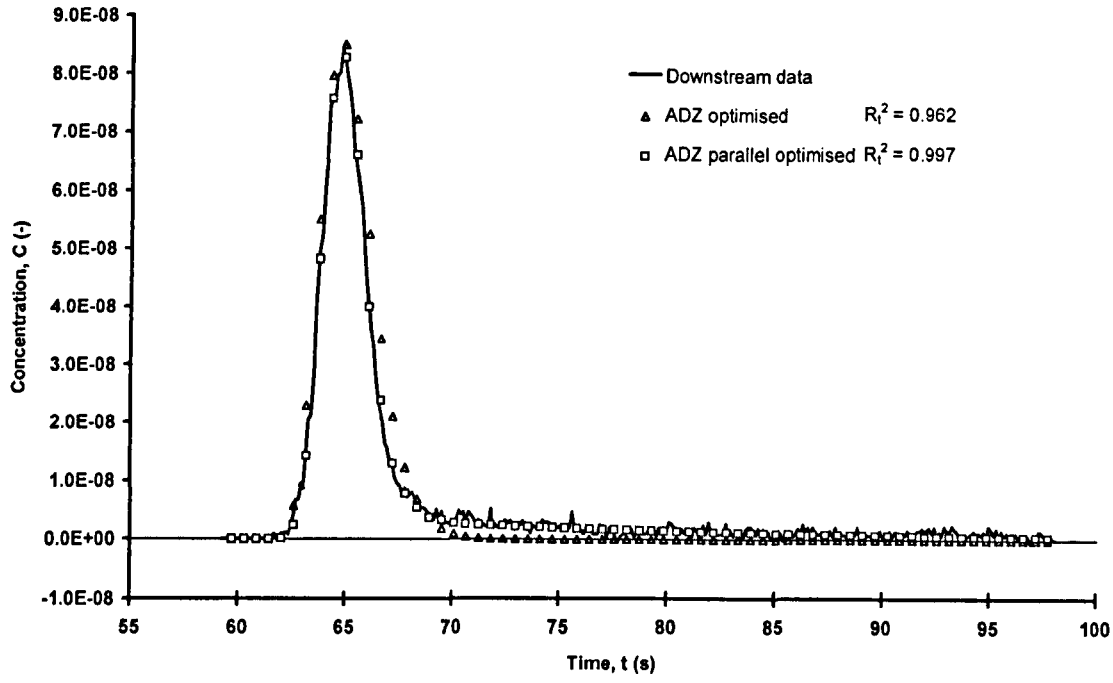

Figure 7.2 Comparison of ADZ parallel and ADZ optimised predictions (388mm unbenched manhole, no step, Q = 6.0l/s, surcharge = 402mm).

	388mm unbenched manhole, no step, Q = 6.0l/s			Straight pipe, Q = 6.0l/s
	ADZ parallel model		ADZ optimised	From Guymer and O'Brien (2000)
	1 (split = 76%)	2 (split = 24%)		
Travel time, $\bar{t}$ (s)	2.69	16.98	2.88	2.78
Time delay, τ (s)	2.53	1.38	2.07	2.44
R_t^2	0.997		0.962	-

Table 7.1 Coefficients for ADZ parallel and ADZ optimised models.

The use of a parallel ADZ model would appear to be a very useful longitudinal dispersion model where more accurate predictions of profiles not well described by the first order model are required. However, a problem with using it further is ensuring the robustness of the optimisation procedure. In the case of a single ADZ model with only two coefficients, it was a simple matter to ensure that there was an individual pair of coefficients that produced a prediction with the best fit to the downstream data. However, with five coefficients in the parallel version, it was not considered possible to be certain that the optimised coefficients were the only combination that gave a best fit value.

A possible solution to this problem would be to use a Monte Carlo simulation procedure. Whilst not being an absolute guarantee of the uniqueness of the optimised coefficient set, it would provide the extra confidence necessary to use the parallel model throughout the manhole data that have been gathered. The process is simple, but rather cumbersome and time consuming. The idea is to calculate the best fit coefficient, R_t^2, for each of the downstream predictions generated from a large number of

random combinations of the five ADZ parallel coefficients. In this way, when the best fit values from these repeats are plotted against each coefficient in turn it is possible to have confidence in whether or not the coefficient has a single best fit value. This is shown in Figure 7.3, where darker shading represents a greater density of data points in that region. Figure 7.3a shows the potential results for a coefficient that is statistically shown to have single, critical value that could be obtained through optimisation. In Figure 7.3b it can be observed that the coefficient concerned may generate more than one maximum best fit value, and therefore an attempt at optimisation may lead to misleading results. The final figure represents the expected result for a coefficient that has no significant effect on the best fit outcome (Figure 7.3c). This circumstance would occur if the use of a higher model caused overparamatisation and the coefficient in the figure was redundant in the optimisation process. Undertaking analysis such as this for different data sets would be necessary before continuing with ADZ parallel optimisation data analysis, and drawing conclusions from the results.

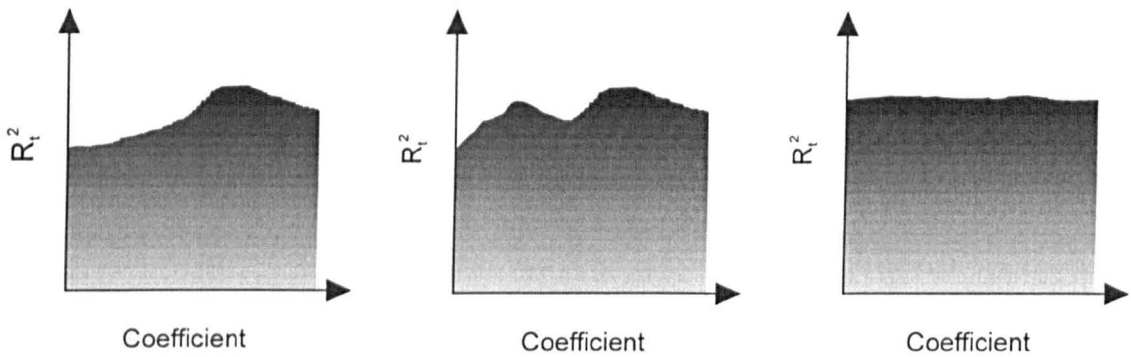

Figure 7.3a Figure 7.3b Figure 7.3c

Figure 7.3 Possible Monte Carlo simulation results.

7.4 Numerical modelling

Rapid developments in computing technology mean that accurate and reliable modelling of complex fluid flow problems is becoming available. Software manufacturers such as Fluent are releasing increasingly powerful versions of their packages. Fluent has the ability to model more than one chemical species, each of which can have independent values for density and viscosity, and thus can make predictions for the concentration of a soluble tracer added to a water filled domain. This could be used as a means of numerically modelling the longitudinal dispersion due to a manhole.

Whilst channel flow, contact tank and large scale reservoir modelling is commonly reduced to a two dimensional flow problem, the submerged jet interaction with the manhole surcharge volume has a considerable three-dimensional aspect. This means that a large and complex computational grid is required to obtain reliable hydrodynamic predictions, upon which solute transport predictions from CFD models have been shown to be highly dependent (Wang and Falconer, 1998). It is regrettable that a more refined grid could not be achieved with the CFD software employed. The greatest restriction was the requirement for a structured computational grid. This meant that for the manhole and pipes combination a large number of cells were required in unused volumes of the three-dimensional domain. These cells are known as dead cells, and the Fluent software undertakes no calculations for them. However, the total number of cells available for computations is fixed and thus having large numbers of dead cells reduces the available number of cells that can be part of the live

domain. The simulation of solute transport processes requiring time dependent flow modelling using time steps at least an order of magnitude smaller than the smallest time constant being modelled (Fluent, 1993). This, in combination with the large computational grid leads to converged solutions describing the full passage of the injected species requiring considerable computational time.

Continual developments in CFD software mean that a more recent version of Fluent allows greater flexibility in the formatting of the computational grid, using an unstructured system that produces grids with less distortion and enables efficient use of cell numbers. This increases the efficiency of the numerical modelling procedure and enables a high quality grid to be applied to complex geometries. Other improvements in the software include the development of new solver algorithms that result in huge reductions in processing time. This makes three-dimensional time dependent modelling with short time steps more feasible. In addition, specific consideration has been given to improving the boundary layer modelling, thus reducing the restrictions on the critical boundary layer cell sizing. It is expected that continued application of CFD to manhole research would be rewarded with improvements in the results for velocities, head loss and dispersion effects. However, the numerical models would require successful calibration of the hydrodynamic conditions by means of reliable laboratory measurements.

It is recommended that an investigation into the use of CFD for modelling solute dispersion begins with a more simple geometrical case than a surcharged manhole. The ideal starting point would be with a three dimensional straight pipe. The flow patterns and dispersive characteristics are well documented by theory and observation and this would provide a reliable verification for the CFD model without the need for intensive laboratory measurements detailing the flow conditions. A fine and well-formed grid could be applied to this less complex geometrical form. Furthermore, the travel time for a simulated soluble tracer cloud would be significantly reduced and therefore the model simulation would be operated over a reduced time period. Only if it were possible to produce a CFD model pipe with accurate velocity, pressure and dispersion predictions would it be reasonable to extend the work to manhole geometries.

7.5 Field testing

The primary aims of establishing an understanding of the mixing that occurs as sewer flow passes through surcharged manholes is to increase the reliability of sewer water quality models. Naturally these computer models are applied to real urban drainage networks, either operational or planned, rather than the idealised conditions of a laboratory. For this reason it is proposed that the work is now at a standard whereby a significant understanding would be gained by undertaking research on longitudinal dispersion through sewer networks using a controlled series of tracer studies.

The laboratory tests have shown that certain manhole configurations cause a marked increase in the dispersion and retention of a cloud of soluble tracer. It is felt that the non-uniform nature of many older sewers that may be suffering from a lack of maintenance will increase longitudinal dispersion effects even more. It is important to determine whether these factors are actually significant in the ability of a sewer quality model to accurately predict the times of arrival and concentrations of soluble pollutants throughout the network.

If a computer model fails to calculate the travel times through an urban drainage network accurately then the application of time rates of decay coefficients for different pollutants is rendered less meaningful. Likewise, the failure to accurately predict first arrival times and peak concentrations of pollutants that may enter the sewer system will cause a lack of reliability in any real time control analysis or operation based on these times.

A large quantity of data would be required from a field test schedule and it is likely that difficulties would be encountered. Measurements of water depth and velocity at critical points through the system, as well tracer concentration measurements would be necessary. Furthermore, interpretation of the results would be greatly assisted by testing being carried out under a variety of flow conditions. Ahyerre *et al* (1998) comment that improvement in knowledge of the water quality processes occurring in sewer systems will rely on high quality data being gathered. They recommend that it would be better to study a limited number of small, experimental watersheds in great detail, rather than gather lower quality data over more or larger catchments. This would allow an accurate assessment of sewer water quality modelling capabilities at present and provide results that could be incorporated in future model development.

Chapter 8

Conclusions

The longitudinal dispersion due to surcharged manholes has been investigated. A laboratory system was developed that allowed the measurement of soluble tracer concentration profiles upstream and downstream of a manhole structure.

A 388mm internal diameter circular manhole with 88mm internal diameter pipe lengths in a straight through configuration was studied. Five step height conditions between the inlet and outlet pipes were considered, with the inlet pipe being raised in equal steps between 0.0 and 2.0 times the pipe diameter, whilst the downstream pipe remained aligned with the manhole base. Surcharges up to approximately 1250mm above the outlet pipe soffit were employed. The experiments were conducted at flow rates between 1.0 and 8.0 litres per second. Specially adapted fluorometers located upstream and downstream of the manhole were used to measure the cross-sectional average temporal concentration profiles of a fluorescent tracer injected into the flow. Pressure measurements were recorded simultaneously by means of pressure transducers fitted to the delivery pipes. O'Brien (2000) supplied additional data relating to the longitudinal dispersion due to surcharged manholes of various internal diameters.

The longitudinal dispersion data were analysed using the advection dispersion equation and the aggregated dead zone models. Coefficients for these models were optimised by a procedure that calculated the pair of coefficients for each equation that gave the best downstream profile prediction when compared with the measured data. This procedure was written as a FORTRAN computer program.

It has been determined that surcharged manhole chambers without a step between the inlet and outlet pipes, and manholes with a benching arrangement, have similar longitudinal dispersion characteristics to an equivalent length of straight pipe. A step height between the inlet and outlet pipes causes increased dispersion. This effect is most significant for step heights less than one pipe diameter. Alterations to the diffusion and entrainment pattern of the submerged jet occur when it is located close to the free surface and this makes the longitudinal dispersion predictions for low surcharges less reliable. Additional work is required to establish data for other manhole configurations that would enable satisfactory predictions of the dispersion processes in the low surcharge region to be made.

The dispersive fraction has been used as a means of comparing the characteristics of different manhole configurations. A relationship between the dispersive fraction and the head loss coefficient for stepped manholes with or without benching has been proposed. This, used in combination with an estimate of the reach time delay for the manhole, would allow sewer water quality models to predict the transport of soluble pollutants through manholes with a simple first order aggregated dead zone model.

References

Ahyerre M., Chebbo G., Tassin B. and Gaume E. (1998) 'Storm Water Quality Modelling, an Ambitious Objective?' *Water, Sci. & Tech.*, vol. 37, no. 1, pp 205-213.

Albertson M. L., Dai Y. B., Jensen R. A. and Rouse, H. (1950) 'Diffusion of Submerged Jets' *ASCE Transactions*, vol. 115, pp 639-697.

Ali K. H. M. and Othman K. (1997) 'Investigation of Jet Forced Water Circulation in Reservoir' *Proc. Instn. Civ. Engrs., Wat., Marit. & Energy*, vol. 124, March, pp 44-62.

Anderson J. D. (1995) Computational Fluid Dynamics: The Basics with Applications' McGraw-Hill. ISBN 0-07-001685-2

Antonopoulos C. (1997) *MSc. (Eng) Thesis*, Dept. of Civil and Structural Engineering, University of Sheffield, UK.

Arao S. and Kusuda T. (1999) 'Effects of Pipe Bending Angle on Energy Losses at Two-Way Circular Drop Manholes' *Proc. 8th Int. Conf. on Urban Storm Drainage*, Sydney, Australia, pp 2163-2168.

Archer B., Bettess F. and Colyer P. J. (1978) 'Head Losses and Air Entrainment at Surcharged Manholes' *Report Number IT 185*, HR Wallingford, UK.

Asztély M. and Lyngfelt S. (1996) 'Three-Dimensional Modelling of Energy Losses in a Manhole' *Proc. 7th Int. Conf. on Urban Storm Drainage*, Hanover, Germany, pp 647-652.

Bartlett R. E. (1970) 'Public Health Engineering - Design in Metric - Sewerage' *Applied Science Publishers*, London. ISBN 444-20064-9

Bartlett R. E. (1981) 'Surface Water Sewerage' *2nd Edition, Applied Science Publishers*, London. ISBN 0-85334-925-8

Beer T. and Young P. C. (1983) 'Longitudinal Dispersion in Natural Streams' *Proc ASCE, J. Env. Eng.*, vol. 109, no. 5, pp 1049-1067

Bo Pedersen F. B. and Mark O. (1990) 'Head Losses in Storm Sewer Manholes: Submerged Jet Theory' *Proc. ASCE., J. Hyd. Eng.*, vol. 116, no. 11, pp 1317-1328.

Cambridge Electronic Design (1990) 'Spike2 Software Version 3 - User Guide' *Cambridge Electronic Design*, Cambridge UK.

Colyer P. J. and Pethick R. W. (1976) 'Storm Drainage Design Methods – A Literature Review' *Report No. INT 154*, HR Wallingford, UK.

Crabtree R., Garsdal H., Gent R., Mark O. and Dorge J. (1994) 'Mousetrap - a Deterministic Sewer Flow Quality Model' *Water, Sci. & Tech.*, vol. 30, no. 1, pp 107-115.

Dennis P., Guymer I and Antonopoulos C. (1999) 'Optimisation of the Aggregated Dead Zone Model for Solute Dispersion in Surcharged Manholes' *Proc. 8th Int. Conf. on Urban Storm Drainage*, Sydney, Australia, pp 763-770.

Dimenna R. A. and Lee S. Y. (1996) 'Validation Analysis for a Computational Fluid Dynamics Calculation of a Turbulent Free Jet in Water' *Proc. 1996 ASME Fluid Eng. Div. Summer Meeting*, vol. 2, no. 2, pp 821-828.

Elgattas M. S. (1995) 'Pressure Loss Coefficient at Straight Through Manholes' *PhD Thesis*, no. 8628, Department of Civil and Structural Engineering, University of Sheffield, UK.

Fischer H. B. (1966) 'A Note on the One-Dimensional Dispersion Model' *Air and Wat. Pollut. Int. J.*, vol. 10, pp443-452.

Fischer H. B. (1967) 'The Mechanics of Dispersion in Natural Streams' *Proc. ASCE., J. Hyd. Eng.*, vol. 93, no. 6, pp 187-216.

Fischer H. B. (1968) 'Dispersion Predictions in Natural Streams' *Proc. ASCE., J. Sanitary Eng.*, vol. 94, no. SA6, pp 927-943.

Fischer H. B., List E. J., Koh R. C. Y. Imberger J. and Brooks N. H. (1979) 'Mixing in Inland and Coastal Waters' *Academic Press*, New York. ISBN 0-12-258150-4

Fluent (1993) 'Fluent User's Manual' Fluent Europe, Sheffield, UK.

Foundation for Water Research (1994) 'UPM Manual. A Planning Guide for the Management of Urban Wastewater Discharges During Wet Weather' *FR/CL 002*, Foundation for Water Research, Marlow, UK. ISBN 0-9521712-1-X

French R. (1986) 'Open Channel Hydraulics' *McGraw-Hill*. ISBN 0-07-Y66342-4

Garsdal H., Mark O., Dørge J. and Jepsen S. E. (1995) 'Mousetrap - Modelling of Water-Quality Processes and the Interaction of Sediments and Pollutants in Sewers' *Water, Sci. & Tech.*, vol. 31, no. 7, pp 33-41.

Guymer I. and O'Brien R. (1995) 'The Effects of Surcharged Manholes on the Travel Time and Dispersion of Solutes in Sewer Systems' *Water, Sci. & Tech.*, vol. 31, no. 7, pp 51-59.

Guymer I. and Harry A. (1996) 'Use of Laser Induced Fluorescence and Video Imaging Techniques in an Investigation of Mixing across the Dead Zone / Flow Zone Boundary' *Proc. Int. Sem. Optical Methods & Data Processing in Heat & Fluid Flow*, I. Mech. E., London, UK, pp 419-428.

Guymer I., O'Brien R. and Harrison C. (1996) 'Representation of Solute Transport and Mixing within a Surcharged Benched Manhole using an Aggregated Dead Zone (ADZ) Technique' *Water, Sci. & Tech.*, vol. 34, no. 3-4, pp 95-101.

Guymer I., O'Brien R., Mark O. and Dennis P. (1998) 'An Investigation of Fine Sediment Mixing within Free-Flowing and Surcharged Manholes' *Water, Sci. & Tech.*, vol. 37, no. 1, pp 215-222.

Guymer I., Boxall J., Marion A., Potter R., Trevisan P., Bellinello M., and Dennis P. (1999) 'Longitudinal Dispersion in a Natural Formed Meandering Channel' *Proc. IAHR XXVIII Congress*, Graz, Austria, 22nd - 27th August 1999 (On compact disc).

Guymer I. and O'Brien R. (2000) 'Longitudinal Dispersion due to Surcharged Manhole' *Proc. ASCE., J. Hyd. Eng.*, vol. 126, no. 2, pp 137-149.

Hammer M. J. (1986) 'Water and Wastewater Technology' *2nd Edition, John Wiley & Sons*. ISBN 0-471-05650-2.

Harwood R. and Saul A. J. (1996) 'CFD and Novel Technology in Combined Sewer Overflow' *Proc. 7th Int. Conf. on Urban Storm Drainage*, Hanover, Germany, pp 1025-1030.

Herath S. K., Jayasuriya, L. N. and Hussey C. J. (1999) 'Modelling Wastewater Quality in Sewerage Systems' *Proc. 8th Int. Conf. on Urban Storm Drainage*, Sydney, Australia, vol. 1, pp 179-186.

Holley E. R. (1969) 'Unified view of Diffusion and Dispersion' *Proc. ASCE., J. Hyd. Div.*, vol. 95, no. HY2, pp 621-631.

Howarth D. and Saul A. J. (1984) 'Energy Loss Coefficients at Manholes' *Proc. 3rd Int. Conf. on Urban Storm Drainage*, Goteborg, Sweden, vol. 1, pp 127-136.

Johnston A. J. and Volker R. E. (1990) 'Head Losses at Junction Boxes' *Proc. ASCE., J. Hyd. Eng.*, vol. 116, no. 3, pp 326-341.

Kusuda T. and Arao S. (1996) 'Energy Losses at Circular Drop Manholes' *Proc. 7th Int. Conf. on Urban Storm Drainage*, Hanover, Germany, pp 85-90.

Kusuda T., Arao S. and Moriyama K. (1993) 'Energy Losses at Junction and Transient Flow in Sewer Networks' *Proc. 6th Int. Conf. on Urban Storm Drainage*, pp 121-127.

Lancaster J. and Hildrew, A. G. (1993) 'Characterizing In-stream Flow Refugia' *Can. J. Fish. Aquat. Sci.*, vol. 50, pp 1663-1675.

Lindvall G. (1984) 'Head Losses at Surcharged Manholes with a Main Pipe and a 90 Degree Lateral' *Proc. 3rd Int. Conf. on Urban Storm Drainage*, Goteborg, Sweden, vol. 1, pp 137-146.

Mark O., Appelgren C. and Košir M. (1996) 'Water Quality Modelling for the Ljubljana Master Plan' *Proc. 7th Int. Conf. on Urban Storm Drainage*, Hanover, Germany, pp 1109-1114.

Marsalek J. (1984) 'Head Losses at Sewer Junction Manholes' *Proc. ASCE., J. Hyd. Eng.*, vol. 110, no. 8, pp 1150-1154.

Marsalek J and Greck B. J. (1988) 'Head Losses at Manholes with a 90 Degree Bend' *Canadian J. of Civ. Eng.*, vol. 15 no. 5 pp 851-858.

O'Brien R. (2000) 'Dispersion due to Surcharged Manholes' *PhD Thesis*, Department of Civil and Structural Engineering, University of Sheffield, UK.

Petruck A., Cassar A. and Dettmar J. (1998) 'Advanced Real Time Control of a Combined Sewer System' *Water, Sci. & Tech.*, vol. 37, no. 1, pp 319-326.

PreBFC (1993) 'PreBFC User's Manual' Fluent Europe, Sheffield, UK.

Rodi W. (1984) 'Turbulence Models and their Applications in Hydraulics – A State of the Art Review' 2nd Revised Edition, *IAHR*, Delft, The Netherlands.

Rutherford J. C. (1994) 'River Mixing' *John Wiley and Sons*, Chichester, UK. ISBN 0-471-94282-0

Sangster W. M., Wood H. W., Smerdon E. T. and Bossy H. G. (1958) 'Pressure Changes at Storm Drain Junctions' *Bulletin No. 41*, Engineering Experimental Station, University of Missouri, Columbia, USA.

Saul A. J., Ruff S. J., Walsh A. M. and Green M. J. (1993) 'Laboratory Studies of CSO Performance' *WRC report*, no. UM1421, Water Research Centre, UK.

Schilling W. (1996) 'Potential and Limitations of Real Time Control' *Proc. 7th Int. Conf. on Urban Storm Drainage*, Hanover, Germany, pp 803-807.

Smart P. L. and Laidlaw I. M. (1977) 'An Evaluation of some Fluorescent Dyes for Water Tracing' *Water Resources Research*, vol. 13, no. 1, pp 15-33.

Stefan H. G. and Demetracopoulos A. C. (1981) 'Cells in Series Simulation of Riverine Transport' *Proc. ASCE., J. Hyd. Eng.*, vol. 107, no. HY6, pp 675-697.

Taylor G. I. (1953) 'Dispersion of Soluble Matter in Solvent Flowing Slowly through a Tube' *Proc. Roy. Soc. Series A*, vol. 219, pp 186-203.

Taylor G. I. (1954) 'The Dispersion of Matter in Turbulent Flow through a Pipe' *Proc. Roy. Soc. Series A*, vol. 223, pp 446-468.

Thornton R. C. and Saul A. J. (1986) 'Some Quality Characteristics of Combined Sewer Flows' *Public Health Engineer*, vol. 3, no. 14, pp 35-38

Valentine E. and Wood I. (1977) 'Longitudinal Dispersion with Dead Zones' *Proc. ASCE., J. Hyd. Eng.*, vol. 103, no. HY9, pp 975-990.

Verbanck M. A., Ashley, R. M. and Bachoc A. (1994) 'International Workshop on the Origin, Occurrence and Behaviour of Sediments in Sewer Systems: Summary of Conclusions' *Water Research*, vol. 28, no. 1, pp 187-194.

Wallis S. G., Young P. C. and Beven K. J. (1989a) 'Experimental Investigation of the Aggregated Dead Zone Model for Longitudinal Solute Transport in Stream Channels' *Proc. ICE*, Part 2, vol. 87, pp 1-22.

Wallis S. G., Guymer I. and Bilgi A. (1989b) 'A Practical Engineering Approach to Modelling Longitudinal Dispersion' *Proc. Int. Conf. on the Hyd. and Env. Modelling of Coastal, Estuarine and River Waters*, University of Bradford, UK, pp 291-300.

Wang H. and Falconer R. (1998) 'Simulating Disinfection Processes in Chlorine Contact Tanks using various Turbulence Models and High Order Accurate Difference Schemes' *Water Res.*, vol. 32, no. 5, pp 1529-1543.

Weinreich G., Schilling W., Birkely A. and Moland T. (1997) 'Pollution Based Real Time Control Strategies for Combined Sewer Systems' *Water, Sci. & Tech.*, vol. 36, no. 8-9, pp 331-336.

White J. B. (1987) 'Wastewater Engineering' *3rd Edition, Edward Arnold Ltd.* ISBN 0-7131-3614-6

Young P. C. and Wallis S. G. (1986) 'The Aggregated Dead Zone (ADZ) model for Dispersion in Rivers' *Proc. Int. Conf. on Water Quality Modelling in the Inland Natural Environment*, BHRA, Bournemouth, UK, Paper L1, pp 421-433.

Young P., Jakeman A. and McMurtrie R. (1980) 'An Instrumental Variable Method for Model Order Identification' *Automatica*, vol. 16, pp 281-294.

Acknowledgements

Firstly, a very big thank you to my supervisor Dr. Ian Guymer. Without his ever willing support, guidance and advice this thesis simply would not exist. Also to Dr. Robert O'Brien for his assistance in the early stages of my work and for making his data available for re-analysis.

I would like to extend grateful thanks to the excellent team of technicians within the Civil and Structural Engineering department at the University of Sheffield. I have great appreciation for the efforts of all those who have applied their time and skills to the laboratory test facility. Special mentions for Mr G. Brawn, Mr P. Osbourne, Mr S Richards, Mr A. Lumby, Mr D. Unwin, Mr D. Callaghan and Mr M. Moore.

Two persons deserve thanks for their direct assistance in collecting laboratory data. Miss C. Mezzani, whose careful approach and hard work enabled extra data to be collected and made available as part of the study, and Mr A. Buxton for his perseverance in obtaining particle image velocimetry data. Also, thanks to Mr. I. Spooner, whose generous loan of photographic equipment at short notice made possible the high powered laser photography.

Finally, special thanks to my parents and my family, my girlfriend Claire, and all my friends who have supported my efforts and provided the light relief from my academic work.